

***NON-INVASIVE CARDIAC
IMAGING FOR THE
QUANTIFICATION OF
VENTRICULAR FUNCTION:
POTENTIAL AND FUTURE
APPLICATIONS***

DR RAE F. DUNCAN

DOCTORATE OF MEDICINE

Postgraduate Institute of Medicine,
University of Newcastle
Tyne and Wear, England
UNITED KINGDOM

And

Cardiovascular Research Centre,
Royal Adelaide Hospital,
Adelaide, SA 5000
AUSTRALIA

November 2012

TABLE OF CONTENTS

Abstract Summary.....	
Acknowledgement.....	xii
Declaration of Originality.....	
Awards.....	
Publications.....	
Presentations.....	
List of Figures.....	
List of Tables.....	
List of Equations.....	
List of Abbreviations.....	
<u>SYNOPSIS</u>	1
<u>CHAPTER 1: INTRODUCTION</u>	5
1.1 Cardiovascular demographics and the evolving role of non-invasive cardiac imaging.....	6
THE LEFT VENTRICLE	
1.2 Anatomy of the normal left ventricle.....	6
1.3 Anatomical relationship of the coronary circulation to the left ventricle and its importance in assessing regional left ventricular function.....	8
1.4 Physiology of the normal left ventricle.....	11
1.4.1 Left ventricular systole.....	11
1.4.2 Left ventricular diastole.....	13
1.4.3 Systolic and diastolic interdependence.....	16
THE RIGHT VENTRICLE	
1.5 Anatomy of the normal right ventricle.....	17
1.6 Anatomical relationship of the coronary circulation to the right ventricle.....	19
1.7 Physiology of the normal right ventricle.....	20
1.7.1 Contribution of the interventricular septum to right ventricular contractility.....	20

1.7.2	Right ventricular haemodynamics.....	21
1.8	Ventricular-ventricular interdependence.....	24
1.9	The origins of diagnostic cardiology.....	26
1.9.1	Invasive catheter studies.....	26
1.9.2	Echocardiography.....	27
1.9.3	Nuclear cardiology.....	28
1.9.4	Cardiac magnetic resonance.....	28
1.9.5	Cardiac computed tomography.....	29
1.10	Multi-modal imaging for the assessment of ventricular function.....	30
1.10.1	Assessment of resting ventricular function.....	31
1.10.2	Assessment of dynamic ventricular function: Stress-perfusion imaging.....	31
1.10.3	Safety issues.....	31
1.11	The non-invasive assessment of left ventricular systolic function.....	32
1.11.1	Haemodynamic assessments of global left ventricular function.....	32
1.11.2	Volumetric assessments of global left ventricular systolic function.....	35
1.11.3	New two-dimensional echocardiographic assessments of left ventricular systolic function.....	43
1.11.4	The assessment of regional left ventricular systolic function.....	50
1.11.5	Concept behind Study 1: Creating a Global Strain Score using regional myocardial deformation imaging to quantify global left ventricular systolic function.....	53
1.11.6	Concept behind Study 2: Regional Wall Motion Scoring for calculating global left ventricular systolic function.....	54
1.12	The non-invasive assessment of left ventricular diastolic function.....	55
1.12.1	The importance of accurately diagnosing left ventricular diastolic dysfunction...55	55
1.12.2	Traditional assessments of left ventricular diastolic function.....	56
1.12.3	New assessments of left ventricular diastolic function.....	64
1.12.4	Current guidelines for evaluating left ventricular diastolic function.....	70
1.12.5	Concept behind Study 3: The potential application of velocity encoded CMR for the estimation of left ventricular end-diastolic pressure.....	73
1.13	The non-invasive assessment of right ventricular function.....	74
1.13.1	The prognostic importance of right ventricular function.....	74
1.13.2	Volumetric assessments of global right ventricular systolic function.....	74

1.13.3	Non-volumetric assessments of global right ventricular systolic function.....	76
1.13.4	Concept behind Study 4: A comparison of ten two-dimensional echocardiographic non-volumetric indices of right ventricular systolic function: Correlation with CMR-derived RVEF.....	81

CHAPTER 2: AIMS **83**

2.1	General aims of this thesis.....	84
2.2	Specific aims of this thesis.....	84
2.2.1	Study 1: Left ventricular systolic function - Speckle tracking strain.....	84
2.2.2	Study 2: Left ventricular systolic function - Regional wall motion score index.....	84
2.2.3	Study 3: Left ventricular diastolic function – MRI phase encoded velocity mapping for estimating left ventricular end diastolic pressure.....	85
2.2.4	Study 4: Right ventricular systolic function – Non-volumetric indices of right ventricular function.....	85

CHAPTER 3: METHODOLOGY **86**

3.1	General methods.....	87
3.2	Study design.....	87
3.3	Cardiac catheterisation protocol.....	88
3.3.1	Left heart catheterisation.....	88
3.3.2	Limitations of the technique.....	89
3.4	Cardiac magnetic resonance imaging protocols.....	90
3.4.1	Left ventricular systolic function protocol.....	90
3.4.2	Right ventricular systolic function protocol.....	91
3.4.3	Left ventricular diastolic function protocol.....	92
3.5	Three-dimensional echocardiography imaging protocol.....	92
3.6	Two-dimensional echocardiography imaging protocols.....	94
3.6.1	Quantifying left ventricular systolic function by two dimensional echocardiography.....	95
3.6.2	Quantifying right ventricular systolic function by two dimensional echocardiography.....	97

3.6.3	Quantifying left ventricular diastolic function by two dimensional Echocardiography.....	99
3.7	Statistical analyses.....	102

CHAPTER 4: LEFT VENTRICULAR SYSTOLIC FUNCTION – PART ONE 104

“TWO-DIMENSIONAL SPECKLE TRACKING STRAIN FOR THE EVALUATION OF LEFT VENTRICULAR SYSTOLIC FUNCTION: A COMPARISON AGAINST CARDIAC MAGNETIC RESONANCE IMAGING, THREE-DIMENSIONAL ECHOCARDIOGRAPHY AND SIMPSON’S BIPLANE METHOD OF DISCS”

4.1	Introduction.....	105
4.2	Study aims.....	106
4.3	Methods.....	106
4.3.1	Study design.....	106
4.3.2	Patient selection.....	107
4.3.3	Imaging methods.....	107
4.3.4	Image analysis.....	108
4.3.5	Reproducibility.....	112
4.3.6	Statistical analysis.....	112
4.4	Results.....	113
4.4.1	Correlation of global strain score with Simpson’s left ventricular ejection Fraction.....	113
4.4.2	Correlation of global strain score, Simpson’s left ventricular ejection fraction and 3D echocardiography left ventricular ejection fraction with CMR-derived left ventricular ejection fraction.....	113
4.4.3	Receiver operator characteristics.....	117
4.4.4	Calculation of left ventricular ejection fraction from the global strain score, and validation of regression equation.....	117
4.4.5	Acquisition and analysis times.....	118
4.4.6	Reproducibility.....	118
4.5	Discussion.....	121

4.5.1	Study limitations.....	123
4.5.2	Conclusion	123
4.5.3	Future work.....	124

CHAPTER 5: LEFT VENTRICULAR SYSTOLIC FUNCTION – PART TWO 125

“A STUDY OF THE 16-SEGMENT REGIONAL WALL MOTION SCORING INDEX AND BIPLANE SIMPSON’S RULE FOR THE CALCULATION OF LEFT VENTRICULAR EJECTION FRACTION: A COMPARISON WITH CARDIAC MAGNETIC RESONANCE IMAGING”

5.1	Introduction.....	126
5.2	Study aims.....	127
5.3	Methods.....	127
5.3.1	Study design.....	127
5.3.2	Patient selection.....	128
5.3.3	Imaging methods.....	128
5.3.4	Image analysis.....	129
5.3.5	Reproducibility.....	130
5.3.6	Statistical analysis.....	131
5.4	Results.....	131
5.4.1	Correlation and inter-technique agreement of regional wall motion score index derived LV ejection fraction with Simpson’s LV ejection fraction.....	131
5.4.2	Correlation and inter-technique agreement of regional wall motion score index derived LV ejection fraction and Simpson’s LV ejection fraction with CMR derived LV ejection fraction.....	133
5.4.3	Correlation and inter-technique agreement of regional wall motion score index derived LV ejection fraction and Simpson’s LV ejection fraction with CMR derived LV ejection fraction in patients with normal LV systolic function.....	134
5.4.4	Correlation and inter-technique agreement of regional wall motion score index derived LV ejection fraction and Simpson’s LV ejection fraction with CMR derived LV ejection fraction in patients with impaired LV systolic function.....	135
5.4.5	Reproducibility.....	136

5.5	Discussion.....	138
5.5.1	Study limitations.....	141
5.5.2	Conclusion	141

CHAPTER 6: LEFT VENTRICULAR DIASTOLIC FUNCTION 142

“PHASE CONTRAST VELOCITY ENCODED CARDIAC MAGNETIC RESONANCE IMAGING FOR THE ASSESSMENT OF LEFT VENTRICULAR DIASTOLIC FUNCTION: A COMPARISON STUDY WITH ECHOCARDIOGRAPHY E/Em RATIO AND INVASIVE CATHETER MEASUREMENTS OF LEFT VENTRICULAR END DIASTOLIC FILLING PRESSURE”

6.1	Introduction.....	143
6.2	Study aims.....	145
6.3	Methods.....	145
6.3.1	Study design.....	145
6.3.2	Patient selection.....	146
6.3.3	Imaging methods.....	147
6.3.4	Image analysis.....	152
6.3.5	Reproducibility.....	154
6.3.6	Statistical analysis.....	155
6.4	Results.....	155
6.4.1	Correlation and intertechnique agreement of mitral E velocities, mitral A velocities and E/A ratio recorded using velocity encoded magnetic resonance, with spectral Doppler echocardiography mitral E and A velocities and E/A ratios.....	156
6.4.2	Correlation and intertechnique agreement of velocity encoded magnetic resonance early diastolic myocardial tissue relaxation velocities (Em) with pulsed-wave tissue Doppler echocardiography Em velocities, recorded from the basal segment/mitral annular junction of all six LV walls, in patients exhibiting a range of LV ejection fractions.....	158
6.4.3	Correlation of velocity encoded magnetic resonance E/Em ratio with invasive measurements of left ventricular end diastolic filling pressure in patients	

exhibiting a range of LV ejection fractions.....	161
6.4.4 Correlation of velocity encoded magnetic resonance E/Em ratio pulsed-wave tissue Doppler E/Em ratio in patients exhibiting a range of LV ejection fractions.....	164
6.4.5 Correlation and intertechnique agreement of mitral E velocities, mitral A velocities and E/A ratio recorded using velocity encoded magnetic resonance, with spectral Doppler echocardiography mitral E and A velocities and E/A ratios in patients with normal LV systolic function.....	166
6.4.6 Correlation of velocity encoded magnetic resonance E/Em ratio with invasive measurements of left ventricular end diastolic filling pressure in patients with normal LV systolic function.....	168
6.4.7 Correlation of velocity encoded magnetic resonance E/Em ratio with pulsed-wave tissue Doppler E/Em ratio in patients with normal LV systolic function.....	170
6.4.8 Regression analysis for comparing variations in velocity encoded magnetic resonance E/Em ratio calculation compared to left ventricular end diastolic pressure in patients with normal LV systolic function.....	172
6.4.9 Correlation and intertechnique agreement of mitral E velocities, mitral A velocities and E/A ratio recorded using velocity encoded magnetic resonance, with spectral Doppler echocardiography mitral E and A velocities and E/A ratios in patients with impaired LV systolic function.....	172
6.4.10 Correlation of velocity encoded magnetic resonance E/Em ratio with invasive measurements of left ventricular end diastolic filling pressure in patients with impaired LV systolic function.....	174
6.4.11 Correlation of velocity encoded magnetic resonance E/Em ratio with pulsed-wave tissue Doppler E/Em ratio in patients with impaired LV systolic function.....	176
6.4.12 Receiver-operator characteristics for velocity encoded magnetic resonance E/Em ratios.....	178
6.4.13 Diagnosing diastolic dysfunction by velocity encoded magnetic resonance in a heterogeneous patient cohort, based on a modification of the American Society of Echocardiography/European Association Echocardiography 2010 Guidelines....	178
6.4.14 Reproducibility.....	182
6.5 Discussion.....	192
6.5.1 Comparing velocity encoded magnetic resonance peak transmitral inflow	

velocities, myocardial tissue velocities and E/A ratios with spectral and tissue Doppler echocardiography recordings and LV filling pressures.....	193
6.5.2 Comparing velocity encoded magnetic resonance E/Em with echocardiography E/Em and LV filling pressures.....	194
6.5.3 Comparing velocity encoded magnetic resonance E/Em results in this study with current research.....	196
6.5.4 Study limitations.....	198
6.5.5 Conclusion and future work.....	199

CHAPTER 7: RIGHT VENTRICULAR FUNCTION

201

“TEN QUANTITATIVE METHODS FOR ANALYSING RIGHT VENTRICULAR SYSTOLIC FUNCTION USING TWO-DIMENSIONAL AND TISSUE DOPPLER ECHOCARDIOGRAPHY: A COMPARISON WITH CARDIAC MAGNETIC RESONANCE IMAGING”

7.1 Introduction.....	202
7.2 Study aims.....	204
7.3 Methods.....	204
7.3.1 Study design.....	204
7.3.2 Patient selection.....	205
7.3.3 Imaging methods.....	205
7.3.4 Image analysis.....	208
7.3.5 Acquisition and analysis times.....	218
7.3.6 Visual assessment of right ventricular systolic function.....	219
7.3.7 Reproducibility.....	219
7.3.8 Statistical analysis.....	219
7.4 Results.....	220
7.4.1 Patient characteristics.....	220
7.4.2 Correlation of ten echocardiographic indices of right ventricular function against magnetic resonance derived right ventricular ejection fraction.....	221
7.4.3 Receiver operator characteristics.....	227
7.4.4 Regression analysis of echocardiographic right ventricular indices indexed	

against magnetic resonance derived right ventricular ejection fraction.....	236
7.4.5 Calculation of right ventricular ejection fraction.....	236
7.4.6 Comparison of the ten echocardiographic indices of right ventricular systolic function with visual assessment of right ventricular systolic function.....	236
7.4.7 Acquisition and analysis times.....	238
7.4.8 Reproducibility.....	240
7.5 Discussion.....	253
7.5.1 Study limitations.....	255
7.5.2 Conclusion.....	256
<u>CHAPTER 8: GENERAL DISCUSSION AND CONCLUSION</u>	257
8.1 General discussion and future work.....	258
8.2 Thesis conclusion.....	263
<u>APPENDICES</u>	264
Appendix A Example patient information sheet.....	264
Appendix B Example patient consent form.....	268
Appendix C British Society of Echocardiography Investigator of the Year Winner Certificate.....	270
Appendix D British Society of Echocardiography Investigator of the Year Finalist Certificate.....	272
<u>REFERENCES</u>	274

ABSTRACT SUMMARY

Background: Non-invasive cardiac imaging provides important diagnostic and prognostic information in cardiovascular disease. Assessment of ventricular function remains the fundamental imaging request in clinical practice. Cardiac magnetic resonance (CMR) is now the recognised reference standard for quantification of left and right ventricular systolic function, but not diastolic filling. Due to cost and limited availability of CMR, echocardiography remains the first line imaging modality for assessing ventricular function in most cases. Several echocardiographic methods are available for quantifying global ventricular function however despite significant advances in cardiac imaging techniques, visual assessment of ventricular systolic function remains the standard by which ventricular function is reported in many centres. This method is subjective and introduces inter-observer bias. In an era of multi-modal imaging, accurate, reproducible and widely available methods for quantifying ventricular function, which exhibit good inter-modal inter-technique concordance, are desirable. The overall aim of this thesis was to examine the accuracy and reproducibility of several new echocardiographic imaging techniques for quantifying left and right ventricular systolic function, indexed against CMR reference standards, and to examine a novel CMR technique for assessing diastolic function, indexed against current reference standards (invasive catheter recording of left ventricular end diastolic filling pressure (LVEDP)), in a heterogeneous cohort of patients as seen in clinical practice.

Methods: All imaging modalities were performed within three hours of each other.

Study 1 was designed to compare the accuracy of speckle tracking strain echocardiography for quantifying LV systolic function against biplane Simpson's rule (SR) and 3D-echocardiography, using CMR LV ejection fraction (LVEF) as the reference standard.

Study 2 was designed to investigate the accuracy of a novel modified regional wall motion scoring index (RWMSI) for calculating LVEF, and compare its accuracy against SR and CMR LVEF.

Study 3 was designed to explore the clinical utility of velocity encoded (VEC) CMR for diagnosing LV diastolic dysfunction. VEC CMR E/Em velocity ratio was compared to LVEDP recorded during left heart catheterisation.

Study 4 was a head-to-head comparison of 10 echocardiographic non-volumetric indices of right ventricular systolic function, based on current European Association of Echocardiography recommendations, indexed against CMR RVEF as the reference standard.

Results: In study 1 we demonstrate that speckle tracking strain may be superior to SR for quantifying LV systolic function. In study 2 we suggest that, when specialist imaging software is unavailable, a modified RWMSI may be superior to SR for calculating LVEF. In study 3, we demonstrate a significant correlation between VEC-CMR E/Em ratios and LVEDP, and conclude that VEC-CMR may be a useful tool to diagnose diastolic dysfunction, especially in patients with preserved LVEF. In study 4, we demonstrate that RV free wall strain has a closer correlation to CMR-RVEF than nine alternative echocardiographic indices of RV function, and may be the method of choice for assessing RV systolic function by 2D-echocardiography in the future.

Conclusions: This series of studies has confirmed that novel non-invasive cardiac imaging techniques may be used to accurately quantify cardiac ventricular function, and may confer significant advantage over current methods.

ACKNOWLEDGEMENTS

I would firstly like to acknowledge the contribution my co-supervisors have made to my education and the production of this thesis. To my Australian supervisor; Professor Stephen Worthley has been an outstanding and enthusiastic leader, whose unwavering support has permitted the success of many research projects in the field of cardiovascular science. I have learnt invaluable lessons from our association that have shaped and moulded my approach to both the research and clinical spheres of my career. To my UK supervisors; I thank Dr Azfar Zaman for his work ethic and continued support which has helped ensure the realisation of this thesis; Professor Bernard Keavney I thank for sharing his extensive knowledge and expertise in the field cardiovascular research.

I would also like to thank my co-workers in Australia. In particular, I must make special note of three people. Dr Cynthia Piantadosi for her experience as a clinical research scientist, her professional assistance and her friendship allowing the realisation of many productive projects together during this time. Also Dr Benjamin Dundon and Dr Adam Nelson for their unending enthusiasm and assistance in data analysis – their camaraderie was greatly appreciated on the many occasions we shared long late nights and weekends of data analysis in the research lab. Special mention must also be made to Dr Karen Teo and Ms Kerry Williams our superb magnetic resonance team leaders who taught me all I know about cardiac magnetic resonance imaging, and to Janet and her staff in the echocardiography laboratory at Adelaide Cardiac Imaging, Wakefield Private Hospital, Adelaide for allowing me access and use of all their equipment.

From the Freeman Hospital, Newcastle Upon Tyne, UK, I would like to thank Dr Antoinette Kenny, Consultant Cardiologist and Clinical Head of Freeman Echocardiography Laboratory for her support and guidance. I must also thank Mrs Julie Schuster, Technical Head of Freeman Echocardiography Laboratory for providing blinded inter-observer reproducibility data for this study.

I must thank the Sir Michael Straker Travelling Fellowship trustees, Newcastle, UK for awarding me a travelling fellowship to assist with my relocation costs to South Australia,

and to the Cardiovascular Research Centre, Adelaide, Australia for financially supporting this research.

I would like to thank all the staff in the Cardiovascular Research Centre, Adelaide, Australia for their support during my stay in Australia as well as their friendship. The CRC was an extremely warm, welcoming and enthusiastic environment to work in and the excellent research that continues to emerge from the centre is testament to the leadership of the CRC Professors, Professor Stephen Worthley and Professor Prash Sanders, and the team work of the staff. I hope in the future I will have the privilege of working on further international collaborations with my new friends.

Finally, and most importantly I wish to thank my family. To my young children Callum and Bethany for their patience and understanding; and to my husband Ross, for his love and support, and for helping me realise that I can achieve despite challenging circumstances.

DECLARATION OF ORIGINALITY

I declare this thesis is a record of original work and contains no material previously accepted for the award of any other degree or diploma in any university or other tertiary institution. To the best of my knowledge and belief, this thesis contains no material previously published or written by another person, except where due reference is made in the text.

I give consent to this copy of my thesis, when deposited in the University Library, being available for loan and photocopying.

THESIS RELATED AWARDS

1. BRITISH SOCIETY OF ECHOCARDIOGRAPHY INVESTIGATOR OF THE YEAR FINALIST 2012 for the study:

“Two-dimensional speckle tracking strain for the evaluation of global left ventricular systolic function: A comparison against magnetic resonance imaging and Simpson’s biplane method of discs” **Rae Duncan**

Due for presentation at the British Society of Echocardiography Annual Scientific Sessions, Harrogate, England on Sat 3rd November 2012.

2. BRITISH SOCIETY OF ECHOCARDIOGRAPHY INVESTIGATOR OF THE YEAR WINNER 2011 for the study:

“A study of the 16-segment regional wall motion scoring index and biplane Simpson’s rule for the calculation of left ventricular ejection fraction: A comparison with cardiac magnetic resonance imaging.” **Rae Duncan**

Presented at the British Society of Echocardiography Annual Scientific Sessions, Edinburgh, Scotland, 7-8th October 2011.

3. BRITISH SOCIETY OF ECHOCARDIOGRAPHY INVESTIGATOR OF THE YEAR FINALIST 2011 for the study:

“Right ventricular free wall strain has a closer correlation with right ventricular ejection fraction than other echocardiographic indices of right ventricular function: Validation with cardiac magnetic resonance imaging” **Rae Duncan**

Presented at the British Society of Echocardiography Annual Scientific Sessions, Edinburgh, Scotland, 7-8th October 2011.

**4. AMERICAN COLLEGE OF CARDIOLOGY SPOTLIGHT ELECTRONIC
POSTER PRESENTATION 2008 for the study:**

“The 17-Segment Regional Wall Motion Scoring Index for the calculation of left ventricular ejection fraction: A comparison against cardiac magnetic resonance imaging and 2D echocardiography biplane Simpson’s rule.”

Presented at the 57th Annual Scientific Session of the American College of Cardiology, Chicago, Illinois, USA, April 2008.

**5. JAPANESE CIRCULATION SOCIETY FIRST PLACE POSTER AWARD 2008
for the study:**

“Velocity Encoded Cine MRI for the assessment of Left Ventricular Diastolic Function.”

Presented at the 72nd Annual Scientific Meeting of the Japanese Circulation Society, Fukuoka, Japan, 28th-30th March 2008.

6. THE SIR MICHAEL STRAKER TRAVELLING FELLOWSHIP AWARD:

Awarded by the Special Trustees, to a physician likely to make a significant contribution to clinical medicine or clinical medical research in North East England.

Awarded June 2006.

THESIS RELATED

PUBLICATIONS/PUBLISHED ABSTRACTS/ARTICLES IN PRESS

- **Duncan RF**, Nelson AJ, Dundon BK, Worthley MI, Rasheed E, Williams K, Kenny A, Zaman A, Worthley SG. Two-dimensional speckle tracking strain for the evaluation of global left ventricular systolic function: A comparison against magnetic resonance imaging and Simpson's biplane method of discs. *Echo* 2012: IN PRESS
- **Duncan RF**, Dundon BK, Nelson AJ, Pemberton J, Williams K, Worthley MI, Zaman A, Thomas H, Worthley SG. A study of the 16-segment regional wall motion scoring index and biplane Simpson's rule for the calculation of left ventricular ejection fraction: A comparison with cardiac magnetic resonance imaging. *Echocardiography* 2011;28(6):597-604.
- **Duncan RF**, Nelson AJ, Schuster J, Dundon BK, Worthley MI, Carbone A, Zaman A, Worthley SG. Right ventricular free wall strain has a closer correlation with right ventricular ejection fraction than other indices of right ventricular systolic function: A comparison with cardiac magnetic resonance imaging. *European Heart Journal* 2011;32:S651.
- **Duncan RF**, Dundon BK, Nelson AJ, Pemberton J, Williams K, Worthley MI, Zaman A, Thomas H, Worthley SG. A study of the 16-segment regional wall motion scoring index and biplane Simpson's rule for the calculation of left ventricular ejection fraction: A comparison with cardiac magnetic resonance imaging. *Echo* 2011;75:
- **Duncan RF**, Nelson AJ, Dundon BK, Schuster J, Worthley MI, Carbone A, K Williams K, Zaman A, Worthley SG. Right ventricular free wall strain has a closer correlation with right ventricular ejection fraction than other echocardiographic indices of right ventricular function: Validation with cardiac magnetic resonance imaging. *Echo* 2011;75:

- **Duncan RF**, Dundon BK, Disney P, Nelson AJ, Leung MC, Brackenridge K, Worthley MI, Piantadosi C, Cumberledge B, Kenny A, Worthley SG. The 17 Segment Regional Wall Motion Scoring Index may be superior to Simpson's Rule for calculation of LVEF. *Journal of the American College of Cardiology* 2008;51:A109.
- **Duncan RF**, Nelson AJ, Dundon B, Worthley MI, Piantadosi C, Williams K, Rasheed E, Worthley SG. Effectiveness of two-dimensional speckle tracking strain for evaluation of left ventricular systolic function: A comparison against 3D echo and cardiac MRI. *European Journal of Echocardiography* 2008; doi:10.1093/ejechocard/jen281.
- **Duncan RF**, Dundon BK, Nelson AJ, Worthley MI, Williams K, Leung MC, Piantadosi C, Liew GY, Mole P, Worthley SG. Velocity encoded cine MRI for the assessment of left ventricular diastolic function. *Heart Lung Circulation* 2008;17:S57.
- **Duncan RF**, Nelson AJ, Dundon BK, Worthley MI, Piantadosi C, Leung M, Williams K, Rasheed E, Zaman A, Worthley SG. Effectiveness of two-dimensional speckle tracking strain for the evaluation of left ventricular systolic function: A comparison against cardiac magnetic resonance and 3D echocardiography. *Heart Lung Circulation* 2008;17:S28.
- **Duncan RF**, Dundon B, Nelson AJ, Disney P, Williams K, Rashed E, Leung M, Piantadosi C, Cumberledge B, Kenny A, Worthley MI, Zaman A, Worthley SG. The 17 Segment Regional Wall Motion Scoring Index may be superior to Simpson's Rule for calculation of LVEF. *Heart Lung Circulation* 2008;17:S28.
- **Duncan RF**, Nelson AJ, Worthley MI, Dundon BK, Brackenridge K, Leung M, Piantadosi C, Liew GYH, Soon K, Molae P, Roberts-Thompson R, Zaman A, Worthley SG. Velocity encoded cine magnetic resonance imaging for the assessment of left ventricular diastolic function. *Circulation Journal* 2008;72:I474.

INTERNATIONAL PRESENTATIONS AS A RESULT OF THIS THESIS

1. The British Society of Echocardiography Annual Conference 2012,
HIC, Harrogate, England.
2-3rd November 2012.

“Two-dimensional speckle tracking strain for the evaluation of global left ventricular systolic function: A comparison against magnetic resonance imaging and Simpson’s biplane method of discs”

RF Duncan, AJ Nelson, BK Dundon, MI Worthley, E Rasheed, K Williams, A Kenny, A Zaman, SG Worthley.

2. The British Society of Echocardiography Annual Conference 2011,
EICC, Edinburgh, Scotland.
7-8th October 2011.

“Right ventricular free wall strain has a closer correlation with right ventricular ejection fraction than other echocardiographic indices of right ventricular function: Validation with cardiac magnetic resonance imaging”

RF Duncan, AJ Nelson, BK Dundon, J Schuster, MI Worthley, A Carbone, K Williams, A Zaman, SG Worthley.

3. The British Society of Echocardiography Annual Conference 2011,
EICC, Edinburgh, Scotland.
7-8th October 2011.

“A study of the 16-segment regional wall motion scoring index and biplane Simpson’s rule for the calculation of left ventricular ejection fraction: A comparison with cardiac magnetic resonance”

RF Duncan, BK Dundon, AJ Nelson, J Pemberton, K Williams, MI Worthley,
A Zaman, H Thomas, SG Worthley.

4. The European Society of Cardiology Congress 2011,
Paris, France.
27th-31st August 2011.

“Right ventricular free wall strain has a closer correlation with right ventricular ejection fraction than other echocardiographic indices of right ventricular function: A comparison with cardiac MRI”

RF Duncan, AJ Nelson, J Schuster, BK Dundon, MI Worthley, A Carbone, A Zaman,
SG Worthley.

5. Euroecho 2008,
Lyon, France.
10th-13th Dec 2008.

“Effectiveness of two-dimensional speckle tracking strain for evaluation of left ventricular systolic function: a comparison against cardiac magnetic resonance and 3D echocardiography”

RF Duncan, AJ Nelson, BK Dundon, K Brackenridge, MC Leung, L Moffet, C Piantadosi,
E Rasheed, MI Worthley, SG Worthley.

6. The Cardiac Society of Australia and New Zealand 56th Annual Scientific Session, Adelaide Convention Centre, Adelaide, South Australia, Australia.
7th-10th August 2008.

“Velocity encoded cine MRI for the assessment of left ventricular diastolic function”

RF Duncan, AJ Nelson, MI Worthley, BK Dundon, K Brackenridge, MC Leung, C Piantadosi, G Liew, A Zaman, SG Worthley.

7. The Cardiac Society of Australia and New Zealand 56th Annual Scientific Session, Adelaide Convention Centre, Adelaide, South Australia, Australia.
7th-10th August 2008.

“Effectiveness of two-dimensional speckle tracking strain for evaluation of left ventricular systolic function: a comparison against cardiac magnetic resonance and 3D echocardiography”

RF Duncan, AJ Nelson, BK Dundon, K Brackenridge, MC Leung, L Moffet, C Piantadosi, E Rasheed, MI Worthley, SG Worthley.

8. The Cardiac Society of Australia and New Zealand 56th Annual Scientific Session, Adelaide Convention Centre, Adelaide, South Australia, Australia.
7th-10th August 2008.

“The 17-Segment Regional Wall Motion Scoring Index may be superior to Simpson’s Rule for the calculation of left ventricular ejection fraction”

RF Duncan, BK Dundon, AJ Nelson, P Disney, K Williams, E Rasheed, C Piantadosi, MC Leung, MI Worthley, B Cumberlandge, A Zaman, SG Worthley.

9. American College of Cardiology 57th Annual Scientific Session,
Chicago, Illinois, USA.
April 2008.

“The 17-Segment Regional Wall Motion Scoring Index may be superior to Simpson’s Rule for the calculation of left ventricular ejection fraction”

RF Duncan, BK Dundon, AJ Nelson, P Disney, K Williams, MC Leung, C Piantadosi,
E Rasheed, MI Worthley, SG Worthley.

10. The Japanese Circulation Society 72nd Annual Scientific Session,
Fukuoka, Japan.
28th-30th March, 2008.

“Velocity encoded cine MRI for the assessment of left ventricular diastolic function”

RF Duncan, AJ Nelson, MI Worthley, BK Dundon, K Brackenridge, MC Leung,
C Piantadosi, G Liew, A Zaman, SG Worthley.

INVITED PRESENTATIONS AS A RESULT OF THIS THESIS

South Tees Regional Network Echo Meeting,
Durham, England.
22nd November 2011.

“Myocardial deformation imaging: Is it ready for prime time?” Rae Duncan

LIST OF FIGURES

- Figure 1.1** Myocardial fibre orientation in the normal heart.....
- Figure 1.2** Schematic diagram of normal coronary artery anatomy.....
- Figure 1.3** Coronary angiography images of the normal coronary tree.....
- Figure 1.4** Relationship of coronary blood supply to left ventricular regional wall segments.....
- Figure 1.5** Intracardiac pressure changes during the cardiac cycle in the normal left ventricle.....
- Figure 1.6** Anatomy and geometry of the normal right ventricle.....
- Figure 1.7** Right ventricular myocardial fibre orientation.....
- Figure 1.8** The Frank-Starling curve.....
- Figure 1.9** Right ventricular volume overload and “D” shaped flattening of the interventricular septum affecting ventricular filling.....
- Figure 1.10** Cardiac loading conditions alter the right ventricular pressure-volume relationship.....
- Figure 1.11** Measuring dP/dt.....
- Figure 1.12** Calculating left ventricular volumes using Simpson’s biplane method of discs.....
- Figure 1.13** Change in American Heart Association 17 segment regional left ventricular volumes over time with 3D echocardiography.....
- Figure 1.14** Calculating left ventricular ejection fraction by cardiac magnetic resonance.....
- Figure 1.15** Pulsed-wave tissue velocity trace in a normal subject.....
- Figure 1.16** Colour coded tissue velocity trace in a normal subject.....
- Figure 1.17** Tissue Doppler longitudinal strain profile.....
- Figure 1.18** Two-dimensional speckle tracking radial strain recording in the apical 4-chamber of view of the heart in a subject with normal left ventricular systolic function.....
- Figure 1.19** Two-dimensional speckle tracking longitudinal strain recording in the apical 4-chamber of view of the heart in a subject with normal left ventricular systolic function.....

Figure 1.20	The American Heart Association 16 and 17 myocardial segment models of the left ventricles.....
Figure 1.21	Assessing regional left ventricular systolic function: Regional wall motion scoring.....
Figure 1.22	Normal diastolic pressure/flow patterns.....
Figure 1.23	The four phases of diastole.....
Figure 1.24	Phase 1 diastole: Measuring the isovolumic time.....
Figure 1.25	Phase 2 diastole: Early passive ventricular filling – measuring peak mitral E wave and mitral E deceleration time.....
Figure 1.26	Calculating the E:A ratio.....
Figure 1.27	Left ventricular filling patterns in diastolic dysfunction.....
Figure 1.28	Example of a pulsed-wave tissue Doppler velocity trace of the mitral annulus.....
Figure 1.29	Diastolic dysfunction: Patterns of abnormal mitral inflow velocities and mitral annular diastolic relaxation velocities.....
Figure 1.30	Kaplan-Meier curve demonstrating survival benefit in patients with an early peak diastolic mitral annular relaxation velocity $\geq 3\text{cm/s}$ compared to $< 3\text{cm/s}$.....
Figure 1.31	EAE/ASE diagnostic algorithm for the estimation of left ventricular filling pressures in patients with normal left ventricular ejection fraction.....
Figure 1.32	EAE/ASE diagnostic algorithm for the estimation of left ventricular filling pressures in patients with impaired left ventricular ejection fraction.....
Figure 3.1	Recording left ventricular end diastolic filling pressure from a fluid-filled catheter trace.....
Figure 3.2	Tracing left ventricular endocardial and epicardial contours and calculating left ventricular volumes using CMR Argus analysis software.....
Figure 3.3	Tracing right ventricular endocardial and epicardial contours and calculating right ventricular volumes using CMR Argus analysis software.....

Figure 3.4	Calculating left ventricular ejection fraction using 3DQ advanced software.....
Figure 3.5	Calculating left ventricular ejection fraction using Simpson’s biplane method of discs.....
Figure 3.6	Measuring the event timing intervals.....
Figure 3.7	Calculating the E/A ratio.....
Figure 3.8	Example of a pulsed-wave tissue Doppler velocity trace of the mitral annulus.....
Figure 3.9	Estimating left ventricular end diastolic pressure from E/Em ratio.....
Figure 4.1	Determining the correct aortic valve closure time using AFI strain software.....
Figure 4.2	Semi-automated border tracking with AFI 2D strain imaging.....
Figure 4.3	Segmental distribution of AFI 2D strain imaging.....
Figure 4.4	Segmental and global strain results recorded from the apical 4 chamber view.....
Figure 4.5	Correlation of 2D speckle tracking strain with 2D Simpson’s rule.....
Figure 4.6	Correlation of cardiac magnetic resonance-derived left ventricular ejection fraction with 3D echocardiography left ventricular ejection fraction.....
Figure 4.7	Correlation of cardiac magnetic resonance-derived left ventricular ejection fraction with 2D echocardiography Simpson’s rule left ventricular ejection fraction.....
Figure 4.8	Correlation of cardiac magnetic resonance-derived left ventricular ejection fraction with 2D speckle tracking strain.....
Figure 4.9	Receiver operator characteristic curve of global strain score.....
Figure 4.10	Correlation of cardiac magnetic resonance-derived left ventricular ejection fraction with global strain score LV ejection fraction equivalent score in a validation cohort of 20 patients.....
Figure 4.11	Bland-Altman plot of intra-observer and inter-observer variation for measuring left ventricular systolic function using cardiac magnetic resonance.....

Figure 4.12	Bland-Altman plot of intra-observer and inter-observer variation for measuring left ventricular systolic function using 3D-echocardiography.....
Figure 4.13	Bland-Altman plot of intra-observer and inter-observer variation for measuring left ventricular systolic function using 2D Simpson's rule..
Figure 4.14	Bland-Altman plot of intra-observer and inter-observer variation for measuring left ventricular systolic function using 2D speckle tracking strain.....
Figure 5.1	Calculating left ventricular ejection fraction using the modified regional wall motion scoring index.....
Figure 5.2	Correlation and Bland-Altman analyses between Regional wall motion score index and Simpson's rule.....
Figure 5.3	Correlation and Bland-Altman analyses between CMR and Regional wall motion score index and CMR and Simpson's rule.....
Figure 5.4	Correlation and Bland-Altman analyses between CMR and Regional wall motion score index and CMR and Simpson's rule in patients with normal left ventricular systolic function.....
Figure 5.6	Bland-Altman analysis of intra-observer and inter-observer variation for measuring left ventricular ejection fraction using Regional wall motion scoring index and biplane Simpson's rule.....
Figure 6.1	Analysis of peak mitral inflow velocity using velocity encoded magnetic resonance imaging.....
Figure 6.2	Calculating E:A ratio from reconstructed velocity versus time curves
Figure 6.3	Analysis of peak mitral annular velocities from six sides of the mitral annulus/basal left ventricle using velocity encoded magnetic resonance imaging.....
Figure 6.4	Calculating Em from reconstructed velocity versus time curves.....
Figure 6.5	Calculating E/Em as a non-invasive estimate of left ventricular end diastolic filling pressure using (A) velocity encoded magnetic resonance and (B) tissue Doppler echocardiography.....

- Figure 6.6** Correlation and Bland Altman analysis of velocity encoded magnetic resonance mitral E velocity, mitral A velocity and E/A ratio with Doppler echocardiography mitral E velocity, mitral a velocity and E/A ratio in all subjects.....
- Figure 6.7** Correlation and Bland Altman analysis of velocity encoded magnetic resonance Em(A) velocity, with tissue Doppler echocardiography Em(A) velocity in all subjects.....
- Figure 6.8** Correlation and Bland Altman analysis of velocity encoded magnetic resonance Em(L) velocity, with tissue Doppler echocardiography Em(L) velocity in all subjects.....
- Figure 6.9** Correlation and Bland Altman analysis of velocity encoded magnetic resonance Em(P) velocity, with tissue Doppler echocardiography Em(P) velocity in all subjects.....
- Figure 6.10** Correlation and Bland Altman analysis of velocity encoded magnetic resonance Em(I) velocity, with tissue Doppler echocardiography Em(I) velocity in all subjects.....
- Figure 6.11** Correlation and Bland Altman analysis of velocity encoded magnetic resonance Em(S) velocity, with tissue Doppler echocardiography Em(S) velocity in all subjects.....
- Figure 6.12** Correlation and Bland Altman analysis of velocity encoded magnetic resonance Em(AS) velocity, with tissue Doppler echocardiography Em(AS) velocity in all subjects.....
- Figure 6.13** Correlation of invasive LVEDP with velocity encoded magnetic resonance E/Em(S), E/Em(L), E/Em(S+Lav), E/Em(5av), E/Em(6av) in all subjects.....
- Figure 6.14** Correlation between echocardiography and magnetic resonance derived E/Em ratios in all subjects.....
- Figure 6.15** Correlation and Bland Altman analysis of velocity encoded magnetic resonance mitral E velocity, mitral A velocity and E/A ratio with Doppler echocardiography mitral E velocity, mitral a velocity and E/A ratio in patients with normal LV systolic function.....

Figure 6.16 Correlation of invasive LVEDP with velocity encoded magnetic resonance E/Em(S), E/Em(L), E/Em(S+Lav), E/Em(5av), E/Em(6av) in patients with normal LV systolic function.....

Figure 6.17 Correlation between echocardiography and magnetic resonance derived E/Em ratios in patients with normal LV systolic function.....

Figure 6.18 Correlation and Bland Altman analysis of velocity encoded magnetic resonance mitral E velocity, mitral A velocity and E/A ratio with Doppler echocardiography mitral E velocity, mitral a velocity and E/A ratio in patients with impaired LV systolic function.....

Figure 6.19 Correlation of invasive LVEDP with velocity encoded magnetic resonance E/Em(S), E/Em(L), E/Em(S+Lav), E/Em(5av), E/Em(6av) in patients with impaired LV systolic function.....

Figure 6.20 Correlation between echocardiography and magnetic resonance derived E/Em ratios in patients with impaired LV systolic function...

Figure 6.21 Simplified EAE/ASE diagnostic algorithm for the estimation of left ventricular filling pressures in patients with normal left ventricular ejection fraction: Modified for use in patients undergoing velocity encoded magnetic resonance imaging.....

Figure 6.22 Simplified EAE/ASE diagnostic algorithm for the estimation of left ventricular filling pressures in patients with impaired left ventricular ejection fraction: Modified for use in patients undergoing velocity encoded magnetic resonance imaging.....

Figure 6.23 Bland-Altman plot of (A) intra-observer and (B) inter-observer variation for measuring mitral E velocity using cardiac magnetic resonance imaging.....

Figure 6.24 Bland-Altman plot of (A) intra-observer and (B) inter-observer variation for measuring mitral A velocity using cardiac magnetic resonance imaging.....

Figure 6.25 Bland-Altman plot of (A) intra-observer and (B) inter-observer variation for measuring E/A ratio using cardiac magnetic resonance imaging.....

Figure 6.26	Bland-Altman plot of (A) intra-observer and (B) inter-observer variation for measuring peak myocardial tissue velocity of the basal LV septum (EmS) using cardiac magnetic resonance imaging.....
Figure 6.27	Bland-Altman plot of (A) intra-observer and (B) inter-observer variation for measuring peak myocardial tissue velocity of the basal LV lateral wall (EmL) using cardiac magnetic resonance imaging....
Figure 6.28	Bland-Altman plot of (A) intra-observer and (B) inter-observer variation for measuring E/Em(S) ratio by cardiac magnetic resonance imaging.....
Figure 6.29	Bland-Altman plot of (A) intra-observer and (B) inter-observer variation for measuring E/Em(L) ratio by cardiac magnetic resonance imaging.....
Figure 6.30	Bland-Altman plot of (A) intra-observer and (B) inter-observer variation for measuring E/Em(S+Lav) ratio by cardiac magnetic resonance imaging.....
Figure 7.1	Calculating the right ventricular fractional area change.....
Figure 7.2	Calculating the right ventricular myocardial performance index by spectral Doppler.....
Figure 7.3	Calculating the right ventricular myocardial performance index by pulsed wave tissue Doppler.....
Figure 7.4	Measuring the tricuspid annular plane systolic excursion score using colour M-mode.....
Figure 7.5	Measuring the tricuspid annular peak systolic tissue velocity using pulsed-wave tissue Doppler imaging.....
Figure 7.6	Measuring the tricuspid annular peak systolic tissue velocity using colour tissue Doppler imaging.....
Figure 7.7	Measuring myocardial acceleration during isovolumic contraction of the right ventricle.....
Figure 7.8	Measuring tricuspid annular plane systolic excursion using colour tissue Doppler displacement imaging.....
Figure 7.9	Right ventricular global strain recorded from the apical 4-chamber view.....

Figure 7.10 Measuring right ventricular free wall strain using 2D speckle tracking software.....

Figure 7.11 Correlation of right ventricular free wall strain with RV ejection fraction calculated by cardiac magnetic resonance imaging.....

Figure 7.12 Correlation of right ventricular global strain with RV ejection fraction calculated by cardiac magnetic resonance imaging.....

Figure 7.13 Correlation of right ventricular fractional area change with RV ejection fraction calculated by cardiac magnetic resonance imaging....

Figure 7.14 Correlation of M-mode tricuspid annular plane systolic excursion with RV ejection fraction calculated by cardiac magnetic resonance imaging.....

Figure 7.15 Correlation of right ventricular tricuspid annular peak systolic tissue velocity recorded using colour tissue Doppler imaging with RV ejection fraction calculated by cardiac magnetic resonance imaging....

Figure 7.16 Correlation of right ventricular tricuspid annular peak systolic tissue velocity recorded using colour tissue Doppler imaging with RV ejection fraction calculated by cardiac magnetic resonance imaging....

Figure 7.17 Correlation of colour tissue Doppler tricuspid annular plane systolic excursion with RV ejection fraction calculated by cardiac magnetic resonance imaging.....

Figure 7.18 Correlation of pulsed-wave tissue Doppler myocardial performance index with RV ejection fraction calculated by cardiac magnetic resonance imaging.....

Figure 7.19 Correlation of spectral Doppler myocardial performance index with RV ejection fraction calculated by cardiac magnetic resonance imaging.....

Figure 7.20 Correlation of right ventricular isovolumic acceleration with RV ejection fraction calculated by cardiac magnetic resonance imaging.....

Figure 7.21 Receiver-operator characteristic curve of RV free wall strain indexed against RV ejection fraction calculated by cardiac magnetic resonance imaging.....

Figure 7.22 Receiver-operator characteristic curve of RV global strain indexed against RV ejection fraction calculated by cardiac magnetic resonance imaging.....

Figure 7.23 Receiver-operator characteristic curve of M-Mode TAPSE indexed against RV ejection fraction calculated by cardiac magnetic resonance imaging.....

Figure 7.24 Receiver-operator characteristic curve of tissue Doppler TAPSE indexed against RV ejection fraction calculated by cardiac magnetic resonance imaging.....

Figure 7.25 Receiver-operator characteristic curve of RV fractional area change indexed against RV ejection fraction calculated by cardiac magnetic resonance imaging.....

Figure 7.26 Receiver-operator characteristic curve of pulsed-wave tricuspid annular peak systolic tissue velocity indexed against RV ejection fraction calculated by cardiac magnetic resonance imaging.....

Figure 7.27 Receiver-operator characteristic curve of RV colour tissue Doppler tricuspid annular systolic tissue velocity indexed against RV ejection fraction calculated by cardiac magnetic resonance imaging.....

Figure 7.28 Receiver-operator characteristic curve of RV tissue Doppler myocardial performance index indexed against RV ejection fraction calculated by cardiac magnetic resonance imaging.....

Figure 7.29 Bland-Altman plot of (A) intra-observer variation and (B) inter-observer variation for measuring RV systolic function using cardiac magnetic resonance (RVEF) (%).....

Figure 7.30 Bland-Altman plot of (A) intra-observer variation and (B) inter-observer variation for measuring RV systolic function using myocardial performance index derived by spectral Doppler (MPI)....

Figure 7.31 Bland-Altman plot of (A) intra-observer variation and (B) inter-observer variation for measuring RV systolic function using colour M-Mode tricuspid annular plane systolic excursion (MM TAPSE) (cm)...

Figure 7.32 Bland-Altman plot of (A) intra-observer variation and (B) inter-observer variation for measuring RV systolic function using tricuspid annular peak systolic velocity using pulsed-wave tissue Doppler (PWTDE S') (cm/s).....

Figure 7.33 Bland-Altman plot of (A) intra-observer variation and (B) inter-observer variation for measuring RV systolic function using tricuspid annular peak systolic velocity using colour tissue Doppler (CTDE S') (cm/s).....

Figure 7.34 Bland-Altman plot of (A) intra-observer variation and (B) inter-observer variation for measuring RV systolic function using isovolumic acceleration (IVA) (cm/s^2).....

Figure 7.35 Bland-Altman plot of (A) intra-observer variation and (B) inter-observer variation for measuring RV systolic function using tricuspid annular peak systolic displacement measured using colour tissue Doppler (TDE TAPSE) (cm).....

Figure 7.36 Bland-Altman plot of (A) intra-observer variation and (B) inter-observer variation for measuring RV systolic function using RV global strain score (-%).....

Figure 7.37 Bland-Altman plot of (A) intra-observer variation and (B) inter-observer variation for measuring RV systolic function using RV free wall strain score (-%).....

Figure 7.38 Bland-Altman plot of (A) intra-observer variation and (B) inter-observer variation for measuring RV systolic function using RV fractional area change (%).....

Figure 7.30 Bland-Altman plot of (A) intra-observer variation and (B) inter-observer variation for measuring RV systolic function using myocardial performance index derived by spectral Doppler (MPI)....

Figure 7.39 Bland-Altman plot of (A) intra-observer variation and (B) inter-observer variation for measuring RV systolic function using myocardial performance index derived by tissue Doppler (TDE MPI).....

LIST OF TABLES

Table 1.1	The left ventricle – Normal ranges.....
Table 1.2	Normal resting haemodynamic indices of left ventricular function....
Table 1.3	Degrees of left ventricular dysfunction according to left ventricular ejection fraction.....
Table 1.4	Reference values for dP/dt.....
Table 1.5	Left ventricular quantification methods: Use, advantages and Limitations.....
Table 1.6	Pulsed-wave tissue Doppler systolic myocardial velocities of the normal left ventricle.....
Table 1.7	Reference ranges for longitudinal and radial strain in the left ventricle.....
Table 1.8	Normal and abnormal ranges of diastolic function.....
Table 1.9	Pulsed-wave tissue Doppler myocardial early relaxation velocities of the normal left ventricle.....
Table 1.10	Normal intracardiac pressures.....
Table 4.1	Clinical characteristics of the study population.....
Table 4.2	Stepwise regression analysis of 3D echo, global strain score and 2D echo Simpson’s rule against CMR as the reference standard for the quantification of global LV systolic function.....
Table 4.3	Comparing 2D echo imaging modalities: Stepwise regression analysis of global strain score and 2D Simpson’s rule against CMR as the reference standard for the quantification of global LV systolic function.....
Table 4.4	Intra-observer variability for measurements of global left ventricular systolic function.....
Table 4.5	Inter-observer variability for measurements of global left ventricular systolic function.....
Table 5.1	Clinical characteristics of study subjects who completed both CMR and 2D echocardiography protocols.....

Table 5.2 Intra-observer and inter-observer variability for measurements of LVEF using the regional wall motion scoring index.....

Table 5.3 Intra-observer and inter-observer variability for measurements of LVEF using biplane Simpson’s rule.....

Table 6.1 Clinical characteristics of study subjects.....

Table 6.2 Intra-observer variability for echo and CMR measurements of left ventricular diastolic function.....

Table 6.3 Inter-observer variability for echo and CMR measurements of left ventricular diastolic function.....

Table 7.1 Clinical characteristics of study subjects who completed both RV-CMR and 2D echocardiography protocols.....

Table 7.2 Comparison of CMR-RVEF and ten echocardiographic indices of right ventricular function with visual assessment of right ventricular systolic function.....

Table 7.3 The acquisition and analysis times for each index of right ventricular function.....

Table 7.4 Intra-observer variability for measurements of right ventricular systolic function.....

Table 7.5 Inter-observer variability for measurements of right ventricular systolic function.....

LIST OF EQUATIONS

Equation 1.1	Calculating cardiac output and factors influencing stroke volume....
Equation 1.2	Calculating stroke volume.....
Equation 1.3	Calculating cardiac output.....
Equation 1.4	Calculating dP/dT.....
Equation 1.5	Calculating left ventricular volumes using biplane Simpson's rule...
Equation 1.6	Calculating left ventricular ejection fraction.....
Equation 1.7	The Doppler shift equation.....
Equation 1.8	Calculating RV fractional area change.....
Equation 4.1	Calculating the global strain score of the left ventricle.....
Equation 4.2	Regression equation for calculating left ventricular ejection fraction from the global strain score.....
Equation 5.1	Calculating left ventricular ejection fraction using the modified regional wall motion scoring index.....
Equation 7.1	Calculating right ventricular ejection fraction.....
Equation 7.2	Calculating the RV myocardial performance index.....
Equation 7.3	Calculating RV isovolumic acceleration.....
Equation 7.4	Regression equation for calculating right ventricular ejection fraction from the RV free wall strain score.....

LIST OF ABBREVIATIONS

A	peak transmitral A-wave velocity
AFI	Automated Functional Imaging
AHA	American Heart Association
ASE	American Society of Echocardiography
BSE	British Society of Echocardiography
CMR	cardiac magnetic resonance
CSE	Canadian Society of Echocardiography
CT	computed tomography
CTDE	colour tissue Doppler echocardiography imaging
CW	continuous wave
E	peak transmitral E-wave velocity
Em	peak early diastolic myocardial tissue velocity
EAE	European Association of Echocardiography
ECG	electrocardiograph
FAC	fractional area change
GE	General Electric
GSS	global strain score derived using 2D speckle tracking strain
IVA	isovolumic acceleration
IVCT	isovolumic contraction time
IVRT	isovolumic relaxation time
LAP	left atrial pressure
LHC	left heart catheterisation
LV	left ventricle
LVEDD	left ventricular end diastolic dimension
LVEDP	left ventricular end diastolic pressure
LVEDV	left ventricular end diastolic volume
LVEF	left ventricular ejection fraction
LVEFES	left ventricular ejection fraction equivalent score
LVESV	left ventricular end systolic volume
M-Mode	time-motion mode
MPI	myocardial performance index measured by spectral Doppler

MRI	magnetic resonance imaging
NS	not significant
PW	pulsed wave
PWTDE	pulsed wave tissue Doppler echocardiography
ROC	receiver-operator curve
ROI	region of interest
RV	right ventricle
RVEDA	right ventricular end diastolic area
RVEDV	right ventricular end diastolic volume
RVEF	right ventricular ejection fraction
RVESA	right ventricular end systolic area
RVESV	right ventricular end systolic volume
RVET	right ventricular ejection time
RVFWS	right ventricular free wall strain
RVGS	right ventricular global strain
RWMS	regional wall motion score
RWMSI	regional wall motion score index
S'	right ventricular peak systolic myocardial tissue velocity
SCMR	Society for Cardiac Magnetic Resonance
SR	biplane Simpson's rule/modified Simpson's biplane method of discs
SSFP	steady state free precession imaging
SPECT	single photon emission computed tomography
TAPSE	tricuspid annular plane systolic excursion (measured by M-Mode)
TDE	tissue Doppler echocardiography
TDE MPI	tissue Doppler myocardial performance index
TDE TAPSE	tricuspid annular plane systolic excursion (measured by tissue Doppler)
TTE	transthoracic echocardiography
TR	tricuspid regurgitation
TVI	tissue velocity imaging
VEC	velocity encoded cine MRI/phase encoded velocity mapping
2DE	two-dimensional echocardiography
3DE	three-dimensional echocardiography

SYNOPSIS

The mechanical pump action of the heart makes this organ unique within the thoraco-abdominal viscera. The continual pumping motion of the heart has for years also made it one of the most difficult organs to image accurately. Invasive recordings of changes in intra-cardiac pressures throughout the cardiac cycle convey indirect information about cardiac pump function but are subject to changes in preload and afterload. Fluoroscopic left ventriculography during cardiac catheterisation provided the first images of the moving heart together with information on regional wall motion abnormalities (RWMAs) within the anterior wall, inferior wall and apex of the left ventricle (LV).^{1,2} However, the use of left ventriculography for calculation of left ventricular ejection fraction (LVEF), the ubiquitous measure for quantifying LV systolic function, is at best crude.

The application of sonar ultrasound to imaging cardiac structures by Edler and Hertz in the 1950's signalled the birth of echocardiography.³ Since then advances in cardiac ultrasound have been considerable. Two-dimensional echocardiography today remains the first line investigation for the assessment of cardiac structure and quantification of LV function. In recent years advances in diagnostic ultrasound techniques now enable visualisation of cardiac structures in three-dimensions in real time and new imaging software permits the calculation of LVEF from reconstructed three dimensional (3D) left ventricular volumes.

Alternative non-invasive imaging modalities also play increasingly important roles in diagnostic cardiology. Nuclear single-photon emission computed tomography (SPECT) scanning is used regularly in some cardiac centres for identification of individuals with infarcted myocardium and/or the presence of inducible ischaemia. The use of multi-detector computed tomography angiography (MDCTA) is gaining popularity for the non-invasive assessment of coronary artery disease. Most recently, cardiac magnetic resonance imaging (CMR) is being increasingly used to enhance cardiac diagnoses. The excellent spatial resolution of CMR makes it ideal for the accurate anatomical assessment of congenital cardiac anomalies and intra-cardiac masses. In specialist centres CMR is now being used to assess post-infarct myocardial viability using delayed enhancement gadolinium CMR and to identify inducible cardiac ischaemia in patients with chest pain syndromes using

adenosine stress-perfusion CMR or dobutamine stress CMR. The ability of CMR to image the heart in multiple planes and to enable highly reproducible 3D volumetric reconstructions from contiguous slice imaging throughout the ventricles mean it has now become widely accepted as the new reference standard for the quantification of baseline left ventricular and right ventricular systolic function.

As several device and pharmacological therapies within cardiology and other medical specialties require accurate quantification of LVEF and serial monitoring of left ventricular systolic function as a prerequisite for treatment, it is important that available techniques for assessing left ventricular systolic function are sensitive, safe, accurate and reproducible. They also need to be standardized and widely available across institutions. In this respect CT and nuclear SPECT have limited application due to repeated patient exposure to ionising radiation. Although CMR and three dimensional echocardiography (3DE) have superior spatial resolution to conventional two-dimensional (2D) echocardiographic imaging techniques, at present due to high costs and limited availability of CMR and 3DE, these imaging modalities are not widely available outside specialist centres and 2D echocardiography (2DE) remains the first line non-invasive imaging modality for quantifying left ventricular systolic function. To retain its clinical utility, it is therefore important that 2DE techniques for quantifying left ventricular systolic function improve in line with other non-invasive imaging modalities as 2DE technology advances.

Cardiac diastole is a complex process and left ventricular diastolic dysfunction is difficult to quantify non-invasively. Traditional echocardiographic assessments of diastolic function are semi-quantitative and load-dependent. Recently much work has been done using tissue Doppler echocardiography E/Em ratio as an estimate of left ventricular filling pressure.⁴⁻¹³ Revised American and European echocardiographic guidelines now recommend the use of tissue Doppler E/Em to assess LV diastolic function, despite recent research questioning the accuracy of this technique in certain patient cohorts.¹⁴⁻¹⁹ CMR is already being used in selective centres, including the Royal Adelaide Hospital, as the superior imaging modality for the detection of cardiac structural anomalies, perfusion defects and accurate assessment of systolic function. At present, however, it is difficult to routinely assess and diagnose diastolic dysfunction with current clinical CMR scan protocols. It has recently become possible however, using a phase contrast cardiac MRI sequence, to record and encode

velocity profiles of both myocardial tissue motion during diastole and blood as it passes through the mitral valve.^{20,21} From the reconstructed velocity versus time curves of LV filling, it should theoretically be possible to estimate left ventricular end diastolic filling pressure (LVEDP) using velocity encoded cine CMR (VEC-CMR) E/Em imaging in similar manner to tissue Doppler echocardiography (TDE).

For many years the right ventricle has largely been the “forgotten” ventricle. As the understanding of cardiac contractile function has improved so too has the understanding of the important role of right ventricular contractility in the normal heart and across a range of cardiac and pulmonary disorders. The excellent spatial resolution of CMR, and its ability to image the heart in any plane enables accurate assessment of right ventricular volumes.²²⁻³⁶ In specialist centres, CMR is increasingly being used to quantify right ventricular ejection fraction (RVEF) and has become the widely accepted non-invasive reference standard for doing so. However, due to the current limited access to CMR, the majority of institutions rely on 2DE assessment of the RV. The complex geometry of the RV, and limited echocardiographic imaging windows precludes accurate volumetric quantification of RV systolic function by 2DE. For this reason, several 2DE *non-volumetric* indices of RV systolic function have been developed. In response to increasing research in this field, the American Society of Echocardiography, in association with the European Association of Echocardiography and Canadian Society of Echocardiography, have recently published revised guidelines on the 2DE assessment of the right heart.³⁷ The guidelines review all the available non-volumetric measures of RV function, the evidence behind the use of these indices, and where appropriate have published lower normative cut-off values based on a meta-analysis of the published literature. The guidelines conclude that at least one non-volumetric quantitative index of RV function should be measured in addition to a visual assessment of RV function, and should be incorporated into every routine transthoracic echocardiography report. At the time of writing, there have been no head-to-head studies comparing the accuracy and reproducibility of all these non-volumetric indices of RV function, and the guidelines are unable to draw conclusions as to which of the available non-volumetric quantitative indices of RV function is superior in accuracy and reproducibility to the others and should therefore be the method of choice.

In an era of increasing multi-modal imaging, it is important that current techniques are comparable in accuracy and reproducibility. The overall objective of this thesis was to assess the accuracy and reproducibility of novel non-invasive imaging indices of LV systolic function, LV diastolic function and RV systolic function, by indexing them against the respective reference standards. The study aim was to assess firstly, the diagnostic accuracy of identifying and quantifying ventricular dysfunction and secondly inter-modality concordance between different imaging techniques.

The first objective of this thesis was to examine the potential of novel 2DE myocardial deformation imaging software to establish if this software was comparable to CMR and 3DE for quantifying left ventricular systolic function.

The second objective of this thesis was to utilise a widely available regional wall motion scoring system in a novel way to assess global left ventricular systolic function. The accuracy of this novel method was compared against CMR and current recommended 2DE assessment of LVEF.

The third objective of this thesis was to explore the utility of VEC-CMR imaging as a method of quantifying left ventricular diastolic function by comparing it to TDE assessments and invasive catheter recordings of LVEDP.

The final objective of this thesis was to perform a head-to-head comparison study of ten different 2DE non-volumetric measures of RV systolic function, indexed against CMR-derived RVEF as the reference standard. The aim was to establish which method was superior in accuracy, reproducibility and clinical applicability, compared to the others, and should therefore be the quantitative index of choice for assessing RV systolic function by 2DE in routine clinical practice.

CHAPTER 1

INTRODUCTION

CHAPTER 1: INTRODUCTION

1.1 CARDIOVASCULAR DEMOGRAPHICS AND THE EVOLVING ROLE OF NON-INVASIVE CARDIAC IMAGING

As the incidence of cardiovascular disease continues to rise, the demand for prompt, accurate non-invasive cardiac imaging for early diagnosis, monitoring and prognosis, across all aspects of cardiovascular disease becomes more important. As more treatment options become available, and conversely as the importance of preventative strategies are increasingly realised, there is an increasing demand for sensitive non-invasive cardiac imaging methods that can reliably detect cardiovascular disease processes at a sub-clinical level enabling the cardiologist to implement early disease modification strategies to enable reduction in morbidity and mortality from the condition.

THE LEFT VENTRICLE

1.2 ANATOMY OF THE NORMAL LEFT VENTRICLE

The LV is the systemic ventricle and its normal geometry is that of a prolate ellipse. For imaging purposes the boundaries of the left ventricular cavity are divided into six walls – four free walls; the anterior, lateral, posterior and inferior walls of the LV, and the interventricular septum, which for imaging purposes is conventionally subdivided into the anteroseptum, and the inferoseptum (often simply referred to as the septum). For descriptive purposes the left ventricle is subdivided into 16 or 17 regional myocardial segments according to the American Heart Association model and is described in more detail in section 1.11.4 (Figure 1.20).³⁸

Left ventricular size and mass vary according to the body surface area of individuals. Normal ranges for left ventricular mass, as determined by CMR,^{22,24} and for left ventricular wall thickness, cavity dimensions and volumes, as agreed by joint American Society of Echocardiography/European Association of Echocardiography and British Society of Echocardiography Guidelines, are shown in Table 1.1.³⁸

Comment [DZ1]: Do we really need a 6th form biology lesson at this level?

Index	Females	Females/BSA	Males	Males/BSA
LV mass		31-79 g/ m ²		45-81 g/ m ²
LV wall thickness	0.6-1.2 cm		0.6-1.2 cm	
LVEDD	3.9-5.3 cm	2.4-3.2 cm/m ²	4.2-5.9cm	2.2-3.1 cm/m ²
LVEDV	56-104ml	35-75 ml/ m ²	67-155ml	35-75ml/ m ²
LVESV	19-49ml	12-30 ml/ m ²	22-58ml	12-30 ml/ m ²
LVEF	≥55%		≥55%	

Table 1.1. The Left Ventricle – Normal Ranges^{22,24,38}

BSA, body surface area; LV, left ventricle; LVEDD, left ventricular end-diastolic diameter; LVEDV, left ventricular end-diastolic volume; LVEF, left ventricular ejection fraction; LVESV, left ventricular end-systolic volume

The alignment of myofibres within the ventricular wall appears to be unique to the heart.³⁹ The angulation of the long axis of the fibres relative to the equatorial axis of the left ventricle changes within the level of the left ventricle from base to apex (Figure 1.1).³⁹ The myofibres in the immediate subendocardial and subepicardial parts of the ventricular wall are aligned in a longitudinal fashion in relation to the ventricular equator, with changing angulations when measured on a radial axis. At the base of the left ventricle there is a distinct collection of circular fibres aligned parallel to the ventricular equator.³⁹ It is this complex fibre orientation in all three planes of the heart: radial, longitudinal and circumferential, that is believed to account for the unique “twisting” motion of the left ventricle during cardiac systole witnessed by cardiothoracic surgeons during operative procedures. An understanding of this complex myofibre orientation of the left ventricle is important from an imaging perspective, as different disease processes can affect myocardial

deformation in the longitudinal, radial and circumferential planes of the LV to differing extents. Our understanding of the relationship between the complex myofibre architecture of the LV and LV systolic contractile function in the different axes of the heart has been greatly enhanced in recent years by myocardial deformation imaging in the form of tissue Doppler strain and speckle tracking strain echocardiography and grid-tagged CMR cardiac magnetic resonance imaging.

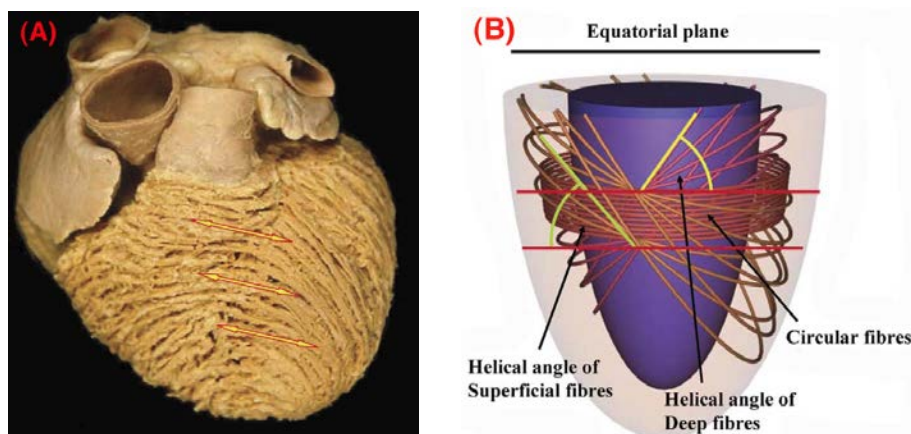


Figure 1.1. Myocardial fibre orientation within the normal heart.³⁹

(A) Blunt dissection of the normal heart reveals varying myocardial fibre orientation in relation to the ventricular plane from base to apex (B) Schematic diagram highlights the complex myofibre alignment within the left ventricle.

1.3 ANATOMICAL RELATIONSHIP OF THE CORONARY CIRCULATION TO THE LEFT VENTRICLE AND ITS IMPORTANCE IN ASSESSING REGIONAL LV FUNCTION

To understand the origin of abnormalities in regional left ventricular function due to ischaemia or infarction, it is important to appreciate the arterial territories of the heart. The coronary circulation consists of the left and right coronary arteries, the ostia of which arise immediately superior to the left and right coronary cusps of the aortic valve. The coronary vasculature, unlike the rest of the arterial tree is perfused during diastole, when not occluded by the valve cusps or squeezed during cardiac systole. The right coronary artery

arises from the right coronary sinus and descends through the right side of the atrioventricular groove giving off branches that supply the right atrium and right ventricle. The right coronary artery supplies the sinus node and the AV node in about 60% and 90% of individuals respectively.⁴⁰ If the right coronary artery is dominant, it gives off the posterior left ventricular branches then continues as the posterior descending artery which runs in the posterior interventricular groove and supplies the basal inferoseptum and inferior left ventricular wall. The left coronary system arises from the left coronary sinus and continues as the left main stem before it branches, usually within 2.5 cm from its origin, into the left anterior descending artery and left circumflex artery. The left anterior descending artery runs in the anterior interventricular groove and supplies the anteroseptum and anterior left ventricular wall. The left circumflex artery travels along the left atrioventricular groove and gives off branches to the left atrium and lateral and posterior walls of the left ventricle. If the left circumflex artery is dominant, then it gives rise to the posterior descending artery.⁴⁰ Figures 1.2 and 1.3 show schematic and fluoroscopic images of the normal coronary anatomy. Figure 1.4 demonstrates the arterial territories of the left ventricle, a relationship that is important to understand when assessing patients with left ventricular dysfunction secondary to regional wall motion abnormalities.

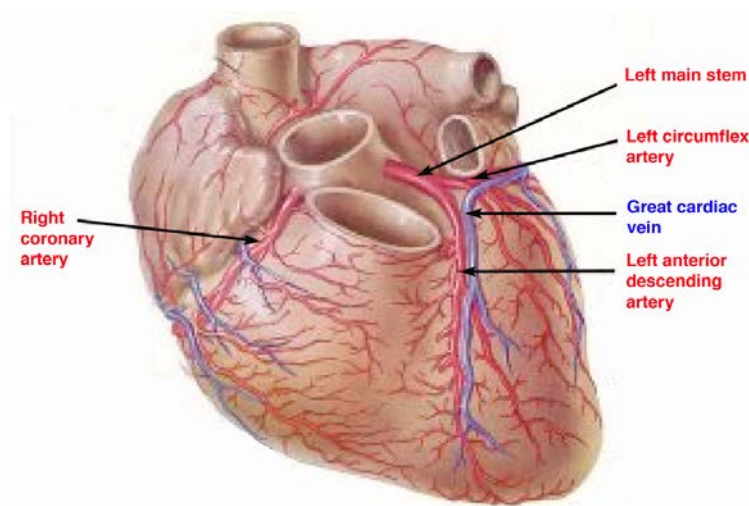


Figure 1.2. Schematic diagram of normal coronary artery anatomy⁴¹

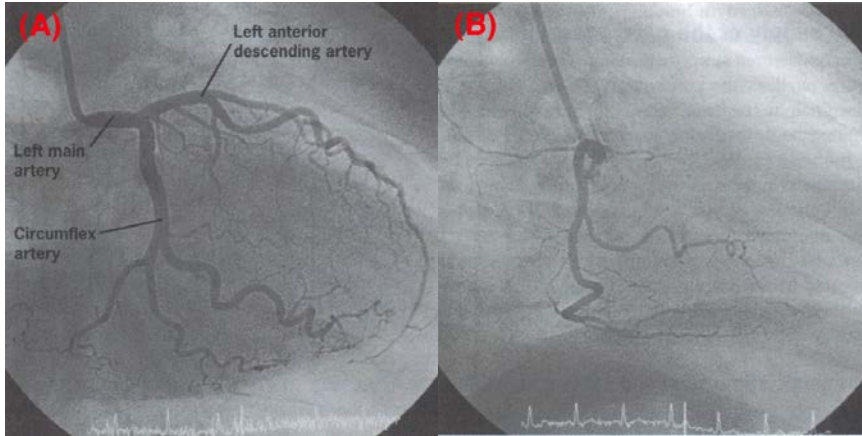


Figure 1.3. Coronary angiography images of the normal coronary circulation.⁴⁰ (A) Dominant left coronary arterial system and (B) non-dominant right coronary artery from the same patient

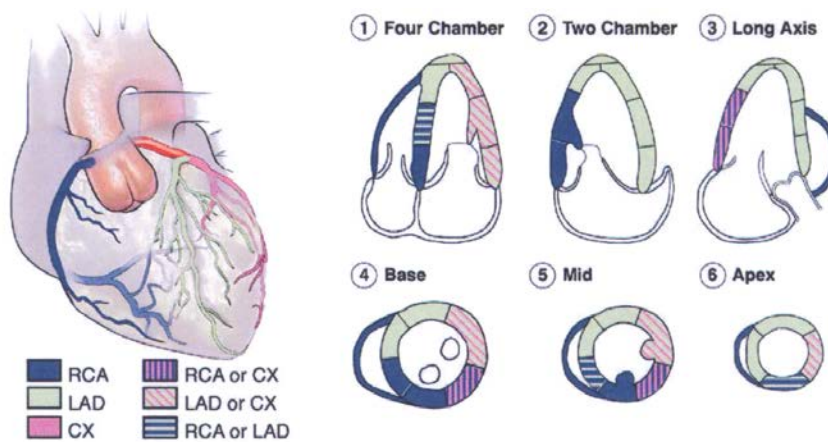


Figure 1.4. Relationship of coronary blood supply to left ventricular regional wall segments³⁸

Cx, left circumflex artery; LAD, left anterior descending artery; RCA, right coronary artery

1.4 PHYSIOLOGY OF THE NORMAL LEFT VENTRICLE

The cardiac cycle refers to the physiological events that occur from the beginning of one heart beat to the commencement of the following heart beat. The cardiac cycle consists of a period of ventricular contraction (systole) and ventricular relaxation and filling (diastole).

1.4.1 Left ventricular systole

The onset of systole occurs when the left ventricular pressure exceeds that of the atrial pressure and approximates with the closure time of the mitral valve. As more and more myofibres enter the contracted state, the pressure generated within the left ventricle continues to rise until it exceeds the aortic pressure. This first phase of systole is known as isovolumic contraction because the volume within the left ventricle is fixed as both the mitral and aortic valves are closed. Once the left ventricular pressure exceeds the aortic pressure, the aortic valve opens and the systolic ejection phase occurs. The rate of ejection of blood through the aortic valve is determined by the pressure gradient across the valve and also by the elastic properties of the aorta and the arterial tree. The volume of blood that is ejected through the aortic valve during cardiac systole expressed as a percentage of the total volume of blood present in the left ventricular cavity at the end of ventricular filling (diastole) is called the ejection fraction. The volume of blood that is ejected by the LV during each heart beat is called the stroke volume. Changes in the stroke volume are dependent on both the myocardial contractility of the LV and the cardiac loading conditions. The overall cardiac output of the heart is the product of the stroke volume and the heart rate (Equation 1.1). Normal LV haemodynamics are shown in Table 1.2.

Equation 1.1:

$$\text{Cardiac Output} = \text{Stroke volume} \times \text{Heart Rate}$$

The diagram illustrates the equation $\text{Cardiac Output} = \text{Stroke volume} \times \text{Heart Rate}$. Below the equation, three terms are listed: **Preload**, **Contractility**, and **Afterload**. Three red arrows point upwards from these terms to the equation: one from **Preload** to **Stroke volume**, one from **Contractility** to **Stroke volume**, and one from **Afterload** to **Heart Rate**.

Haemodynamic Index	Normal Range
LV velocity-time integral (cm)	15-35
Stroke Volume (ml/m ²)	75-100
Cardiac Output (l/min)	4.0-8.0
Cardiac Index (l/min/m ²)	2.5-4.0

Table 1.2. Normal resting haemodynamic indices of left ventricular function (95% confidence interval)^{42,43}

Currently used non-invasive imaging methods for quantifying global LV systolic performance can be divided into haemodynamic and volumetric assessments of the LV. Haemodynamic assessment of LV systolic function includes the non-invasive quantification of stroke volume and dp/dt. Volumetric assessment of LV systolic function is performed non-invasively by calculating the ejection fraction of the LV. LVEF quantification is the most common measure of left ventricular systolic function and can be assessed using several different methods.³⁸ LVEF is the most commonly requested quantitative index on a diagnostic imaging scan request, and is also used to monitor disease progression.^{44,45} LVEF has also been shown to be a reliable indicator of prognosis in cardiovascular disease.⁴⁶⁻⁵⁰ Differing degrees of LV systolic impairment according to LVEF are shown in Table 1.3.

LV Systolic Function	LVEF range
Normal	≥ 55%
Mildly impaired	45-54%
Moderately impaired	36-44%
Severely impaired	≤ 35%

Table 1.3. Degrees of LV dysfunction according to left ventricular ejection fraction.³⁸

Current non-invasive imaging guidelines for assessing LV systolic function by haemodynamic and volumetric means are described in section 1.11.

1.4.2 Left ventricular diastole

Diastole has four phases:

- 1) Isovolumic relaxation
- 2) Early passive left ventricular filling
- 3) Diastasis
- 4) Late active left ventricular filling associated with atrial contraction

Phase 1: Isovolumic relaxation

Isovolumic relaxation is an active energy dependent process during which the myocytes return to their presystolic length and tension. This event occurs early in diastole and starts with the closure of aortic valve which occurs when the left ventricular pressure falls below the aortic pressure. As the left ventricle actively relaxes, the left ventricular pressure falls without a change in left ventricular volume. Once the left ventricular pressure falls below that of the left atrial pressure, the mitral valve opens, signalling the end of the isovolumic relaxation phase.⁴² The isovolumic period lasts 50-100ms (approximately 15-20% of cardiac diastole), during which time the ventricular pressure drops to 85% of its diastolic value.⁵¹ The rapidity with which left ventricular pressure declines during phase 1 diastole cannot adequately be explained by the isovolumic relaxation of the myocardium alone. Buckberg and colleagues have nicely demonstrated using sonomicrometer crystals in a pig model, that contraction of subendocardial fibres in the LV anterior wall ceases at end-systole, but contraction of sub-epicardial fibres persists 92 ± 20 ms longer. This dissociation between the end of sub-endocardial and sub-epicardial contraction corresponds with the isovolumic relaxation period, suggesting the presence of an active “suction” mechanism contributing to the rapid left ventricular pressure decent seen during phase 1 diastole.⁵¹

Phase 2: Early passive ventricular filling

After the mitral valve opens the early passive left ventricular filling phase starts. Early diastolic filling depends on the magnitude of the pressure gradient between the left atrium (LA) and left ventricle which propels blood into the left ventricular cavity. The rate at which the LA:LV pressure gradient declines is dependant on 1) the elastic recoil of the left ventricle, 2) chamber compliance and 3) left atrial pressure. Normally the rate of left ventricular filling and left atrial emptying is rapid and approximately 80% of left ventricular filling occurs during this phase.⁴²

Phase 3: Diastasis

Diastasis occurs due to equalization of the pressures across the mitral valve. Despite the equilibrium of pressures reduced blood flow can continue through the mitral valve due to inertia. The duration of diastasis is determined by the heart rate, being longer during bradycardia and shorter during tachycardia.

Phase 4: Late active ventricular filling

During diastasis, the left atrial and left ventricular pressures are at equilibrium. To enable further left atrial emptying and left ventricular filling, atrial contraction occurs. This increases left atrial pressure and enables a further volume of blood to be propelled into the left ventricular cavity. This final phase of diastole accounts for approximately 20% of left ventricular filling.⁴²

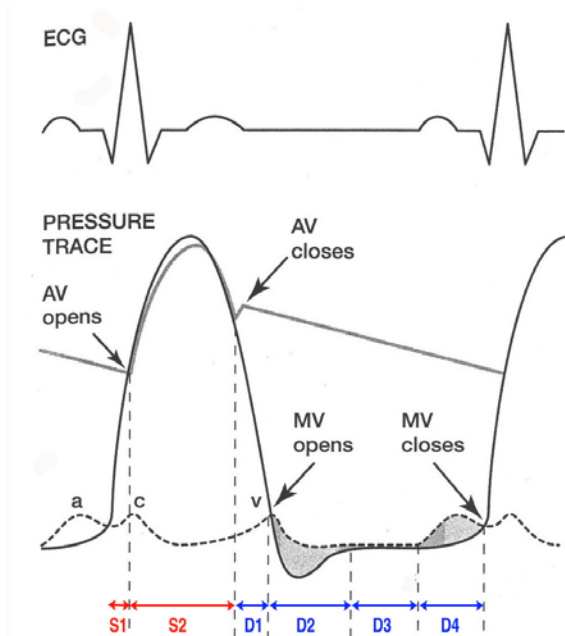


Figure 1.5. Intracardiac pressure changes during the cardiac cycle in the normal left ventricle

S1; Systole Phase 1: isovolumic contraction

S2; Systole Phase 2: systolic ejection phase

D1; Diastole Phase 1: isovolumic relaxation

D2; Diastole Phase 2: early passive filling

D3; Diastole Phase 3: diastasis

D4; Diastole Phase 4: late active filling associated with atrial contraction

LV diastole is a complex multi-stage process. This makes a quantitative non-invasive assessment of global diastolic function difficult. For many years, the diastolic relaxation of the heart has been assessed by Doppler echocardiography by studying mitral inflow and pulmonary vein flow patterns. Unfortunately these indices are only semi-quantitative at best, and are load dependent. In recent years, with the development of tissue Doppler echocardiography (TDE) techniques, there has been an increasing move to assess diastolic function by non-invasively estimating LV filling pressures. This physiology behind this technique is described in detail in section 1.10.3. CMR may provide useful in assessing LV

diastolic function in the future, but at the time of writing has no clinical application in this field.

1.4.3 Systolic and diastolic interdependence

Currently left ventricular systolic failure is diagnosed in the presence of a reduced LVEF. Diastolic heart failure is traditionally defined as heart failure symptoms in the presence of preserved LVEF. In reality, this classification is an over-simplification. It seems unlikely that systolic and diastolic heart failure are two distinct entities as systole and diastole are intrinsically linked within the cardiac contractile cycle. Diastolic filling patterns and filling pressures are often abnormal in patients with systolic dysfunction.⁵²⁻⁵⁶ Furthermore, recent insights from myocardial deformation imaging studies by our research group⁵⁷ and others⁵⁸ have suggested the presence of reduced long axis systolic contractility in patients with elevated diastolic filling pressures, abnormal diastolic filling patterns and preserved LVEF. Despite this overlap, distinguishing between predominantly systolic dysfunction and predominantly diastolic dysfunction is important for prognostic reasons. Furthermore, the correct diagnosis of diastolic heart failure as a cause of dyspnoea is important for prognostic reasons. In the Framington Heart study, patients with symptoms of congestive heart failure and impaired LV systolic function had an annual mortality of 18.9%.⁵⁹ By comparison, symptomatic heart failure due to diastolic dysfunction with preserved ejection fraction has a more benign prognosis with an annual mortality rate of 8.7%.^{60,61}

THE RIGHT VENTRICLE

1.5 ANATOMY OF THE NORMAL RIGHT VENTRICLE

“Thus the right ventricle may be said to be for the sake of transmitting blood through the lungs, not for nourishing them”

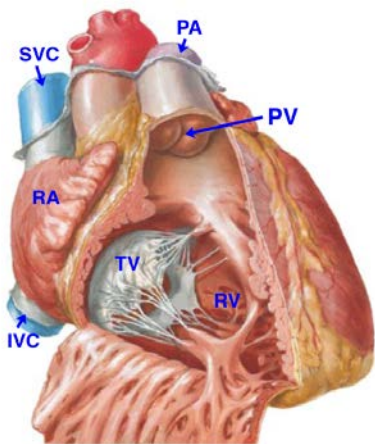
- Sir William Harvey, De Motu Cordis 1616⁶²

Despite the insight of Sir Harvey into the function of the right ventricle (RV), the RV was historically viewed by most as a passive conduit connecting the venous circulation to the pulmonary circulation. The RV was not considered nearly as important as the left ventricle in maintaining normal cardiovascular haemodynamics, and as such study of the RV has been largely neglected in favour of research into LV physiology. It is not until recent years that the importance of this “forgotten” ventricle in cardiovascular pathophysiology is finally being appreciated, and it is now recognised that the RV and LV are interdependent and have similar vitally important functions.

In the normal heart, the RV is the most anteriorly situated chamber and lies immediately behind the sternum. The normal RV is delimited by the tricuspid valve annulus at the inlet and the pulmonary valve at the outlet. Because the RV operates as a lower pressure system than the left heart, it is a thin walled and more compliant structure than the LV by the law of LaPlace, and its septal contour is indented by the dominant LV. As a result the RV is a complex shape that appears triangular when viewed side on, and a crescent when viewed in cross-section. This complex geometry of the right ventricle and its relation to the left ventricle within the thorax renders two-dimensional volumetric assessment of RV function inaccurate.

Morphologically the RV is distinguished from the LV by having coarser trabeculae, a moderator band and lack of fibrous continuity between the inlet and outflow valves.⁶³ Anatomically the RV can be subdivided into three component parts – 1) the inlet, which consists of the tricuspid valve, chordae tendinae and papillary muscles, 2) the trabeculated apical myocardium and 3) the infundibulum or conus which corresponds with the smooth

walled outflow region of the RV which lies immediately below the pulmonary valve (Figure 1.6). Three prominent muscular bands are present in the RV: the moderator band, the septomarginal band and the parietal band. The septomarginal band extends inferiorly and becomes continuous with the moderator band which attaches to the anterior papillary muscle. The parietal band and the infundibular septum together make up the crista supraventricularis.⁶⁴



(A) Schematic diagram demonstrating the anatomy of the normal right ventricle from the anterior aspect. Note the heavily trabeculated RV endocardial surface and RV moderator band.

(B) Geometric illustration of the normal right ventricle. The complex crescentic shape of the RV prevents accurate volumetric assessment of RV function by 2D echocardiography

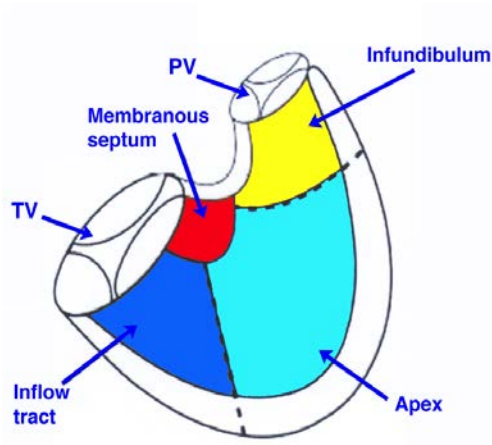


Figure 1.6. (A) Anatomy & (B) geometry of the normal right ventricle⁶⁴

The myofibre architecture of the RV differs from that of the LV. The RV has transverse and longitudinally orientated fibres and but lacks the middle constrictor fibre layer of the LV (Figure 1.7). The RV therefore must rely more heavily on longitudinal shortening during systole to maintain ejection fraction.⁶³

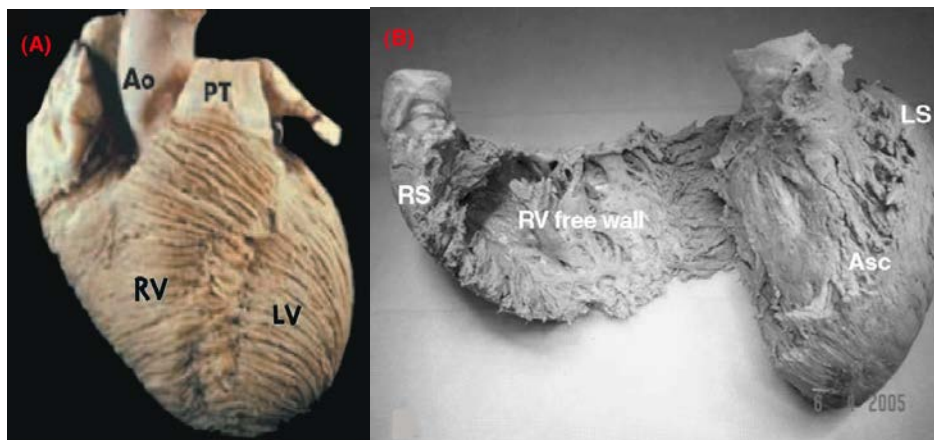


Figure 1.7. Schematic of RV myocardial fibre orientation^{64,65}

The RV wall is mainly composed of superficial and deep muscle layers. (A) The fibres of the superficial layer are arranged transversely in a direction that is parallel to the atrioventricular groove. (B) The deep muscle fibres are longitudinally aligned from base to apex adjacent to the trabeculated endocardial surface of the RV.

Ao, aorta; LV, left ventricle; PT, pulmonary trunk; RV, right ventricle

1.6 ANATOMICAL RELATIONSHIP OF THE CORONARY CIRCULATION TO THE RIGHT VENTRICLE

The blood supply to the right ventricle depends on the anatomy of the coronary tree. Approximately 80% of the population have a dominant right coronary system, in which case the right coronary artery (RCA) supplies most of the right ventricle. The lateral wall of the RV is supplied by the marginal branches of the RCA. The posterior wall and inferoseptum are supplied by the posterior descending artery. The infundibulum or conus is supplied by the conal artery, which has a separate ostial origin to the RCA in up to 30% of individuals. The anteroseptum and anterior wall of the RV are perfused by branches of the

left anterior descending artery.^{63,66} However, as the degree of RV dysfunction post myocardial infarction is often out of keeping with the findings on coronary angiography, a segmental model cannot be applied to the RV in the same manner as the AHA segmental model used to describe regional wall motion abnormalities of the LV.^{66,67}

1.7 PHYSIOLOGY OF THE NORMAL RIGHT VENTRICLE

The primary function of the RV is to receive systemic venous return and pump it to the pulmonary system. Under normal circumstances the RV is connected in series with the LV and so is required to pump the same stroke volume as the LV. However compared to the systemic circulation, the pulmonary circulation has a much lower vascular resistance and greater pulmonary artery distensibility. Right-sided intracardiac pressures are therefore much lower than left sided pressures, giving the RV its unique physiology.

Due to the anatomy and myofibre orientation of the RV, the RV contracts by three different mechanisms; 1) inward movement of the RV free wall (which produces a bellows effect) 2) contraction of the longitudinal fibres (long axis shortening), and 3) traction on the free wall at the points of attachment secondary to LV contraction.^{64,68} RV contraction is greater longitudinally than radially.⁶³ Also, due to the higher surface-to-volume ratio of the RV, a smaller inward motion is required to eject the same stroke volume. Understanding these fundamental differences between the physiology of RV and LV systole are important when developing and comparing different methods for quantitative assessment of RV function.

1.7.1 Contribution of the interventricular septum to right ventricular contractility

The role of the septum in ventricular-ventricular interactions is incompletely understood. The oblique fibre orientation of the LV enables ventricular torsion which helps to create the high pressures required to eject blood into high systemic vascular resistance. By contrast, under normal conditions the pulmonary vascular resistance is approximately one sixth of systemic resistance, and so the transverse constriction (bellows effect) and longitudinal shortening of the RV free wall is satisfactory to eject blood into the lower pressure pulmonary tree. In situations where septal akinesis is present, and RV free wall function is

preserved, RV haemodynamics may remain normal as long as pulmonary vascular resistance is low.⁶⁵ However, the contribution of septal contraction to RV systole becomes increasingly important in situations of increased pulmonary vascular resistance, where the oblique fibre orientation of the septum and subsequent septal twisting becomes a vital mechanism for the RV to maintain output against increased pulmonary vascular resistance.⁶⁵

Recent advances in TDE have enabled preliminary research into the functional contributions of the interventricular septum to left and right ventricular contraction respectively showed that differences in thickening and radial strain could be observed between the two sides of the septum, which were not present in the longitudinal axis.⁶⁹ Knowledge of fibre architecture with an abrupt change in the middle of the septum together with the above study suggests the septum to be a morphologically and functionally bilayered structure.⁶³

1.7.2 Right Ventricular Haemodynamics

Under normal conditions, unlike the LV, the right ventricle is an energy efficient pump. The RV produces approximately the same stroke volume as the LV, but at 25% of the stroke work. However this efficiency is largely predicated by the low hydraulic impedance of the pulmonary vascular bed. That coupled with the highly compliant nature of the RV wall means the contractile properties of the RV are significantly influenced by changes in cardiac loading conditions.

Preload

Preload is the load present on the right ventricle in end-diastole, prior to systolic contraction, and is a reflection of the venous filling pressure. Within physiological limits an increase in RV preload improves myocardial contractility as per the Frank-Starling relationship (Figure 1.8). Due to the increased compliance of the RV free wall, the RV may tolerate volume overloaded states well for a long time without a significant decrease in RVEF.⁶³ However beyond a certain point, excessive RV volume loading can alter septal

geometry, compress the LV and impair global ventricular function due to the mechanism of ventricular interdependence (Figure 1.9).

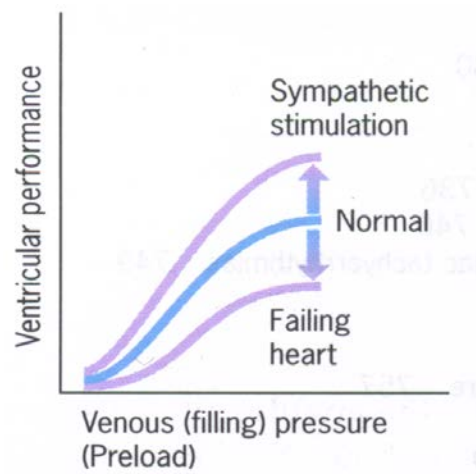


Figure 1.8. The Frank-Starling Curve.

The Frank-Starling curve demonstrates the effect of altered filling pressures on ventricular performance in the normal, failing and sympathetically stimulated ventricle.

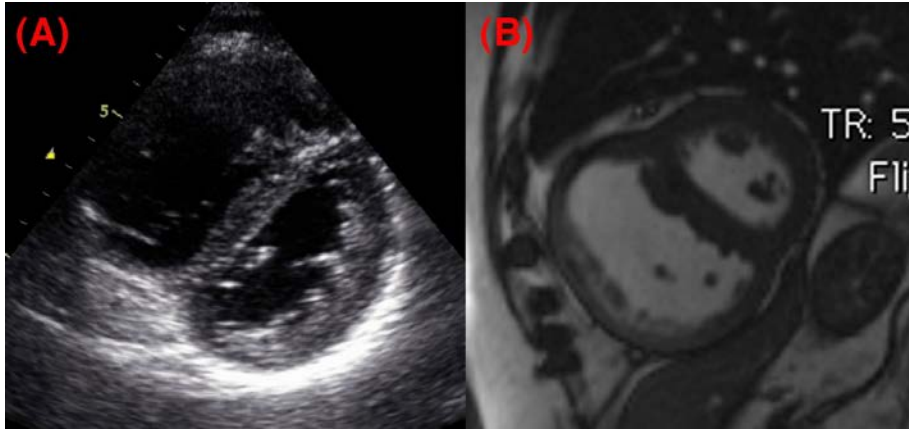


Figure 1.9. RV volume overload and “D” shaped flattening of the interventricular septum affecting LV filling. (A) parasternal short axis echocardiography view of the volume overloaded RV (left) causing D-shaped flattening of the interventricular septum and reversal of the transeptal gradient with resultant underfilling of the LV cavity (right). (B) Corresponding steady state free precession short axis cine CMR image demonstrating the same pathophysiology.

Myocardial contractility

Myocardial contractility is the inherent capacity of the myocardium to perform work independent of changes on preload or afterload. RV myocardial contractility differs to that of the LV due to the different myofibre orientation, however there is also limited evidence to suggest that the RV myocardium is intrinsically different with a faster twitch velocity in RV muscle bundles than those of the LV.⁷⁰⁻⁷²

Afterload

As the RV is “coupled” to its low impedance pulmonary vascular bed, acute changes in afterload lead to major changes in RV pressure-volume relationships (see Figure 1.10). Compared to the LV, the RV is therefore extremely sensitive to changes in afterload, and the presence of pressure overloaded states such as acquired pulmonary hypertension often leads to RV dilatation and failure.

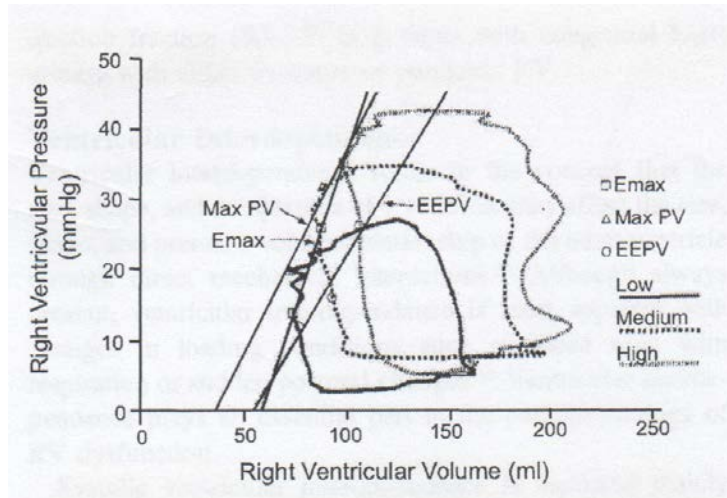


Figure 1.10. Right ventricular pressure-volume loops under different loading conditions.^{64,73} Cardiac loading conditions alter the RV pressure-volume relationship as shown above. The slopes of maximum time-varying elastance (E_{max}), maximum pressure-volume ratio (Max PV) and end-ejection pressure/volume (EEPV) are displayed on the graph.

1.8 VENTRICULAR-VENTRICULAR INTERDEPENDENCE

While it has been traditional to consider left and right ventricular physiology as independent of each other, this concept is flawed. The right and left ventricle share the constraints of the pericardial cavity and are interconnected via the interventricular septum. Ventricular interdependence refers to the concept that the size, shape, compliance and function of one ventricle effects the size, shape and pressure-volume relationship of the other. It is now well recognised that normal right ventricular function is dependent on normal left ventricular function, and conversely abnormalities of the left ventricle are important in the pathophysiology of RV failure.

Research suggests systolic ventricular interdependence is mediated predominantly through the interventricular septum. Damiano and colleagues electrically isolated contractility of the left and right heart, and demonstrated that LV systole caused pronounced pressure

generation in the right ventricle, estimated to account for up to 30% of the contractile energy of the RV.⁷⁴ Furthermore, animal experiments have shown that normal contractility of the septum is able to maintain RV pressure generation and circulatory stability when the RV free wall is scarred or replaced by a non-contractile patch, as long as the RV itself is not dilated.⁷⁵

Diastolic ventricular interdependence is believed to be mediated through pericardial constraints on the dilated heart. In RV overloaded states, the compliant RV dilates. Eventually due to the constraint of the pericardial sac, the RV free wall cannot dilate outwards any further, and so pressure or volume overload within the right ventricle causes the interventricular septum to be displaced leftwards, altering the LV geometry and increasing the pericardial constraint on the left heart. The LV diastolic pressure-volume curve is displaced upwards. The reduced LV cavity size impairs diastolic filling and results in a reduction in cardiac output.

Systolic septal motion is influenced by the transeptal gradient. Under conditions of severe RV free wall dysfunction, paradoxical septal motion reflects the left to right systolic transeptal gradient because depressed RV contraction allows unopposed LV septal tension development.^{66,76-80} The compensatory contribution of septal contraction to global RV systolic function is highlighted in the presence of septal hypokinesis. Unsurprisingly, haemodynamic compromise and morbidity associated with RV ischaemia is exacerbated by the presence of septal dysfunction.⁷⁶

Right ventricular infarction is known to complicate approximately 50% of cases of acute inferior myocardial infarction and is a predictor of major complications and mortality.^{81,82} However, right ventricular dysfunction following acute inferoposterior myocardial infarction may not be fully explained by right ventricular wall ischaemia. The dominant right coronary artery supplies the inferior and posterior walls of the left ventricle and acute ischaemic LV dysfunction results in elevated filling pressures and increases the afterload pressure on the right ventricle. The right ventricle is sensitive to pressure overloaded states, which further exacerbates RV systolic dysfunction. The fact that significant transient RV

systolic dysfunction has been noted in 77% of study subjects within 48 hours after anterior myocardial infarction further supports this theory.⁸³

The physiology of the right ventricle is unique, and the early detection and quantification of RV systolic dysfunction has important prognostic implications in cases of both primary RV failure due to cardiomyopathic processes, or more commonly secondary RV dysfunction in response to conditions of increased RV afterload (pressure overloaded RV secondary to pulmonary hypertension +/- elevated LV filling pressures), or pre-load (volume overloaded RV).

1.9 THE ORIGINS OF DIAGNOSTIC CARDIOLOGY

1.9.1 Invasive catheter studies

The history of diagnostic cardiology can be traced back to 1711 when Stephen Hales placed catheters into the left and right ventricles of a living horse.⁸⁴ More than a century later, the first formal studies of cardiac physiology were performed using invasive cardiac catheterisation by Claude Bernard in animal models.⁸⁵ The first clinical cardiac catheter procedure on a human was performed by Werner Forssmann in 1929 when he inserted a catheter into a vein in his own forearm, guided it fluoroscopically into his right atrium.⁸⁶ A decade later Professor Andre Cournand and colleagues developed the techniques for left and right heart catheterisation that we still use today.⁸⁷ Cardiac catheterisation provides valuable well-validated haemodynamic information on intra-cardiac pressures which are still used for diagnostic purposes and to guide clinical decision making. Invasive techniques however, by their very nature, carry inherent risks and discomfort for the patient. Non-invasive alternatives for quantifying ventricular systolic and diastolic function and measuring haemodynamic indices of contractility, ventricular relaxation and diastolic filling are safer and more patient-friendly and should therefore be considered first line investigations in diagnostic cardiology, provided the technique itself is robust and reproducible.

The currently recommended methods for quantifying ventricular function are well validated within the differing imaging modalities. However, current techniques have recognised

limitations as subsequently discussed in section 1.11. In an era of multi-modal imaging, intermodality concordance is also important. There have been major technological advances in the field of non-invasive cardiac imaging in recent years, and the objective of this thesis is to explore the use of novel imaging methods to quantify resting ventricular function.

1.9.2 Echocardiography

The existence of ultrasonic radiation in nature was first demonstrated by Lazzaro Spallanzani in the seventeen hundreds during a study of bats.⁸⁸ Edler (a Swedish cardiologist) and Hertz (a physicist) were the first clinical team to successfully utilize ultrasound technology to non-invasively image the heart in Europe in 1954.⁸⁹ Using similar principles to the SONAR (sound navigation and ranging) ultrasound system used to detect enemy submarines during World War I, Edler and Hertz recorded the first moving images of the heart by M-Mode and used this technology to aid the pre-operative selection of patients with mitral stenosis for a new closed mitral commissurotomy technique.⁸⁹ This signified the birth of transthoracic echocardiography (TTE). The early progression of echocardiography in the 1960's was largely as a result of the scientific work of Professor Harvey Feigenbaum of the Indiana University School of Medicine, Indianapolis, USA.⁹⁰⁻⁹³ Since this time, major advances in TTE have occurred including the development of fast Fourier transformation and Doppler colour flow mapping, resulting in TTE becoming the "Gold Standard" bedside cardiac imaging modality for the diagnosis of a variety of cardiac complaints. Standard TTE is the most widely available, and often first line, non-invasive imaging modality for diagnosing abnormalities of cardiac morphology (using 2D and time-motion mode measurements), valvular pathologies (combining abnormalities on both 2D imaging and spectral Doppler flow patterns) and cardiac contractile dysfunction (resting global systolic and diastolic impairment, regional wall motion abnormalities, and the use of dobutamine stress/viability protocols for the diagnosis of inducible ischaemia and myocardial viability). The recent development of tissue Doppler echocardiography, myocardial deformation imaging and three-dimensional echocardiography has further provided new and exciting tools in clinical imaging research and clinical echocardiography.

1.9.3 Nuclear Cardiology

The history of nuclear medicine originated in the 1920s. The first diagnostic application of nuclear medicine was in the field of cardiology, when in 1927 Herman Blumgart used injectable solutions of radon gas and a Geiger tube to measure the “velocity of the circulation” in normal volunteers.⁹⁴ Clinical nuclear cardiology began in the early 1960’s. The production of the scintillation camera and commercial development of radioisotopes enabled the imaging of radio-labelled tracers as they circulated through the heart in real-time. The first uses of nuclear cardiology included measurement of regional myocardial perfusion, regional function and detection of intra-cardiac shunts.⁹⁵ The 1970’s and 1980’s heralded the development of 201-thallium, technetium-99m and myocardial stress-perfusion imaging for the detection of inducible myocardial ischaemia.⁹⁶ This is performed today using single-photon emission computed tomography (SPECT). From the late 1970’s onwards first-pass ventriculography and equilibrium ventriculography have become available for assessing right and left ventricular function, and quantification of cardiac stroke volumes and ejection fractions.

1.9.4 Cardiac Magnetic Resonance

Cardiac magnetic resonance imaging is a new and continually evolving sub-specialty within the field of diagnostic cardiology which is at present limited to specialist centres. However the origins of magnetic resonance imaging (MRI) can be traced back over one hundred years.

The rotating magnetic field was first discovered by Nicola Tesla in 1885.⁹⁷ The concept of nuclear magnetic resonance however was not established until 1946 when Felix Bloch and Edward Purcell, independently discovered that certain nuclei placed in a magnetic field absorbed energy in the electromagnetic spectrum and re-emitted this energy as a radiofrequency pulse when the nuclei transferred to their resting state, with the frequency of the radiofrequency pulse being proportional to the strength of the magnetic field.^{98,99} This finding eventually led to the production of the first magnetic resonance images some 30 years later by Lauterbur and Mansfield. Paul Lauterbur in New York, USA and Peter Mansfield from Nottingham, UK, independently described the use of magnetic field

gradients to enable spatial localisation of nuclear magnetic resonance signals.^{100,101} The first published magnetic resonance image of a living creature, a clam, in 1974 was produced by Lauterbur and colleagues.¹⁰² The first in vivo human MRI image, the cross section of a finger, was published by Mansfield in colleagues in 1977.¹⁰² Lauterbur and Mansfield were jointly awarded the Nobel prize in 2003 for inventing magnetic resonance imaging.¹⁰³

Goldman and colleagues from Harvard Medical School were the first to describe the future potential of MRI in diagnostic cardiology in 1980.¹⁰⁴ A year later Hawkes and colleagues in Nottingham, UK described what is believed to be the first recorded cardiac magnetic resonance image,¹⁰⁵ followed by the first ECG gated moving cardiac image by Lauterbur's group in 1983.¹⁰⁶ Since this time advances in MRI imaging of the heart have been considerable, and include the development of delayed enhancement CMR for assessing myocardial viability, steady state free precession CMR for assessing cardiac anatomy and chamber quantification, adenosine stress-perfusion CMR and dobutamine stress CMR for detecting inducible myocardial ischaemia, velocity encoded CMR for calculating valvular haemodynamics and grid-tagging to assess regional myocardial deformation. CMR is emerging as its own distinct sub-specialty within the field of diagnostic cardiology. The clinical research for this thesis was performed during a research fellowship at the Cardiovascular Research Centre, Royal Adelaide Hospital, South Australia. During the writing of this thesis, the Department of Cardiology at the Royal Adelaide Hospital became the first cardiology centre in Australasia to set up a dedicated clinical cardiac MRI service under the leadership of Prof Stephen Worthley and Dr Karen Teo.

1.9.5 Cardiac Computed Tomography

British engineer, Godfrey Hounsfield, a former employee of UK record company EMI, and American physicist Allan M Cormack invented computed tomography (CT) in 1972 by combining computer technology with X-ray technology, for which they received the Nobel prize in medicine.¹⁰⁷ Two years later the first commercially available CT system was produced by Siemens Medical Systems.¹⁰⁸ Multiplanar reformatting became available in 1984, and the development of slip-ring technology in 1988 enabled the production of the first spiral CT scanner. The first CT angiogram was performed in 1997 from a single-slice

spiral CT reconstruction. However it was not until 2002 that cardiac CT progressed from research dream to reality with the development of 16-slice multi-detector CT (MDCT) for imaging the coronary arteries. Since this time we have seen the development of 64-slice MDCT in 2004, the dual source scanner in 2006, and 128-, 256- and 320-slice MDCT in 2007-2008.¹⁰⁷ Gantry rotation speeds and collimeter slice thickness have decreased with each generation of CT scanner, and it is now possible to image the whole heart in seconds with high spatial and reasonable temporal resolution.¹⁰⁷

1.10 MULTI-MODAL IMAGING FOR THE ASSESSMENT OF VENTRICULAR FUNCTION

1.10.1 Assessment of resting ventricular function

Historically 2D-echocardiography has been the imaging modality of choice for the assessment of resting LV and RV global systolic function, LV diastolic function and regional myocardial function. Radionuclide ventriculography has also been used to quantify right and left ventricular ejection fractions, but has fallen out of favour with the development of newer imaging modalities and techniques. The development of 3D-echocardiography has improved accuracy of cardiac volume quantification, however the most exciting development in cardiac ventricular functional imaging is CMR. The superior spatial resolution of CMR compared to echocardiography and nuclear techniques, and its ability to image the heart in any plane, now makes it the generally accepted reference standard for quantification of right and left ventricular ejection fraction. At the present time, CMR is not the recommended standard for assessing diastolic function. Cardiac CT also has excellent spatial resolution. Although the major current clinical application for cardiac CT is for the non-invasive imaging of the coronary arteries, a recent study by Brodoefel and colleagues has demonstrated the feasibility of CT for quantifying LV systolic function with excellent inter-technique correlation in both ventricular volume quantification (LVEDV: R=0.98; LVESV: R=0.99) and LVEF calculation (R=0.95), when compared to CMR.¹⁰⁹

1.10.2 Assessment of dynamic ventricular function: Stress-perfusion imaging

A major application of cardiac functional imaging is in the diagnosis, assessment and risk stratification of patients with known or suspected coronary artery disease. Nuclear SPECT, dobutamine stress echocardiography, dobutamine stress CMR and adenosine stress-perfusion CMR can all be used to assess areas of regional ventricular infarction and inducible ischaemia. Low-dose dobutamine viability stress echocardiography and delayed enhancement gadolinium CMR imaging protocols are also used to differentiate between viable and non-viable ventricular myocardium. Each imaging modality has its advantages and limitations, the further discussion of which is out-with the scope of this thesis.

1.10.3 Safety issues

The quantification of resting ventricular function is the most common imaging request in diagnostic cardiology. Furthermore, ejection fraction quantification is often used serially as a monitoring tool to aid clinical decision-making in both cardiac and non-cardiac pathologies. The safety of a diagnostic imaging test, which will be used to assess many millions of patients world-wide, often serially, is therefore of paramount importance. Currently no adverse biological effects have been observed in humans at diagnostic ultrasound intensity levels. Similarly, excluding patients with ferromagnetic implants and implanted device therapies, CMR performed in a 1.5T scanner, is believed to be safe.

The UK department of Health's Administration of Radioactive Substances Advisory Committee (ARSAC) limit for a single administered dose of radioactive-thallium is 80Mbq.¹¹⁰ The effective dose equivalent is 0.23mSv/Mbq giving a total dose of 17-18mSv radiation exposure during a thallium-SPECT scan and the 8.6-10.7mSv radiation exposure during a technetium-labelled SPECT scan depending on the protocol used.¹¹¹ The radiation dose to patient during radionuclide ventriculography is in the region of 800 Mbq giving a dose equivalent of approximately 7mSv.¹¹² For a 64-slice MDCT scan the radiation exposure for a retrospectively ECG gated scan is 13-15mSv for a man and 18-21mSv for a woman, although these doses may be less in newer generation scanners.¹¹¹

Due to repeated exposure to ionising radiation, we believe nuclear cardiology and cardiac CT are not suitable or justifiable imaging modalities for assessing resting ventricular function in patients that require serial monitoring, when safer alternatives are available. For this reason the investigation of potential novel methods to improve the diagnosis of cardiac dysfunction within this thesis will concentrate on the use of new echocardiographic and CMR imaging techniques.

1.11 THE NON-INVASIVE ASSESSMENT OF LEFT VENTRICULAR SYSTOLIC FUNCTION

Traditionally and currently, the first line non-invasive imaging modality for the assessment of left ventricular systolic function remains 2D echocardiography. Left ventricular systolic function is assessed globally (overall ventricular performance) and regionally (for the presence of regional wall motion abnormalities indicating the site and extent of previous myocardial infarct).

1.11.1 Haemodynamic assessments of global left ventricular function

Echocardiographic quantification of global left ventricular systolic function is traditionally assessed using either haemodynamic or volumetric measurements.

Stroke distance, Stroke volume and Cardiac Output

Haemodynamic assessments of left ventricular function are measured using spectral Doppler indices. The stroke distance is equivalent to the left ventricular systolic velocity time integral (LV VTI) and is easily measured from a pulsed wave Doppler trace recorded in the left ventricular outflow tract (LVOT).¹¹³ From the stroke distance, both the stroke volume (the volume of blood ejected from the heart during each systolic contraction) and the cardiac output (the volume of blood pumped out by the heart per minute) can be calculated as shown in Equations 1.2 and 1.3.

Equation 1.2:

$$SV = \pi(LVOT D/2)^2 \times LV VTI$$

where: SV = stroke volume

LVOT D = LV out flow tract diameter

LV VTI = LV velocity time integral

Equation 1.3:

$$CO = SV \times HR$$

where: CO = cardiac output

SV = stroke volume

HR = heart rate

The normal ranges for LV VTI (stroke distance), stroke volume and cardiac output are as previously shown in Table 1.2.

Limitations of the technique

Doppler assessment of LV VTI and SV are influenced by cardiac loading conditions, dysrhythmias and ectopy. Further more, any errors in LVOT diameter measurements are magnified during cross-sectional area calculations.

Left ventricular pressure-time relationship (dP/dT)

An alternative non-invasive haemodynamic estimate of LV systolic function can be determined from the LV pressure-time relationship (dP/dT). Doppler indices obtained during the non-ejection phase of the cardiac cycle are less dependent on loading conditions.⁴² DP/dT is a measure of the rate of rise of left ventricular pressure during the isovolumic contraction period and is calculated as shown in Equation 1.4.⁴²

Equation 1.4: Calculating dP/dT

$$dP/dT = 32/\Delta t \quad \text{where } \Delta t = \text{time interval}$$

measured between velocity points
1 and 3 m/s on the mitral regurgitant
spectral Doppler envelope.

An example of the echo Doppler measurement of dP/dT is shown in Figure 1.11.

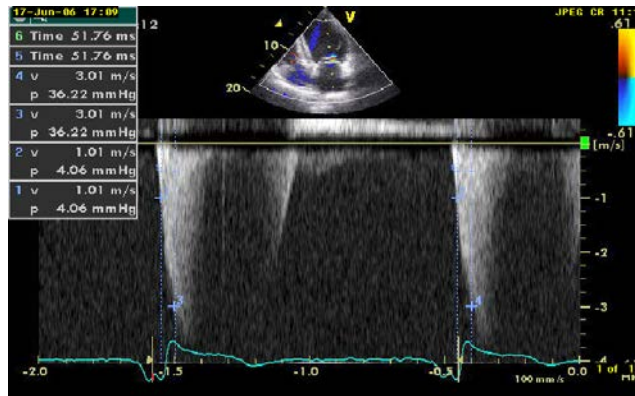


Figure 1.11. Measuring dP/dT.

The time interval between 1 and 3 m/s is 51.76ms as shown. The corresponding dP/dT is therefore 620.16mmHg/s indicating severe left ventricular dysfunction.

Reference values for dP/dT are shown in Table 1.4 below.

LV Systolic Function	DP/dt values (mmHg/s)	Time taken to generate 32mmHg
Normal	> 1,200	< 27ms
Mild-Moderate dysfunction	800 –1,200	27-40ms
Severe dysfunction	< 800	> 40ms

Table 1.4. Reference values for dP/dT.⁴²

To minimise error during this measure, care must be taken to ensure correct Doppler alignment and to optimise gain and filter settings. The velocity scale and sweep speed should be set consistently – for example, 0-4m/s with a sweep speed of 100mm/s. This technique is dependant on the presence of a well-defined mitral regurgitant Doppler envelope.

1.11.2 Volumetric assessments of global left ventricular systolic function

Diagnostic and prognostic importance of left ventricular ejection fraction

Due to geometric assumptions and load dependent nature of haemodynamic estimations of LV systolic function, calculation of LVEF by volumetric methods is the universally accepted measure of LV systolic function in clinical practice. LVEF is one of the basic quantitative indices of any cardiac imaging study and is diagnostically important in identifying patients with LV systolic dysfunction and heart failure. The LVEF is the total blood volume ejected from the LV during each cardiac cycle, expressed as a percentage of the total volume of blood present in the LV at the end of the diastolic filling period. Degrees of systolic dysfunction are categorised according to specified ranges of LVEF into normal contractile function, mild, moderate and severely impaired function as previously shown in Table 1.3. A LVEF \geq 55% is considered normal.³⁸

Not only is LVEF important diagnostically, it is arguably the most important index of prognosis. The prognostic value of LVEF is well established.⁴⁶⁻⁵⁰ Patients with symptomatic heart failure have a significantly increasing 12 month mortality per 10% reduction in LVEF.¹¹⁴ Furthermore, quantification of LVEF aids clinical decision making when forming medical management plans for patients with a variety of cardiac and non-cardiac pathologies alike.

Patients with impaired LVEF due to ischaemic and non-ischaemic cardiomyopathies have been shown to prognostically benefit from pharmacological therapies such as angiotension converting enzyme inhibitors,¹¹⁵⁻¹²⁰ beta-blockers¹²¹⁻¹²⁴ and aldosterone antagonists.^{125,126} The monitoring of left ventricular dimensions and LVEF is important in patients with

valvular heart disease and guides the optimal timing of surgical interventions.¹²⁷ Cardiac resynchronisation therapy (CRT) has been shown to improve both morbidity and mortality in heart failure patients with New York Heart Association functional class III-IV symptoms, a broad QRS on ECG and severe left ventricular dysfunction in several multicentre trials.¹²⁸⁻¹³⁵ The presence of a LVEF \leq 35% is a prerequisite for consideration of CRT under current National Institute of Clinical Excellence (NICE) (2007) UK Guidelines.¹³⁶ Similarly AVID,¹³⁷ MADIT II¹³⁸ and COMPANION¹³⁴ clinical trials demonstrated significant survival benefit with the implantation of internal cardioverter defibrillator (ICD) device therapies for the prevention of sudden arrhythmia-induced cardiac death in patients with severe left ventricular dysfunction of ischaemic origin, who had no evidence of untreated ischaemia. Again accurate quantification of LVEF is a prerequisite for consideration of ICD device therapy according to NICE Guidance number 95.¹³⁹

The importance of LVEF quantification in the management of patients with non-cardiac disorders and diseases should not be underestimated either. Quantification of LVEF in patients prior to non-cardiac surgery is increasingly common and aids surgeons and anaesthetists in risk stratification of their patients pre-operatively. Initial quantification of LVEF and subsequent monitoring of LV systolic function is also important during the treatment of oncology patients to ensure the avoidance of chemotherapy induced cardiomyopathy due to the potentially cardiotoxic nature of these agents.¹⁴⁰

Two-dimensional echocardiography assessments of left ventricular ejection fraction

Despite the clear importance of accurately calculating LVEF in clinical practice, it is a measure that is often performed sub-optimally. Although accurate quantification of LVEF is one of the fundamental indications for performing a non-invasive cardiac imaging study, the accuracy and reproducibility of this measurement is modality, method and operator dependent. Traditionally, 2D transthoracic echocardiography has been the imaging modality used to quantify LVEF and a variety of different methods for calculating LVEF have been developed. Each of these methods has advantages and limitations which are summarised in Table 1.5.

Dimensions/volumes	Use/advantages	Limitations
<u>Linear</u>		
M-Mode (Teicholtz)	<ul style="list-style-type: none"> - Reproducible - High frame rates - Wealth of accumulated data - Most representative in normally shaped ventricles 	<ul style="list-style-type: none"> - Beam orientation frequently off axis - Single dimension may not be representative in distorted ventricles - Inaccurate in ventricles with RWMA's
<u>2D Guided</u>	<ul style="list-style-type: none"> - Assures orientation perpendicular to ventricular long axis 	<ul style="list-style-type: none"> - Lower frame rates than M-Mode - Single dimension only
<u>Volumetric</u> Simpson's Biplane	<ul style="list-style-type: none"> - Corrects for shape distortion - Minimises mathematical assumption 	<ul style="list-style-type: none"> - Apex frequently foreshortened - Endocardial dropout - Relies on only two planes - Few accumulated data on normal population
Area-length	<ul style="list-style-type: none"> - Partial correction for shape distortion 	<ul style="list-style-type: none"> - Based on mathematical assumptions - Few accumulated data
<u>Mass</u> M-Mode or 2D guided	<ul style="list-style-type: none"> - Wealth of accumulated data 	<ul style="list-style-type: none"> - Inaccurate in ventricles with RWMA's - Beam orientation (M-mode) - Small errors magnified - Overestimated LV mass - Insensitive to distortion in ventricular shape
Area-length	<ul style="list-style-type: none"> - Allows for contribution of papillary muscles 	<ul style="list-style-type: none"> - Based on a number of mathematic assumptions
Truncated ellipsoid	<ul style="list-style-type: none"> - More sensitive to distortions in ventricular Shape 	<ul style="list-style-type: none"> - Minimal normal data

Table 1.5. Left ventricular quantification methods: Use, advantages & limitations³⁸

2D, two dimensional; RWMA's, regional wall motion abnormalities

Due to the inherent problems of the Teicholtz and Area-Length methods for quantifying LV systolic function, both the American Society of Echocardiography and the European Association of Echocardiography guidelines favour the use of the biplane method of discs (modified Simpson's rule) as the 2D echocardiographic standard for calculating LVEF, despite the recognised limitations of this technique.³⁸

The principle underlying this method is that the total left ventricular volume is calculated from a stack of elliptical discs, the calculated volume of which is derived from left ventricular cavity measurements recorded in the apical four chamber and apical two chamber views in end diastole (EDV) and end systole (ESV) (Figure 1.12).¹⁴¹

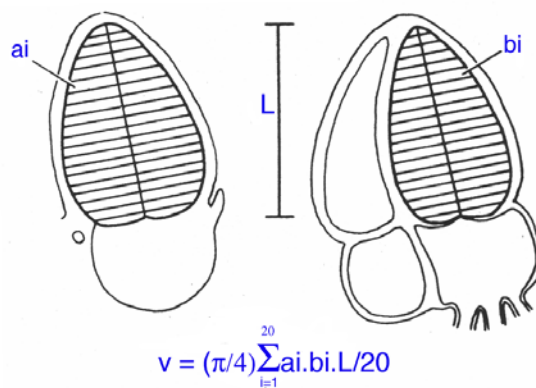


Figure 1.12 & Equation 1.5. Calculating left ventricular volumes using Simpson's Biplane Method of Discs.⁴²

The left ventricle is divided into a series of 20 discs along its length (L). The total volume of the left ventricle is then calculated from the above equation where a = area of disc in plane 1 (cm²), b = area of disc in plane 2 (cm²) and L = length (cm).

LVEF is then calculated as follows:

Equation 1.6. Calculating left ventricular ejection fraction

$$\text{LVEF (\%)} = \frac{\text{EDV} - \text{ESV}}{\text{EDV}}$$

Limitations of Biplane Simpson's Rule

The modified Simpson's biplane method of discs, which is not a true Simpson's, relies on imaging in only two planes and therefore makes geometric assumptions. This technique requires both the presence of good endocardial definition and the absence of apical foreshortening during image acquisition. In echogenic subjects and with the introduction of second harmonic imaging in the absence of contrast enhancement, interobserver errors are still significant. Thompson et al showed that the interobserver variability in calculating the LV end diastolic volume (LVEDV), LV end systolic volume (LVESV) and LVEF are 13%, 17% and 18% respectively.¹⁴² Even with the use of both second harmonic imaging and contrast enhancement, which requires intravenous cannulation and medical supervision and is therefore not practical for routine use in a busy clinical echocardiography laboratory, interobserver variability for LVEDV, LVESV and LVEF are 8%, 15% and 6% respectively.¹⁴²

Three-dimensional echocardiography

The recent development of three-dimensional echocardiography (3DE) largely overcomes the geometrical limitations of standard 2DE. A 3D acquisition of the LV is performed from the apical window, from data gathered over 4-5 cardiac cycles. Using semi-automated endocardial border detection, the LVEDV and LVESV are measured from the resulting three-dimensional left ventricular volume (see Chapter 3, Section 3.5). The LVEF is then calculated from the LV volumes as described previously. The changes in regional volumes between end-diastole and end-systole are also displayed by the software (Figure 1.13). Jacobs et al have shown 3DE to have significantly better reproducibility than standard 2D TTE, with 3DE interobserver variabilities of 10%, 11%, 5% for LVEDV, LVESV and LVEF respectively.¹⁴³ Volumetric calculations using 3DE correlate well with cardiac MRI derived measurements,¹⁴⁴⁻¹⁴⁶ although 3DE significantly underestimates ventricular volumes when compared to CMR.^{147,148} However, due to cost and limited availability of 3DE, routine use of this technology is limited to specialist centres.

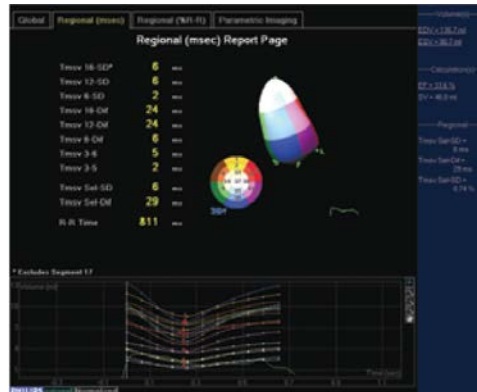


Figure 1.13. Change in American Heart Association 17 segment regional LV volumes over time with 3DE

Cardiac magnetic resonance imaging

As technology has advanced, a variety of alternative cardiac imaging modalities can be used to quantify LVEF – most notably nuclear SPECT and cardiac magnetic resonance imaging. Unfortunately, LVEF calculated by these different imaging modalities are often used interchangeably when close intertechnique agreement has not been established.¹⁴⁹ Two dimensional volumetric assessments of LV function have been previously shown to have a sub-optimal correlation with CMR,^{150,151} and nuclear techniques tend to underestimate LVEF compared to 2DE.¹⁴⁹ Quantification of global LV systolic function by 3DE has a closer correlation with CMR, but significantly underestimates left ventricular volumes.^{144,148}

Nuclear imaging is limited by the fact it exposes patients to ionising radiation. In an era where safer alternative imaging modalities are available, diagnosis and monitoring of LV dysfunction by SPECT scanning is no longer justifiable. Nuclear imaging is therefore out with the scope of this thesis and will not be discussed further.

CMR has superior spatial resolution to both 2D and 3D echocardiography and the advantage of being able to image the heart in any plane, unlike echocardiography which is limited to standardised transthoracic windows. Furthermore, the ability of CMR to acquire sequential short axis steady state free precession (SSFP) imaging sequences in a contiguous

manner through the heart from the left ventricular base to apex (Figure 1.14a), enables a geometrically accurate 3D volumetric reconstruction of the left ventricular cavity. Proprietary analysis software allows endocardial border tracing in end diastole and end systole for each imaging sequence within the left ventricular short axis stack (Figure 1.14b). Indeed, by applying Simpson's method of discs to a CMR SSFP breath hold cine LV short axis series, multiple slice by slice LV volumes are actually measured and summated, resulting in fewer mathematical assumptions and a high reproducibility with an interobserver variability for LVEDV, LVESV and LVEF of 8%, 4% and 5% respectively¹⁵² – a significant improvement on standard TTE techniques. For these reasons it is now generally accepted that CMR is the reference standard for assessing resting global LV systolic function.

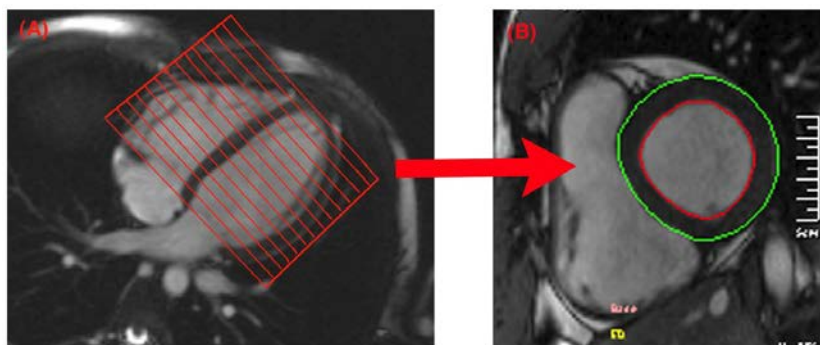


Figure 1.14. Calculating LVEF by cardiac magnetic resonance.

(A) Acquisition of retrospectively gated steady state free precession short-axis cine images from left ventricular base to apex. Subsequent manual endocardial border tracing in end-diastole (B) and end-systole (not shown) for each LV short axis slice enables multiple slice by slice LV volumes to be measured and summed. LVEF is therefore calculated by CMR using a true Simpson's method of discs with minimal mathematical assumptions – in contrast with the Biplane Simpson's method used in 2D echocardiography

Cardiac magnetic resonance imaging for assessing left ventricular dysfunction in heart failure however, has several potential limitations. A full cardiac magnetic resonance study, depending on the clinical indication, can take from 40-70 minutes to complete. During this

time, the patient needs to be supine within the magnet. Dyspnoea is a common symptom of heart failure, often exacerbated in the supine position and therefore lying flat may be difficult. Furthermore, most steady state free precession imaging sequences are acquired as breath-hold sequences over several cardiac cycles which again can be difficult for the dyspnoeic patient. Cardiac magnetic resonance imaging is ECG-gated and in most routine imaging sequences the resultant 2D image is a reconstruction of data acquired over several heartbeats. Variation in the R-R interval of the ECG, as occurs in the presence of atrial fibrillation and ventricular ectopy, therefore has adverse effects on image quality. The prevalence of atrial dysrhythmias and ventricular ectopy are significantly higher in patients with left ventricular dysfunction than those without.¹⁵³⁻¹⁵⁵ In the in-patient setting, patients requiring left ventricular functional assessment are often acutely unwell. Transferring an unstable patient from ITU or CCU to the MRI scanner for the purpose of ventricular assessment is not justifiable when a bedside echocardiogram is an available alternative. Cardiac magnetic resonance imaging is contra-indicated in patients with ferromagnetic metallic implants. The prevalence of device therapies in patients with impaired left ventricular function is rising.¹⁵⁶ Although this may be set to change in the future, at the time of writing, most pacemakers, CRT and ICD devices currently implanted are not MRI compatible, thus prohibiting the use of CMR imaging in this (growing) patient population. Finally, although widely accepted as the reference standard technology for assessing left ventricular systolic function, the considerable cost and expertise required for CMR imaging means access to a dedicated clinical CMR programme is at present limited to specialist centres. Until this changes, or until 3DE becomes routinely available, 2DE will remain the standard by which most clinicians will quantify left ventricular function and subsequently base clinical decisions.

For the reasons above, and due to the portable nature and wide availability of echocardiography, the 2D echocardiogram will continue to play an important role in cardiovascular diagnostics. Due to the recognised limitations of current 2D echocardiographic assessments of LVEF, it is important that clinical research seeks to improve 2DE methods for quantifying global LV systolic function. A 2DE technique that is quick to perform, reproducible, recognises contractile information from all six walls of the left ventricle and makes minimal geometric assumptions is desirable. Furthermore, as the clinical availability of CMR grows, it will become increasingly common to use both

imaging technologies in parallel. For this reason, it is important that CMR and echocardiographic methods used to assess ventricular systolic function have good inter-technique agreement.

1.11.3 New 2DE assessments of left ventricular systolic function

Tissue Doppler Echocardiography (TDE)

Ultrasonic imaging utilizes a physical phenomenon first recognised by Christian Johann Doppler in 1842.¹⁵⁷ The Doppler principle states that when a transmitted ultrasound beam hits a moving object (for example red blood cells) the ultrasound beam is reflected back at an altered, or “shifted” frequency.¹¹³ The magnitude of this Doppler shift frequency is proportional to the velocity and direction in which the moving object is travelling. By ensuring the Doppler beam is directly in line with the direction of myocardial blood flow, the blood flow velocity can be calculated using the Doppler Shift equation (Equation 1.7).

Equation 1.7. The Doppler Shift Equation¹¹³

$$V = \frac{\Delta F \cdot c}{2F_0 \cdot \cos \theta}$$

where: ΔF = Doppler shift frequency
 F_0 = transducer frequency
 c = velocity of sound in tissue (1540m/s)
 θ = angle of incidence (assumed to be 0°
if Doppler alignment correct)

Myocardial tissue movement occurs at an amplitude of forty decibels higher and a velocity ten times slower than myocardial blood flow.¹⁵⁸ By applying standard autocorrelation processing but reversing low amplitude and high velocity filters it is possible to obtain images of tissue Doppler motions of high temporal resolution without significant artefact originating from the blood pool.^{158,159} This is the basis underlying tissue Doppler echocardiography (TDE) techniques.

By employing the above gain/filter settings regional myocardial tissue velocities, strain and strain rates can be recorded throughout the whole of the cardiac cycle with excellent temporal resolutions.

Tissue velocity imaging

Tissue velocity imaging (TVI) allows accurate recording of regional velocity profiles within the myocardium. Using either pulsed-wave TVI or colour TVI with post processing, myocardial velocity profiles can be generated throughout the whole of the cardiac cycle for the basal and mid segments of all LV walls. Ensuring a Doppler angle error of <20 degrees in the apical views, the resultant velocity profiles equate to the velocity profiles of myocardial contraction and relaxation in the longitudinal plane of the heart. The velocity information can be displayed in real-time as colour-coded data superimposed on the two-dimensional grey scale image. With post-processing techniques this data can be displayed as tissue velocity waveforms of mean myocardial velocities. The main disadvantage is the time consuming nature of the offline analysis. Alternatively, online pulsed-wave TVI permits measurement of tissue velocities, within the pre-determined sample volume, over time. This method quantifies peak rather than mean myocardial velocities. It is limited however, in its inability to record data from more than one site at a time, meaning direct comparisons in regional wall motion must be made using different cardiac cycles.

It is important to note with both these techniques, as with all Doppler measurements, correct Doppler alignment is of paramount importance to minimise error. The heart contracts in three directions: radially, longitudinally and circumferentially. Due to Doppler angle dependence, it is only possible to simultaneously assess longitudinal contraction of the basal and mid myocardial segments of the left ventricle using colour tissue Doppler imaging techniques. In the normal heart, the velocities at the base are higher than those at the apex and the velocities in the right ventricle are higher than those in the left. Normal tissue velocity profiles using pulsed-wave tissue velocity imaging and colour-coded tissue velocity imaging with post processing are shown below in Figure 1.15 and Figure 1.16 respectively.

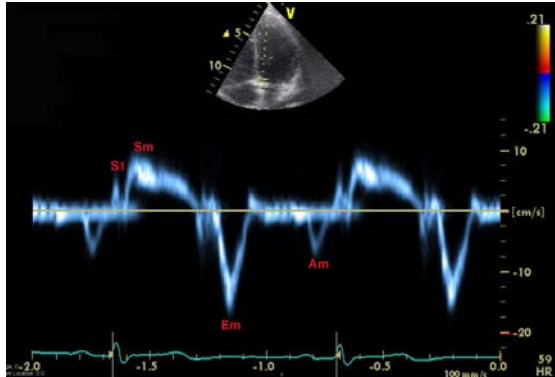


Figure 1.15. Pulsed-wave tissue velocity trace in a normal subject.

S1 = myocardial velocity associated with isovolumic contraction

Sm = peak systolic shortening velocity

Em = peak early diastolic myocardial relaxation velocity

Am = late diastolic myocardial velocity associated with atrial contraction.

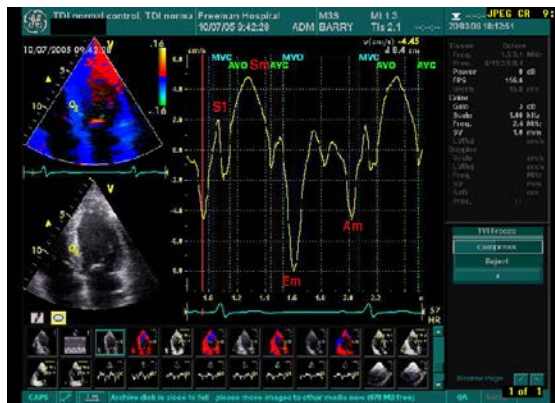


Figure 1.16. Colour coded tissue velocity trace in a normal subject.

S1 = myocardial velocity associated with isovolumic contraction

Sm = maximal systolic shortening velocity

Em = maximal early diastolic myocardial relaxation velocity

Am = late diastolic myocardial velocity associated with atrial contraction

MVC = mitral valve closure

AVO = aortic valve opening

AVC = aortic valve closure

MVO = mitral valve opening

The peak systolic velocities of the basal walls of the LV in a normal heart are as shown in Table 1.6.

PW sample position	Peak systolic myocardial tissue velocity (cm/sec)
Basal septum	7.5 ± 1.3
Basal lateral wall	10.3 ± 1.9
Basal anterior wall	10.3 ± 1.6
Basal inferior wall	9.6 ± 0.9
Basal posterior wall	9.9 ± 1.3

Table 1.6. Pulsed-wave tissue Doppler systolic myocardial velocities of the normal left ventricle.¹⁶⁰

Tissue Doppler strain and strain rate imaging

One of the drawbacks of tissue velocity imaging is that it cannot distinguish between active and passive movement. It is unclear if the velocity profile recorded for a severely hypokinetic/akinetic myocardial segment actually represents the velocity of contraction for that segment or if the segment is being passively dragged inwards by pulling forces from adjacent contracting myocardium.

Lagrangian strain is the degree of myocardial deformation, at a given time point within the cardiac cycle, in relation to end-diastole as the reference point.¹⁶¹ Strain analysis enables calculation of the instantaneous velocity gradient between two sample points at a pre-defined distance. This velocity gradient is then divided by the sample distance to yield the temporal changes of deformation known as myocardial strain rate. The potential advantages of myocardial strain and strain rate over current assessments of LV systolic function are four fold: 1) they allow sensitive assessment of regional myocardial function at high temporal resolutions, far excelling those of the naked eye; 2) the resultant strain graphs are both objective and quantifiable; 3) Strain assesses myocardial deformation not myocardial velocity and so distinguishes between active contraction and passive inward motion of akinetic myocardium being “dragged” inwards by pulling forces from adjacent

observer and intra-observer variability in tissue Doppler strain analysis are high, in the region of >16% compared to $\leq 5\%$ for tissue velocity imaging analysis.¹⁵⁹

While undoubtedly CMR has superior spatial resolution to echocardiography, TDE has the advantage over CMR, by virtue of the fact that it is a real time technique, and unlike CMR is not dependant on frame (phase) averaging. High frame rates with TDE (≥ 100 fr/sec) are readily achievable and so although the spatial resolution is not as good as CMR, the temporal resolution is superior.

Myocardial deformation imaging – 2D Speckle tracking Strain

As previously described, tissue Doppler derived strain imaging is a measure of myocardial deformation. Longitudinal strain, measured from the apical views of the heart, enable quantification of myocardial fibre shortening and therefore, in theory, a very accurate and sensitive representation of regional myocardial systolic function in the longitudinal plane of the heart. As strain imaging can detect differences between active and passive motion, it may be superior to tissue velocity imaging for assessment of left ventricular systolic function. In reality, tissue Doppler strain is prone to both “drift” and “noise” artefact. Due to the angle dependency of tissue Doppler derived strain imaging and the globular nature of the dilated heart, there are further problems with the accuracy of this technique. Furthermore, it is not possible to accurately measure strain values in the apical regions of the heart due to the unacceptable Doppler angles or therefore combine the segmental systolic strain readings to calculate a global strain score for the heart as a whole when measuring myocardial deformation using tissue Doppler methods. The development of 2D speckle-tracking strain imaging has largely overcome these problems. Speckle tracking strain is a Doppler independent measure of myocardial deformation. Speckle tracking strain utilizes a speckle tracking software program which ‘recognizes’ the unique “speckle” patterns within the left ventricular myocardium and tracks their movement throughout the cardiac cycle in an automated manner. As speckle tracking strain is [relatively](#) angle independent it overcomes the problem of reproducibility and enables a segmental strain score to be applied to each of the 16 AHA myocardial segments of the left ventricle. Speckle tracking strain also enables the calculation of strain in the radial plane of the heart.

Although speckle tracking strain has several advantages over tissue Doppler techniques as described above, it also has some limitations. The temporal resolution of 2D speckle tracking strain is inferior to tissue Doppler strain, with achievable frame rates in the region of 50fr/sec in comparison to >100fr/sec with tissue Doppler techniques. While this temporal resolution is still clinically acceptable, and indeed remains superior to CMR, the temporal resolution with newer 3D and 4D speckle tracking software is degraded further, resulting in potential underestimation of true peak myocardial deformation. At present, there are no published normative values for speckle tracking derived strain indices, and this is partly due to the fact that inter-technique concordance between speckle tracking strain software produced by different manufacturers has not been established. Finally, strain imaging, although relatively load independent, is heart rate dependent, thus limiting the clinical usefulness of strain imaging in individuals undergoing dobutamine stress echocardiography.

An example of a radial speckle tracking strain recording taken from the parasternal short-axis view is illustrated in Figure 1.18. An example of a longitudinal speckle tracking strain recording taken from the apical four-chamber (A4C) view is illustrated in Figure 1.19. The normal reference ranges for longitudinal and radial strain are shown in Table 1.7.

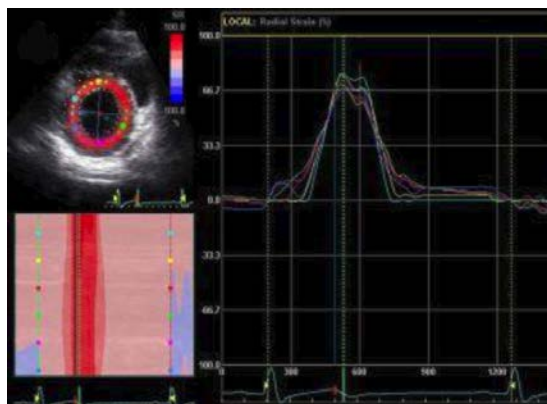


Figure 1.18. Two-dimensional radial strain recording in the apical 4-chamber view of the heart of a subject with normal left ventricular systolic function.

Radial strain is represented as a positive value reflecting the myocardial wall thickening in the radial plane of the LV during systole.

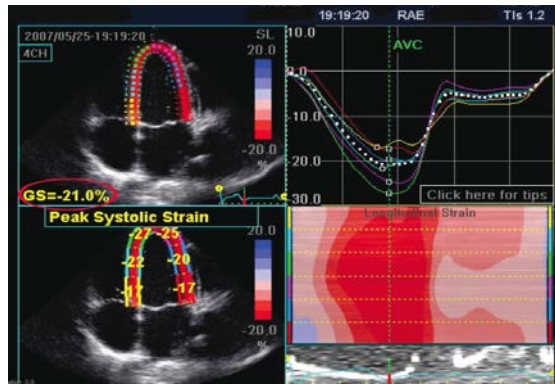


Figure 1.19. Two-dimensional longitudinal strain recording in the apical 4-chamber view of the heart of a subject with normal left ventricular systolic function. A segmental strain score is applied to each AHA myocardial segment. An overall strain score for that apical view is then automatically calculated (circled).

Strain Imaging Plane	Normal Peak Systolic Strain values
Radial strain ¹⁶⁵	+ 41.0 +/- 17.0%
Longitudinal strain ¹⁶⁶	- 18.7 +/- 3.7%

Table 1.7. Reference ranges for longitudinal and radial strain in left ventricle.

1.11.4 The assessment of regional left ventricular systolic function

The assessment of regional left ventricular function is particularly important in patients with ischaemic heart disease due to the nature of the coronary artery blood supply to the left ventricle (as previously highlighted in Figure 1.4). The detection of areas of regional infarction (by low dose viability dobutamine stress echocardiography, nuclear SPECT or delayed enhancement gadolinium magnetic resonance imaging) or inducible ischaemia

using stress-perfusion techniques (such as dobutamine stress echocardiography, nuclear SPECT, adenosine stress-perfusion magnetic resonance imaging and dobutamine stress magnetic resonance imaging) confers important information about the presence and extent of myocardial scar tissue and presence of haemodynamically significant coronary stenoses. In addition to this, viability and stress-perfusion imaging also confer important information on the coronary territory involved and the likely culprit coronary artery, thus in turn giving diagnostically and prognostically useful information to aid decision making for targeting coronary revascularisation procedures.

At a more basic level in patients with known or suspected ischaemic heart disease a standard 2D echocardiogram, as a first line investigation can provide much information on regional myocardial function. Regional wall motion abnormalities in the anterior wall and apex of the left ventricle following chest pain for example, indicates myocardial infarction in the left anterior descending artery territory of the heart. The echocardiographic measurement of the diameter of each myocardial segment in end-diastole has been shown to provide a relatively sensitive measure of myocardial viability. An end diastolic wall thickness (EDWT) $>0.6\text{cm}$ diagnoses the presence of viability in severely hypokinetic/akinetic segments with a sensitivity, specificity and negative predictive value of 80%, 51% and 80% respectively.¹⁶⁷

The American Heart Association 16- and 17-segment models of the left ventricle

To enable a universally standardised description of regional wall motion abnormalities (RWMA), the American Heart Association (AHA) have subdivided the left ventricle into 16 or 17 myocardial segments. The AHA 16 and 17 myocardial segment models of the left ventricle are essentially identical, with the exception of the addition of an apical cap in the 17-segment model. Both models have been endorsed by the American Society of Echocardiography (ASE) and European Association of Echocardiography (EAE) for use in clinical practice.³⁸ The 17-segment model is more commonly used in myocardial stress-perfusion studies and the 16-segment model for the description of resting LV regional wall

motion abnormalities. Figure 1.20 is a schematic representation of the AHA 17-segment model of the left ventricle.

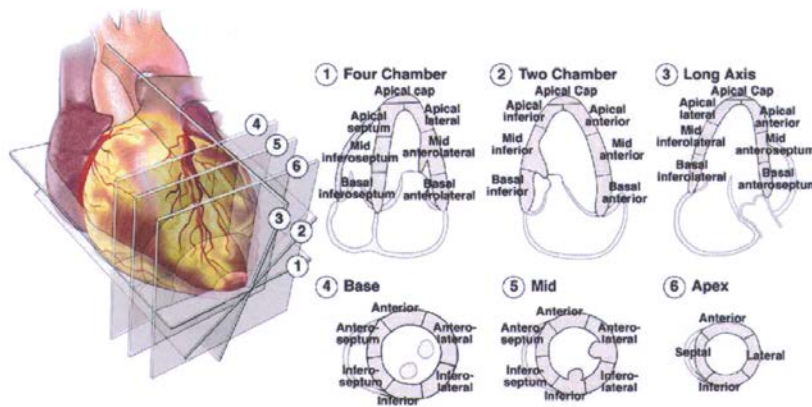


Figure 1.20. The American Heart Association 16- & 17-myocardial segment models of the left ventricle. The schematic below represents the AHA 17-segment model which is often used in stress-perfusion studies. The 16-segment model is more commonly used to assess resting regional wall motion abnormalities, and is essentially the same as the 17-segment model with the exception of the apical cap.³⁸

Regional Wall Motion Scoring

Regional wall motion scoring refers to the regional assessment of systolic function of each of the myocardial segments of the left ventricle. The radial contraction of each myocardial segment is visually assessed by the cardiac sonographer and a score is applied. A score of 0 = hyperkinesis, 1 = visually normal contraction; 2 = hypokinesis; 3 = akinesis; 4 = dyskinesis and 5 = aneurysmal. An overall regional wall motion score index of 1.00 is indicative of normal global left ventricular systolic function. A wall motion score index approaching 3.00 is consistent with severely impaired radial contraction within the left ventricle as a whole. Figure 1.21 highlights the use of regional wall motion scoring to assess regional left ventricular function in a patient with ischaemic cardiomyopathy.





	LAX	SAX	4C	2C
WMSI 2.00				
X - Cannot Interpret 4 - Dyskinetic	0 - Hyperkinetic 5 - Aneurysmal	1 - Normal 6 - Akinetic w/scar	2 - Hypokinetic 7 - Dyskinetic w/scar	3 - Akinetic

Figure 1.21. Assessing regional left ventricular systolic function: Regional wall motion scoring. This patient has ischaemic cardiomyopathy. Akinesis of the inferoposterior LV walls is in keeping with the previously known inferior myocardial infarction and right coronary artery occlusion. There are also wall motion abnormalities in the anterolateral regions of the left ventricle.

LAX, parasternal long axis view; SAX, parasternal short axis view; WMSI, wall motion score index; 4C, apical four-chamber view; 2C, apical two-chamber view.

New assessments of regional left ventricular function

Strain imaging has the advantage over tissue velocity imaging due to the fact that it records myocardial deformation during systolic contraction therefore differentiating between active contraction and passive inward motion of akinetic myocardial segments due to tethering and drag effects from adjacent viable myocardium. The clinical application of tissue Doppler strain is limited due to its high signal to noise ratio, moderately poor reproducibility and angle dependency as previously discussed. Due to the angle dependency of tissue Doppler techniques, radial strain can only be measured in the anterior and posterior walls of the left ventricle in the parasternal short axis view. Longitudinal strain can be assessed in the basal-mid segments of all left ventricular walls in the apical views. The increased angle of incidence between the tissue Doppler beam and apex of the heart means that opposing apical myocardial segments of the left ventricle cannot be assessed from the same cardiac cycle by tissue Doppler strain. The need for manual myocardial tracking throughout systole and long analysis times severely limits the clinical application of this technique for assessing regional myocardial function.

Speckle tracking strain by contrast has semi-automated border tracking and tracks unique myocardial “speckle” patterns through-out systole in an automated and angle independent fashion. The automated nature of this technique makes it potentially highly reproducible and easy to use. Further more, the angle independent nature of the 2D speckle tracking software means that all 16 segments of the AHA model can be analysed, thus giving speckle tracking strain the potential to assess global as well as regional myocardial function. General Electric Automated Functional imaging (AFI) software enables automated quantification of the mean myocardial deformation recorded within each of the 16 AHA LV myocardial segments, using speckle tracking techniques. Speckle tracking AFI imaging therefore provides an alternative sensitive quantitative method for assessing regional (and global) myocardial function of the LV, in addition to current visual assessments of regional LV function.

1.11.5 Concept behind Study 1: Creating a Global Strain Score using regional myocardial deformation imaging to quantify global left ventricular systolic function

The hypothesis behind both Study 1 and Study 2 of this thesis was that methods for analysing regional cardiac function, that encompass a comprehensive assessment of all LV myocardial segments of the AHA-segment model, could potentially be used to quantify global as well as regional systolic function. Further-more, mathematical equations could be derived to convert the sum of the regional LV myocardial segment scores into a global LVEF-equivalent score.

Volumetric assessments of global LV function are load dependent. Furthermore biplane Simpson’s rule makes geometric assumptions as previously discussed. Strain imaging assesses myocardial deformation, therefore should not be subject to changes in loading conditions, and can differentiate between active and passive movement. Longitudinal strain is affected early in cardiomyopathic disease processes and impaired longitudinal strain is therefore an early sensitive marker of left ventricular systolic dysfunction. Two dimensional speckle tracking strain imaging has several advantages over tissue Doppler strain imaging techniques as previously discussed. Currently longitudinal strain speckle

tracking software enables semi-automated quantification of mean longitudinal strain for each of the AHA-16 myocardial segments within the left ventricle. We hypothesised that current speckle tracking software could be utilised to calculate a global strain score for the left ventricle, and that this global strain score would correlate more closely to CMR derived LVEF than biplane Simpson's rule. Furthermore, we believed that the results of this study would enable derivation of a regression equation that would enable the global strain score to be converted in to more easily recognisable LVEF-equivalent score. Finally, due to the semi-automated nature of the speckle tracking, we hypothesised that our new technique would be more reproducible than the currently used biplane Simpson's method.

1.11.6 Concept behind Study 2: Regional wall motion scoring for calculating global left ventricular systolic function

The regional wall motion score index (RWMSI) is a basic but well validated method for quantifying regional radial contraction. By taking the principle of the regional wall motion scoring system and restructuring it to give hyperkinesis a score of 3, normal radial contraction a score of 2, hypokinesis a score of 1, akinesis a score of 0 and dyskinesis a score of -1, we hypothesised that the regional wall motion scoring system could be used to calculate a LVEF-equivalent score by using the equation:

$$\text{LVEF(\%)} = \Sigma(16\text{segRWMS})/16 \times 30$$

Furthermore, we believe there is a significant difference between myocardial segments that are mildly hypokinetic and those that are severely hypokinetic, which are not currently differentiated between in the ASE/EAE endorsed regional wall motion score index. We believed that sub-classifying hypokinetic segments as mild-moderately hypokinetic, and moderately-severely hypokinetic and applying a score of 1.25 and 0.75 respectfully would improve the accuracy of the resultant LVEF calculation.

We hypothesised that this new LVEF index may have a closer correlation and better inter-technique agreement with CMR-derived LVEF (as the reference standard) than 2DE biplane Simpson's rule. The main advantage of this new method for assessing global LV

function is 1) it is quick and easy to perform in clinical practice and 2) it does not require the application of specialist software therefore it can be performed on any echo machine, in any situation by any experienced sonographer anywhere in the world.

1.12 THE NON-INVASIVE ASSESSMENT OF LEFT VENTRICULAR DIASTOLIC FUNCTION

1.12.1 Importance of accurately diagnosing left ventricular diastolic dysfunction

Diastolic heart failure accounts for approximately 50% of all cases of heart failure.¹⁶⁸⁻¹⁶⁹ Originally believed to be a relatively benign condition, it is only in recent years that the true prognostic implications of diastolic heart failure have been recognised.¹⁷⁰⁻¹⁷³ Furthermore, diastolic dysfunction has now become recognised as the primary mechanism responsible for dyspnoea and exercise intolerance in patients with systolic heart failure irrespective of the severity of the systolic dysfunction.^{14,174-176} Diastolic dysfunction is an independent indicator of adverse prognosis in patients with left ventricular systolic impairment.^{53,177-180} For these reasons, the importance of accurate diagnosis of diastolic dysfunction is now recognised by the cardiology community as clinically important. Unfortunately, as diastole is a complex process, the accurate diagnosis and quantification of diastolic impairment is difficult.

1.12.2 Traditional assessments of left ventricular diastolic function

Diastolic dysfunction contributes to symptoms of heart failure due to the elevation of the left ventricular filling pressure.^{181,182} This is associated with a rise in left atrial pressure which promotes pulmonary oedema and dyspnoea. Left ventricular filling pressures are measured invasively during cardiac catheterisation and are directly associated with functional capacity and prognosis in patients with heart failure.^{16,183-185} Because of patient discomfort and the potential complications involved with invasive procedures, the routine use of invasive catheterisation procedures for assessing diastology has decreased significantly over recent years.¹⁸⁶ Over the last two decades, the non-invasive evaluation of

LV diastolic function has been based on echocardiography spectral Doppler LV filling patterns.

Diastole is a complex process that depends on both relaxation of the left ventricle (an active and energy dependent process) and compliance of the left ventricle, which is defined as the volume related pressure changes that occur during diastole.¹⁸⁷ In diastolic dysfunction, relaxation abnormalities occur first, followed by abnormalities of ventricular compliance.⁴² Since diastole is a complex four-stage process, accurate assessment of diastolic dysfunction cannot be traditionally measured echocardiographically from a single diastolic index instead the diagnosis of diastolic dysfunction is based upon a combination of diastolic measurements including mitral inflow patterns, mitral E and A wave deceleration times, abnormal E:A ratios, abnormal pulmonary vein flow patterns and prolonged isovolumic relaxation times (Figure 1.22).

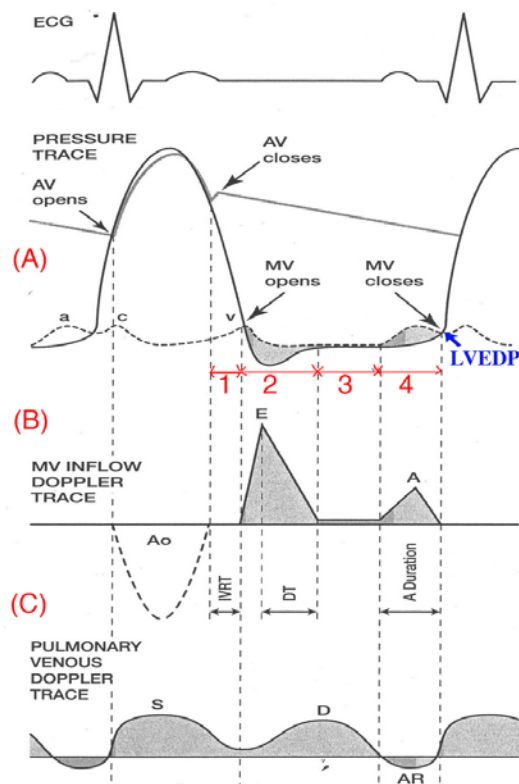


Figure 1.22. Normal diastolic pressure/flow patterns recorded during (A) cardiac catheterisation; (B) mitral inflow Doppler trace during TTE; (C) pulmonary vein flow during TTE.⁴² 1: IVRT, 2: Early passive LV filling, 3: Diastasis, 4: Late LV filling associated with atrial contraction.

AV, aortic valve; DT, deceleration time; IVRT, isovolumic relaxation time; MV, mitral valve; LVEDP, left ventricular end diastolic pressure

Each of the four phases of cardiac diastole can be depicted on the mitral inflow spectral Doppler profile and on the tissue Doppler profile as shown (Figure 1.23). Measurements of these distinct phases are used in the traditional combined assessment of diastolic function as described below.

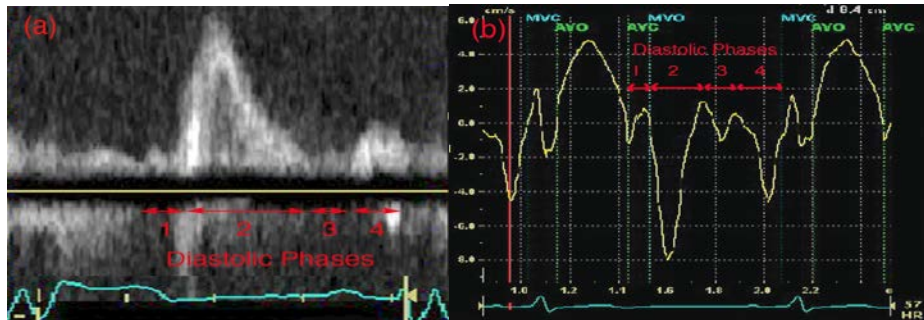


Figure 1.23. The Four Phases of Diastole shown on a (a) Spectral Doppler trace of mitral inflow (b) Tissue velocity trace of mitral annular motion. (1) Isovolumic relaxation (2) Early passive filling (3) Diastasis (4) Late active filling associated with atrial contraction.

Phase 1: Isovolumic relaxation time

Isovolumic relaxation is an active energy dependent process during which the myocytes return to their presystolic length and tension. This event occurs early in diastole and starts with the closure of aortic valve. As the left ventricle actively relaxes, the left ventricular pressure falls without a change in left ventricular volume. Once the left ventricular pressure falls below that of the left atrial pressure, the mitral valve opens, signalling the end of the isovolumic relaxation phase.⁴²

The duration of the isovolumic relaxation period can be measured as the interval between aortic valve closure and mitral valve opening. This is known as the isovolumic relaxation time (IVRT).⁴²

In conditions causing abnormally slow relaxation of the myocardial fibrils, it takes longer for the left ventricular pressure to fall below left atrial pressure, hence mitral valve opening is delayed and the IVRT is prolonged.⁴² In conditions of reduced left ventricular compliance, left atrial pressure is high. Myocardial relaxation is still impaired but the high left atrial pressure largely masks the relaxation abnormalities. In conditions where left

atrial pressure is high, the time taken for the left ventricular pressure to fall below the left atrial pressure is reduced, and so mitral valve opening occurs early and IVRT is short.⁴² Thus changes in IVRT can be used as a marker of Phase 1 diastolic dysfunction.

IVRT is traditionally measured from spectral Doppler flow patterns obtained in the modified apical five-chamber view. A pulsed-wave Doppler trace is recorded by angling the Doppler beam at an intermediate position between mitral inflow and aortic outflow to record both velocities simultaneously. IVRT is measured as the time interval from end of aortic outflow to start of mitral inflow (Figure 1.24).

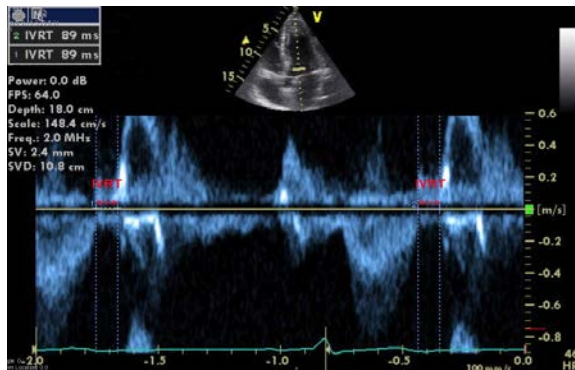


Figure 1.24. Phase 1 Diastole: Measuring the isovolumic relaxation time.

The timing interval from end aortic out flow to commencement of mitral inflow is measured from the spectral Doppler signal recorded at a sweep speed of 100mm/s.

Phase 2: Early passive ventricular filling - Peak mitral E wave velocity and mitral deceleration time

After the mitral valve opens, the early passive left ventricular filling phase starts. Early diastolic filling depends on the magnitude of the pressure gradient between the left atrium (LA) and left ventricle which propels blood into the left ventricular cavity. The rate at which the LA:LV pressure gradient declines is dependent on 1) the elastic recoil of the left ventricle, 2) chamber compliance and 3) left atrial pressure. Normally the rate of left

ventricular filling and left atrial emptying is rapid and approximately 80% of left ventricular filling occurs during this phase.⁴²

In conditions of abnormal left ventricular relaxation, the IVRT is prolonged and delayed mitral valve opening occurs. This causes a reduction in the early transmitral pressure gradient and hence the amplitude of the peak mitral E wave is reduced. As the ventricular myocardium continues to relax in an abnormal fashion, equalisation between left atrial pressure and left ventricular pressure is delayed and so mitral E wave deceleration time is prolonged. Thus reduced E peak velocity and prolonged mitral deceleration time are phase 2 diastolic indices of diastolic dysfunction due to abnormal diastolic relaxation.¹⁸⁸

In conditions causing abnormal left ventricular compliance, left atrial pressure is high and mitral valve opening occurs early. The early transmitral pressure gradient is larger than normal and hence the peak mitral E velocities are abnormally high. Due to the reduced compliance of the ventricle there is rapid equalisation of transmitral pressure resulting in a short deceleration time before the start of diastasis which occurs early. An increased peak mitral E wave velocity and a short mitral deceleration time are phase 2 indices of diastolic dysfunction due to abnormal left ventricular compliance.¹⁸⁸

Mitral inflow patterns are recorded using pulsed-wave Doppler from the apical four-chamber view with the pulsed-wave sample volume located adjacent to the tips of the mitral valve leaflets.¹¹³ Peak mitral E wave velocity is measured as the maximal modal velocity recorded during early diastole (see Figure 1.25). The mitral deceleration time is measured as the interval between the peak mitral E wave velocity and the point of deceleration extrapolated to the zero baseline as shown in Figure 1.25.⁴²

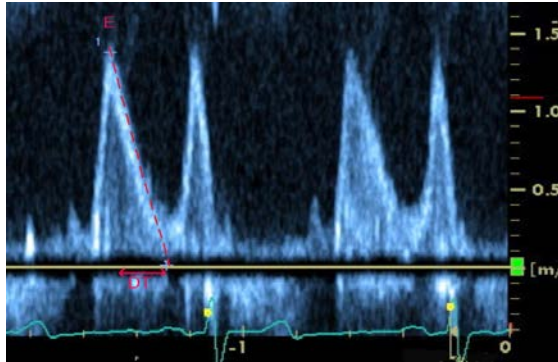


Figure 1.25. Phase 2 Diastole: Early passive ventricular filling - Measuring Peak Mitral E wave and Mitral E wave deceleration time (DT).

Phase 3: Diastasis

Diastasis occurs due to equalization of the pressures across the mitral valve. Despite the equilibrium of pressures reduced blood flow can continue through the mitral valve due to inertia. The duration of diastasis is determined by the heart rate, being longer during bradycardia and shorter during tachycardia. It is therefore not a reliable measure of diastolic dysfunction.

Phase 4: Late active ventricular filling - Peak mitral A wave velocity and E:A ratio

During diastasis, the left atrial and left ventricular pressures are at equilibrium. To enable further left atrial emptying and left ventricular filling, atrial contraction occurs. This increases left atrial pressure and enables a further volume of blood to be propelled into the left ventricular cavity. This final phase of diastole accounts for approximately 20% of left ventricular filling.⁴² The peak velocity generated during left ventricular filling secondary to left atrial contraction is represented by the peak mitral A wave on the Doppler spectrum.

In conditions of abnormal myocardial relaxation, early passive left ventricular filling is reduced and there is a compensatory increase in left ventricular filling due to atrial contraction, thus the peak mitral A valve velocity is increased. This is usually expressed as a ratio of peak E:A. In abnormal diastolic relaxation E:A ratio is reduced.

In conditions of abnormal left ventricular compliance, rapid equalisation across the transmitral gradient occurs along with elevated LVEDP. As a result of the elevated LVEDP, little or no transmitral gradient is re-established during atrial contraction and so the peak mitral A wave is reduced in size or absent. The E:A ratio is increased in conditions due to abnormal left ventricular compliance.

Peak mitral A velocities are recorded as part of the mitral inflow pattern in the manner described above. Peak mitral A wave velocity is measured as the maximal modal velocity recorded during late diastole as shown in Figure 1.26 and E:A ratio is then calculated.

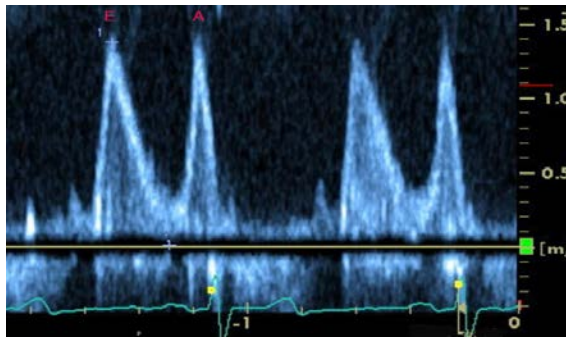


Figure 1.26. Calculating the E:A ratio. In this example the peak E wave and A wave velocities were identical at 1.48m/s giving a ratio of 1:1.

Caveat

As myocardial disease progresses there may be a transition from predominantly abnormal diastolic relaxation to restrictive physiology (reduced left ventricular compliance and elevated left atrial pressure). During this period the transmitral inflow pattern may look normal despite the presence of significant diastolic dysfunction. This is known as “pseudonormalisation”.⁴² In patients exhibiting a pseudonormal inflow pattern, it is traditional to perform a Valsalva manoeuvre to unmask the underlying diastolic abnormalities. Abnormal mitral annular velocities confirm the diastolic abnormalities in this cohort of heart failure patients as described in section 1.10.3.

Abnormalities recorded in traditional echocardiographic indices of diastolic function occur in a U-shaped non-linear fashion, depending on whether impaired ventricular relaxation or restrictive LV filling predominates (see Table 1.8). Thus traditional indices of diastolic function are best used to describe the grade of diastolic function determined by the overall LV filling pattern, rather than used as quantitative nominal variables. Diastolic impairment is traditionally graded as 1) abnormal relaxation 2) pseudonormal 3) restrictive filling as shown in Figure 1.27. Restrictive left ventricular filling patterns, are associated with greater filling pressures and a worse prognosis than left ventricular filling patterns consistent with abnormalities predominantly of diastolic relaxation.¹⁸⁹ Furthermore, although mitral filling patterns have shown to correlate with invasive diastolic pressure recordings in patients with dilated cardiomyopathy, traditional mitral inflow indices of diastolic function correlate poorly with haemodynamic data in patients with normal or near normal LVEF (LVEF>50%).^{13,14,190-192}

Diastolic Parameter	Abnormal Range	Normal Range	Abnormal Range
Mitral E wave (m/s)	<0.4	0.4-1.0	>1.0
E:A ratio	<0.7	0.7-3.1	>3.1
MV DT (ms)	<139	139-219	>219
IVRT (MS)	<54	54-100	>100

Table 1.8. Normal and abnormal ranges of diastolic function (95% Confidence Intervals).¹⁸⁸

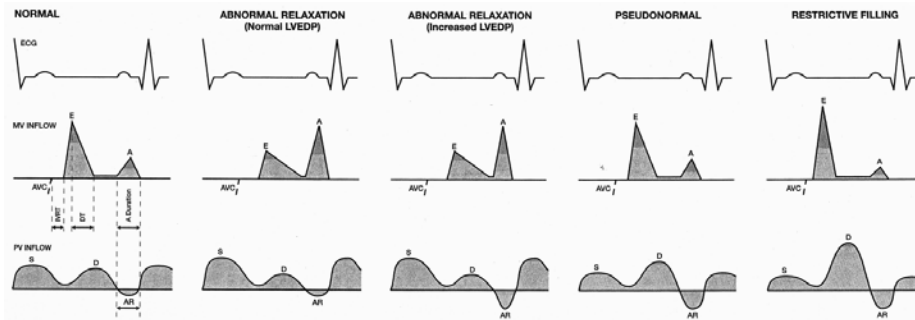


Figure 1.27. Left ventricular filling patterns in diastolic dysfunction.

Mitral inflow and pulmonary vein flow patterns in normal diastolic function through to progressively severe diastolic dysfunction as shown⁴²

Thus one of the major drawbacks of using IVRT, E/A ratios, mitral deceleration times and pulmonary vein flow patterns to assess diastolic function, is that they are only semi-quantitative, making it difficult to assess absolute improvements in diastolic function in response to treatment strategies. A further drawback of these methods, is that the results are dependent on the haemodynamic loading conditions of the heart.¹⁸⁹

1.12.3 New assessments of left ventricular diastolic function

Echocardiography: Mitral annular peak early diastolic relaxation velocities (Em), E/Em and the non-invasive estimation of left ventricular end diastolic filling pressure

Elevated LVEDP occurs when significant diastolic dysfunction is present. In the absence of significant mitral valve disease LVEDP approximately equals mean left atrial pressure (mLAP), which in turn, approximates pulmonary capillary wedge pressure (PCWP). LVEDP and PCWP are measured invasively at the time of left and right heart catheterisation respectively (see Figure 1.22 above). In the last decade much work has been done looking at peak early diastolic tissue relaxation velocities at the mitral valve annulus (Em). Em, provides an index of left ventricular relaxation that is relatively independent of preload.^{5,193-195} In addition to providing load-independent information, Em can be used to differentiate between normal and pseudonormal filling patterns.⁴² Em velocities have been

shown to be reproducible.^{193,194,196} They also have the advantage of being quantifiable. An Em velocity recorded from the septal side of the mitral valve annulus (Em(s)) of <8cm/s has been shown to accurately predict impaired diastolic relaxation with a sensitivity of 73% and a specificity of 100%.¹⁹⁷ The normal values for Em velocities recorded from the septal, lateral, anterior and inferior sides of the mitral valve annulus are shown in Table 1.9.

Mitral Annular Position	Em (cm/sec)
Basal septum	12.3 ± 2.8
Basal lateral wall	15.8 ± 3.8
Basal anterior wall	13.7 ± 4.0
Basal inferior wall	13.6 ± 3.6

Table 1.9. Pulsed-wave tissue Doppler myocardial early relaxation velocities of the normal left ventricle¹⁹⁷

The ratio of E/Em (where 'E' is peak velocity of mitral inflow during early passive filling and Em is the peak tissue velocity of early diastolic relaxation at the mitral valve annulus) has been shown to correlate with invasive LVEDP measurements and PCWP measurements.^{4,9} For example, Agricola *et al* demonstrated E/Em(s) >10 predicts elevated left ventricular filling pressure (LVEDP >15) with a sensitivity and specificity of 90% and 83% respectively.¹⁹⁸ Bruch *et al* demonstrated an E/Em >15 has a sensitivity and specificity of 80% and 100% respectively for predicting an LVEDP ≥15.¹⁹⁹ Ommen *et al* assessed the clinical utility of E/Em in patients with both normal and impaired LV systolic function. They reported that E/Em correlated better with mean LV diastolic pressure measured using micromanometer-tipped catheter than any other traditional echocardiographic index of LV diastolic function over a wide range of LVEFs (r=0.64) and when confined to a patient cohort with documented coronary artery disease (r=0.65).⁴ Furthermore, they reported that their correlations with invasive diastolic pressure measurements were consistently equivalent or better when Em was measured at the septal side of the mitral annulus, compared to the lateral mitral annulus, or the combination of the septal and lateral mitral annulus. Subsequent studies have noted that in patients with normal LVEF, E/Em ratios have the best correlations with LV filling pressures and invasive

indices of LV stiffness when Em is recorded from the lateral mitral annulus.^{6,200} Based on these and other studies, an Em(S) >8cm/s and Em(L) >10cm/s reflect normal mitral annular early diastolic relaxation velocities.¹⁴ E/Em >15 is believed to indicate elevated diastolic filling pressures and E/Em ≤8, to indicate normal filling pressures, with E/Em of 8-15 representing a grey area when Em is measured at the septal mitral annulus.¹⁴ When Em is measured at the lateral mitral annulus, E/Em >12 indicates elevated diastolic filling pressure^{14,201} An example of a pulsed-wave Em recording is shown in Figure 1.28. and examples of E/Em diastolic patterns are shown in Figure 1.29. Using these two methods, (Em and E/Em) changes in diastolic function can be recorded quantitatively.

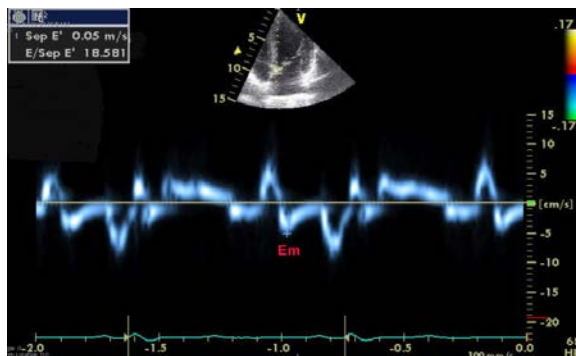


Figure 1.28. Example of a pulsed-wave tissue Doppler velocity trace of the mitral annulus. The peak mitral annular early diastolic relaxation velocity (Em) was recorded as shown. In this example taken from the septal mitral annulus of a patient with dilated cardiomyopathy, Em = 5cm/s which is significantly reduced.

The physiology behind E/Em as an estimate of LV diastolic filling pressure

At end systole, cardiac myocytes are in a contracted state, and the elastic properties of the LV myocardium are compressed and twisted resulting in stored energy within the myocardium. Relaxation of myocardial contraction results in release of this energy which causes LV pressure to fall rapidly during isovolumic relaxation. Under normal conditions the rate of relaxation of the LV wall tension is rapid enough to cause the LV pressure to continue to decline after mitral valve opening. This fall in LV pressure produces an early diastolic pressure gradient from the LA to LV which “sucks” blood from the atria down

towards the LV apex. The rate of early LV filling is determined by the size of this LA-LV pressure gradient. The lower the early diastolic LV pressure is, the greater the gradient for filling, enabling the LV to fill without requiring an elevated left atrial pressure (LAP). The ability of the normal heart to decrease the early diastolic LV pressure in response to stress enables an increase in cardiac stroke volume without much increase in LAP. Relaxation properties of the LV are affected early in myocardial dysfunction, and the ability of the heart to increase LV filling without an increase in LAP is reduced or absent in heart failure.²⁰¹⁻²⁰³ Changes in LV filling through progressive grades of diastolic impairment can be non-invasively assessed from Doppler measurements of mitral inflow (E and A) and measurements of peak early mitral annular myocardial tissue relaxation velocities (Em). As the cardiac apex remains fixed throughout the cardiac cycle, Em provides a measure of the long-axis lengthening rate of the LV in early diastole. Under normal conditions, Em occurs at the same point in diastole as the peak transmitral E wave velocity as a result of the symmetrical expansion of the LV during early diastolic filling. In Grade 1 diastolic dysfunction, diastolic relaxation of the LV is impaired but without a significant increase in LAP. This results in a decrease in both E and Em, an increase in the peak transmitral A wave velocity reflecting the increased importance of atrial contraction to maintain LV filling, and E/A is <1 (Figure 1.29 below). With progressively worsening diastolic dysfunction, LVEDP rises closely followed by a rise in LAP, resulting in restoration of the early diastolic LA-LV pressure gradient, and pseudonormalisation of the transmitral E velocity, despite elevated LV filling pressures (Grade 2 diastolic dysfunction). As LV relaxation becomes more impaired Em becomes both reduced and delayed and occurs after E, suggesting that in \geq Grade 2 diastolic dysfunction, the LV does not expand in a symmetrical manner in diastole, but instead long-axis lengthening and propagation of blood to the LV apex occurs after the LV is filled by movement of blood into the LV inflow tract across the LA-LV gradient. In the presence of impaired relaxation, Em does not occur during the time of the LA-LV pressure gradient, so Em is both delayed and reduced and becomes almost independent of LAP.^{201,204} Em therefore provides a quantitative preload independent measure of diastolic function in situations of elevated LAP.²⁰¹ In addition to this, both the peak Em velocity and the delay in Em relative to E, directly correlate with the time constant of LV relaxation.²⁰⁵⁻²⁰⁷ The peak transmitral E wave velocity is altered directly by changes in LAP and inversely by changes in the time constant of LV relaxation. Dividing E by Em effectively corrects for changes in the time constant of LV relaxation,

therefore changes in E/Em ratio should closely reflect changes in LAP giving a non-invasive estimate of left ventricular filling pressure. Thus in Grade 2 diastolic function, the pseudonormal mitral filling pattern is distinguished from normal by reduced and delayed Em, and an elevated E/Em ratio reflecting the rise in LAP. In severe Grade 3 diastolic dysfunction, filling is restrictive and LV diastolic filling pressures are very high – this is reflected in marked elevation of E/Em ratio (Figure 1.29).

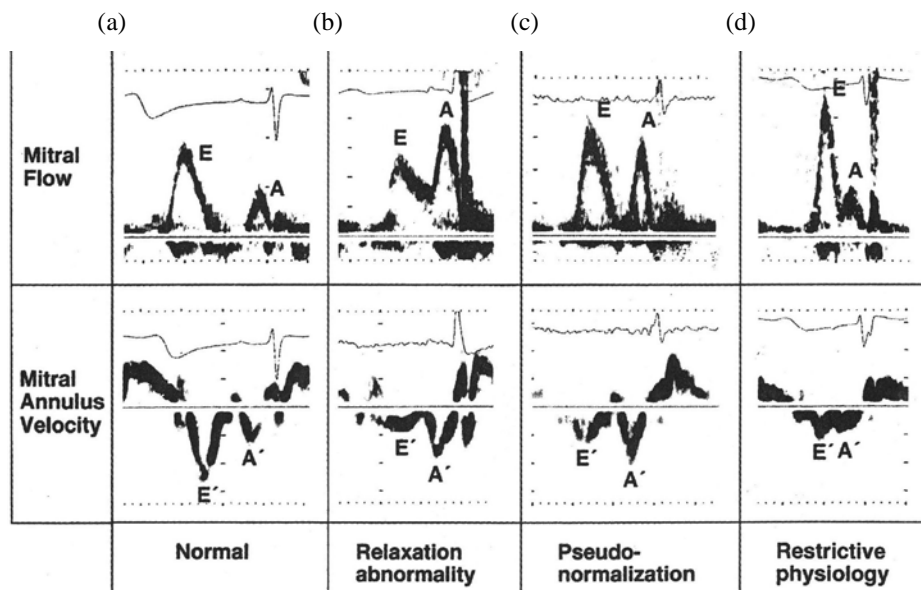


Figure 1.29. Diastolic dysfunction: Patterns of abnormal mitral inflow velocities and mitral annular diastolic relaxation velocities (b) Grade 1 Diastolic dysfunction, (c) Grade 2 diastolic dysfunction and (d) grade 3 diastolic dysfunction, compared to normal diastolic function (a).⁴²

Not only has E/Em been shown to correlate with elevated diastolic filling pressures, both Em and E/Em ratios confer important prognostic information. Elevated filling pressures are associated with increased mortality in heart failure patients. Wang et al have demonstrated an incremental survival benefit in heart failure patients with $Em > 3$ and $E/Em \leq 15$ at one year follow-up.⁵⁴ This survival benefit was not only maintained, but cumulatively

increased over 5 years (see Figure 4.2.9).⁵⁴ Subsequent studies have confirmed the prognostic importance of E/Em in differing patient cohorts.^{10,11,208-214}

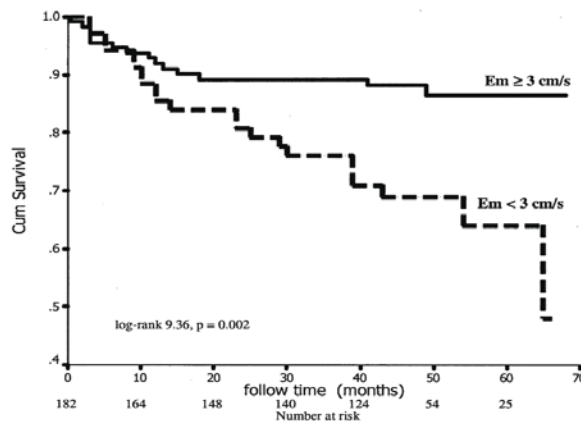


Figure 1.30. Kaplan-Meier curve demonstrating survival benefit in patients with an early peak diastolic mitral annular relaxation velocity ≥ 3 compared to < 3 cm/s.⁵⁴ Cum; cumulative.

The assessment of diastolic function by cardiac magnetic resonance imaging

At the time of writing there is no standard CMR method for diagnosing and quantifying left ventricular diastolic dysfunction in clinical practice. Small single centre studies have explored the potential of using grid-tagged myocardial deformation CMR imaging sequences to assess diastolic relaxation.²¹⁵⁻²¹⁹ This has increased our understanding of left ventricular torsion and the contribution of diastolic “untwisting” and LV suction to LV filling in early diastole.²¹⁸⁻²²⁰ Diastole however is a multi-stage process and CMR myocardial deformation imaging has limited ability to assess late diastolic events due to the degradation of the grid-tags in end-diastole.²²¹ Azevedo and colleagues²²¹ have recently developed a method of assessing diastolic strain rate which shows potential but needs to be validated in a larger prospective study.²²² While myocardial deformation imaging by CMR shows potential, it is not yet applicable to clinical practice. Furthermore, grid-tagging analysis software is at present available in only a few specialist centres, further limiting the

clinical applicability of this technique. Research studies have demonstrated a relatively good correlation between CMR and echocardiography for calculating E/A ratios using VEC-CMR sequences, however, the same problems surrounding the load-dependent nature of these indices remains.²²³⁻²²⁵

1.12.4 Current Guidelines for evaluating left ventricular diastolic function

Currently, invasive cardiac catheterisation remains the gold standard for quantifying left ventricular diastolic filling pressures (see Table 1.10), with Doppler echocardiography as the non-invasive standard by which left ventricular diastolic function is assessed in most cases.

Catheter derived Pressures	Average (mmHg)	Range (mmHg)
PCWP (mean)	9	4-12
LAP		
- a wave	10	4-16
- v wave	12	6-21
- mean	8	2-12
LVP		
- peak systolic	130	90-140
- end diastolic	8	5-12

Table 1.10. Normal Intracardiac Pressures.²²⁶

In the absence of mitral valve disease and pulmonary arterial hypertension, mean pulmonary capillary wedge pressure, mean left atrial pressure and left ventricular end-diastolic pressure approximate each other.

PCWP, pulmonary capillary wedge pressure; LAP, left atrial pressure; LVP, left ventricular pressure.

Due to the increased prevalence of diastolic heart failure, and recognition of its prognostic implications the joint EAE and ASE writing group have recently stated that “the assessment of left ventricular diastolic function and filling pressures is of paramount clinical

importance".¹⁴ Increasing evidence surrounding the use of tissue Doppler E/Em ratios to estimate left ventricular filling pressures has led the EAE/ASE joint task force to recently publish revised guidelines for assessing LV diastolic function (these new guidelines were published following recruitment completion of this thesis study population).¹⁴ When using E/Em calculations, the new EAE/ASE guidelines recommend Em is recorded using pulsed-wave tissue Doppler with a sweep-speed of 50-100mm/s at end-expiration. For the assessment of global diastolic function acquisition, measurement and averaging of tissue Doppler signals from a minimum of two sides (the septal and lateral sides) of the mitral annulus is recommended, to minimise the effects of regional wall motion abnormalities on these velocities.^{14,227}

There are several situations in which E/Em may not provide an accurate representation of LV diastolic filling pressure. Firstly, Em is usually reduced in patients with mitral stenosis, significant mitral annular calcification, surgical mitral rings and mitral prostheses. Secondly, peak mitral E wave is elevated in patients with moderate to severe primary mitral regurgitation and normal LV relaxation, due to increased flow across the regurgitant mitral valve. Both these situations may lead to a falsely elevated E/Em ratio.¹⁴ Finally, E/Em does not increase in patients with constrictive pericarditis despite the presence of elevated filling pressures. In constrictive pericarditis annulus paradoxus may occur – whereby E/Em becomes inversely proportional to the severity of the constriction and degree of elevation of the LVEDP. This is because of an increase in Em which is believed to be due to relative preservation of LV longitudinal expansion compensating for the limited lateral and anteroposterior diastolic excursion.²²⁸ In these situations, E/Em should not be used to estimate LV diastolic filling pressure.

A recent paper, published since completion of our study recruitment, suggests E/Em may not provide accurate assessment of pulmonary capillary wedge pressure (a surrogate marker of LAP and LVEDP) in the structurally normal heart.²²⁹ Although in general terms E/Em is relatively independent of haemodynamic loading conditions, in the normal heart Em is related to preload and responds to changes in LAP. This was demonstrated by Masutani et al in normal experimental animals where E/Em was demonstrated to actually decrease, not increase, in response to massive fluid loading.²²⁹ A further study by Mullens et al, also published since completion of our study recruitment, failed to demonstrate a clear

relationship between E/Em and pulmonary capillary wedge pressure in patients with severe LV systolic impairment (LVEF \leq 30%) leading the research group to conclude that tissue Doppler E/Em was not reliable in predicting LV filling pressures in advanced systolic heart failure.¹⁶ These later studies, in conjunction with the exclusion criteria above, now call into question the accuracy of echocardiographic E/Em ratios for the quantification of LV diastolic filling pressures in routine clinical practice.

Based on a meta-analysis of current research, the new revised EAE/ASE guidelines¹⁴ recommend a differing stepwise approach to assessing diastology in patients with preserved and impaired left ventricular systolic function as shown in Figures 1.31 and 1.32.

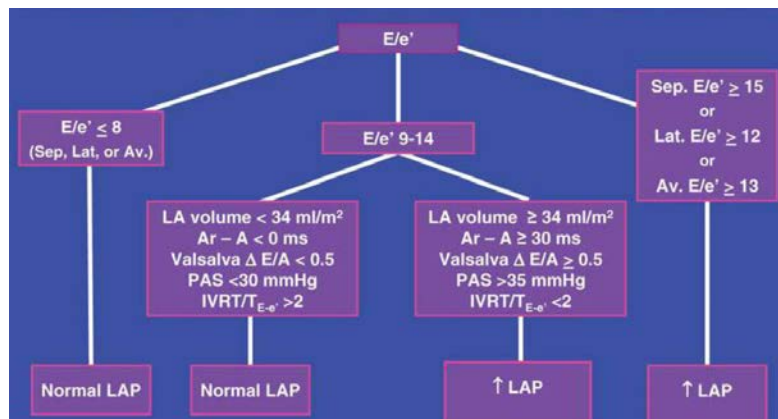


Figure 1.31. EAE/ASE diagnostic algorithm for the estimation of left ventricular filling pressures in patients with normal LVEFs.¹⁴

A, mitral A wave associated with left atrial contraction; Ar-A, the time difference between the pulmonary vein Ar wave duration and the mitral A-wave duration; Av, average; E, peak early mitral inflow velocity; e', mitral annular early diastolic relaxation velocity; IVRT, isovolumic relaxation time; LA, left atrial; LAP, left atrial pressure; Lat, lateral; PAS, pulmonary artery systolic pressure; T_{E-e'}, the time interval difference between QRS onset and E, and QRS onset and e'.

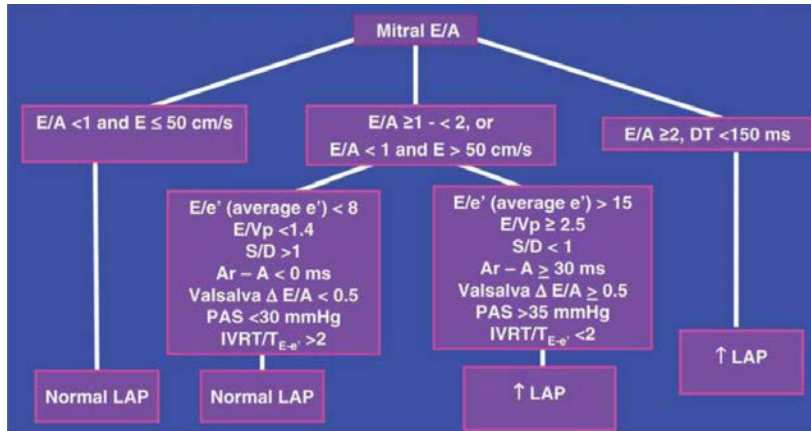


Figure 1.324. EAE/ASE diagnostic algorithm for the estimation of left ventricular filling pressures in patients with impaired LVEFs.¹⁴

A, mitral A wave associated with left atrial contraction; Ar-A, the time difference between the pulmonary vein Ar wave duration and the mitral A-wave duration;; D, pulmonary venous diastolic flow velocity; E, peak early mitral inflow velocity; e', mitral annular early diastolic relaxation velocity; IVRT, isovolumic relaxation time; LA, left atrial; LAP, left atrial pressure; Lat, lateral; PAS, pulmonary artery systolic pressure; S, pulmonary venous systolic flow velocity; T_{E-e'}, the time interval difference between QRS onset and E, and QRS onset and e'; Vp, flow propagation velocity.

1.12.5 Concept behind Study 3: VEC-CMR for the estimation of left ventricular end-diastolic pressure

CMR is now the accepted reference standard for the quantification of left ventricular systolic function. In the future, if CMR is to fulfil it's potential as a "one-stop" imaging modality for anatomical and functional imaging of the heart, an accurate, reproducible and clinically applicable method of quantifying left ventricular diastolic function needs to be developed.

VEC-CMR imaging sequences are part of all standard clinical CMR imaging packages and can be analysed off-line with standard proprietary software. The concept behind Study 3 of this thesis was that VEC-CMR could be used to assess left ventricular diastolic function. We hypothesized that we could modify the amplitude of the bipolar field gradient used in

phase encoded velocity mapping sequences to enable early tissue relaxation velocities of the basal left ventricular myocardium (Em) to be recorded and measured in a manner analogous to tissue Doppler echocardiography techniques. A standard VEC-CMR sequence would then be used to record the early peak mitral inflow velocity (E). The feasibility of using VEC-CMR to detect early diastolic relaxation abnormalities would then be assessed by comparing CMR-derived Em with Em values recorded using pulsed-wave tissue Doppler. The VEC-CMR sequences would then be used to calculate an E/Em ratio which will be compared to LVEDP measured during cardiac catheterisation in subjects exhibiting a wide range of LVEF's. We aimed to establish if VEC-CMR E/Em could be used as a surrogate measure of LVEDP. The overall aim was to create a novel, accurate and user-friendly method of assessing left ventricular diastolic function by cardiac magnetic resonance imaging.

1.13 THE NON-INVASIVE ASSESSMENT OF RIGHT VENTRICULAR FUNCTION

1.13.1 The prognostic importance of right ventricular function

Prognostic studies have confirmed that RV function is a major determinant of morbidity in both heart failure^{230,231} and pulmonary disease,^{232,233} with poor outcome in patients with impaired RV long axis function and associated vena cavae and right atrial dilation.^{230,234-236} Since RV function has been shown to be a sensitive marker of exercise tolerance and outcome in a number of cardiac syndromes, identifying the most sensitive markers of RV dysfunction is of immense clinical importance.²³⁰

1.13.2 Volumetric assessments of global right ventricular systolic function:

By Cardiac Magnetic Resonance imaging

There is no “gold standard” for the quantification of RV systolic function. However, as CMR volumetric assessment of the cardiac ventricles is not limited by the anatomy of the thorax or subject to geometric limitations, Simpson’s method of discs by CMR for the

quantification of RVEF is largely considered to be the non-invasive reference standard for accurately assessing RV systolic function. The two most commonly used RV structure and function acquisition protocols, endorsed by the Society for Cardiac Magnetic Resonance imaging (SCMR), include steady state free precession cine imaging in the RV short axis and trans-axial orientations,²³⁷ although other RV image acquisition protocols are available.²³⁸

By 3D Echocardiography

During the recruitment period of this study, 3DE RV volume and ejection fraction quantification software was not commercially available. Since completion of this project 3DE software has been developed and pooled data from a few small single centre studies and one larger study suggest the assessment of RVEF is feasible by 3DE, using either the 3D disc summation or apical rotational methods, with a lower reference limit for RVEF of 44%.²³⁹ Van der Zwaan²⁴⁰ and others²⁴¹⁻²⁴³ have reported intermodality discordance between CMR and 3DE for assessing RV function with RV volumes being underestimated by 3DE when compared to CMR. This is believed to be due to the lack of precise endocardial border definition by RT3DE, which in turn is due to a combination of 1) poor visualisation of the anterior RV wall segments by RT3DE, 2) the presence of the abundant RV trabeculae and 3) the variation in the definition of the RV basal regions and RVOT. Furthermore, RV dysfunction is often secondary to pulmonary disease and pulmonary hypertension. Echocardiographic windows, especially RV windows, are often more difficult in patients with pulmonary disease. Due to differing 3DE RVEF quantification methodologies, limited normative data and a paucity of data for patient cohorts with significant RV dilatation and dysfunction, at present the American Society of Echocardiography (ASE)/ European Association of Echocardiography (EAE)/ Canadian Society of Echocardiography (CSE) 2010 joint guidelines for assessing the right heart, do not endorse the use of 3DE for the diagnosis of RV dysfunction in clinical practice.³⁷

By 2D Echocardiography

The complex geometry of the RV and its anatomical relationship to the LV in addition to the limited 2DE views obtainable of the RV means it is not possible to accurately measure

RV volumes using 2DE. Although biplane Simpson's rule and area-length methods have been used to quantify RVEF in past research studies, due to multiple geometric assumptions, these methods are inherently inaccurate. Volumetric assessment of RVEF by 2DE is therefore not recommended by the ASE, EAE or CSE.³⁷

1.13.3 Non-volumetric assessments of global right ventricular systolic function

Due to the limited availability of CMR, 2DE remains the first line imaging modality for assessing RV function. For the reasons described above, volumetric assessment of RV systolic function is not recommended. As a result a visual "eyeball" assessment of RV function remains the 2DE standard in clinical practice by which the RV is assessed. This method is only semi-quantitative. Furthermore Miller and colleagues have elegantly demonstrated the high and disparate inter-observer variation in the visual assessment of the RV.²⁴⁴ In an era where complex multi-model imaging technologies are available, and the diagnosis and prognostic importance of RV dysfunction is now well recognised, such a subjective assessment of RV function is clearly suboptimal. The need for quantitative 2DE measures of RV performance, has recently led to the development of several non-volumetric indices of RV systolic function using M-Mode, Doppler, tissue Doppler and myocardial deformation echocardiographic imaging techniques. A variety of small single centre studies have demonstrated correlation of these techniques with alternative cardiac imaging modalities including CMR, nuclear ventriculography and right heart catheterisation in addition to providing independent prognostic information.^{243,245-255} In response, the ASE, in conjunction with the EAE and CSE, published in 2010, revised guidelines for the echocardiographic assessment of the right heart in adults. In this paper, they summarize the available non-volumetric indices of RV systolic function from pooled data, and recommend that at least one quantitative measure of RV systolic function, for which there is normative data available (i.e. fractional area change, tricuspid annular plane systolic excursion (TAPSE), peak systolic pulsed wave tissue velocity (PWTDE S') and myocardial performance index (MPI)) be incorporated into the routine echocardiographic examination and report in addition to a visual assessment of RV function.³⁷ However, these guidelines make no recommendation as to which of these non-volumetric indices of RV function should be used. To our knowledge, there have been no head-to-head studies comparing these new techniques and currently it remains unclear which technique, if any, is

superior to the others and which has the best reproducibility. The differing non-volumetric techniques for assessing RV systolic function are discussed below:

RV Fractional Area Change

The geometric complexity of the RV and its orientation within the thorax prevents accurate volumetric quantification of RVEF by 2DE. The percentage change in RV area between end systole and end diastole acts as a ~~two-~~dimensional surrogate marker of RVEF. RV area is measured in end diastole and end systole from an optimised apical four chamber view, by tracing the RV endocardial border along the RV free wall from the lateral tricuspid annulus to the apex, from the apex along the interventricular septum to the medial tricuspid annulus, and from medial to lateral sides of the tricuspid annulus. The RV fractional area change (FAC) is then calculated as:

Equation 1.8. Calculating RV fractional area change³⁷

$$\text{RV FAC (\%)} = \frac{\text{RV ESA}}{\text{RV EDA}} \times 100 \quad \begin{array}{l} \text{where: ESA=end systolic area} \\ \text{EDA=end diastolic area} \end{array}$$

RV FAC has been shown to correlate with RVEF by CMR, and the ASE/EAE recommend a lower normative reference value of 35%.³⁷

RV Myocardial Performance Index

The myocardial performance index (MPI) is a well described Doppler derived index that incorporates assessment of systolic and diastolic function and is calculated by the equation: $\text{MPI} = (\text{IVCT} + \text{IVRT})/\text{ET}$. As myocardial function declines, ejection time is shortened and the isovolumic contraction and relaxation periods are lengthened. MPI is therefore inversely proportional to ventricular function. The use of the MPI as a surrogate marker of LV performance is now validated across a range of cardiac conditions.²⁵⁷⁻²⁶⁵ MPI is independent of heart rate and LV geometry. Furthermore its value as a prognostic indicator of cardiac outcome is now recognised. More recently however, Lavine et al have demonstrated that MPI is load dependent and this is seen as a significant limitation to the

use of the technique as a prognostic indicator of LV function.^{266,269} Paradoxically, the afterload dependency of the MPI, seen as a limitation in LV studies, may prove advantageous when applied to the RV. RV dysfunction is commonly secondary to conditions causing pulmonary hypertension. In practical terms, the echocardiographic assessment of RV function should always be accompanied by the non-invasive estimation of pulmonary artery systolic pressure (PASP). Currently this is achieved by measuring the maximal tricuspid regurgitation (TR) jet velocity and calculating the TR pressure gradient using the modified Bernoulli equation. However, a substantial proportion of individuals have insufficient TR to enable TR velocity measurement and hence PASP estimation. It is possible that the afterload dependency of the MPI means that when applied to the RV, changes in the RV MPI is a reflection of both RV performance and PASP and this warrants further investigation. The RV MPI has been shown to have prognostic value in patients with pulmonary hypertension and changes in RV MPI correlate with change in clinical status in this group.²⁷⁰

The right-sided MPI has now been measured in >1000 normal control subjects across 23 studies with an upper normative reference limit of 0.40 when measured by pulsed-wave spectral Doppler and 0.55 when measured using the tissue Doppler method.³⁷ Although RV MPI has been studied in selected patient populations with RV infarction,²⁷¹ pulmonary hypertension,²⁷⁰ hypertrophic cardiomyopathy²⁷² and congenital heart disease,^{273,274} the use of MPI for assessing RV performance in clinical practice in an unselected cohort of patients exhibiting a wide range of RVEFs is not well established. A limitation of RV MPI is that it is technically more difficult to measure accurately than LV MPI due to shorter RV isovolumic relaxation times. Pseudonormalised values may also occur in situations where the isovolumic contraction time is shortened due to an acute increase in RV diastolic pressure, as occurs in the setting of acute RV myocardial infarction.²⁷⁵

RV MPI can be measured from spectral Doppler patterns of tricuspid inflow and pulmonary outflow, or from a pulsed-wave tissue Doppler velocity profile acquired at the lateral tricuspid annulus.³⁷

RV Strain

The use of myocardial deformation imaging to assess LV systolic function has been discussed previously in section 1.11.3. Global longitudinal strain of the RV and of the RV free wall can be measured using 2D speckle tracking software. Due to the predominant long axis contractility of the RV in the normal heart, RV longitudinal strain is greater than radial strain.^{276,277} The use of RV speckle tracking strain to quantify global RV function should in theory be highly reproducible due to the semi-automated nature of the analysis software, and angle independent. RV strain has also been shown to be relatively load-independent.²⁷⁸ In the clinical research setting, myocardial deformation imaging appears sensitive enough to discern changes in longitudinal strain values in the right ventricles of patients before and after lung transplantation,²⁷⁹ in patients with ischaemic heart disease²⁸⁰ and in patients suffering acute pulmonary embolism.²⁸¹ RV strain analysis may therefore be a potentially good method for quantifying RV function in clinical practice. At present, due to the lack of normative data, this technique is not recommended by the ASE/EAE/CSE for routine clinical use.³⁷

ASSESSMENTS OF TRICUSPID ANNULAR MOTION

Rushmer and Krystal first noted that the RV ejects blood primarily by contraction of the walls in the longitudinal axis, drawing the tricuspid annulus towards the cardiac apex.²⁸² In healthy adults it has been shown that the tricuspid annulus has the greatest motion along its lateral aspect. As a result of these observations several differing measures of tricuspid annular motion have been developed as markers of RV systolic function.

Tricuspid annular plane systolic excursion

Tricuspid annular plane systolic excursion (TAPSE) is an M-Mode measure of RV long axis function and has been shown to correlate with haemodynamic indices of RV function²⁸⁴ and RVEF calculated using radionuclide angiography²⁸⁵ and CMR.²⁸⁶ In a study of 900 patients and normal controls a TAPSE ≤ 1.6 cm had a high specificity, but low sensitivity for diagnosing RV systolic dysfunction.²⁸⁷ Furthermore TAPSE has been shown to be an independent prognostic indicator in patients with congestive cardiac failure.²⁸⁸ The

major advantage of TAPSE is that it is a geometrically independent measure of RV function that is quick and easy to perform. Its major limitation is that it is a single plane measurement, which like other assessments of tricuspid annular motion may not reflect regional changes in RV function.

Peak systolic tissue velocity of lateral tricuspid annular motion

Tissue velocity imaging (TVI) is an alternative method of assessing tricuspid annular motion. The peak systolic tissue velocity (S') of the lateral side of the tricuspid annulus has been measured previously with pulsed-wave TVI and shown to correlate with CMR-derived RVEF.²⁸⁹ A tricuspid annular $S' < 11.5$ cm/s has been shown to predict RVEF $< 45\%$ with a sensitivity and specificity of 90% and 85% respectively.²⁹⁰ From pooled data of > 2000 normal controls across 43 studies the lower reference limit of normal was $S' = 10$ cm/s for pulsed-wave TVI.³⁷ S' can also be measured using colour TVI, although the absolute value recorded is lower than with pulsed-wave TVI, as colour TVI measures the mean of the systolic tissue velocities recorded within the specified region of interest. Mean annular velocities in normal controls average 8.5-10 cm/s with lower normative reference limit of 6 cm/s from pooled studies.³⁷ The main advantages of TVI for assessing RV function include the geometric independence of the technique, and the speed and ease with which the TVI traces can be acquired. Tissue Doppler velocities of the RV are also relatively independent of age.^{283,291,292} Furthermore S' of the tricuspid annulus has been shown to be a prognostic indicator in patients with congestive heart failure.^{254,255} In addition to the single plane nature of the technique, other limitations of tissue velocity imaging for assessing RV function include the Doppler angle dependence of the technique and the fact that tricuspid annular tissue velocities may be altered by cardiac loading conditions.²⁹³

Tricuspid annular motion during isovolumic contraction: "Isovolumic acceleration"

The three independent physiological components determining the magnitude of RV ejection are preload, afterload and myocardial contractility as previously discussed. Although maximal RV elastance is considered the reference standard for measuring RV contractility,⁶³ due to the invasive and time-consuming nature of this investigation it is not

routinely performed.²⁹⁴ An alternative method for assessing RV contractility is by measuring endocardial acceleration by implanting an intracardiac accelerometer into the right ventricular wall.²⁹⁵ However, this method too is invasive. Using the principle of endocardial acceleration, Vogel and colleagues developed a novel non-invasive technique for assessing myocardial acceleration and hence myocardial contractility.²⁴⁶ Isovolumic acceleration (IVA) is calculated as the mean of the isovolumic contraction slope on a colour tissue Doppler trace recorded from the lateral tricuspid annulus.³⁷ In research studies IVA has been shown to be relatively independent of preload and afterload changes within the RV, but is heart rate dependent.^{63,246,293} To date, IVA has been successfully used to assess RV function in patients with congenital heart disease and cardiac transplant recipients.^{293,296-298}

Tricuspid annular plane systolic excursion by tissue Doppler echocardiography

In addition to velocity and strain information, colour tissue Doppler imaging enables assessment of longitudinal myocardial displacement during systole. Tissue Doppler displacement imaging offers a novel method for assessing RV function by assessing tricuspid annular excursion in the longitudinal plane during RV systole, i.e. a TDE measure of TAPSE. One theoretical advantage of this technique over M-Mode TAPSE is that pulmonary valve opening and closure times can be superimposed on the colour TDE displacement curve. This ensures that maximal longitudinal displacement during the systolic ejection period is measured in all patients and excludes measurement of post-systolic motion which does not contribute to RV ejection. To our knowledge, this potential novel method for assessing RV function has not previously been studied.

1.13.4 Concept behind Study 4: Comparison of ten 2DE non-volumetric indices of RV systolic function: Correlation with CMR-derived RVEF.

CMR RVEF is the non-invasive reference standard by which RV systolic function is measured. CMR enables a true Simpson's method of discs to be used to quantify RVEF from multiple short axis slice sequences without geometric assumptions. By contrast, volumetric assessment of the RV by 2DE is limited by the complex geometry of the RV and the limited RV echocardiographic imaging windows. For this reason, RV FAC,

TAPSE, MPI, RV strain, TVI and IVA are being explored for use as new non-geometric indices of RV systolic function, to be used in conjunction with visual assessment. Recent revised ASE/EAE/CSE guidelines recommend the use of at least one quantitative measure of RV systolic function in addition to a visual assessment of RV function to be incorporated into routine echocardiographic examination reports.³⁷ However, these guidelines make no recommendation as to which non-volumetric index of RV function is superior to the others. Although all show promise as adjunctive measures of RV function, direct comparison of all these techniques has to date, not been performed in the heterogeneous population of patients seen in clinical practice. Furthermore there is a paucity of data comparing the reproducibility of these methods in patients exhibiting a wide range of RV ejection fractions. In addition to M-Mode TAPSE, MPI, RV strain, TVI and IVA, we believe TAPSE measured using tissue Doppler displacement imaging, to be a potentially new method of assessing RV function which has not been previously described.

The concept behind study four of this thesis was therefore to directly compare the use of FAC, M-Mode TAPSE, TDE TAPSE, MPI, 2D strain, TVI and IVA for assessing RV function by measuring the correlation of these techniques against CMR-derived RVEF as the reference standard.

CHAPTER 2

AIMS

CHAPTER 2: AIMS

2.1 AIMS OF THESIS

The aims of this thesis were:

- 1) to explore the use of novel imaging methods to improve non-invasive quantification of resting global left and right ventricular function in patients exhibiting a broad spectrum of ventricular function and
- 2) where appropriate, to assess intermodality agreement between echocardiography and cardiac magnetic resonance imaging techniques.

2.2 SPECIFIC AIMS OF THIS THESIS

2.2.1 Study 1: Left ventricular systolic function – Speckle tracking Strain

Formatted: No bullets or numbering

- To explore the clinical utility of 2DE speckle tracking strain imaging for quantifying global LV systolic function by comparing it to CMR LVEF as the reference standard, in a heterogenous cohort of patients as seen in clinical practice.
- To use regression analysis to compare the accuracy of the 2D strain derived “global strain score” (GSS) against 3DE LVEF and 2DE Simpson’s Rule LVEF, indexed against CMR LVEF as the reference standard.
- To compare the reproducibility of the 3 echocardiographic techniques.
- To develop a regression equation to enable GSS to be converted into a LVEF equivalent score.
- To validate this regression equation in a second cohort of patients.

2.2.2 Study 2: Left ventricular systolic function – Regional Wall Motion Score Index

Formatted: Outline numbered +
Level: 3 + Numbering Style: 1, 2, 3, ...
+ Start at: 2 + Alignment: Left +
Aligned at: 0 cm + Indent at: 1.27 cm

- To explore the clinical utility of using a modified 16-myocardial segment regional wall motion scoring index (RWMSI) to calculate LVEF by comparing it to CMR LVEF as the reference standard.
- To use regression analysis to compare the accuracy of RWMSI LVEF against 2DE Simpson's LVEF, indexed against CMR LVEF as the reference standard.
- To compare the correlation and intermodality concordance of both RWMSI and Simpson's rule against CMR LVEF in patients with normal and impaired LV systolic function.
- To compare the reproducibility of these techniques.

2.2.3 Study 3: Left ventricular diastolic function – VEC CMR for estimating LVEDP

Formatted: Outline numbered + Level: 3 + Numbering Style: 1, 2, 3, ... + Start at: 2 + Alignment: Left + Aligned at: 0 cm + Indent at: 1.27 cm

- To compare E/A ratios recorded using VEC CMR against Doppler echocardiography.
- To explore the clinical utility of using VEC CMR to record LV myocardial tissue velocities, by comparing them to Em velocities recorded by pulsed-wave tissue Doppler echocardiography.
- To explore the clinical utility of using CMR to estimate left ventricular filling pressure by comparing VEC CMR E/Em ratio to LVEDP recorded during cardiac catheterisation in patients with normal and impaired LV systolic function
- To establish the reproducibility of this technique.

Study 4: Right ventricular systolic function – Non-volumetric echo indices of RV

Formatted: Outline numbered + Level: 3 + Numbering Style: 1, 2, 3, ... + Start at: 2 + Alignment: Left + Aligned at: 0 cm + Indent at: 1.27 cm

2.2.4 —function

- To perform a head-to-head comparison of ten 2DE non-volumetric indices of global RV function, indexed against CMR RVEF as the reference standard in a heterogeneous cohort of patients as seen in clinical practice.
- To assess receiver-operator characteristics and establish normative cut-off values for the RV indices which do not have previously published normative values.
- To assess the reproducibility of the techniques.

- To use regression analysis to determine which of the ten 2DE techniques is the most accurate when compared to CMR.

CHAPTER 3

METHODS

CHAPTER 3: METHODS

3.1 GENERAL

The research studies were approved by the Regional Ethics committee and Wakefield Ethics board, South Australia. Study volunteers met with the recruiting cardiologist, Dr Duncan, who explained the study protocols to the patients. Patient information sheets were also provided. Written informed consent was obtained.

3.2 STUDY DESIGN

For all ventricular function studies, the aim was to study the clinical usefulness of the new imaging methods across a broad-spectrum of ventricular function. This was achieved by recruiting patients from cardiac catheterisation lists, cardiology outpatient clinics and clinical echocardiography lists.

Study subjects underwent CMR imaging and echocardiography sequentially within two hours of each other to ensure similar loading conditions of the heart. Patients undergoing cardiac catheterisation, had their CMRs, echocardiograms and cardiac catheter procedures performed consecutively within three hours of each other in the fasted state to eliminate significant differences in cardiovascular loading conditions during the different cardiovascular imaging tests.

Patients were included in the studies if they were in sinus rhythm and had no contra-indications to CMR. Patients were excluded from the LV systolic function studies if they had an atrial dysrhythmia, a contra-indication to CMR or poor endocardial wall definition as defined by the inability to assess ≥ 2 AHA myocardial LV segments. Patients were

excluded from the LV diastolic function study if they had an atrial dysrhythmia, a contra-indication to CMR, moderate-severe mitral valve disease, significant mitral annular calcification, a surgical mitral ring, a mitral prosthesis or pericardial constriction. Patients were excluded from the RV function studies if they had a contra-indication to CMR, a tricuspid valve prosthesis or surgical ring, or poor RV echocardiographic images as assessed in the apical 4-chamber view of the heart.

3.3 CARDIAC CATHETERISATION PROTOCOL

3.3.1 Left heart catheterisation

All patients undergoing invasive assessment of left ventricular filling pressures had a clinical indication for left heart catheterisation (LHC). Patients were admitted in the fasted state and LHC was performed aseptically using the Judkins technique. A fluid-filled catheter was placed in the left ventricle after retrogradely crossing the aortic valve. Left ventricular filling pressures were then recorded over three or more cardiac cycles in paused respiration. Filling pressures were recorded prior to left ventriculography and coronary angiography to ensure non-ionic contrast media did not influence the subsequent pressure waveform recordings. Left ventriculography and coronary angiography then proceeded in the standard way.²⁹⁹

LVEDP was defined as the pressure after atrial contraction just before LV systolic pressure rise (Figure 3.1).³⁰⁰ This is usual clinical practice, as previously described.



Figure 3.1. Recording LVEDP from a fluid-filled catheter trace

3.3.2 Limitations of the technique

A number of potential errors can occur when intracardiac pressures are measured using a fluid-filled catheter system. Distortion of the output signal can occur as a result of the pressure damping characteristics of the system. Another potential source of error can occur if the system has not been carefully calibrated against a known pressure to establish a zero reference point at the start of the procedure. Other potential sources of error include catheter whip artifact and catheter impact artifact.

In this study, the LHC procedures were not performed by the research team, but by the clinical cardiologist for clinical indications. As part of the research protocol, the clinicians were asked to take all reasonable measures to minimise pressure damping, ensure correctly zeroed transducers and minimise other potential sources of error.

The use of micromanometer catheters can reduce the error in recording invasive left ventricular pressure measurements. These catheters have a pressure transducer mounted at their tip, have higher natural frequencies and more optimal damping characteristics because the interposing fluid column is eliminated. The pressure waveform is less distorted and they have a decreased incidence of catheter whip artifact. At the outset of this study we aimed to correlate non-invasive estimation of LVEDP recorded using velocity-encoded CMR against LV pressure recordings made using a 4F Millar micromanometer-

tipped catheter system. The initial aim was to use the micromanometer catheter to measure LV pressure, from which its first-time derivative, $LV+dP/dt_{max}$, would be determined (using the catheterization laboratory polygraph).³⁰¹ To eliminate the effects of minor fluctuations in heart rate on $LV+dP/dt_{max}$, patients would be subjected to continuous baseline atrial pacing, slightly faster than the spontaneous heart rate, via a bipolar pacing electrode inserted either into the high right atrium or the coronary sinus. Cardiac output would be determined by the Fick method.³⁰¹ Mechanical restitution curve construction would comprise insertion of an atrial premature stimulus following every eight beats of baseline atrial pacing at progressively shorter test pulse intervals (TPI), until atrial/AV nodal refractoriness was attained. The $LV+dP/dt_{max}$ would be determined at each TPI and expressed as a percent of that observed at baseline. The TPI would be expressed as a percent of baseline atrial pacing cycle length. This is well-validated research technique for assessing load independent left ventricular function.³⁰¹ Unfortunately due to the expense, fragility and added procedural times of these micromanometer catheter systems their subsequent use for this project was not feasible.

In addition to the above reasons, in clinical practice LVEDP is most commonly recorded using fluid-filled catheter systems. Our aim was to find a clinically applicable non-invasive measure of LVEDP using velocity-encoded CMR. Correlation of non-invasive measures of LVEDP against the most common clinically utilised invasive measure of LVEDP was therefore more easily applicable and appropriate.

3.4 CARDIAC MAGNETIC RESONANCE IMAGING PROTOCOLS

General imaging methods and the use of standard imaging sequences are described below. The specific imaging methodologies used in each study are described in detail in the relevant chapters.

3.4.1 Left ventricular systolic function protocol

All CMR studies were performed using a 1.5T MRI scanner (Siemens Sonata, Erlangen, Germany) and a phased array surface coil. Long axis reference views were used for positioning the perpendicular LV short axis slices from the level of the mitral annulus to the

LV apex. Short axis images were obtained with prospectively ECG-gated TrueFISP (Fast Imaging with Steady-State Free Precession) sequences at 6mm slice thickness. Acquisition time was 90% of the RR-interval, image matrix 256 X 150, field of view 380 mm, repetition time 52.05 ms, echo time 1.74 ms, flip angle 70°, and 12 to 17 heart phases were acquired per repetition time interval. All images were acquired during 8 to 10 second breathholds and stored digitally for offline analysis of LV function.

Left ventricular analysis was performed off-line using a proprietary software programme (Argus software, Siemens Medical Solutions, Germany). Short-axis LV endocardial and epicardial contours were manually traced in end-diastole (start of R-wave) and in end-systole (smallest cavity area) (Figure 3.2). Papillary muscles and trabeculations were excluded from the ventricular volume and were included if contiguous with the myocardial mass. The basal slice was selected as the slice where the blood volume was surrounded by >50% of ventricular myocardium. The end-diastolic and end-systolic cavity surface areas were then summed and end-diastolic (EDV) and end-systolic (ESV) volumes calculated by multiplying with interslice intervals as per Simpson's method of discs. LVEF was calculated as $LVEF = ((EDV - ESV) / EDV) \times 100\%$ (Figure 3.2).²²

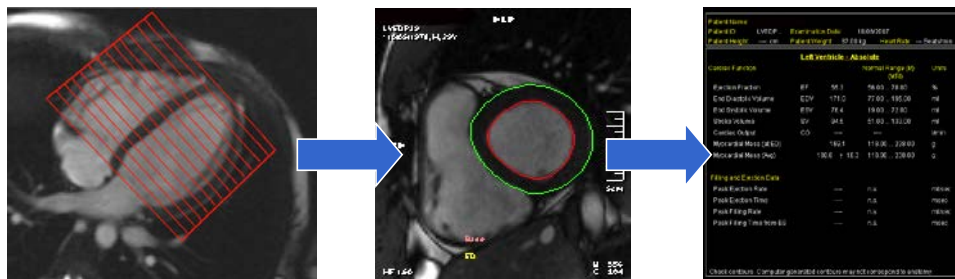


Figure 3.2. Tracing LV endocardial and epicardial contours and calculating LV volumes and LVEF using CMR Argus analysis software.

3.4.2 Right ventricular systolic function protocol

The right ventricle was imaged in the short axis orientation using steady-state free

precession sequences in a similar manner to the LV structure and function protocol. This is one of the two RV imaging protocols endorsed by the Society of Cardiac Magnetic Resonance Imaging.²³⁷ Short-axis RV endocardial contours were traced manually in end-diastole (start of R-wave) and in end-systole (smallest cavity area). Trabeculations were included in the ventricular volume. In the basal slice, both in end-diastole and end-systole, if the pulmonary valve was visible, only the portion of the right ventricular outflow tract below the level of the pulmonary valve was included. For the inflow part of the RV, the blood volume was excluded if the surrounding wall was thin and not trabeculated as it was considered to be in the right atrium. The end-diastolic and end-systolic cavity surface areas were then summed and end-diastolic (EDV) and end-systolic (ESV) volumes calculated by multiplying with interslice intervals as per Simpson's method of discs. RVEF was calculated as $RVEF = ((EDV-ESV)/EDV) \times 100\%$ (Figure 3.3).

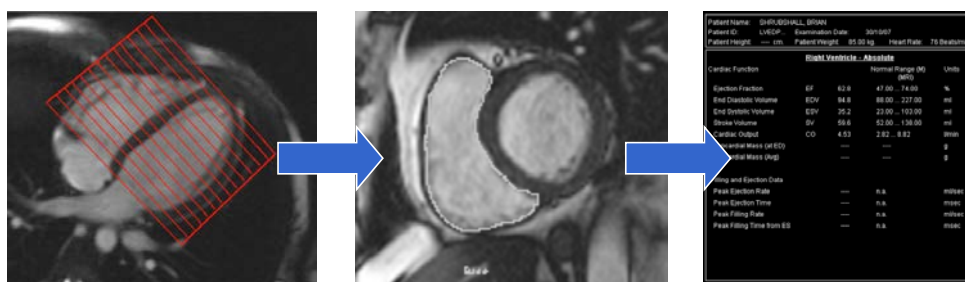


Figure 3.3. Tracing right ventricular endocardial contours and calculating RV volumes and RVEF using CMR Argus analysis software.

3.4.3 Left ventricular diastolic function protocol

VEC-CMR was used to measure early (E) and late (A) transmitral diastolic flow velocities, and E/A ratio calculated. The VEC-CMR protocol was then modified and used to record peak myocardial tissue velocities from the basal segments of all six walls of the left ventricle (Em). LVEDP was estimated from the VEC-CMR E/Em ratio in a manner analogous to the pulsed-wave tissue Doppler technique used in echocardiography. This method is described in detail in chapter 6: LV diastolic function.

3.5 THREE DIMENSIONAL ECHOCARDIOGRAPHY IMAGING PROTOCOLS

3DE imaging was performed from the apical window with the patient in the left lateral decubitus position using a commercial ultrasound system (iE33 intelligent echocardiography, Philips Medical Systems, Andover, MA). Pyramidal 3D volume datasets were obtained in the apical view using a matrix array transducer. Gain and compression controls were adjusted, and fundamental imaging was used to improve image quality. Views were optimized to include the entire LV cavity and walls using 2D biplane, then several full volume 3D data sets with a wide field of view were acquired using medium line density. The temporal resolution was approximately 20 frames per second. Acquisition of the 3D volume dataset was steered electronically without transducer movement. Datasets were recorded over several cardiac cycles in held expiration taking care to avoid stitching artefact.

The 3D full volume images were manipulated with commercial software equipped with the 3DE system (3D QLAB software, Philips Inc.). Each volumetric dataset was displayed in a quadrant screen consisting of the pyramidal view and three planar cross sections; 4-chamber long axis, 2-chamber long axis and a short axis view. The three planar images were manipulated using multiplanar reconstruction to select anatomically correct 4- and 2-chamber views with the largest long axis dimensions (see Figure 3.4A). End diastole was marked on the cine-loop as the frame of mitral valve closure and end systole was the frame preceding mitral valve opening. LV volumes were then calculated using 3D full volume algorithms on the 3DE system (3DQ Advanced, QLAB, Philips Inc.) A semi-automated border tracking system was used to create a full-volume 3D endocardial contour from five user defined points; four points at the junction of the mitral annulus with the basal septum and lateral wall in the 4-chamber view and the basal anterior and inferior wall in the 2-chamber view, and one point at the cardiac apex. Border tracking was then manually manipulated where required, for optimisation in all three planes. An advanced parallel processing algorithm generated 3D wire-mesh endocardial volumes for end diastole and end systole and LVEF was automatically calculated (Figure 3.4B).¹⁴⁷

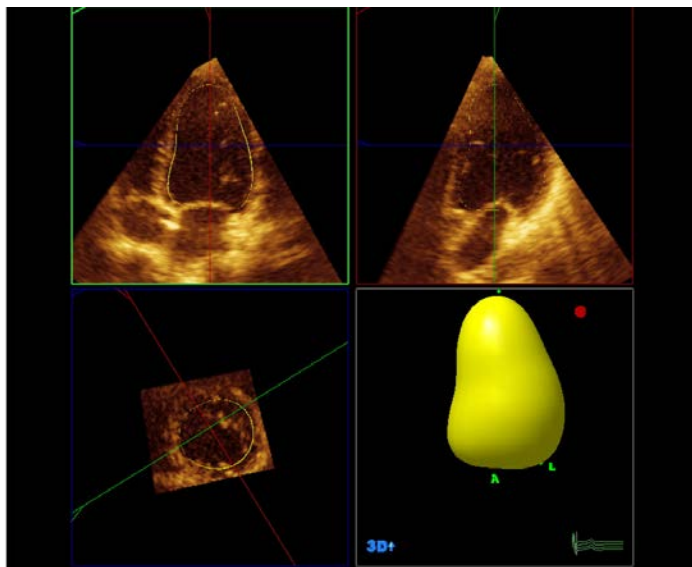


Figure 3.4. Calculating LVEF using 3DQ-Advanced software.

Advanced parallel processing enables rapid generation of a full 3D wire mesh endocardial volume with minimal operator intervention. Three-dimensional pattern matching tracks the mitral annulus and apex over time, providing an “active object” motion presentation of the dynamic 3D shape. This allows 3D borders for the endocardial space in each frame to be combined into a smooth beating volume with accurate spatial and temporal motion detail. LVEF is then calculated by the software from 3D end-diastolic and end-systolic volumes.

3.6 TWO-DIMENSIONAL ECHOCARDIOGRAPHY IMAGING PROTOCOLS

All two-dimensional echocardiograms were performed using a Vivid 7 scanner (GE Medical Systems, Wauwatosa, WI). All patients were imaged in the left lateral decubitus

position with the patients' left arm raised above the head, taking care to avoid apical foreshortening. Images were acquired in paused respiration (in gentle end expiration whenever possible) to prevent excessive translational motion of the heart. Image resolution and endocardial border delineation were maximised by optimising the gain, depth and focus of each image. Second harmonic imaging was used consistently throughout all studies. Full transthoracic imaging studies were performed on all patients. For the assessment of global left ventricular systolic function, optimal images were acquired in the standard parasternal long axis (PSLAX), parasternal short axis (PSSAX), apical four chamber (A4C), apical two chamber (A2C) and apical long axis (ALAX) views of the heart as per ASE/EAE guidelines.³⁸ For the assessment of LV diastolic function, transmitral E and A velocities were recorded using pulsed-wave spectral Doppler as per ASE/EAE guidelines described below. Mitral annular peak systolic tissue velocities were recorded and E/Em ratio calculated as described below. For the non-volumetric assessment of global RV systolic function, optimal images were acquired in the apical-4-chamber view of the heart, and tricuspid inflow and pulmonary outflow spectral Doppler traces recorded for all patients.

3.6.1 Quantifying left ventricular systolic function by 2DE

Calculating LVEF using Simpson's Biplane Method of Discs (Modified Simpson's Rule)

In this study, LVEF was quantified by 2DE using Simpson's Biplane method of discs as per ASE/EAE guidelines. When calculating left ventricular end diastolic volume (LV EDV), end diastole was defined as the frame after mitral valve closure. This is in keeping with the ASE/EAE joint guideline for chamber quantification.³⁸ LV EDV was calculated by manually tracing the endocardial border, excluding the papillary muscles, in the apical four chamber and apical two chamber views. The basal border of the left ventricle was delineated as a straight line, between the insertion of the mitral valve leaflets at the septal and lateral mitral annulus in the apical four chamber view and the insertion of the leaflets at the inferior and anterior mitral annulus in the apical two-chamber view (see Figure 3.5). End systole was defined as the frame preceding mitral valve opening,³⁸ and the left ventricular end systolic volume (LV ESV) was calculated by tracing the endocardial border in the end systolic frame by the method described in Figure 1.12 and Equation 1.5. The automated software then calculated the LVEF as follows: $LVEF (\%) = (EDV - ESV) / EDV$.

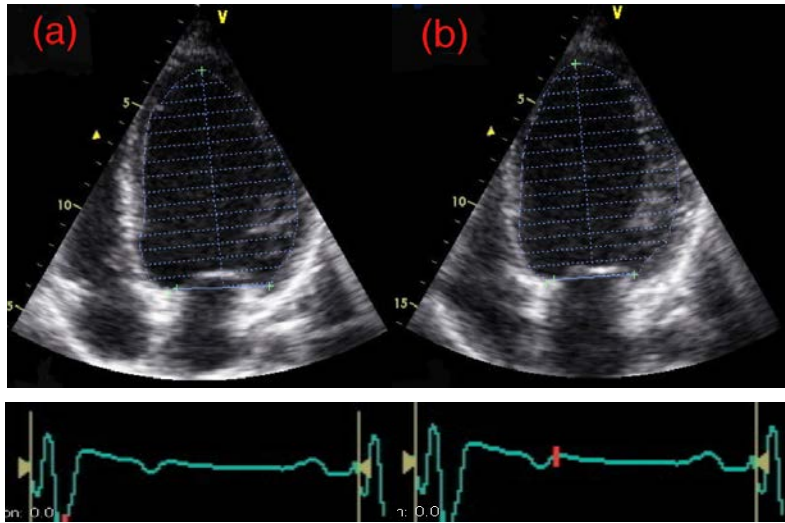


Figure 3.5. Calculating left ventricular ejection fraction using Simpson's Biplane Method of Discs. The endocardial border of the left ventricle was traced as shown in (a) end diastole and (b) end systole in the apical four-chamber view. The same process was repeated in the apical two chamber view and the LVEF calculated.

Quantifying LV systolic function using 2D speckle tracking strain imaging

A regional longitudinal strain score was calculated for each of the AHA 16 segments of the LV, from the 3 apical views of the heart, using GE AFI functional imaging software as described in detail in chapter 4: LV systolic function Part 1. This information was then used to quantify global LV systolic function.

Calculating LVEF from the modified regional wall motion scoring index

A regional wall motion score was applied to each of the 16-AHA myocardial segments of the left ventricle based on a visual assessment of radial contractility as described in detail in

chapter 5: LV systolic function Part 2. The resultant regional wall motion score index was then converted into a LVEF-equivalent score.

3.6.2 Quantifying right ventricular systolic function by 2DE

Due to the complex geometry of the RV, its anatomical relationship to the LV and the limited imaging planes for the RV by transthoracic echocardiography, accurate volumetric assessment of RV systolic function is not possible by 2DE.

Ten non-volumetric indices of RV systolic function were assessed using a combination of M-Mode, spectral Doppler, tissue Doppler and speckle tracking strain imaging techniques. These were 1) M-Mode tricuspid annular systolic plane excursion (TAPSE), 2) Tissue Doppler tricuspid annular systolic plane excursion (TDE-TAPSE), 3) RV myocardial performance index by spectral Doppler (RV MPI), 4) RV myocardial performance index by pulsed tissue Doppler (RV TDE MPI), 5) RV peak systolic myocardial tissue velocity measured using pulsed-wave tissue Doppler echocardiography (RV PWTDE S'), 6) RV peak systolic myocardial tissue velocity measured using colour tissue Doppler echocardiography (RV CTDE S'), 7) RV isovolumic acceleration (RV IVA), 8) RV fractional area change (RV FAC), 9) RV "global" strain (RVGS) and 10) RV free wall strain (RVFWS).

M-Mode imaging used to assess TAPSE was recorded from the apical 4-chamber view of the heart with the pulse sample volume at the junction of the lateral tricuspid annulus and RV free wall. M-Mode recording were made taking care to ensure correct cursor alignment with minimal angulation and a sweep speed of 100cm/s. Pulsed-wave (PW) spectral Doppler recordings of tricuspid inflow and pulmonary outflow were made from the apical-4 chamber view and parasternal short axis view respectively, ensuring correct Doppler angulation and a sweep speed of 100cm/s. These measures were subsequently used to calculate RV MPI. The PW TDE RV myocardial peak systolic tissue velocity (S') was recorded from the apical 4-chamber view of the heart with the pulse sample volume at the junction of the lateral tricuspid annulus and RV free wall. PW TDE recordings were made taking care to ensure Doppler angulation of ≤ 20 degrees, with a sweep speed of 100cm/s. S' was defined as the peak systolic deflection, after the isovolumic contraction spike, from the PW tissue velocity trace. This PW tissue velocity trace was also used to measure RV

TDE MPI. Colour tissue Doppler images of the right ventricle were acquired from the apical 4 chamber views with frame rates ≥ 100 frames/sec and pulse repetition frequencies between 500 Hz to 1 KHz. Three consecutive beats were stored and analysed during post processing. A continuous-wave Doppler tracing of pulmonary outflow was recorded through the pulmonary valve from the parasternal short axis view to enable event timing during post-processing. Pulmonary valve opening and closure times were recorded by placing event-timing markers at the start and end of the pulmonary outflow spectral envelope (Figure 3.6A). The recorded pulmonary valve opening and closure times were then superimposed on the tissue velocity/time graph during post processing (Figure 3.6B).

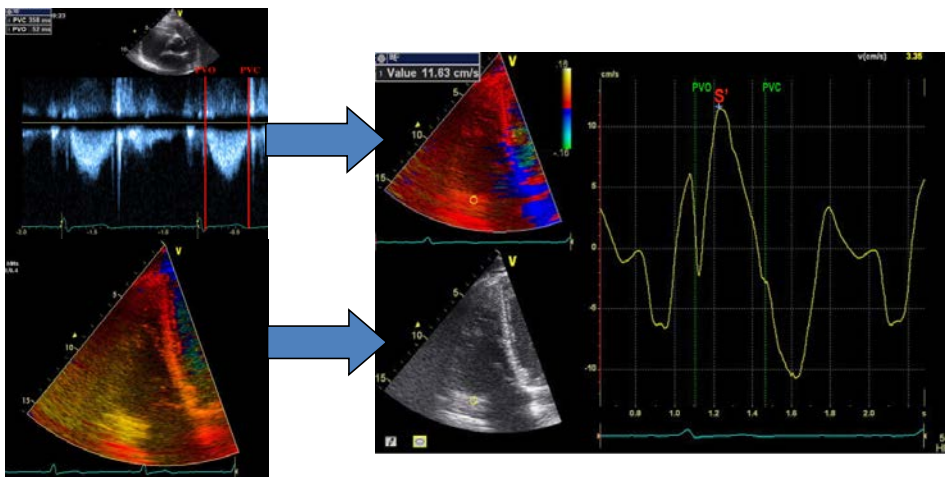


Figure 3.6. Measuring the event timing intervals.

Event timing markers for pulmonary valve opening (PVO) and closure (PVC) are applied at the start and end of pulmonary outflow spectral Doppler trace. These event timing markers are superimposed onto the tissue velocity-time graph during post processing.

Myocardial tissue velocity and tissue displacement parameters were then measured from the colour images during further post processing. The tissue Doppler sample volume, also known as the ROI (region of interest) marker was placed at the junction of the basal right ventricular free wall with the lateral tricuspid annulus, and the ROI was manually tracked throughout the cardiac cycle. CTDE S' and RV IVA indices were calculated from this

position on the subsequent colour tissue velocity imaging graph. TDE TAPSE was recorded from the same position on the subsequent colour tissue displacement graph. RV “global” strain and RV free wall strain were quantified by speckle tracking strain using GE AFI automated functional imaging software. Detailed descriptions of each technique are discussed in chapter 7: RV systolic function.

3.6.3 Quantifying left ventricular diastolic function by 2DE

Mitral filling patterns and E:A ratio

Mitral inflow patterns were recorded using pulsed-wave Doppler from the apical four-chamber view, with the pulsed sample volume placed at the mitral leaflet tips as per ASE/EAE guidelines.¹⁴ Peak mitral E wave velocity was measured as the maximal modal velocity recorded during early diastole (see Figure 3.7). Peak mitral A wave velocity was measured as the maximal modal velocity recorded during late diastole as shown in Figure 3.7. E:A ratio was then calculated.

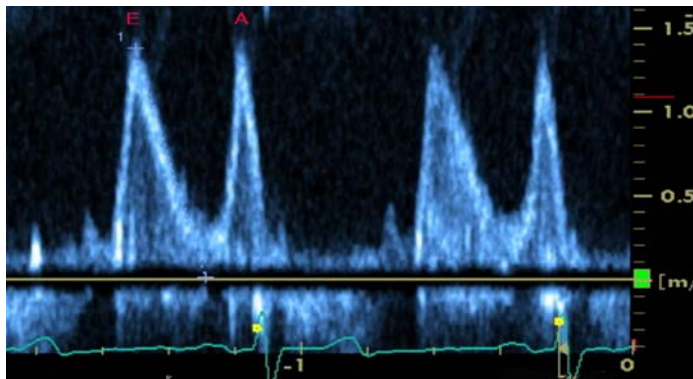


Figure 3.7 Calculating the E:A ratio. In this example the peak E wave and A wave velocities were identical at 1.48m/s giving a ratio of 1:1.

Mitral annular peak early diastolic relaxation velocities

The mitral annular early diastolic relaxation velocity, E_m , provides an index of left ventricular relaxation that is independent of preload.^{5,194,302} In addition to providing load-independent information, E_m can be used to differentiate between normal and pseudonormal filling patterns.⁴²

Mitral annular velocities were recorded from the apical window using pulsed-wave mode. The gain and filters were set low and the frame rate optimised. The pulsed-wave sample volume was placed at the junction of the left ventricular wall and mitral valve annulus on the septal side of the mitral valve. The resultant tissue Doppler velocity profile was then acquired with a sweep speed of 100mm/s. The process was then repeated at the lateral, anterior, inferior and posterior and anteroseptal sides of the mitral valve annulus. The peak E_m velocity was measured from the pulsed-wave tissue Doppler profile as shown below in Figure 3.8. The E_m value recorded from the septal and lateral sides of the mitral valve annulus are the positions most often quoted in the literature and are subsequently referred to as $E_m(S)$ and $E_m(L)$ respectively. As we wished to compare myocardial tissue early diastolic relaxation velocities with diastolic tissue velocity traces derived using VEC-CMR sequences, we measured mitral annular peak early diastolic relaxation velocities from all sides of the mitral annulus in the apical views.

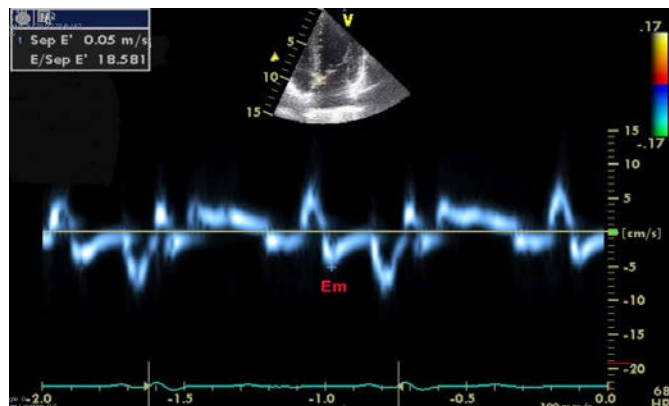


Figure 3.8. Example of a pulsed-wave tissue Doppler velocity trace of the mitral annulus. The peak mitral annular early diastolic relaxation velocity (E_m) was recorded as shown. In this example taken from the septal mitral annulus of a patient with dilated cardiomyopathy, $E_m = 5\text{cm/s}$ which is significantly reduced.

Calculating the left ventricular end diastolic filling pressure

The ratio of transmitral E wave velocity to mitral annular tissue velocity has been shown to correlate with both pulmonary capillary wedge pressure and left ventricular end diastolic filling pressure (LVEDP) in various patient cohorts.^{4,5,13,303}

The revised EAE guidelines for assessing LV diastolic function recommend estimating LVEDP from E/ E_m ratios where E_m is measured from either the septal side of the mitral annulus $E_m(S)$, the lateral side of the mitral annulus $E_m(L)$, or where E_m is the averaged recordings from both septal and lateral sides of the mitral annulus $E_m(S+L_{av})$.¹⁴ We calculated E/ $E_m(S)$ by dividing the peak E wave velocity by E_m recorded at the septal mitral annulus (Figure 3.9).¹⁹⁹ We then repeated this ratio calculation using E/ $E_m(L)$ and E/ $E_m(S+L_{av})$. As 12 of our 19 study subjects with impaired LV systolic function had ischaemic heart disease with regional wall motion abnormalities, we also calculated the E/ E_m ratio by dividing the peak E wave velocity by E_m averaged from recordings at all 6 sides (septal, lateral, anterior, antero-septal, inferior and posterior) of the mitral annulus (E/ $E_m(6_{av})$.) This was to ensure the E/ E_m ratios were not significantly influenced by regional changes in diastolic relaxation. Finally, as the antero-septal side of the mitral annulus is in continuity with the aortic annulus in the apical long axis view, we also calculated the E/ E_m ratio from the remaining 5 sides of the mitral annulus, with the exclusion of the antero-septum (E/ $E_m(5_{av})$).

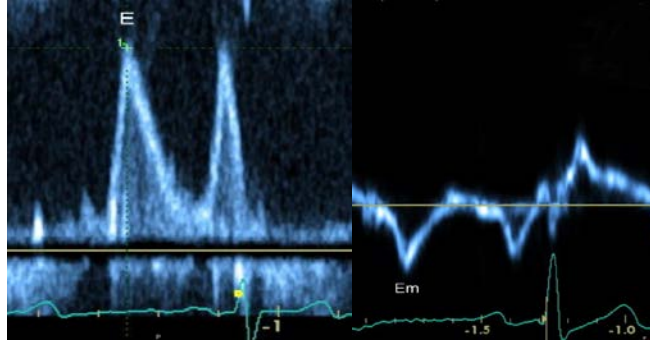


Figure 3.9 Estimating left ventricular end diastolic pressure from E/Em ratio.

E, peak velocity of early mitral inflow; Em, peak mitral annular early diastolic relaxation velocity.

3.7 STATISTICAL ANALYSES

All data sets were assessed for normality using the Kolmogorov-Smirnov test when the sample size was <50 and the Shapiro-Wilk test when the sample size was ≥ 50 . Parametric data is displayed as mean \pm two standard deviations. Non-parametric data is displayed as median (first to third interquartile range).

Bivariate correlations were performed using Pearson correlation coefficient for parametric data and Spearman correlation coefficient for non-parametric data. For normally distributed data sets, different echocardiographic indices of left and right ventricular function were compared against each other when indexed against cardiac magnetic resonance imaging as the reference standard, using step-wise regression analysis. If data was non-parametrically distributed it was transformed where possible and stepwise regression analysis was performed to compare different techniques as previously described. If it was not possible to transform non-parametric data, then bivariate correlations were performed.

For functional imaging techniques where normative cut-off values have been previously published, these values were used to classify patients as having normal or impaired ventricular function. Several of the echocardiographic functional imaging techniques studied in this thesis have no published normative values. For these techniques, receiver

operator characteristics were studied to determine normative threshold values, by indexing them appropriately against either CMR LVEF or RVEF, as the reference standards.

A p value of <0.05 was considered statistically significant.

CHAPTER 4

LEFT VENTRICULAR SYSTOLIC FUNCTION - PART ONE

**“TWO-DIMENSIONAL SPECKLE TRACKING
STRAIN FOR THE EVALUATION OF LEFT
VENTRICULAR SYSTOLIC FUNCTION: A
COMPARISON AGAINST CARDIAC MAGNETIC
RESONANCE IMAGING, THREE-DIMENSIONAL
ECHOCARDIOGRAPHY AND SIMPSON’S BIPLANE
METHOD OF DISCS”**

CHAPTER 4: LV SYSTOLIC FUNCTION PART 1

4.1 INTRODUCTION

The quantification of LVEF is important for therapeutic and prognostic reasons.³⁰³ The high spatial resolution of CMR imaging makes it the reference standard for LVEF calculation.²² 3DE is also an effective methodology for assessment of LVEF. However due to limited availability and high costs of CMR and 3DE, 2DE remains the most widely utilized imaging modality for LV systolic function. Currently joint ASE and EAE guidelines recommend that Simpson's biplane method of discs remains the preferred 2D method for calculating LVEF despite the recognised limitations of this technique.³⁸

In recent years there have been major advantages in 2DE software particularly in the field of strain imaging.³⁰⁵⁻³¹⁰ Two dimensional speckle tracking strain imaging involves the use of a semi-automated endocardial border tracking system to quantify myocardial deformation based on the recognition and tracking of unique "speckle" patterns within the myocardium. This technique has several theoretical advantages over both volumetric assessments of LV function and tissue Doppler strain. Lagrangian strain measures the percentage deformation of the myocardium throughout systole in relation to end diastole as the reference point, rather than volumetric changes within the ventricle and therefore theoretically should be less affected by cardiac loading conditions than volumetric methods.³¹¹ The 2D strain automated tracking results in faster analysis times and improves reproducibility compared to manual tracking used with tissue Doppler strain. Unlike tissue Doppler strain, 2D strain is an angle independent technique which improves accuracy and reproducibility and enables strain analysis of all 16 myocardial segments of the American Heart Association (AHA) model, thus potentially allowing quantification of global as well as regional strain data.^{306,312} Finally global longitudinal strain has recently been shown to confer important prognostic information.³¹³ Stanton et al have recently demonstrated that individuals with a global longitudinal strain score $\geq -12\%$ had significantly worse survival than those with a global longitudinal strain score of $\leq -12\%$ ($p < 0.001$).³¹³

4.2 STUDY AIMS

The aim of this study was to establish a novel 2DE technique to quantify LV systolic function by utilising global longitudinal systolic strain data. Furthermore we sought to

assess the accuracy and reproducibility of this technique compared to CMR, 3DE and biplane Simpson's rule and whether global longitudinal strain can be used to calculate a LVEF equivalent score (LVEFES).

4.3 METHODS

4.3.1 Study Design

Eighty-three patients exhibiting a broad spectrum of LVEF's (Range 15-79%) were recruited from outpatient clinics, elective echocardiography and cardiac catheterisation lists. All study subjects underwent standard 2DE (GE Vivid 7) and 2D speckle tracking strain imaging (GE Automated Functional Imaging). LVEF was calculated by 2DE using Simpson's Rule in as previously described.³⁸ A global longitudinal strain score (GSS) was calculated by 2D speckle tracking strain as described below. The GSS was correlated against Simpson's rule in all patients to validate the technique. An initial sub-study cohort of 33 patients successfully underwent 3DE (Phillips iE33) and CMR (1.5T Siemens Sonata) (LVEF range by CMR: 24-73%). LVEF was calculated by 3DE and CMR in these patients as previously described. The three echocardiographic methods for quantifying LV function were then compared against each other using multivariate analysis to establish the echocardiographic technique with the closest correlation to CMR-derived LVEF and the highest reproducibility.

Linear regression was used to convert the GSS into a measure of LVEF. A second cohort of 20 patients (LVEF range: 12-72%) was then recruited from outpatient clinics, elective echocardiography and cardiac catheterisation lists and underwent 2DE and CMR. This second cohort of patients was used to validate the regression equation used to convert the GSS into a LVEFES.

4.3.2 Patient Selection

Patients were included in the study if they were in sinus rhythm and had no contraindications to CMR. Patients were excluded if they were in atrial fibrillation, had a

contraindication to CMR or had poor endocardial wall definition as defined by the inability to accurately visualize ≥ 2 AHA myocardial segments. Clinical characteristics of the study population are shown in Table 4.1.

Gender (M:F)	21:12
Mean age (yrs)	60 \pm 15
Cardiac Diagnosis	
- Ischaemic heart disease*	18
- Valvular heart disease	3
- Dilated cardiomyopathy	1
- Pulmonary hypertension	4
- Atrial septal defect	1
- Other	1
- No cardiac diagnosis	5

Table 4.1. Clinical characteristics of the study population (N=33).

F, female; M, male

*diagnosed either on coronary angiography, or clinical diagnosis of angina/previous myocardial infarction.

4.3.3 Imaging Methods

CMR, 2DE and 3DE were performed consecutively, within 2 hours of each other, to ensure similar cardiac loading conditions.

Cardiac Magnetic Resonance Imaging

The CMR LV systolic function acquisition protocol was performed as previously described in section 3.4.1.

3D Echocardiography Imaging

The 3DE LV systolic function acquisition protocol was performed as previously described in section 3.5.

2D Echocardiography Imaging

2DE imaging was performed from the apical window with the patient in the left lateral decubitus position using a Vivid 7 scanner (GE Medical Systems, Wauwatosa, WI). Depth and frame rate were optimized and 2D images recorded of the apical 4-chamber (A4C), apical-2chamber (A2C) and apical long axis (ALAX) views of the left ventricle and stored for subsequent LV analysis. Harmonic imaging was used consistently throughout each study. Speckle tracking strain analysis was performed from standard apical views of the heart therefore image acquisition times for 2D speckle tracking strain imaging was the same as that of a standard echocardiogram.

4.3.4 Image Analysis

Cardiac Magnetic Resonance

LV volumes were quantified and LVEF calculated by CMR using the method described in section 3.4.1.

3D Echocardiography

LV volumes were quantified and LVEF calculated by 3DE using the method described in section 3.5.

2D Echocardiography

LVEF was calculated from the A4C and A2C views using Simpson's biplane method of discs as described in section 3.6.1.³⁸

Two-dimensional longitudinal strain was analysed using Automated Functional Imaging (AFI) software (GE Medical Systems, Wauwatosa, WI) from the apical four-chamber, apical two-chamber and apical long axis views after optimising gain, depth and filter settings to ensure optimal endocardial border definition and frame rates. The aortic valve closure time in relation to QRS onset was determined from the apical long axis view as shown in Figure 4.1.

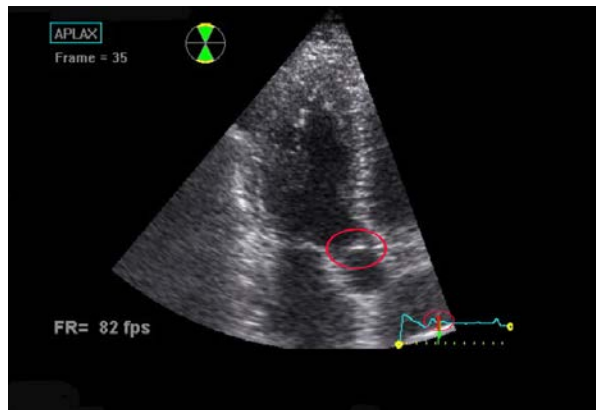


Figure 4.1. Determining the correct aortic valve closure time using AFI strain software. The point of closure of the aortic valve is selected after frame-to-frame analysis of aortic valve motion in the apical long axis view (large circle). The aortic valve closure time is represented as a green line on the ECG (small circle).

Once the aortic valve closure time has been selected, the endocardial and epicardial borders were selected manually. Points are positioned at the junction of the basal walls and mitral annulus, and at the apex. The endocardial border tracking system (shown in Figure 4.2) is re-positioned manually by selecting the appropriate coloured dots, until the operator was satisfied that each myocardial segment was being tracked correctly throughout that cardiac cycle.

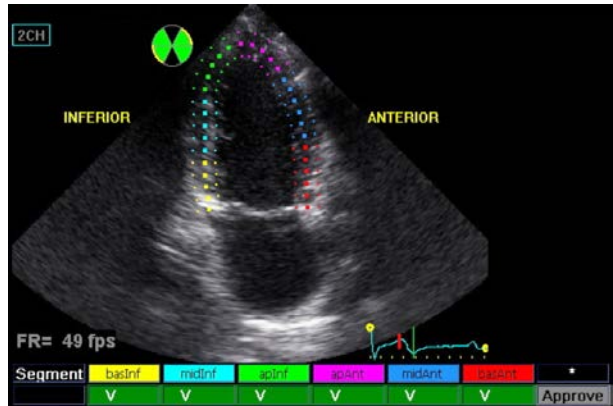


Figure 4.2. Semi-automated border tracking with AFI 2D Strain Imaging.

The semi-automated endocardial border tracking system is positioned as shown. Once the operator is satisfied that each myocardial segment is being correctly tracked throughout the cardiac cycle, the positions are finalised by selecting the approve button shown below.

The AFI strain software automatically divides the left ventricle into the standard AHA myocardial segments using the 16-segment model as shown in Figure 4.3.

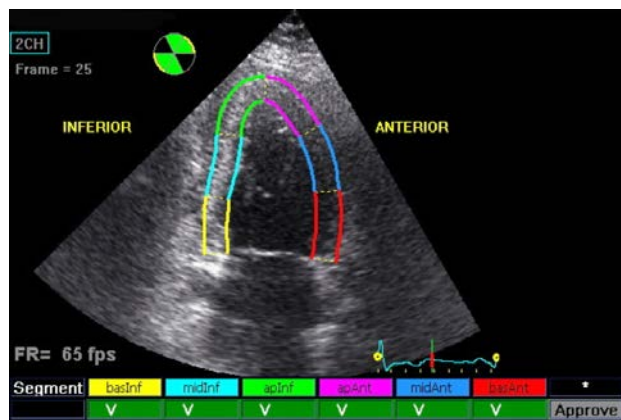


Figure 4.3. Segmental distribution of AFI 2D strain imaging. The left ventricular walls are automatically divided in to the standard AHA myocardial segments as shown.

Using the software “quad” function, a peak systolic strain score is automatically calculated for each myocardial segment as shown in the bottom left quadrant of Figure 4.4. The top right and bottom right quadrants of Figure 4.4 are a graphical representation and parametric representation of the same data. A global strain score for the apical image is shown in the upper left quadrant of Figure 4.4.

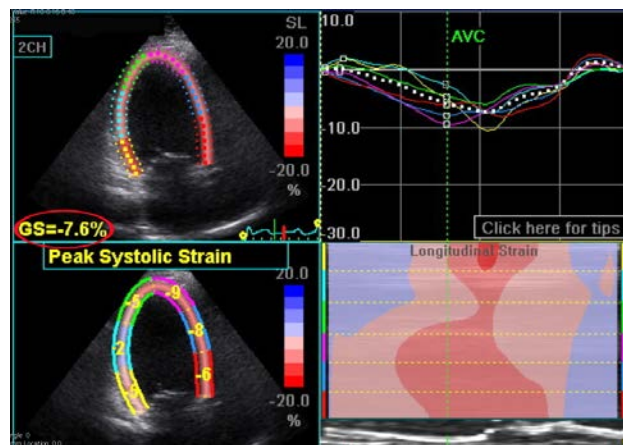


Figure 4.4. Segmental and global strain results recorded from the apical 4-chamber view. A segmental strain score is automatically applied to each myocardial segment. A global strain score is also applied to each apical view imaged (circled). Note the abnormally low segmental and global strain recordings this heart failure patient in comparison to the scores recorded in the normal control subject shown in Figure 1.19.

The global strain score for each apical view was recorded, and a global strain score for the entire left ventricle was calculated as the average of these three recordings as shown in Equation 4.1.

Equation 4.1. Calculating the Global Strain Score of the left ventricle:

$$\text{Global Strain Score (LV)} = (\text{GS(A4C)} + \text{GS(A2C)} + \text{GS(ALAX)})/3$$

(GS, global strain; A4C, apical four-chamber view; A2C, apical two-chamber view; ALAX, apical long axis view)

The semi-automated border tracking system ensured rapid quantification of 2D strain (analysis time <2 minutes per view) thus enabling online calculation of GSS during each standard echocardiographic study.

4.3.3 Reproducibility

Interobserver variability in CMR-LVEF, 3DE-LVEF, biplane Simpson's LVEF and GSS were assessed in 10 patients by two independent observers. These measurements were repeated by one observer six months later.

4.3.4 Statistical Analysis

All data sets were tested for normality using the Shapiro-Wilk test when sample size was greater than fifty and the Kolmogorov-Smirnov test when it was not. GSS was compared to biplane Simpson's LVEF using bivariate correlation (Spearman correlation coefficient). Each echocardiographic technique was correlated against CMR-derived LVEF using bivariate correlation (Pearson correlation coefficient). Intertechnique agreement was tested through Bland-Altman analyses. Stepwise regression analysis was then performed to establish which echocardiographic technique had the strongest correlation to CMR-derived LVEF. A regression equation was derived from the results and used to convert the GSS into an ejection fraction equivalent score (LVEFES). Inter- and intra-observer variability was expressed as the co-efficient of variation, mean bias, limits of agreement and standard deviation of the difference for each echocardiographic technique. A value of $p < 0.05$ was considered statistically significant.

4.4 RESULTS

Eight patients were excluded from the study due to poor endocardial wall definition. One patient was unable to complete the CMR scan due to claustrophobia and was excluded from the CMR/3DE study arm. Seventy-five patients successfully completed the 2DE validation study and thirty-three patients successfully completed the CMR/3DE arm of the study.

4.4.1 Correlation of GSS with Simpson's LVEF

GSS was compared to LVEF calculated using biplane Simpson's rule in 75 patients (EF range: 15-79%). GSS had a good correlation with biplane Simpson' rule ($p < 0.001$, $r = 0.768$). Correlation between the two different 2D echocardiographic methods are shown in Figure 4.5.

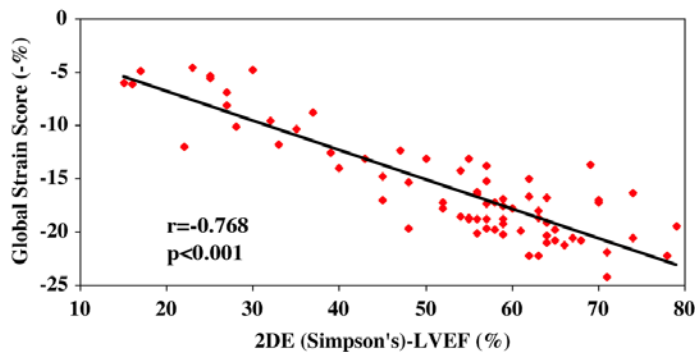


Figure 4.5. Correlation of 2D Speckle tracking strain (Global Strain Score -%) with 2DE Simpson's Rule.

LVEF, left ventricular ejection fraction; 2DE, two dimensional echocardiography

4.4.2 Correlation of GSS, Simpson's LVEF and 3DE-LVEF with CMR-LVEF

Quantification of global LV systolic function by GSS, Simpson's-LVEF and 3DE-LVEF methods were compared to CMR-LVEF as the reference standard in 33 patients (LVEF range: 24-73%). GSS had a moderately-strong correlation with CMR-LVEF ($p < 0.001$,

$r=0.700$) compared to 3DE-LVEF which had a strong correlation with CMR-LVEF ($p<0.001$, $r=0.839$). GSS had a better correlation with CMR-LVEF than Simpson's-LVEF ($p<0.001$, $r=0.652$). Correlation between imaging modalities are shown in Figure 4.6-4.8.

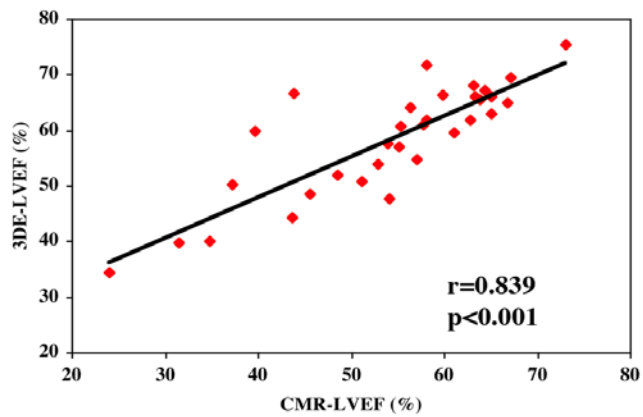


Figure 4.6. Correlation of CMR-derived LVEF (%) with 3DE-LVEF (%).

CMR, cardiac magnetic resonance; LVEF, left ventricular ejection fraction; 3DE, three-dimensional echocardiography.

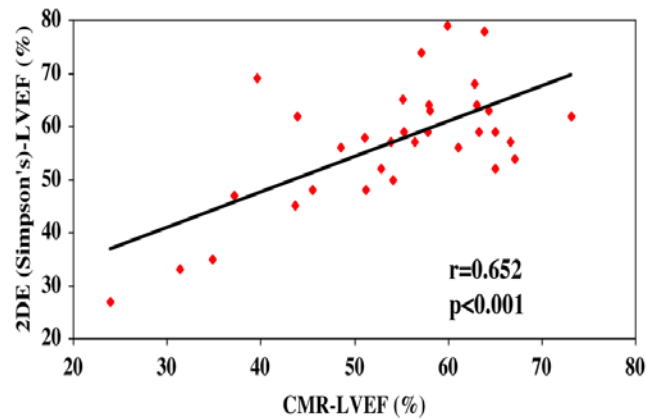


Figure 4.7. Correlation of CMR-derived LVEF (%) with 2DE Simpson's Rule LVEF (%)

CMR, cardiac magnetic resonance; LVEF, left ventricular ejection fraction; 2DE, two-dimensional echocardiography

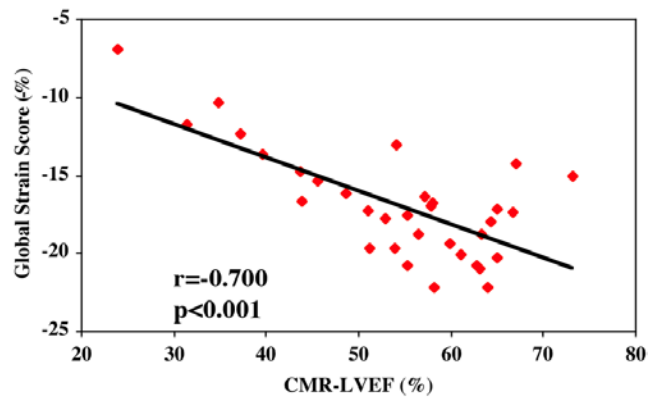


Figure 4.8. Correlation of CMR-derived LVEF (%) with 2D Speckle tracking strain (Global Strain Score -%).

CMR, cardiac magnetic resonance; LVEF, left ventricular ejection fraction

Table 4.2 shows the results of stepwise regression analysis of the three echocardiographic imaging modalities against CMR. On stepwise regression analysis, a combined assessment using 3DE and GSS, correlated most strongly with CMR-LVEF. Of the 2DE methods, the GSS had a significantly stronger relationship to CMR-LVEF than biplane Simpson's Rule (Table 4.3).

Stepwise Regression of CMR-derived LVEF vs. 3DE, GSS and Simpson's Rule

- 1) 3DE: T= 5.38, p<0.001
- 2) GSS: T= -2.08, p<0.05

- 1) 3DE: R = 0.839
- 1) + 2) 3DE + GSS: R = 0.860

Table 4.2. Stepwise regression analysis of 3DE, GSS and 2DE Simpson's Rule against CMR as the reference standard for the quantification of global LV systolic function.

CMR, cardiac magnetic resonance; GSS, global strain score; LV, left ventricular; 3DE, three-dimensional echocardiography; 2DE, two-dimensional echocardiography

Stepwise Regression of CMR-derived LVEF vs. GSS and Simpson's Rule

- 1) GSS: T= -2.74, p<0.01
- 2) Simpson's : T= 1.80, p=NS

- 1) GSS: R = 0.735

Table 4.3. Comparing 2DE imaging modalities: Stepwise regression analysis of GSS and 2DE Simpson's Rule against CMR as the reference standard for the quantification of global LV systolic function.

CMR, cardiac magnetic resonance; GSS, global strain score; LV, left ventricular; 2DE, two-dimensional echocardiography

4.4.3 Receiver operator characteristics

The cut-off point for calculating sensitivity and specificity for GSS was determined from the ROC curve (Figure 4.9). Using CMR-LVEF<55% (abnormal LV function was considered positive), a GSS of $\geq -17\%$ predicted abnormal LV systolic function with a specificity of 84% and a sensitivity of 71%.

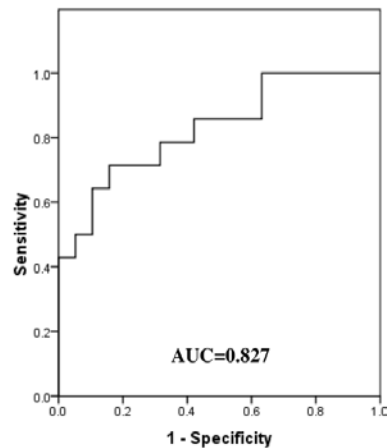


Figure 4.9. Receiver operator characteristic curve of global strain score.

AUC, area under the curve

4.4.4 Calculation of left ventricular ejection fraction and validation of regression equation

From linear regression analysis, the GSS can be converted into a LVEFES using the regression equation: $LVEFES = -2.28(GSS) + 15.46$. Applying this formula to our patient population we confirmed that a GSS less than -17% is associated with a normal LVEF ($LVEF \geq 55\%$) by CMR. This regression equation was validated in a separate cohort of 20 patients who were also recruited from outpatient clinics, elective echocardiography and cardiac catheterization lists (validation cohort LVEF range: 12-72% as measured by CMR). Correlation analysis showed similar agreement in the validation group ($p=0.001$, $r=0.683$) as in the test group (Figure 4.10). Of the patients diagnosed with impaired LV systolic function ($LVEF < 55\%$) by CMR, 86% were correctly classified by GSS LVEFES. By

comparison, 79% were correctly classified as having impaired LVEF by 3DE and only 64% were correctly classified using biplane Simpson's rule.

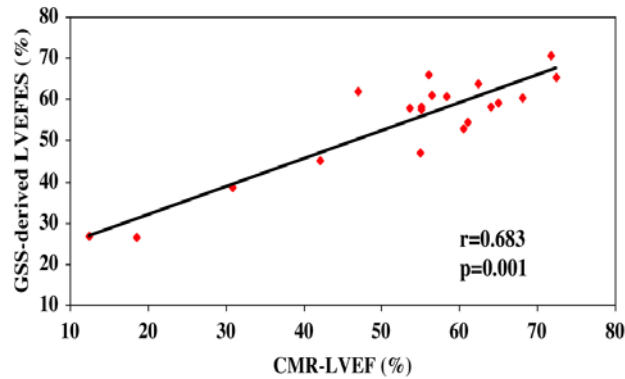


Figure 4.10. Correlation of CMR-derived LVEF (%) with GSS LVEFES (%) in the validation cohort of 20 patients.

CMR, cardiac magnetic resonance; GSS, global strain score; LV, left ventricular ejection fraction equivalent score

4.4.5 Acquisition and analysis times

For a technique to have wide spread clinical application it must be easy and quick to perform. As speckle strain analysis is derived from standard apical imaging views of the heart, additional image acquisition time over and above that of a standard transthoracic study was negligible. Analysis time for the GSS was in the region of 4 minutes.

4.4.6 Reproducibility

Intra- and inter-observer variability for CMR LVEF, 3DE-LVEF, biplane Simpson's LVEF and GSS are expressed as the co-efficient of variation, and as the mean bias, limits of agreement and standard deviation of the difference (Table 4.4 and 4.5). The corresponding Bland-Altman plots are shown in Figure 4.11-4.14.

Imaging modality used to quantify LV function	% Co-efficient of variation	Mean bias	Limits of agreement	SDD
CMR - LVEF (%)	2.79%	-0.98	-5.59 to 3.62	2.30
3DE - LVEF (%)	4.72%	1.3	-9.06 to 11.66	5.18
Simpson's LVEF (%)	3.19%	0.82	-5.16 to 6.79	2.99
Global Strain Score (-%)	2.22%	0.45	-1.30 to 2.20	0.88

Table 4.4. Intra-observer variability for measurements of global left ventricular systolic function.

CMR, cardiac magnetic resonance; LVEF, left ventricular ejection fraction; 3DE, three dimensional echocardiography; SDD, standard deviation of the difference.

Imaging modality used to quantify LV function	% Co-efficient of variation	Mean bias	Limits of agreement	SDD
CMR - LVEF (%)	3.60%	1.29	-5.19 to 7.78	3.24
3DE - LVEF (%)	5.26%	-0.26	-13.25 to 12.72	6.49
Simpson's LVEF (%)	6.91%	-0.69	-13.45 to 12.07	6.38
Global Strain Score (-%)	3.15%	0.44	-1.25 to 2.13	0.84

Table 4.5. Inter-observer variability for measurements of global left ventricular systolic function.

CMR, cardiac magnetic resonance; LVEF, left ventricular ejection fraction; RT3DE, real time three dimensional echocardiography; SDD, standard deviation of the difference.

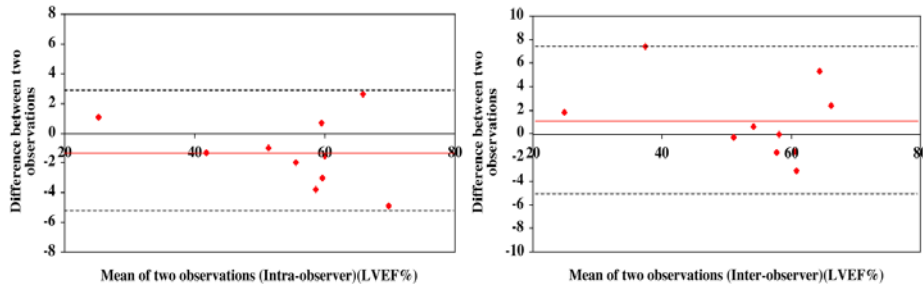


Figure 4.11. Bland-Altman Plot of (A) intra-observer and (B) inter-observer variation for measuring LV systolic function using cardiac magnetic resonance (LVEF %)

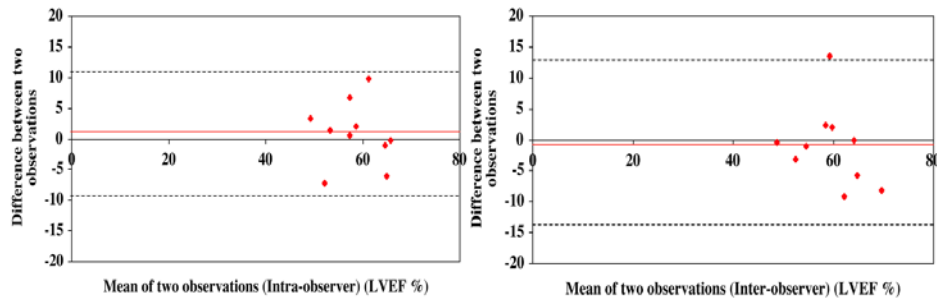


Figure 4.12. Bland-Altman Plot of (A) intra-observer and (B) inter-observer variation for measuring LV systolic function using 3D echocardiography (LVEF %)

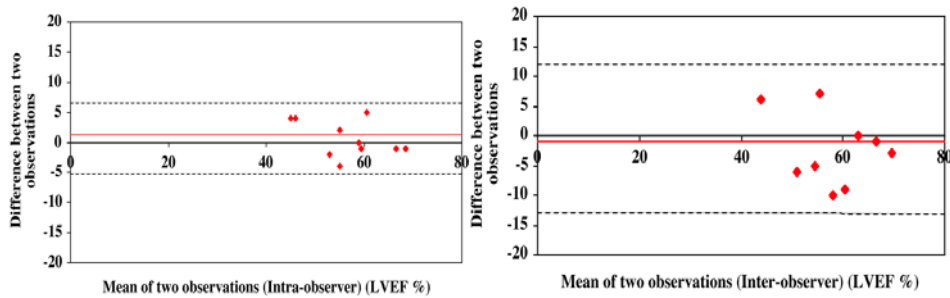


Figure 4.13. Bland-Altman Plot of (A) intra-observer and (B) inter-observer variation for measuring LV systolic function using 2DE Simpson’s Rule (LVEF %)

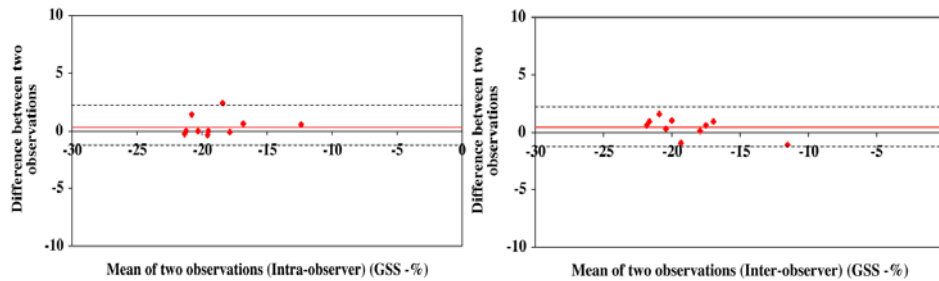


Figure 4.14. Bland-Altman Plot of (A) intra-observer and (B) inter-observer variation for measuring LV systolic function using 2D Speckle tracking strain (Global Strain Score - %)

Intra- and inter-observer variability for calculating the GSS was excellent (co-efficient of variation = 2.3% and 3.0% respectively). The average time taken for calculating the GSS was ≤ 4 minutes.

4.5 DISCUSSION

This study has shown that using 2D speckle tracking strain is a fast, accurate and reproducible method for quantifying global LV systolic function.

At the outset of this study we sought to explore the use of speckle tracking strain imaging as a novel rapid 2D assessment of global LV function and compare its accuracy against other cardiac imaging modalities. The GSS is a novel, reproducible measure of LV function with good correlation when compared to with CMR-derived LVEF. On stepwise regression analysis, the GSS had a significantly stronger relationship to CMR-LVEF than biplane Simpson’s rule.

CMR has rapidly become the reference standard for assessing cardiac anatomy and function. The technique for quantifying LVEF by CMR is highly reproducible as demonstrated in table 4.4.and 4.5 above. However, there remain major limitations to its

widespread use due to initial cost and inability of some individuals to enter an enclosed space. Furthermore, patients with severe LV dysfunction may be unable to lie flat for the duration of the investigation, or may be contraindicated from undergoing CMR due to the increasing prevalence of cardiac resynchronisation therapy and internal cardioverter defibrillator devices in this cohort. Three-dimensional echocardiography measurements compare favourably to CMR reference values in this study and others,¹⁴⁴⁻¹⁴⁷ however as yet 3DE is not widely available outside specialist centres. Two-dimensional speckle tracking strain, by comparison, now comes as a standard function on most new 2D GE echo machines, and is widely available on echo machines by other manufacturers. Both CMR and 3DE protocols involve image acquisition and frame averaging over several heart beats. Image quality is thus detrimentally affected by respiratory motion artefact, irregular heart rhythms and frequent ventricular ectopy. Two-dimensional speckle tracking strain analysis is performed on images acquired over a single heart-beat with high temporal resolution, and thus in theory may be more accurate in patients with atrial fibrillation, although this remains to be determined.

Standard 2DE is widely available, relatively inexpensive and well tolerated. Its limitation is in the 10-15% of patients in whom satisfactory images cannot be obtained due to poor echocardiographic windows. At present, the ASE/EAE recommend Simpson's rule as the preferred 2D method to calculate LVEF.³⁸ This technique requires both the presence of good endocardial definition and the absence of apical foreshortening during image acquisition. In echogenic subjects and with the introduction of second harmonic imaging in the absence of contrast enhancement, inter-observer errors are still significant. Thomson *et al* showed that the inter-observer variability in calculating the left ventricular end diastolic volume (LV EDV), left ventricular end systolic volume (LV ESV) and LVEF can be as high as 13%, 17% and 18% respectively.¹⁴² Even with the use of both second harmonic imaging and contrast enhancement (which is neither practical or feasible for routine use in a busy technician-led echocardiography laboratory), inter-observer variability for LV EDV, LV ESV and LVEF are 8%, 15% and 6% respectively.¹⁴² By contrast, intra- and inter-observer variability of GSS in this study was 2.3% and 3.2% respectively. Not only does GSS correlate more closely than biplane Simpson's rule to CMR based quantification of LV systolic function, it is more reproducible too. Furthermore it is quick and easy to use, and due to the automated nature of the border tracking can be used by echocardiographers

of varying experience. The results of our study compliment the results of a recently published study by Brown et al³¹⁴ further strengthening the growing body of evidence that 2D speckle tracking strain may be a useful alternative for the quantification of global as well as regional LV systolic function.

As echocardiography reports are interpreted by imaging specialists, general cardiologists, general physicians and trainees alike, it is important that the method used for quantifying LV function is easily recognised across all medical specialties. LVEF ubiquitously is the convention by which LV function is quantified. Strain imaging however, measures myocardial deformation not volumetric changes. We believe it is important that the GSS should be converted into a LVEFES that is easily interpreted by all. The GSS, derived using GE AFI Strain software may be used to calculate a LVEFES using the equation:

$$\text{LVEFES} = -2.28(\text{GSS}) + 15.46$$

4.5.1 Study limitations

This study was designed to examine the feasibility of using 2D strain for quantifying global LV systolic function. In this study we derived GSS using GE Vivid 7 AFI speckle tracking strain software. We cannot comment on the accuracy of 2D strain for quantifying LV systolic function using software from other manufacturers. From the results of our study, we derived a regression equation to enable us to convert the GSS into a more user-friendly and recognisable LVEFES. Preliminary validation of this formula was performed by correlating GSS LVEFES against CMR-derived LVEF in a second independent cohort of 20 patients with encouraging results. However, subgroup analysis in patient subgroups with mild, moderate and severe LV dysfunction was not possible due to the small number of study patients and this warrants further investigation before use of the GSS for calculating LVEF should be introduced into clinical practice.

4.5.2 Conclusion

In centres where CMR and 3DE are not available, the GSS may provide a superior 2DE alternative to biplane Simpson's rule for quantifying global LV systolic function.

4.5.3 Future work

Future work should involve repeating this study in a prospective and blinded manner in a much larger cohort of patients exhibiting a wide range of LVEF. This would enable meaningful sub-group analysis of study subjects with mild, moderate and severe LV systolic impairment. We believe our regression equation should also be tested in a larger cohort of patients. Finally, inter-technique concordance needs to be established between 2D speckle tracking strain software packages produced by different manufacturers.

CHAPTER 5

LEFT VENTRICULAR SYSTOLIC FUNCTION - PART TWO

**“A STUDY OF THE 16-SEGMENT REGIONAL WALL
MOTION SCORING INDEX AND BIPLANE
SIMPSON’S RULE FOR THE CALCULATION OF
LEFT VENTRICULAR EJECTION FRACTION: A
COMPARISON WITH CARDIAC MAGNETIC
RESONANCE IMAGING”**

CHAPTER 5: LV SYSTOLIC FUNCTION PART 2

5.1 INTRODUCTION

The accurate quantification of LVEF is important for the reasons previously discussed. To have a wide clinical application, in addition to being accurate and reproducible, the technique used to quantify LVEF has to be easy to perform, relatively quick and widely available. Currently, high cost and limited availability prohibit the routine application of both CMR and 3DE as the first line imaging modality for assessing resting LV systolic function in clinical practice. The 2DE biplane Simpson's rule although widely available, has limitations which have already been discussed extensively in chapters 1 and 4. In chapter 4, we therefore investigated the use of 2D speckle tracking strain as an alternative method for quantifying LVEF with an encouraging result. Although this 2DE technology now comes routinely as part of the software package on several new echo machines, and is more accessible than 3DE or CMR, it is not available on older machines, and several cardiac imaging centres, especially in less affluent countries, may not have access to this technology. Furthermore, speckle tracking strain software varies between manufacturers, and until more validation studies are performed, it is unclear whether the strain value measured using a GE echo machine will be the same as that measured using an echo machine produced by Philips, Toshiba or other manufacturers.

For this reason we decided to investigate the use of the method recommended by the ASE and EAE for assessing regional LV systolic function, to see if we could use it to quantify global LV systolic function and calculate LVEF. The ASE/EAE guidelines recommend using the American Heart Association (AHA) 16-segment model for the assessment of regional LV function.³⁸ A regional wall score is applied to each myocardial segment classifying it as follows: 1=normal contraction, 2=hypokinetic (reduced contraction), 3=akinetic (no contraction) and 4=dyskinetic (paradoxical motion during systole). The regional wall motion score is applied by visually assessing radial contraction of each AHA myocardial segment within the LV, and therefore does not require the use of specialist software. One limitation of this scoring system is that it does not differentiate between the

contractile differences of mildly hypokinetic and severely hypokinetic myocardial segments.

5.2 STUDY AIMS

The aim of this study was to validate the accuracy of a simple novel 2DE technique to quantify global LV systolic function by using a modified regional wall motion scoring system and comparing it against biplane Simpson's Rule and also CMR as the reference standard.

5.3 METHODS

5.3.1 Study Design

One hundred and ten patients exhibiting a broad spectrum of LVEF's (Range 7-74%) were recruited from outpatient clinics, elective echocardiography and cardiac catheterisation lists.

All study subjects underwent standard 2DE (GE Vivid 7). Due to limited access to MRI facilities, it was not possible to perform CMR scans on all 110 study subjects. Fifty-two~~one~~ of 110 study subjects were randomised to undergo CMR within one hour of echocardiography, successfully underwent CMR. LVEF was calculated by 2DE using Simpson's rule and CMR in the standard way as previously described. A regional wall motion score (RWMS) was applied to each of 16-AHA myocardial segments based on the consensus opinion of two BSE accredited cardiologists experienced in echocardiography and blinded to the other scan results. The modified Regional Wall Motion Score Index (RWMSI) was then used to calculate a global LVEF as described below. The two echocardiographic methods for quantifying LV function were then compared against each other. ~~LVEF~~ calculated by using the RWMSI (RWMSI-LVEF) and by using Simpson's Rule (Simpson's-LVEF) was then correlated against CMR as the reference standard for the subgroup of ~~51~~ patients who successfully~~underwent~~ CMR. There was a broad range of LVEF (12-73%) assessed in this cohort. Subgroup analyses were performed to assess

intertechnique agreement of both the RWMSI and Simpson's rule compared to CMR in patients with normal (LVEF \geq 55%) and impaired (LVEF <55%) LV systolic function.

5.3.2 Patient Selection

Patients with normal LV systolic function, globally impaired LV systolic function and regional wall motion abnormalities were included in the study. Patients were excluded if they had a contraindication to CMR or had poor endocardial wall definition as defined by the inability to accurately visualize \geq 2 AHA myocardial segments. Clinical characteristics of the study population are described in Table 5.1.

Gender (M:F)	29:22
Mean age (yrs)	59
Clinical Diagnosis	
- Ischaemic heart disease*	31
- Valvular heart disease	3
- Dilated cardiomyopathy	3
- Pulmonary hypertension	3
- Restrictive cardiomyopathy	1
- Atrial septal defect	1
- Coronary artery spasm	1
- No cardiac diagnosis	8

Table 5.1. Clinical characteristics of study subjects who completed both CMR and 2D echocardiography protocols (n=51)

F, female; M, male

* diagnosed either on coronary angiography, or clinical diagnosis of angina/previous myocardial infarction.

5.3.3 Imaging Methods

CMR and 2DE were performed consecutively, within 30 minutes of each other, to ensure similar cardiac loading conditions.

Cardiac Magnetic Resonance Imaging

The CMR LV systolic function acquisition protocol was performed as previously described in section 3.4.1.

2D Echocardiography Imaging

2DE imaging was performed from the parasternal and apical windows with the patient in the left lateral decubitus position using a Vivid 7 scanner, (GE Medical Systems, Wauwatosa, WI). Depth and frame rate were optimized and 2D images recorded of the parasternal long axis (PSLAX), parasternal short axis (PSSAX), apical 4-chamber (A4C), apical 2-chamber (A2C) and apical long axis (ALAX) views of the left ventricle and stored for subsequent LV analysis. Harmonic imaging was used consistently throughout each study. Echo contrast agents were not used.

5.3.4 Image Analysis

Cardiac Magnetic Resonance

LV volumes were quantified and LVEF calculated by CMR using the method described in section 3.4.1.

2D Echocardiography

LVEF was calculated from the A4C and A2C views using Simpson's biplane method of discs as described in section 3.6.1.

Regional Wall Motion Score Index

A modified regional wall motion score (RWMS) was applied to each of 16-AHA myocardial segments, based on the consensus opinion of two British Society of Echocardiography accredited cardiologists blinded to other scan results (Figure 5.1). The RWMS was applied as follows: Hyperkinesis = 3; Normal regional contraction = 2; Mild-moderate Hypokinesis = 1.25; Moderate-Severe Hypokinesis = 0.75; Akinesis = 0, Dyskinesis = -1. This modified RWMS includes analysis of hyperkinetic and dyskinetic myocardial segments and differentiates between degrees of hypokinesis. Normal regional contraction was defined by the presence of normal wall thickening in the radial plane of the LV. In cases of partial segment contractility, when half a myocardial segment exhibited akinesis (0) and the other half normal contractility (2) the combined scores were averaged to give an overall score (1) for that segment. LVEF was then calculated using the following equation:

Equation 5.1. The Regional Wall Motion Scoring Index for calculating LVEF:

$$\text{LVEF}(\%) = \Sigma(16\text{segRWMS})/16 \times 30.$$

Formatted: Body Text 3, Left

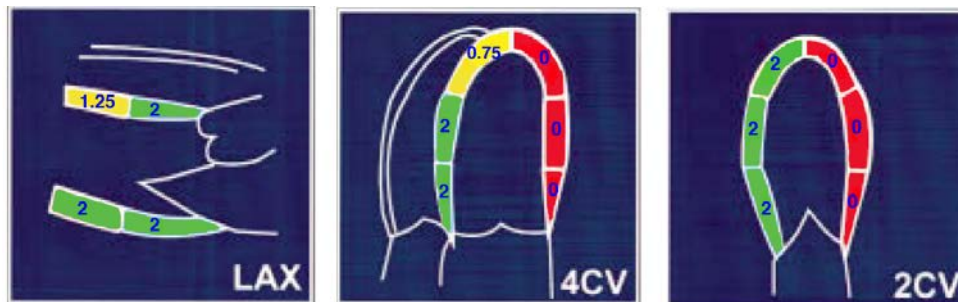


Figure 5.1. Calculating LVEF using the Regional Wall Motion Scoring Index.

A regional wall motion score (RWMS) is applied to each of the 16-American Heart Association myocardial segments. RWMS: Hyperkinesis = 3; Normal regional contraction = 2; Mild-moderate Hypokinesis = 1.25; Moderate-severe Hypokinesis = 0.75; Akinesis = 0; Dyskinesis = -1. LVEF is then calculated by: LVEF (%) =

$\Sigma(16\text{segRWMS})/16 \times 30$. In this example, the RWMS=18, therefore LVEF=18/16 x 30 = 34%.

Formatted: Body Text 3, Left

5.3.5. Reproducibility

Interobserver and intraobserver variability in Simpson's-LVEF and RWMS-LVEF was assessed in 10 patients exhibiting a range of LVEFs (LVEF range: 12-68% by CMR analysis). LVEF was assessed using RWMSI and Biplane Simpson's rule by two independent observers. These measurements were repeated by one observer six months later.

5.3.6. Statistical Analysis

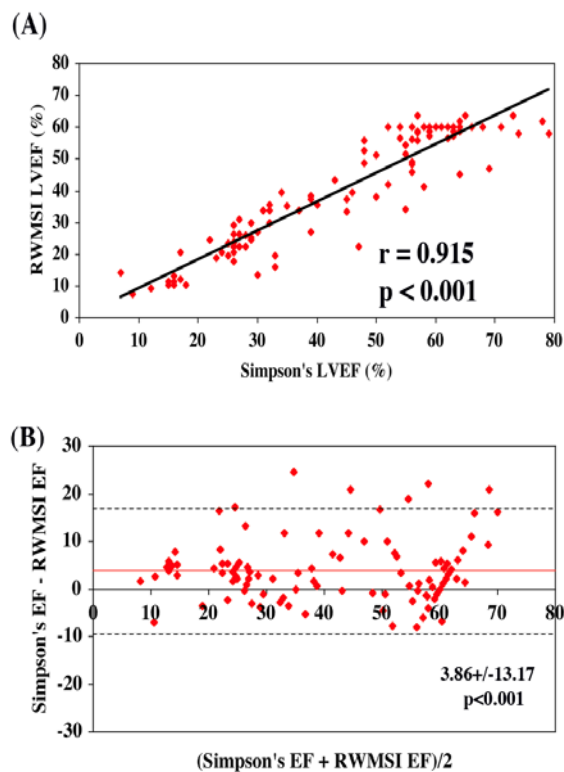
Values are expressed as mean \pm standard deviation (SD). All data sets were tested for normality using the Shapiro-Wilk test when sample size was greater than fifty and the Kolmogorov-Smirnov test when it was not. Each echocardiographic technique was correlated against CMR-LVEF using a bivariate correlation (Pearson correlation coefficient for parametric data and Spearman correlation coefficient for non-parametric data). For parametric data, linear regression analysis was used to directly compare RWMSI-LVEF to Simpson's-LVEF when indexed against CMR-LVEF as the reference standard. Subgroup analysis was performed to assess the accuracy of RWMSI-LVEF and Simpson's-LVEF indexed against CMR-LVEF in patients with normal (LVEF \geq 55%) and impaired (LVEF<55%) LV systolic function. Bland-Altman analysis was used to determine the bias and limits of agreement between the corresponding measurements. Results are expressed as mean bias \pm 1.96SD. The significance of intertechnique biases was tested using the paired samples T-test for parametrically distributed data and Wilcoxon signed ranks test for non-parametrically distributed data. A value of p<0.05 was considered significant.

5.4. RESULTS

Eight patients were excluded from the study due to poor endocardial wall definition and one patient failed to complete the CMR protocol due to claustrophobia. 102 patients successfully underwent 2DE and 51 of [52102](#) completed the CMR [sub-study protocol](#).

5.4.1 Correlation and intertechnique agreement of RWMSI-LVEF with Simpson's-LVEF

LVEF derived using the RWMSI was compared to LVEF calculated using 2D Simpson's rule in 102 patients (EF range: 7-74%). RWMSI-LVEF correlated strongly with 2D Simpson's rule ($p < 0.001$, $r = 0.915$). Mean calculated LVEF was significantly lower using RWMSI compared to Simpson's Rule (mean bias: 4.06 ± 12.94 ; $Z = -5.25$, $p < 0.001$) (Figure 5.2).



Formatted: Centered

Figure 5.2. (A) Correlation of RWMSI-LVEF with Simpson's Rule in 102 subjects (LVEF range: = 7-74%). (B) Bland-Altman analysis between RWMSI and Simpson's Rule; solid horizontal line denotes the mean difference between RWMSI and Simpson's Rule measurements, broken horizontal lines represent the limits of agreement (2SD around the mean intertechnique difference). Bottom right of Bland-Altman plot: mean bias \pm 1.96SD, the mean bias is significant if $p < 0.05$.

LVEF, left ventricular ejection fraction; RWMSI, regional wall motion score index; SD, standard deviation.

Formatted: Font: 11 pt

Formatted: Font: 11 pt

Formatted: Font: 11 pt

Formatted: Font: 9 pt

Formatted: Font: 9 pt

5.4.2 Correlation and intertechnique agreement of RWMSI-LVEF and Simpson's-LVEF with CMR-LVEF

RWMSI-LVEF and Simpson's-LVEF were compared to CMR-LVEF in 51 patients (EF range: 12-73%). Over a wide range of LVEF, RWMSI-LVEF showed a good correlation with CMR-LVEF ($r=0.916$, $p < 0.001$); Simpson's-LVEF showed a moderate correlation with CMR-LVEF ($r=0.647$, $p < 0.001$). RWMSI-LVEF significantly underestimated LVEF compared to CMR (mean bias: 2.47 ± 11.37 ; $Z = -3.281$, $p = 0.001$) and Simpson's-LVEF significantly overestimated LVEF compared to CMR (mean bias; -3.46 ± 16.74 ; $Z = -2.83$, $p = 0.005$). Correlation between imaging modalities and corresponding Bland-Altman analysis of intertechnique agreement are shown in Figure 5.3.

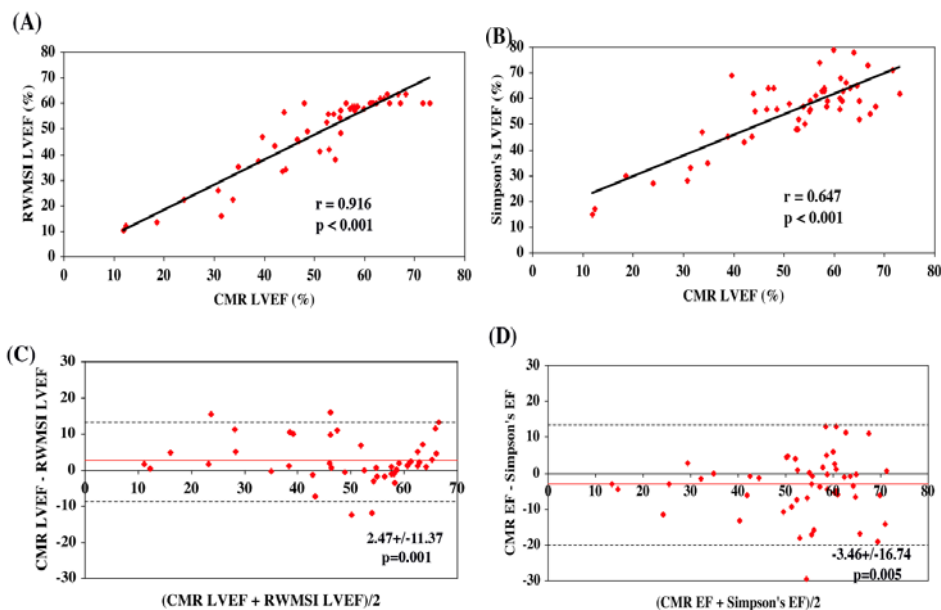


Figure 5.3. Correlation of CMR-LVEF with (A) RWMSI and (B) Simpson's Rule in 51 subjects (LVEF range: 12-73%). (C) Bland-Altman analysis between CMR and RWMSI; solid horizontal line denotes the mean difference between RWMSI and CMR measurements, broken horizontal lines represent the limits of agreement (2SD around the mean intertechnique difference). Bottom right of Bland-Altman plot: mean bias \pm 1.96SD, the mean bias is significant if $p < 0.05$. (D) Bland-Altman analysis between CMR-LVEF and Simpson's Rule in the same format as in Figure 5.3C. LVEF, left ventricular ejection fraction; RWMSI, regional wall motion score index; SD, standard deviation.

5.4.3 Correlation and intertechnique agreement of RWMSI-LVEF and Simpson's-LVEF with CMR-LVEF in patients with normal LV systolic function

Twenty-seven patients who successfully underwent CMR had normal LV systolic function (LVEF \geq 55%). Although a good correlation was noted between RWMSI-LVEF and CMR-LVEF ($r=0.785$, $p<0.001$), RWMSI significantly underestimated LVEF in patients with normal LV systolic function (mean bias: 2.39 ± 7.41 ; $Z=-3.20$, $p=0.001$). There was no significant difference in mean LVEF calculated using Simpson's rule and CMR in patients with normal LV systolic function (mean bias; -1.10 ± 15.86 with 95%CI: -4.30 to 2.11 , $p=NS$), however correlation between these two techniques in patients with normal LV function was surprisingly poor ($r=0.124$, $p=NS$) (Figure 5.4).

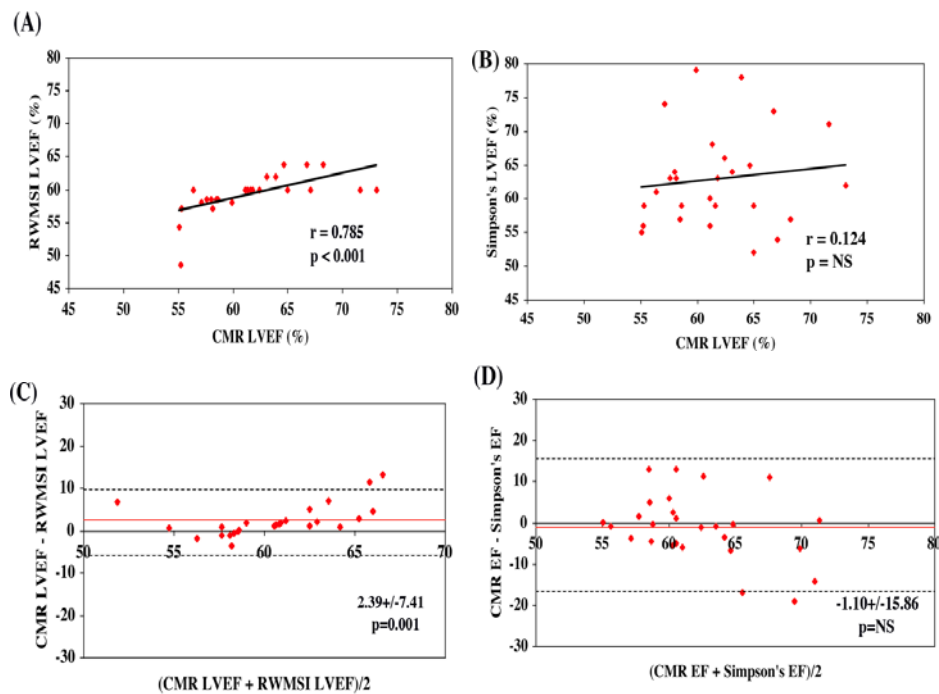


Figure 5.4. Correlation of CMR-LVEF with (A) RWMSI and (B) Simpson's Rule in subjects with normal LV function (LVEF \geq 55%, $n=27$). Lower panels denote Bland-Altman analysis between CMR-LVEF and (C) RWMSI and (D) Simpson's Rule in the corresponding study subjects in the same format as in Figure 5.3.

5.4.4 Correlation and intertechnique agreement of RWMSI-LVEF and Simpson's-LVEF with CMR-LVEF in patients with impaired LV systolic function

Twenty-four of the 51 patients who underwent CMR had impaired LV systolic function (LVEF<55%). RWMSI-LVEF showed a good correlation with CMR-LVEF ($r=0.866$, $p<0.001$) in patients with impaired LV systolic function, this being comparable to the correlation of Simpson's-LVEF with CMR-LVEF ($r=0.826$, $p<0.001$). On linear regression analysis, RWMSI-LVEF had a significantly stronger correlation with CMR-LVEF ($T=3.14$, $p=0.005$) than Simpson's LVEF ($T=1.84$, $p=NS$). In patients with impaired LV systolic function there was no significant difference between LVEF calculated using the RWMSI and using CMR (mean bias: 2.58 ± 14.80 with 95%CI: -0.60 to 5.77 , $p=NS$). Simpson's rule significantly overestimated LVEF compared to CMR with a mean difference of -6.12 ± 16.44 with 95%CI: -9.66 to -2.58 ($p=0.002$) (Figure 5.5).

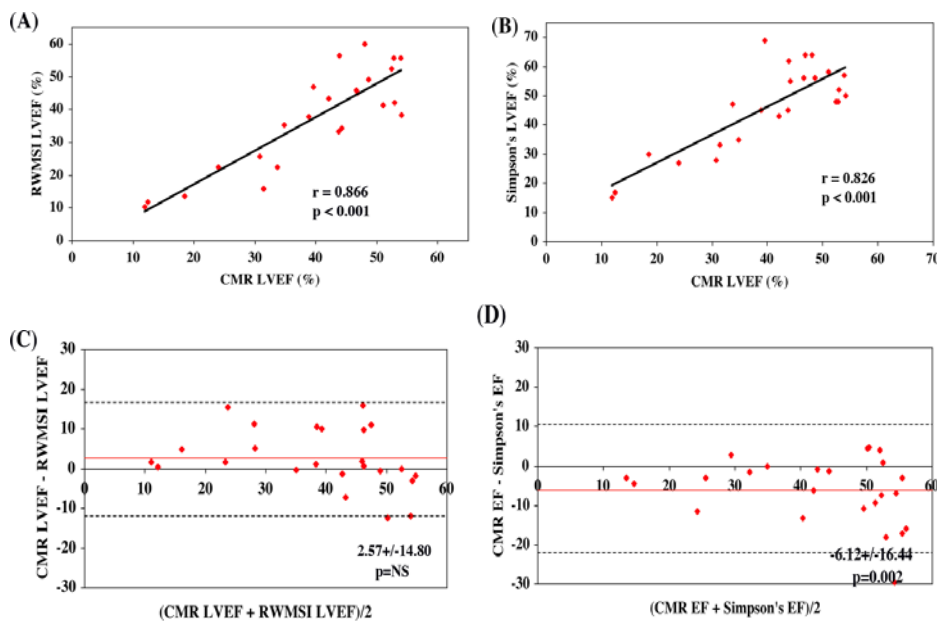


Figure 5.5. Correlation of CMR-LVEF with (A) RWMSI and (B) Simpson's Rule in subjects with impaired LV function (LVEF<55%, n=24). Lower panels denote Bland-Altman analysis between CMR-LVEF and (C) RWMSI and (D) Simpson's Rule in the corresponding study subjects in the same format as in Figure 5.3.

5.4.5 Reproducibility

Intra- and inter-observer variability for RWMSI-LVEF and Simpson's-LVEF are expressed as the co-efficient of variation, and as the mean bias, limits of agreement and standard deviation of the difference as shown in Tables 5.2 and 5.3. The corresponding Bland-Altman plots are shown in Figure 5.6 A-D.

Intra-observer mean of RWMSI-LVEF was 40.42% with difference between the means of $1.68 \pm 10.88\%$. Inter-observer mean of RWMSI-LVEF was 40.48% with difference between the means of $1.64 \pm 12.32\%$. Intra-observer mean of Simpson's-LVEF was 51.20% with difference between the means of $-0.34 \pm 12.33\%$. Inter-observer mean of Simpson's-LVEF was 52.52% with difference between the means of -2.91 ± 9.86 .

RWMSI-LVEF	% Co-efficient of variation	Mean bias	Limits of agreement	SDD
Intra-observer	8.33%	1.68	-9.43 to 12.79	5.55
Inter-observer	11.22%	1.64	-10.93 to 14.21	6.29

Table 5.2. Intra-observer and Inter-observer variability for measurements of LVEF using the Regional Wall Motion Scoring Index

SDD, standard deviation of the difference

Simpsons-LVEF	% Co-efficient of variation	Mean bias	Limits of agreement	SDD
Intra-observer	7.00%	-0.34	-12.92 to 12.24	6.29

Inter-observer	8.45%	-2.91	-12.97 to 7.16	5.03
----------------	-------	-------	----------------	------

Table 5.3 Intra-observer and Inter-observer variability for measurements of LVEF using Biplane Simpson’s Rule

SDD, standard deviation of the difference

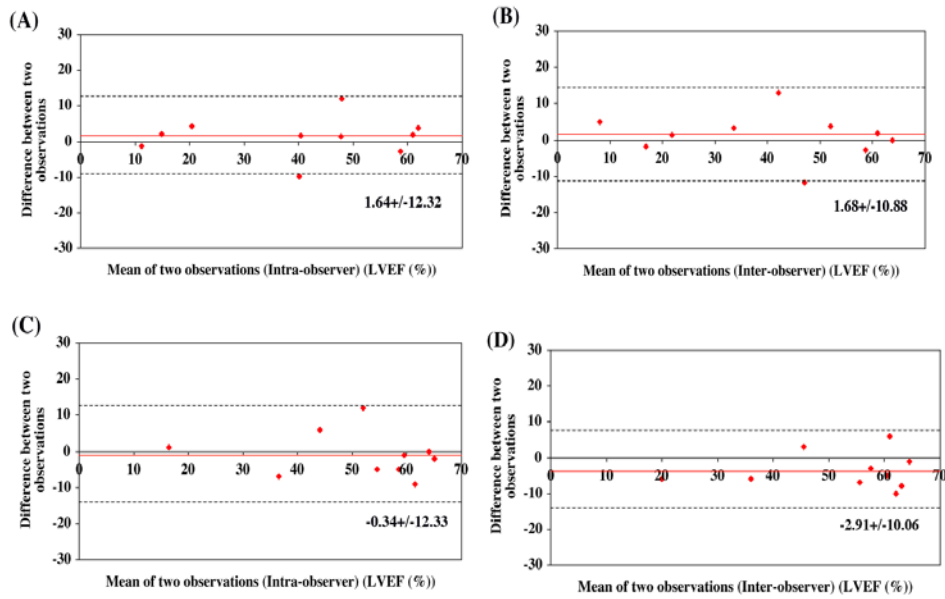


Figure 5.6. Bland-Altman analysis of (A) intra-observer and (B) inter-observer variation for measuring LVEF using RWMSI, and (C) intra-observer and (D) inter-observer variation for measuring LVEF using Biplane Simpson’s Rule.

5.5 DISCUSSION

Cardiac magnetic resonance imaging has rapidly become the reference standard for assessing cardiac anatomy and function. The technique for quantifying LVEF by CMR is highly reproducible as previously reported by our research group.²² However, there remain major limitations to its widespread use due to initial cost and inability of some individuals to enter an enclosed space. Furthermore, patients with severe LV dysfunction may be

unable to lie flat for the duration of the investigation, or may be contraindicated from undergoing CMR due to the increasing prevalence of cardiac resynchronisation therapy and internal cardioverter defibrillator devices in this cohort. 3DE measurements compare favourably to CMR reference values,¹⁴⁴⁻¹⁴⁷ however as yet 3DE is not widely available outside specialist centres. 2DE, on the other hand, is widely available, relatively inexpensive and well tolerated.

At present, the ASE/EAE recommend Simpson's Rule as the preferred 2DE method by which to calculate LVEF despite its recognised limitations.³⁸ Calculation of LVEF by the regional wall motion scoring index is a simple method for quantifying left ventricular systolic function that encompasses information from all 16 AHA myocardial segments of the left ventricle. It has the potential therefore to be of value in quantifying global LV systolic function in patients with impaired LV function due to the presence of regional wall motion abnormalities in addition to patients with global cardiomyopathies. Furthermore, quantification using this method does not require the presence of specialist software, and therefore can be performed in any cardiac centre on any 2D echocardiogram by an experienced operator.

We are not the first research group to use a wall motion score to estimate LVEF. In 2001, McGowan and colleagues used a 9-myocardial segment wall motion score index to quantify LVEF in patients with systolic heart failure secondary to ischaemic heart disease.³¹⁵ They demonstrated moderate agreement with radionuclide ventriculography and moderate reproducibility, and concluded that while a 9-segment wall motion score index was a valid and widely applicable method for assessing LV systolic function, it may not be sensitive enough to detect small changes in LV systolic function that may occur in chronic heart failure. By comparison, we have used a more sensitive 16-segment wall motion score indexed based on the gold standard American Heart Association classification of regional myocardial function.³⁸ Furthermore, McGowan's wall motion score index was validated against radionuclide ventriculography, with a temporal delay of up to four weeks between the echocardiogram and nuclear study. By comparison, in our study we have validated our RWMSI-LVEF against CMR-LVEF, the internationally recognised reference standard. In our study echocardiograms and CMR scans were performed on the same day, within one hour of each other in all patients to ensure similar cardiac loading conditions. In our study,

RWMS-LVEF showed acceptable reproducibility, comparable to that of biplane Simpson's rule. Importantly, LVEF calculated using the RWMSI had a strong correlation to CMR ($p < 0.001$, $R = 0.914$). Biplane Simpson's rule LVEF had a moderate correlation to CMR ($p < 0.001$, $R = 0.647$) when tested over a wide range of LVEFs (range 12-73%).

On sub-group analysis when compared to CMR, Simpson's rule did not correlate with CMR in patients with normal LV systolic function. Although at first this result may seem surprising, on review of the literature, previous comparisons of Simpson's biplane method of discs performed by TTE and volumetric assessment of LVEF performed by CMR have demonstrated large and systematic differences in absolute measurements; Gardner et al¹⁵⁰ reported important differences in CMR volumes and LVEF and echocardiographic volumes and LVEF on indirect comparisons of normal volunteers and Chuang et al¹⁵¹ have demonstrated that intermodality comparison of cardiac volumes and LVEF are significantly better between volumetric CMR analysis and volumetric echocardiography (3D echocardiography) than between volumetric CMR and biplane echocardiography (Simpson's rule). They have also reported wide limits of agreement when comparing volumetric CMR with biplane echocardiography for calculating LVEF.¹⁵¹ These results suggest that LVEF measurements by the two techniques are not interchangeable. By comparison, the RWMSI had a significantly better correlation with CMR-LVEF in patients with normal LV systolic function compared to Simpson's rule, despite a tendency to underestimate absolute LVEF in this cohort (mean RWMSI-LVEF vs. mean CMR-LVEF: $59.37\% \pm 2.99$ vs. $61.75\% \pm 4.82$, $p = 0.001$).

In patients with LV dysfunction, although both echocardiographic techniques correlated well with CMR-LVEF, RWMSI-LVEF had a significantly better correlation with CMR-LVEF than Simpson's-LVEF on step-wise regression analysis. Importantly, RWMSI-LVEF had good intertechnique agreement with CMR in patients with impaired LV systolic function. Simpson's rule significantly overestimated LVEF in the cohort of patients with LV systolic dysfunction. Bellenger et al have previously studied LVEF and cardiac volumes calculated using CMR, 2DE Simpson's rule and radionuclide ventriculography in patients with heart failure and also concluded that biplane echocardiography tends to yield a higher ejection fraction than CMR; a similar finding to this study.¹⁴⁹ This is a clinically important finding. A $LVEF \leq 35\%$ is a prerequisite for heart failure patients to be considered

for certain device therapies such as cardiac resynchronization therapy and internal cardiac defibrillators.^{136,139,316} If Simpson's rule is significantly overestimating LVEF in patients with impaired LV function, patients who would benefit from these devices, may potentially be being excluded. RWMSI did not significantly overestimate or underestimate LVEF in this cohort.

The results of our study suggest that the novel RWMSI-LVEF may be a simple and reliable alternative to biplane Simpson's rule for quantifying LV systolic function. Furthermore RWMSI-LVEF appears to have superior intertechnique agreement with CMR-LVEF compared to biplane Simpson's rule.

5.5.1. Study Limitations

This study was designed to examine the feasibility of using the RWMSI to calculate LVEF and to examine its accuracy compared to CMR and biplane Simpson's echocardiography. Subgroup analysis in patient subgroups with mild, moderate and severe LV dysfunction was not possible due to the small number of study patients and this warrants further investigation.

5.5.2. Conclusion

We have compared the use of the 16-segment RWMSI to biplane Simpson's rule for the quantification of global LV systolic function in patients exhibiting a wide range of LVEF, when indexed against CMR as the reference standard. RWMSI-LVEF correlates strongly with CMR and has good inter-technique agreement. The RWMSI is a simple and widely available method for quantifying left ventricular systolic function using 2DE. In centres where CMR and 3DE are not readily available, the use by experienced individuals, of the RWMSI for calculation of LVEF may offer a simple and reliable 2D echocardiographic alternative to biplane Simpson's rule.

CHAPTER 6

Formatted: Font: 24 pt

LEFT VENTRICULAR DIASTOLIC FUNCTION

“PHASE CONTRAST VELOCITY ENCODED CARDIAC
MAGNETIC RESONANCE IMAGING FOR THE
ASSESSMENT OF LEFT VENTRICULAR DIASTOLIC
FUNCTION – A COMPARISON STUDY WITH
ECHOCARDIOGRAPHY E/Em RATIO AND INVASIVE
CATHETER MEASUREMENTS OF LEFT
VENTRICULAR END DIASTOLIC FILLING
PRESSURE”

CHAPTER 6: LV DIASTOLIC FUNCTION

6.1 INTRODUCTION

Diastolic function is a complex multi-stage active process that remains difficult to measure non-invasively in quantitative terms. The need for accurate diagnosis and quantification of diastolic dysfunction is been designated of “paramount clinical importance” by the European Association of Echocardiography and American Society of Echocardiography.¹⁴ Furthermore, in patients with known systolic heart failure due to dilated cardiomyopathy, the presence and severity of diastolic function correlates better with functional class and prognosis than LVEF.^{177-180,317-331}

Elevated LV filling pressures are the main physiologic consequences of diastolic dysfunction. These are measured invasively during cardiac catheter studies. In patients with normal or near normal LV systolic function (LVEF \geq 50%) traditional non-invasive indices of diastolic function including transmitral E wave velocity, E/A ratio, mitral deceleration time, isovolumic relaxation time and pulmonary vein S:D ratio correlate poorly with LV filling pressures recorded during catheter studies.^{13,191,192} The peak transmitral E wave velocity is dependent on and varied directly with changes in the left atrial pressure and inversely with the time constant of LV relaxation. As abnormal diastolic relaxation and high LV filling pressures commonly co-exist in patients with diastolic heart failure it is therefore unsurprising that peak transmitral E wave velocity correlated poorly with left atrial and left ventricular filling pressures. By dividing the peak transmitral E wave velocity by the early diastolic myocardial tissue relaxation velocity (E_m), we are in effectively correcting the transmitral E wave velocity for the influence of myocardial relaxation, thus improving the relationship with the LV diastolic filling pressure. Therefore

“E” corrected by “Em” (E/Em) gives an estimate of the LV diastolic filling pressure. This is the basis upon which tissue Doppler echo E/Em has been used to non-invasively estimate LVEDP.

The excellent spatial resolution of CMR makes it the gold standard for anatomical imaging of the cardiac chambers. The use of CMR for functional cardiac imaging is also increasing. One of the major advantages of CMR over cardiac CT and nuclear techniques, is that it can provide both accurate anatomical and functional imaging data during a single scan. CMR can be used to assess myocardial viability, using delayed enhancement gadolinium scanning, and inducible myocardial ischaemia using adenosine stress-perfusion and dobutamine stress MRI protocols. CMR is now widely recognised as the reference standard for quantifying LV systolic function. For CMR to fulfil its potential as the one-stop imaging modality for both anatomical and functional imaging of the heart, accurate and reproducible quantitative methods for assessing LV diastolic function by CMR need to be developed.

Research studies have demonstrated a relatively good correlation between CMR and echocardiography for recording mitral inflow patterns using VEC-CMR sequences, however, like echocardiography, these measures are load-dependent and only semi-quantitative.²²³⁻²²⁵ Small single centre studies have explored the potential of using grid-tagged myocardial deformation CMR imaging sequences to assess diastolic relaxation.²¹⁵⁻²¹⁹ This has increased our understanding of left ventricular torsion and the contribution of diastolic “untwisting” and LV suction to LV filling in early diastole.²²⁰ CMR myocardial deformation imaging however has limited ability to assess late diastolic events due to the degradation of the grid-tags in end-diastole.²²¹ Although useful for research purposes, CMR myocardial deformation imaging analysis is time consuming and analysis software is not widely available, limiting the clinical application of this technique at this time. At the time of writing there is no standard CMR method for diagnosing and quantifying left ventricular diastolic dysfunction in clinical practice.

Over the last 10 years, the use of Doppler echocardiography has expanded substantially once it was discovered myocardial tissue velocities could be recorded from heart muscle with high temporal resolution, by applying standard autocorrelation processing but reversing low

amplitude and high velocity filters. Tissue Doppler echocardiography is now used routinely in clinical practice to identify diastolic dysfunction non-invasively and estimate left ventricular end diastolic filling pressure (LVEDP) using the ratio E/Em where E is the peak early diastolic filling velocity of the LV and Em is the peak early diastolic myocardial tissue velocity recorded at the level of the mitral annulus. Based on this principle, we explored the clinical utility of using modified VEC-CMR sequences to measure early diastolic tissue velocities within the LV myocardium, and to use them, along with recorded early diastolic mitral inflow velocities, to estimate LVEDP by calculating a VEC-CMR E/Em ratio.

6.2 STUDY AIMS

The first aim of this study was to use VEC-CMR sequences to record early diastolic mitral inflow velocities (E), and early diastolic myocardial tissue velocities (Em), and compare them to E and Em velocities recorded by Doppler and tissue Doppler echocardiography in patients exhibiting a range of pathologies. The second aim was to use the E and Em values to calculate the E/Em ratio by CMR and to establish if this technique correlated with 1) E/Em ratio recorded by echocardiography and 2) LVEDP as measured invasively by fluid-filled catheter as the reference standard, in a heterogeneous patient cohort as seen in clinical practice.

6.3 METHODS

6.3.1 Study Design

Ethical approval for this study was granted on the basis that patients enrolled into the study must have a clinical indication for undergoing invasive heart catheter studies. Forty-five patients exhibiting a broad spectrum of LVEF's (Range: 18.5-71.6%) were recruited from elective cardiac catheterisation lists.

All study subjects underwent standard 2DE (GE Vivid 7), CMR (1.5T Siemens Sonata) and left heart catheterisation within 3 hours of each other in the fasted state to ensure similar loading conditions. LVEDP was measured during left heart catheterisation as previously

described. Mitral E and A velocities were recorded for all patients by both Doppler echocardiography and VEC-CMR and E/A ratio calculated. VEC-CMR derived E, A and E/A ratios were compared to corresponding echocardiography values. Myocardial tissue Em velocities were recorded from all six LV walls by TDE and VEC-CMR. VEC-CMR Em velocities were compared to corresponding echocardiography values. VEC-CMR E/Em ratios were calculated and compared to Doppler E/Em and to invasively measured LVEDP as the gold standard.

6.3.2 Patient Selection

Patients in sinus rhythm with normal LV systolic function, globally impaired LV systolic function and regional wall motion abnormalities were included in the study. Patients were excluded if they had a contraindication to CMR, had significant mitral valve disease, moderate-severe mitral annular calcification, prosthetic mitral valve or known pericardial disease. Clinical characteristics of the study population are described in Table 6.1.

Gender (M:F)	22:19
Mean age (yrs)	63±10
Clinical Diagnosis	
- Ischaemic heart disease	25
- Valvular heart disease	2
- Dilated cardiomyopathy	2
- Pulmonary hypertension	4
- Restrictive cardiomyopathy	1
- Atrial septal defect	1
- Other	2
- No cardiac diagnosis	4

Table 6.1. Clinical characteristics of study subjects (n=41)

F, female; M, male

6.3.3 Imaging Methods

Left heart catheterisation, CMR and 2DE were performed consecutively, within 3 hours of each other, to ensure similar cardiac loading conditions.

Left heart catheterisation

LVEDP was recorded during left heart catheterisation as previously described in section 3.3.

Cardiac Magnetic Resonance Imaging

The CMR LV diastolic function acquisition protocol was performed as described below:

Cardiac magnetic resonance imaging sequences – Phase encoded velocity imaging for the assessment of left ventricular diastolic function: Image acquisition

Transmitral flow was measured using a retrospectively electrocardiographically triggered FLASH phase-contrast MRI technique with a velocity sensitivity of 130cm/s. The centre of the slice was positioned in the middle of the mitral valve at the level of the valve tips during early diastole with the imaging plane perpendicular to mitral flow, using both two-chamber and four chamber images. In order to cover late diastolic filling, acquisition was performed throughout the cardiac cycle with a retrospective period of 1.2 (scan parameters: slice thickness, 5mm; in-plane resolution, 1.6 x 1.5mm; temporal resolution, 16-18msec; TR/TE = 30/3.2ms; 240 x 256 image matrix and 30⁰ flip angle).¹⁹⁴ Myocardial tissue velocities were measured by repeating this phase-contrast MR sequence with velocity encoding of 30cm/s and a different image slice position. The image slice position was positioned at two-thirds of the long axis, planned on early diastolic two-, three- and four-chamber

images, perpendicular to the interventricular septum. Care was taken during sequence acquisition to ensure aliasing artefact did not occur. If aliasing did occur, the velocity sensitivity was adjusted appropriately and the sequence acquisition was repeated.

**CMR Phase encoded velocity analysis for the quantification of LV diastolic function:
Image analysis**

Offline analysis was performed by tracing a standardised circular region of interest (ROI) on the modulus images and transferring this ROI to the paired phase images, using the LEONARDO analytical software package (Siemens, Erlangen, Germany). For assessment of transmitral flow, tracings were performed manually on the images acquired with a velocity encoding of 130cm/s along the borders of the mitral valve from opening to closing (Figure 6.1). From the reconstructed velocity versus time curves of LV filling, peak velocity in early diastole (E) and peak velocity associated with atrial contraction (A) were determined (Figure 6.2). From these peak velocities the E/A ratio was calculated.

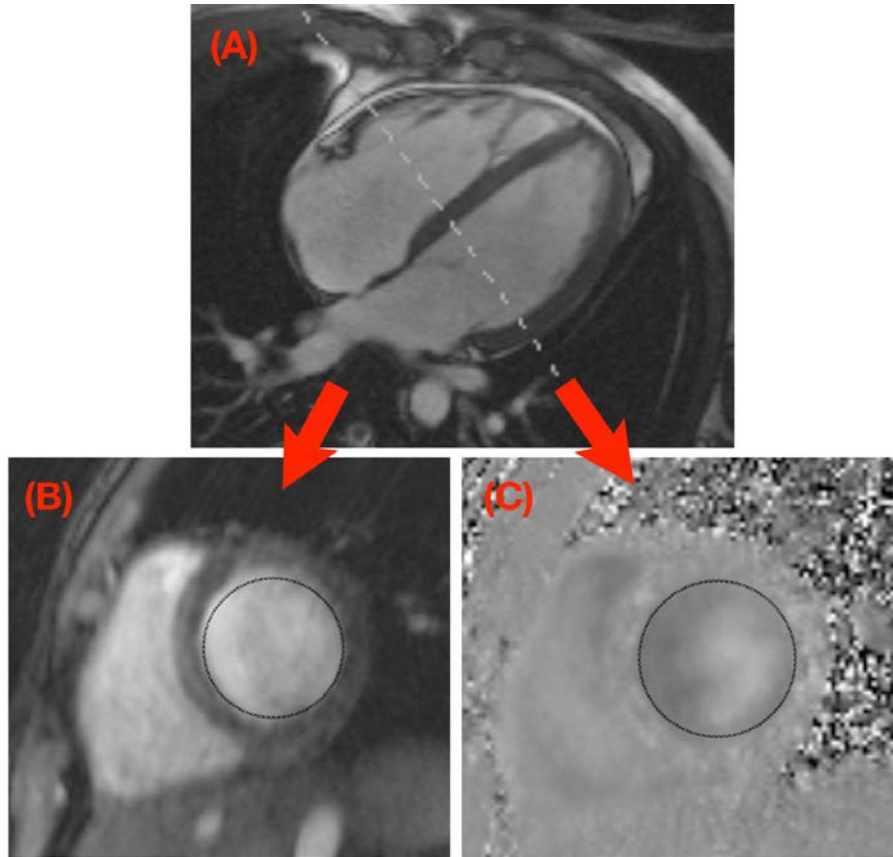


Figure 6.1. Analysis of peak mitral inflow velocity (E) using VEC-CMR.

(A) VEC-CMR short axis imaging plane for transmitral inflow velocity measurement (dotted line) is at the level of the mitral leaflet tips. Resultant magnitude image (B) and velocity map (C) of mitral inflow. Transmitral velocities from within the region of interest (solid circle) are recorded and the information is used to create a peak velocity versus time curve (as shown subsequently in Figure 6.2)

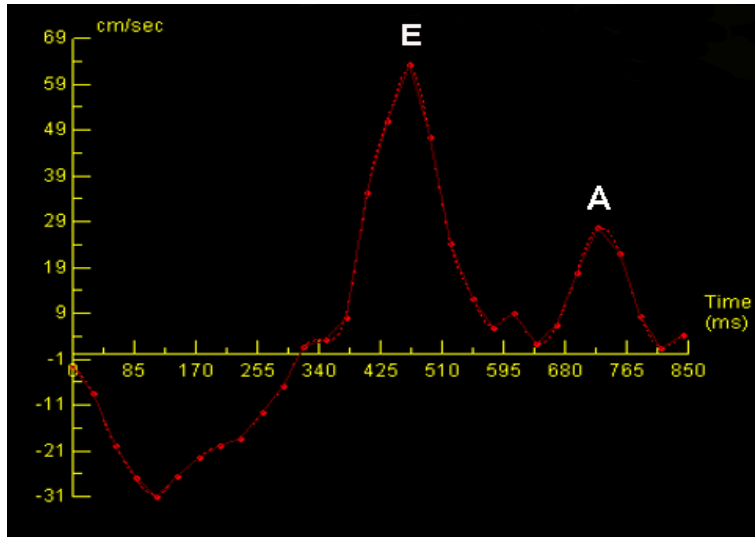


Figure 6.2. Calculating E/A ratio from reconstructed velocity versus time curve.

Early peak diastolic myocardial tissue relaxation velocities (E_m) were recorded using a standardised ROI of 40 pixels placed in the centre of the inferoseptal, anteroseptal, lateral, anterior, posterior and inferior regions of LV myocardium in the LV short axis, at sites approximating to the LV wall positions from which the corresponding early peak tissue relaxation velocities were recorded by tissue Doppler echocardiography (Figure 6.3).

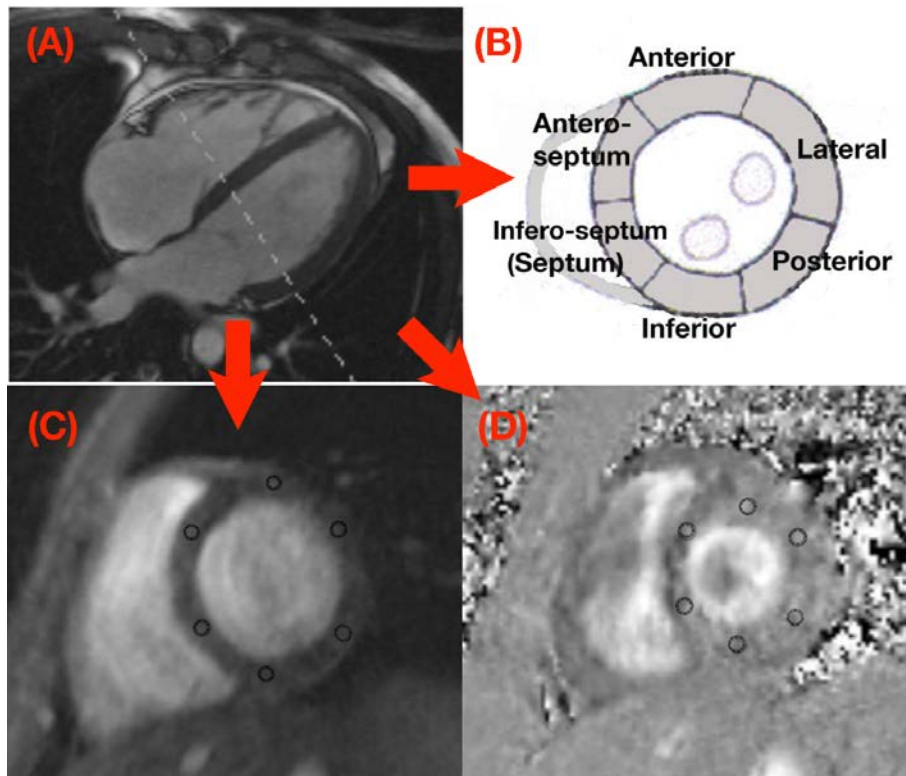


Figure 6.3. Analysis of peak early diastolic myocardial tissue relaxation velocities (E_m) using VEC-CMR.

(A) VEC-CMR short axis imaging plane for early diastolic myocardial tissue relaxation velocity measurements (dotted line) is at the level of the basal third of the LV. Image (B) is a schematic diagram delimiting the six LV basal AHA-myocardial segments. E_m velocities were then recorded from the middle of each of the six basal LV myocardial segments (solid circles) as shown in the resultant magnitude image (C) and velocity map (D). E_m velocity information recorded from within each of the six regions of interest (solid circles) was then used to create six individual peak early myocardial tissue relaxation velocity versus time curves (as shown subsequently in Figure 6.4)

From the reconstructed velocity versus time curves of LV filling, early peak basal myocardial relaxation velocities of the left ventricle were calculated from the basal LV septum (EmS), anteropsetum (EmAS), anterior wall (EmA), lateral wall (EmL), posterior wall (EmP) and inferior wall (EmI) (Figure 6.4).

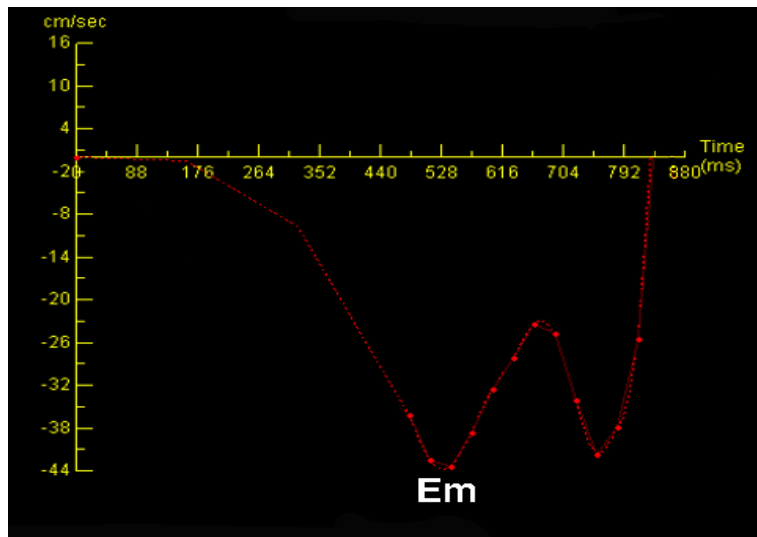


Figure 6.4. Calculating Em from reconstructed velocity versus time curves.

Doppler Echocardiography Imaging

Mitral inflow Doppler velocities and myocardial tissue velocities were recorded as previously described in section 3.6.3.

6.3.4. Image Analysis

Cardiac Magnetic Resonance

E, A and Em values were recorded from reconstructed VEC-CMR velocity-time graphs as previously described. LVEDP was then estimated by recording the ratios of 1) peak mitral inflow velocity: early myocardial relaxation velocity of the septum (E/Em(S)) 2) peak

mitral inflow velocity: early myocardial relaxation velocity of the lateral wall (E/Em(L)) and 3) peak mitral inflow velocity: average of the early myocardial relaxation velocities of the septum and lateral wall (E/Em(S+Lav)). These are the three E/Em ratios recommended for use by the EAE & ASE in their guidelines for the non-invasive assessment of diastolic function.¹⁴ Our study cohort included patients with regional wall motion abnormalities, for this reason we also estimated LVEDP by recording 4) peak mitral inflow velocity: average of the early myocardial relaxation velocities of the left ventricle (averaged from all six basal readings) (E/Em 6av). As the basal anteroseptum is in very close proximity with the aortic valve, we were unsure if this may adversely influence the accuracy of Em recordings made at the level of the basal anteroseptum by VEC-CMR and TDE. For this reason, our fifth and final estimation of LVEDP was performed by recording 5) peak mitral inflow velocity: average of the early myocardial relaxation velocities of the left ventricle (averaged from 5 basal readings, excluding the anteroseptum) (E/Em 5av) (see Figure 6.5).

2D Echocardiography

E, A and Em values were recorded from Doppler velocity-time graphs as previously described. E/Em ratios were then calculated as follows: E/Em(S), E/Em(L), E/Em(S+Lav), E/Em(5av) and E/Em(6av) in a manner analogous to the VEC-CMR E/Em ratios above (Figure 6.5) .

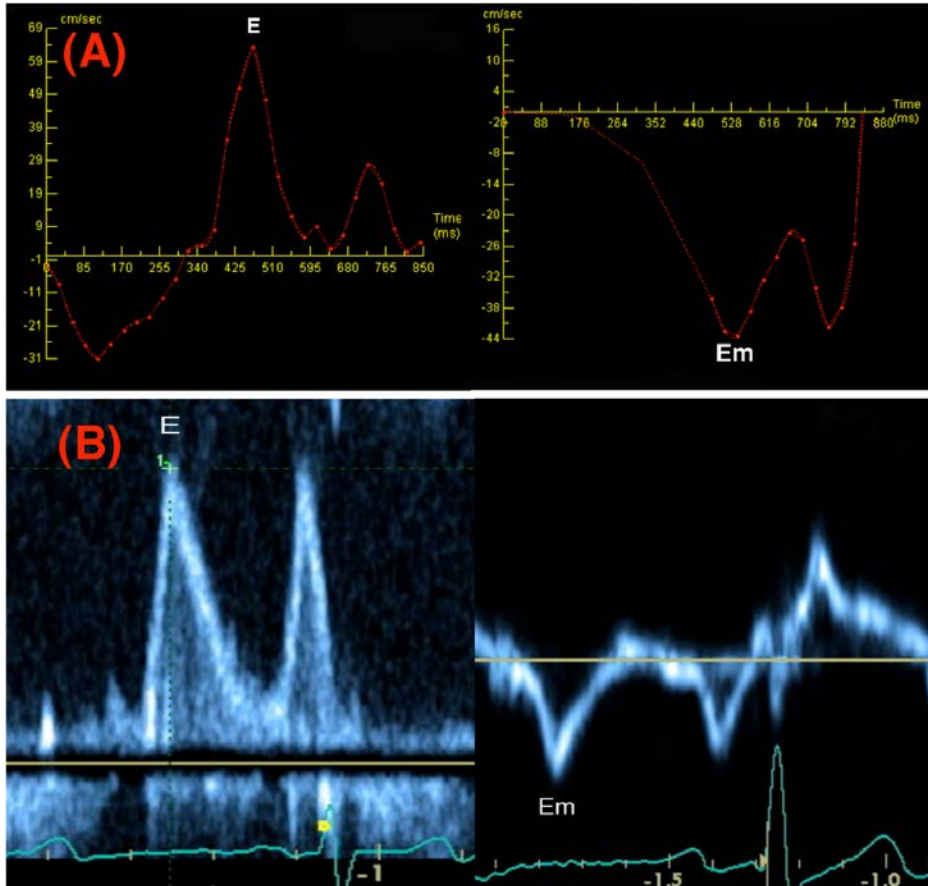


Figure 6.5. Calculating E/Em as a non-invasive estimate of LVEDP using (A) VEC-CMR (B) tissue Doppler echocardiography

6.3.5. Reproducibility

Inter-observer and intra-observer variability for E, A, Em(S) and Em(L) were assessed in 10 patients by two independent observers. These measurements were repeated by one observer six months later.

6.3.6. Statistical Analysis

Values are expressed as mean \pm standard deviation (SD). All data sets were tested for normality using the Kolmogorov-Smirnov test. Each VEC-CMR measure (E, A, Em(S), Em(L), Em(AS), Em(A), Em(I) and Em(P)) was correlated against the equivalent echocardiographic measure using a bivariate correlation (Pearson correlation coefficient for parametric data and Spearman correlation coefficient for non-parametric data). E/Em(S), E/Em(L), E/Em(S+Lav), E/Em(5av) and E/Em(6av) ratios were then calculated by VEC-CMR and echocardiographic techniques, and correlated against LVEDP as the gold standard. For parametric data, linear regression analysis was used to directly compare different combinations of E/Em ratio indexed against LVEDP as the reference standard. Subgroup analysis was performed to assess the accuracy of VEC-CMR E/Em and echo E/Em indexed against LVEDP in patients with normal (LVEF \geq 55%) and impaired (LVEF $<$ 55%) LV systolic function. Receiver operator characteristics were examined. Bland-Altman analysis was used to determine the bias and limits of agreement between the corresponding measurements. Results are expressed as mean bias \pm 1.96SD. The significance of intertechnique biases was tested using the paired samples T-test for parametrically distributed data and Wilcoxon signed ranks test for non-parametrically distributed data. A value of $p<0.05$ was considered significant.

6.4. RESULTS

Four patients were excluded from the study; two patients had incorrectly zeroed catheter traces; the clinician performing the LHC failed to perform an LV pressure recording prior to coronary angiography in one patient; and one patient failed to complete the CMR protocol due to claustrophobia. Forty-one patients successfully completed this study.

6.4.1 Correlation and intertechnique agreement of mitral E velocities, mitral A velocities and E/A ratio recorded using VEC-CMR, with spectral Doppler echocardiography mitral E and A velocities and E/A ratios.

VEC-CMR derived mitral E velocities and mitral A velocities were compared to the corresponding mitral E and A velocities recorded by Doppler echocardiography (n=41). The resultant E/A ratios calculated from the VEC-CMR and Doppler echocardiography velocity traces were also compared. VEC-CMR mitral E velocity had a moderate correlation with Doppler echocardiography mitral E velocity ($p<0.001$, $r=0.657$). Mean calculated mitral E velocity was significantly lower using VEC-CMR compared to Doppler echocardiography (mean bias: 10.98 ± 15.79 ; $Z=-3.94$, $p<0.001$). VEC-CMR mitral A velocity correlated strongly with Doppler echocardiography mitral A velocity ($p<0.001$, $r=0.701$). Mean calculated mitral A velocity was significantly lower using VEC-CMR compared to Doppler echocardiography (mean bias: 17.27 ± 15.83 ; $Z=-3.91$, $p<0.001$). VEC-CMR E/A ratio had a weak correlation with Doppler echocardiography E/A ratio ($p=0.003$, $r=0.481$). Mean calculated E/A ratio was significantly higher using VEC-CMR compared to Doppler echocardiography (mean bias: -0.17 ± 0.41 ; $Z=2.35$, $p<0.016$) (Figure 6.6 A-F).

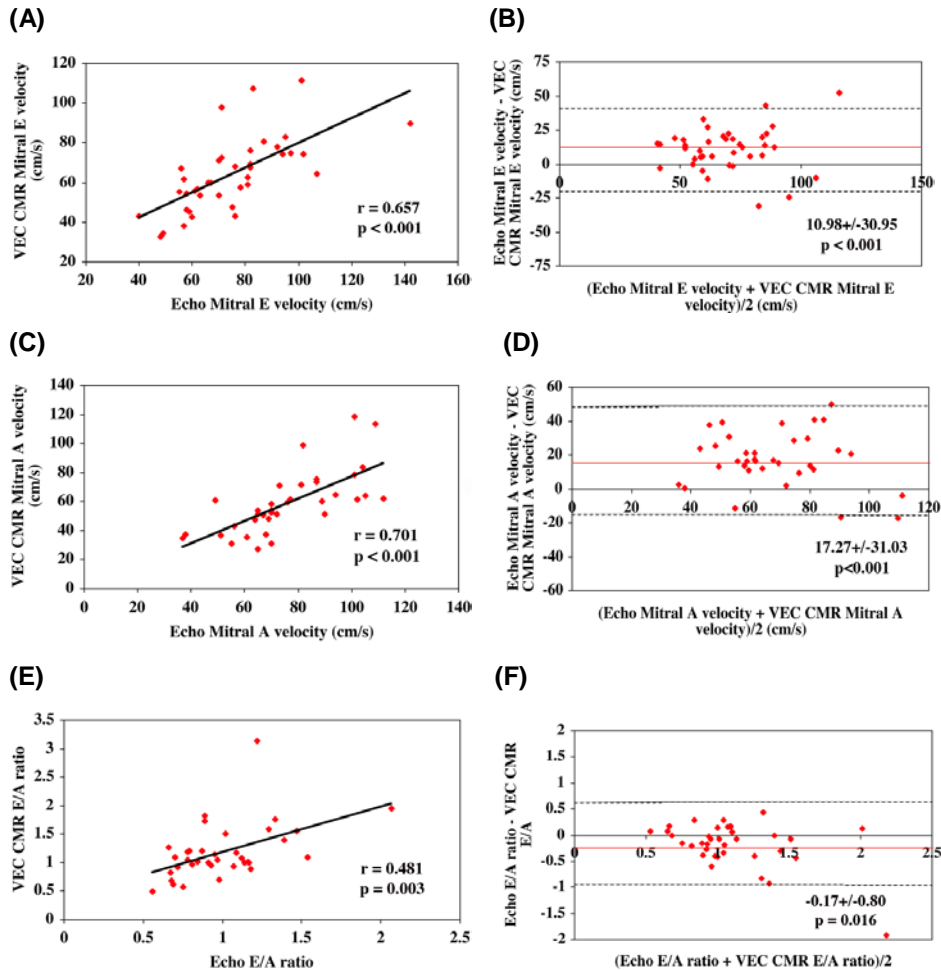


Figure 6.6. (A) Correlation of VEC-CMR mitral E velocity with Doppler echocardiography mitral E velocity in 41 subjects (LVEF range:18.5-71.0%). (B) Bland-Altman analysis between VEC-CMR mitral E velocity and Doppler echocardiography mitral E velocity; solid horizontal line denotes the mean difference between VEC-CMR and Doppler echocardiography measurements, broken horizontal lines represent the limits of agreement (2SD around the mean intertechnique difference). Bottom right of Bland-Altman plot: mean bias \pm 1.96SD, the mean bias is significant if $p < 0.05$. (C) Correlation of VEC-CMR mitral A velocity with Doppler echocardiography mitral A velocity (D) Bland-Altman analysis between VEC-CMR mitral A velocity and Doppler echocardiography mitral A velocity in the same format as in (B) above. (E) Correlation of VEC-CMR E/A ratio with Doppler echocardiography E/A ratio (F) Bland-Altman analysis between VEC-CMR E/A ratio and Doppler echocardiography E/A ratio in the same format as in (B) above. SD, standard deviation.

6.4.2 Correlation and intertechnique agreement of VEC-CMR early diastolic tissue myocardial tissue relaxation velocities (Em) with pulsed-wave tissue Doppler echocardiography Em velocities, recorded from the basal segment/mitral annular junction of all six LV walls, in patients exhibiting a range of LVEF.

The Em velocity was recorded from the basal segment of each LV wall by VEC-CMR as previously described for all study subjects (n=41). The Em velocities recorded from the anterior (EmA), lateral (EmL), posterior (EmP), inferior (EmI), septal (EmS) and anteroseptal (EmAS) LV walls were then compared to the Em velocities recorded from the basal LV wall/mitral annular junction in the corresponding anterior, lateral, posterior, inferior, septal and anteroseptal positions as measured by pulsed-wave tissue Doppler echocardiography (PWTDE) as previously described. Correlation and intertechnique agreement for each Em velocity is shown below (Figures 6.7-6.12).

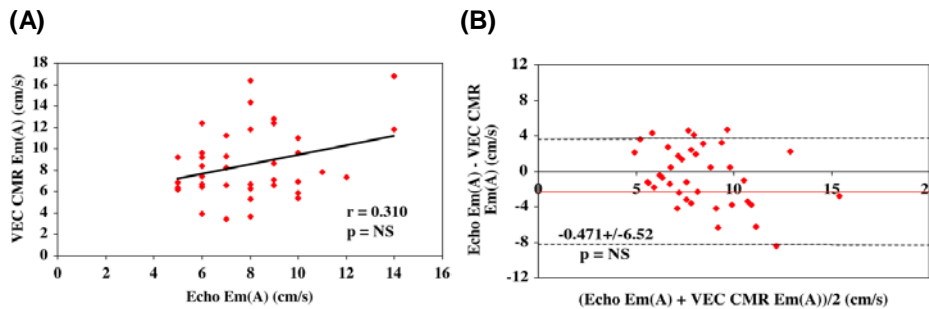


Fig 6.7. (A) Correlation of VEC-CMR Em(A) with PWTDE Em(A) (B) Bland-Altman analysis between VEC-CMR Em(A) and PWTDE Em(A) in the same format as in Figure 6.6. Em(A), early diastolic tissue relaxation velocity recorded from the basal anterior left ventricular wall/mitral annular junction; PWTDE, pulsed-wave tissue Doppler echocardiography; VEC-CMR, velocity encoded cardiac magnetic resonance imaging.

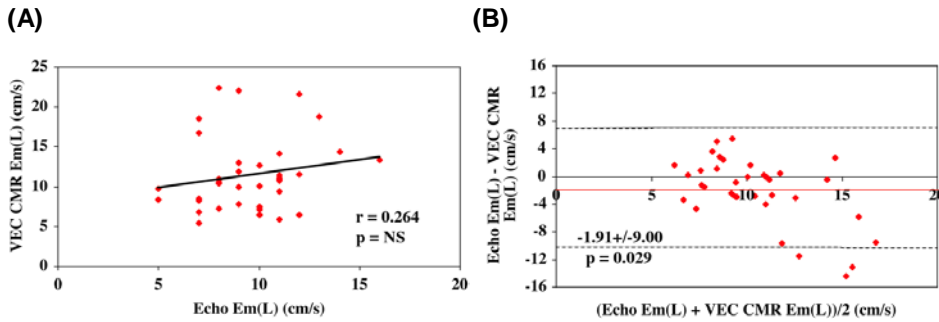


Fig 6.8. (A) Correlation of VEC-CMR Em(L) with PWTDE Em(L) (B) Bland-Altman analysis between VEC-CMR Em(L) and PWTDE Em(L) in the same format as in Figure 6.6. Em(L), early diastolic tissue relaxation velocity recorded from the basal anterior left ventricular wall/mitral annular junction; PWTDE, pulsed-wave tissue Doppler echocardiography; VEC-CMR, velocity encoded cardiac magnetic resonance imaging.

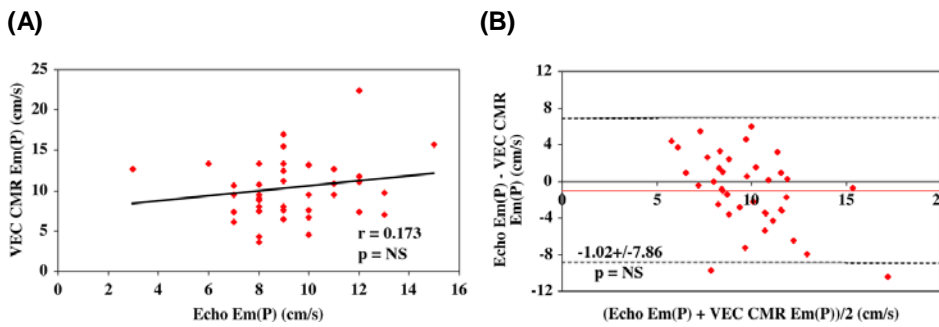


Fig.6.9. (A) Correlation of VEC-CMR Em(P) with PWTDE Em(P) (B) Bland-Altman analysis between VEC-CMR Em(P) and PWTDE Em(P) in the same format as in Figure 6.6. Em(P), early diastolic tissue relaxation velocity recorded from the basal anterior left ventricular wall/mitral annular junction; PWTDE, pulsed-wave tissue Doppler echocardiography; VEC-CMR, velocity encoded cardiac magnetic resonance imaging.

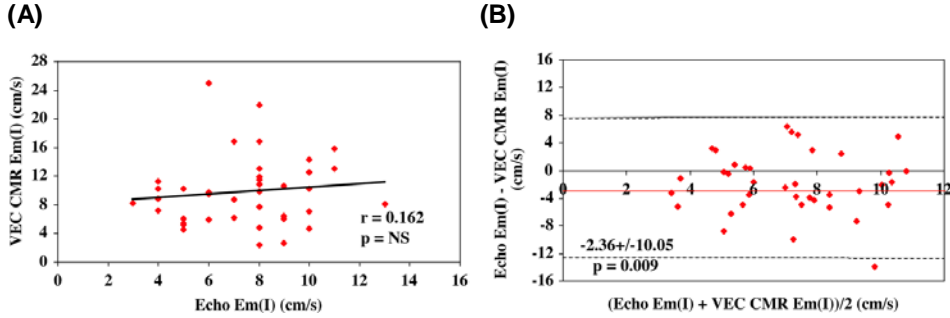


Fig 6.10. (A) Correlation of VEC-CMR Em(I) with PWTDE Em(I) (B) Bland-Altman analysis between VEC-CMR Em(I) and PWTDE Em(I) in the same format as in Figure 6.6. Em(I), early diastolic tissue relaxation velocity recorded from the basal septal left ventricular wall/mitral annular junction; PWTDE, pulsed-wave tissue Doppler echocardiography; VEC-CMR, velocity encoded cardiac magnetic resonance imaging.

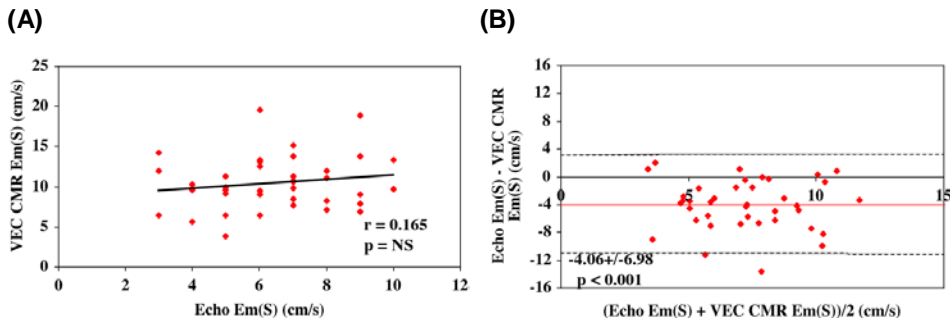


Fig 6.11. (A) Correlation of VEC-CMR Em(S) with PWTDE Em(S) (B) Bland-Altman analysis between VEC-CMR Em(S) and PWTDE Em(S) in the same format as in Figure 6.6. Em(S), early diastolic tissue relaxation velocity recorded from the basal anterior left ventricular wall/mitral annular junction; PWTDE, pulsed-wave tissue Doppler echocardiography; VEC-CMR, velocity encoded cardiac magnetic resonance imaging.

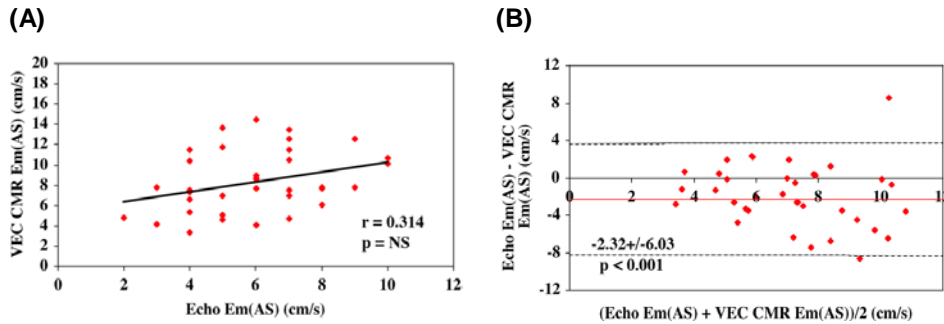


Fig 6.12. (A) Correlation of VEC-CMR Em(AS) with PWTDE Em(AS) (B) Bland-Altman analysis between VEC-CMR Em(AS) and PWTDE Em(AS) in the same format as in Figure 6.6. Em(AS), early diastolic tissue relaxation velocity recorded from the basal anteroseptal left ventricular wall/mitral annular junction; PWTDE, pulsed-wave tissue Doppler echocardiography; VEC-CMR, velocity encoded cardiac magnetic resonance imaging.

None of the Em velocities recorded from the 6 basal LV wall segments by VEC-CMR had any correlation with the PWTDE mitral annular Em velocities in patients over a broad spectrum of LVEF.

6.4.3. Correlation of VEC-CMR E/Em ratio with invasive measurements of left ventricular end diastolic filling pressure in patients exhibiting a range of LVEF.

For all 41 study subjects, E/Em ratio was calculated using firstly the Em velocity recorded from the basal septum (E/Em(S)) and then the basal lateral wall (E/Em(L)). The E/Em ratio was then calculated from the mean of the septal and lateral velocities (E/Em(S+Lav)). These three variations in calculating E/Em are the methods recommended by the ASE/EAE for assessing diastolic function using PWTDE to calculate E/Em. We included patients with ischaemic heart disease in our study, as is common to the patient population assessed by echocardiography and CMR in clinical practice, and felt that a single measure of Em, may reflect regional rather than global changes in early diastolic myocardial tissue relaxation in patients with regional wall motion abnormalities. For this reason, we recorded Em from all six wall of the LV, and calculated E/Em from the mean of all 6 early diastolic tissue velocities (E/Em(6av)). Of note, on the anteroseptal side of the mitral annulus, the

mitral annulus is in fibrous continuity with the aortic annulus. We hypothesised that measurement from this position may be influenced by the anatomical relationship with the aortic valve, and so our final variation in calculating E/Em was made by dividing the peak mitral E velocity with the mean of the 5 basally recorded early diastolic tissue velocities, excluding the anteroseptal LV wall (E/Em(5av)). Each of these variations in calculated E/Em ratio was compared to invasively recorded LVEDP, to establish which ratio, if any, best reflected LV diastolic filling pressure, and was therefore the most accurate in diagnosing and quantifying LV diastolic dysfunction in a heterogeneous population (Figure 6.13).

As demonstrated in Figure 6.13, in a heterogeneous population of patients exhibiting a wide range of LVEF's, only VEC-MRI E/Em(S) had any correlation with invasive LVEDP.

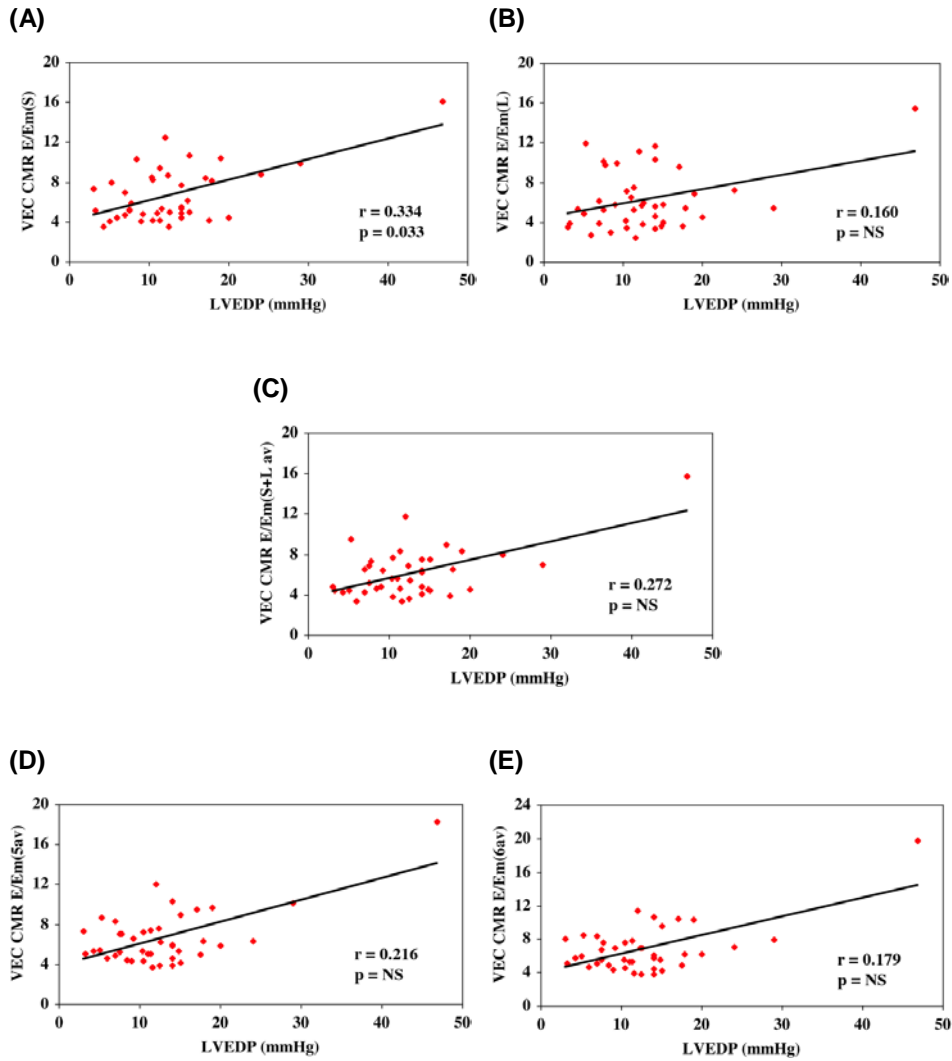


Figure 6.13. Correlation of LVEDP with (A) VEC-CMR E/Em(S), (B) VEC-CMR E/Em(L), (C) VEC-CMR E/Em(S+L.av), (D) VEC-CMR E/Em(5av) and (E) VEC-CMR E/Em(6av) in N=41 patients (LVEF range: 18.5-71.6%). E, peak mitral inflow velocity; Em, early diastolic tissue relaxation velocity; LVEDP, left ventricular end-diastolic filling pressure; VEC-CMR, velocity encoded cardiac magnetic resonance imaging.

6.4.4. Correlation of VEC-CMR E/Em ratio with PWTDE E/Em ratio in patients exhibiting a range of LVEF.

E/Em ratios recorded using VEC-CMR and PWTDE methods were calculated as previously described in section 6.4.3. VEC-CMR E/Em ratios then were compared to corresponding echo E/Em ratios in all patients (N=41) as shown in Figure 6.14.

As shown in Figure 6.14, in a heterogeneous population of patients with a broad spectrum of LVEF, E/Em by CMR had no correlation with Em by echo when Em was measured at the septal or lateral side of the mitral annulus. When Em was averaged from readings recorded from 5 or 6 LV walls however, a weak-moderate correlation was present between echo and CMR methods.

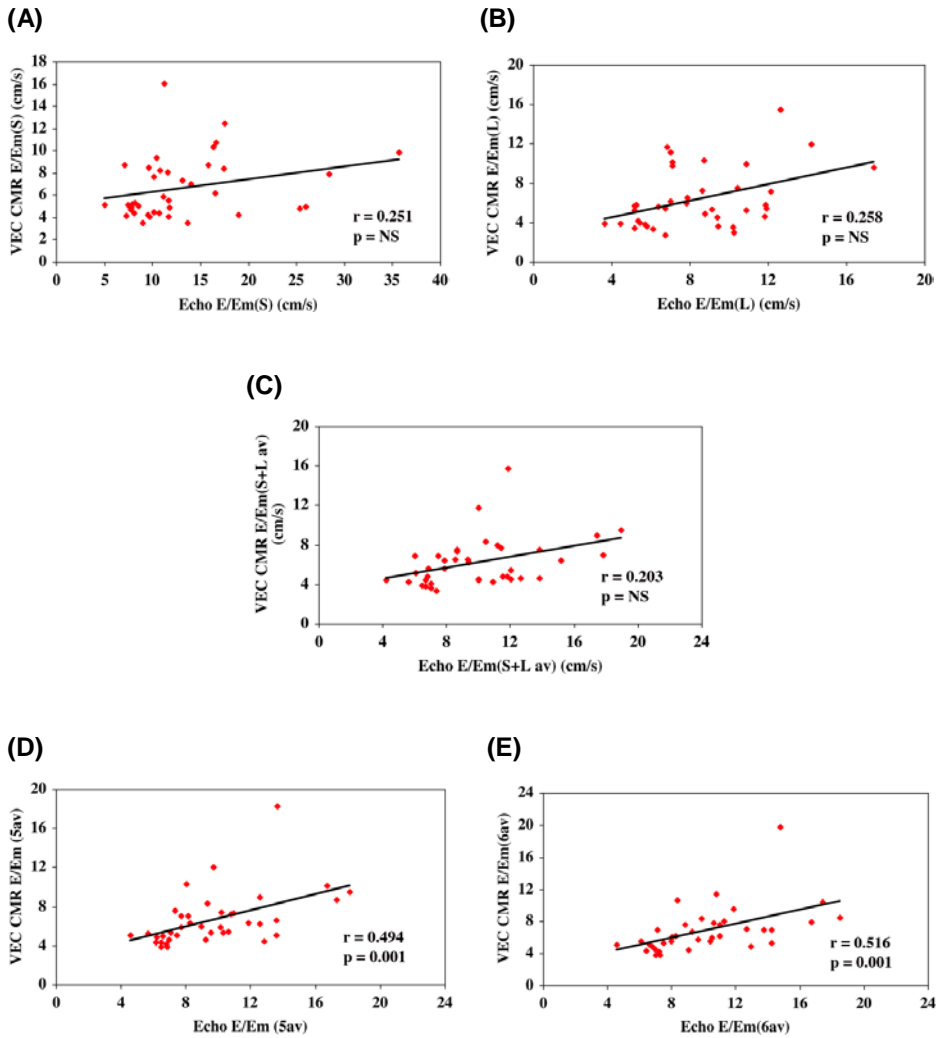


Figure 6.14. . Correlation between echo and CMR-derived E/Em ratios in N=41 patients: (A) Echo vs. VEC-CMR E/Em(S), (B) echo vs. VEC-CMR E/Em(L), (C) echo vs. VEC-CMR E/Em(S+L av), (D) echo vs. VEC-CMR E/Em(5av) and (E) echo vs. VEC-CMR E/Em(6av) in N=41 patients (LVEF range: 18.5-71.6%). E, peak mitral inflow velocity; Em, early diastolic tissue relaxation velocity; LVEDP, left ventricular end-diastolic filling pressure; VEC-CMR, velocity encoded cardiac magnetic resonance imaging.

SUBGROUP ANALYSES: DIASTOLIC MEASUREMENTS IN PATIENTS WITH PRESERVED EJECTION FRACTION (LVEF \geq 55%)

6.4.5. Correlation and intertechnique agreement of mitral E velocities, mitral A velocities and E/A ratio recorded using VEC-CMR, with spectral Doppler echocardiography mitral E and A velocities and E/A ratios in patients with normal LV systolic function

In study subjects with normal LV systolic function, there was a moderate correlation between VEC-CMR mitral E velocity and echo mitral E velocity. A weak-moderate correlation was noted between CMR and echo methods for calculating mitral A velocity and E/A ratio (Figure 6.15).

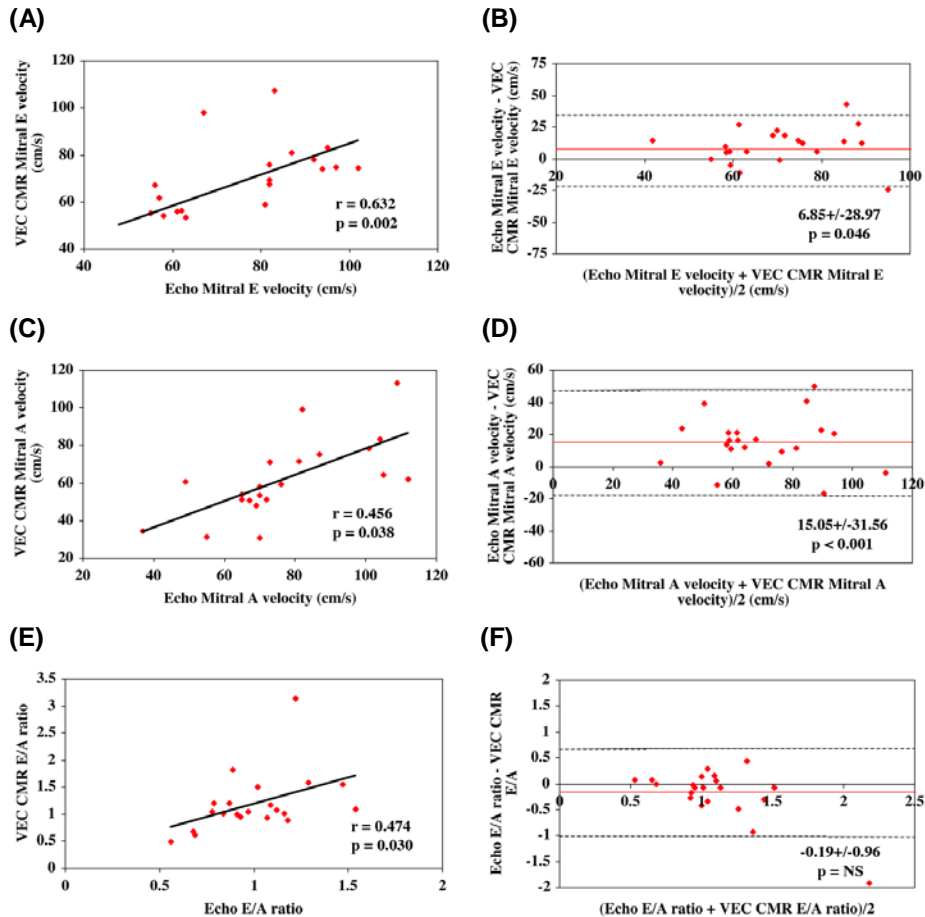


Figure 6.15. (A) Correlation of VEC-CMR mitral E velocity with Doppler echocardiography mitral E velocity in 22 subjects (LVEF ≥ 55). (B) Bland-Altman analysis between VEC-CMR mitral E velocity and Doppler echocardiography mitral E velocity; solid horizontal line denotes the mean difference between VEC-CMR and Doppler echocardiography measurements, broken horizontal lines represent the limits of agreement (2SD around the mean intertechnique difference). Bottom right of Bland-Altman plot: mean bias $\pm 1.96\text{SD}$, the mean bias is significant if $p < 0.05$. (C) Correlation of VEC-CMR mitral A velocity with Doppler echocardiography mitral A velocity (D) Bland-Altman analysis between VEC-CMR mitral A velocity and Doppler echocardiography mitral A velocity in the same format as in (B) above. (E) Correlation of VEC-CMR E/A ratio with Doppler echocardiography E/A ratio (F) Bland-Altman analysis between VEC-CMR E/A ratio and Doppler echocardiography E/A ratio in the same format as in (B) above. SD, standard deviation.

6.4.6. Correlation of VEC-CMR E/Em ratio with invasive measurements of left ventricular end diastolic filling pressure in patients with normal LV systolic function.

E/Em(S), E/Em(L) and E/Em(S+Lav) all correlated with LVEDP in patients with normal LV systolic function. There was a trend to significance between E/Em(5av) and LVEDP and E/Em(6av) and LVEDP (Figure 6.16).

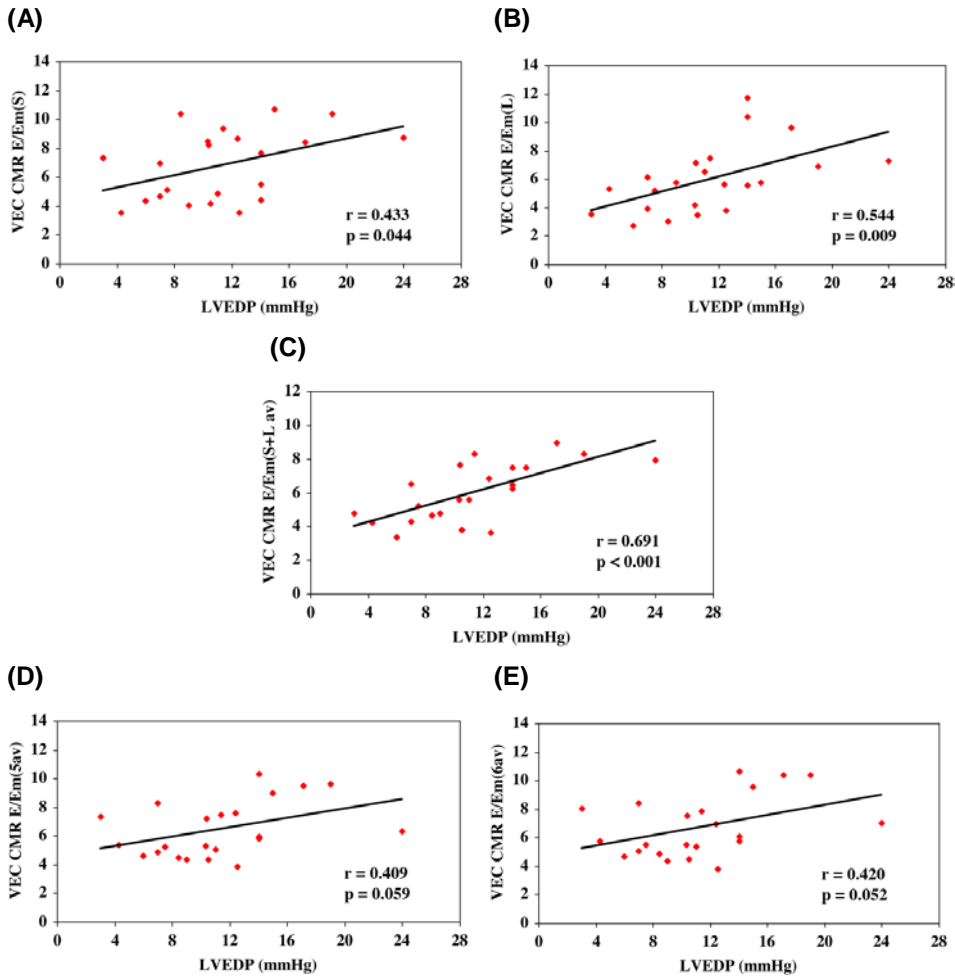


Figure 6.16. Correlation of LVEDP with (A) VEC-CMR E/Em(S), (B) VEC-CMR E/Em(L), (C) VEC-CMR E/Em(S+L,av), (D) VEC-CMR E/Em(5av) and (E) VEC-CMR E/Em(6av) in N=22 patients (LVEF \geq 55%). E, peak mitral inflow velocity; Em, early diastolic tissue relaxation velocity; LVEDP, left ventricular end-diastolic filling pressure; VEC-CMR, velocity encoded cardiac magnetic resonance imaging

6.4.7. Correlation of VEC-CMR E/Em ratio with PWTDE E/Em ratio in patients with normal LV systolic function.

In individuals with normal LV systolic function, with the exception of E/Em(L), all VEC-CMR E/Em indices had a moderate correlation with E/Em measured using pulsed-wave tissue Doppler echocardiography (Figure 6.17).

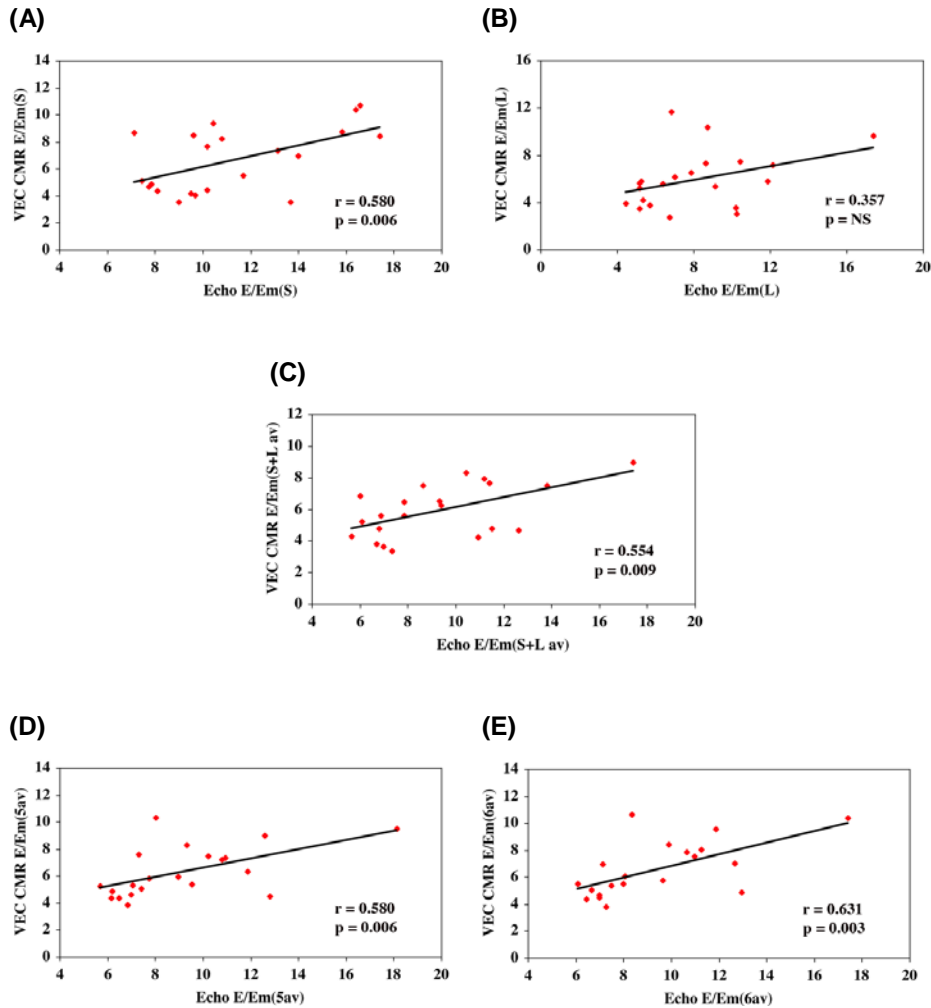


Figure 6.17. Correlation between echo and CMR-derived E/Em ratios in patients with preserved LVEF (LVEF \geq 55; N=22): (A) Echo vs. VEC-CMR E/Em(S), (B) echo vs. VEC-CMR E/Em(L), (C) echo vs. VEC-CMR E/Em(S+L av), (D) echo vs. VEC-CMR E/Em(5av) and (E) echo vs. VEC-CMR E/Em(6av). E, peak mitral inflow velocity; Em, early diastolic tissue relaxation velocity; LVEDP, left ventricular end-diastolic filling pressure; VEC-CMR, velocity encoded cardiac magnetic resonance imaging.

6.4.8. Regression analysis for comparing variations in VEC-CMR E/Em ratio calculation compared to LVEDP in patients with normal LV systolic function.

VEC-CMR E/Em(S), E/Em(L), E/Em(S+Lav), E/Em(5av) and E/Em(6av) were compared to each other, indexed against LVEDP, in all 22 patients with normal LVEFs. This was to establish if any one VEC-CMR E/Em index had a superior correlation with LVEDP when compared to the remaining VEC-CMR E/Em indices. On regression analysis, no single index of VEC-CMR E/Em had a significantly stronger correlation with LVEDP when compared to the other remaining indices in patients with normal LV systolic function.

Calculating VEC-CMR E/Em(5av) and E/Em(6av) involves recording Em velocities from 5 and 6 different regions of interest within the basal left ventricular myocardium respectively, across 30 phases. This is time consuming and is a limitation of the technique. Calculating VEC-CMR E/Em(S), E/Em(L) and E/Em(S+Lav) ratios involve analysing less LV myocardial regions of interest improving analysis times and therefore the potential clinical applicability of the technique. E/Em(5av) only exhibited a correlation with LVEDP that was of borderline significance, and E/Em(6av) did not significantly correlate with LVEDP. As calculating VEC-CMR E/Em(5av) and E/Em(6av) confers no statistical advantage over E/Em(S), E/Em(L) and E/Em(S+Lav), VEC-CMR E/Em(5av) and E/Em(6av) are excluded from further analysis in sections 6.4.14 and 6.4.15.

SUBGROUP ANALYSES: DIASTOLIC MEASUREMENTS IN PATIENTS WITH IMPAIRED EJECTION FRACTION (LVEF<55%)

6.4.9 Correlation and intertechnique agreement of mitral E velocities, mitral A velocities and E/A ratio recorded using VEC-CMR, with spectral Doppler echocardiography mitral E and A velocities and E/A ratios in patients with impaired LV systolic function.

A moderately strong correlation was present between VEC-MR and Doppler echocardiography methods for measuring mitral E velocity, mitral A velocity and E/A ratio in patients with impaired LV systolic function (Figure 6.18).

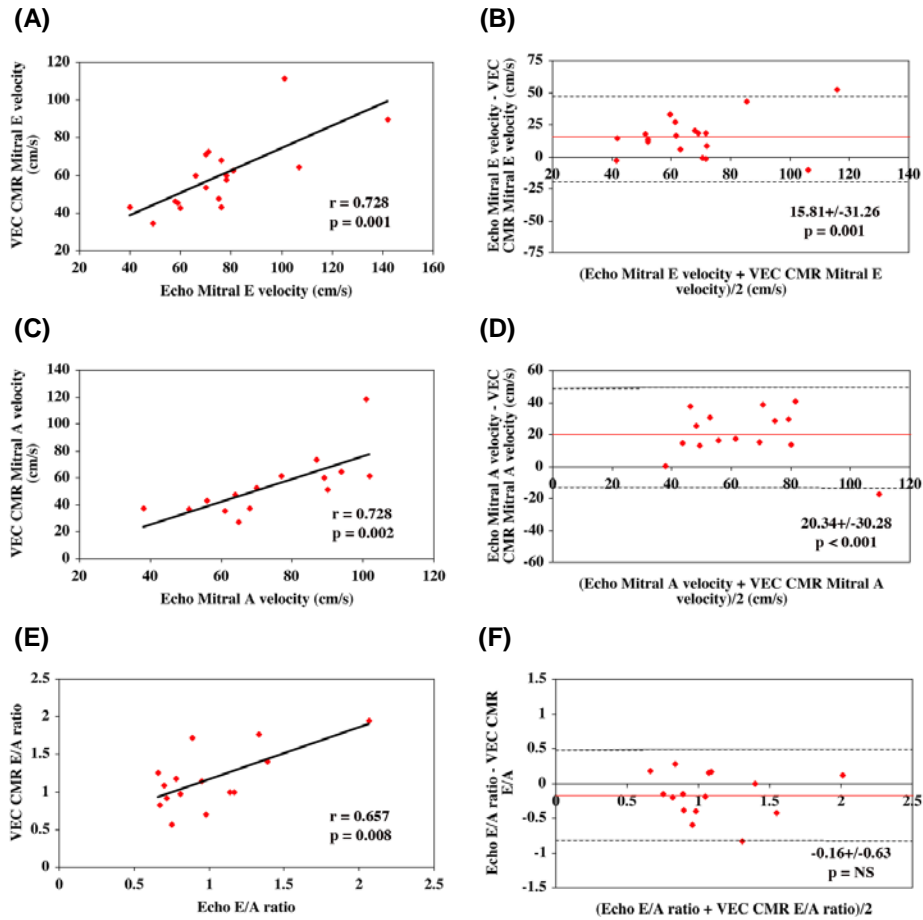


Figure 6.18. (A) Correlation of VEC-CMR mitral E velocity with Doppler echocardiography mitral E velocity in 19 subjects (LVEF <55%). (B) Bland-Altman analysis between VEC-CMR mitral E velocity and Doppler echocardiography mitral E velocity; solid horizontal line denotes the mean difference between VEC-CMR and Doppler echocardiography measurements, broken horizontal lines represent the limits of agreement (2SD around the mean intertechnique difference). Bottom right of Bland-Altman plot: mean bias \pm 1.96SD, the mean bias is significant if $p < 0.05$. (C) Correlation of VEC-CMR mitral A velocity with Doppler echocardiography mitral A velocity (D) Bland-Altman analysis between VEC-CMR mitral A velocity and Doppler echocardiography mitral A velocity in the same format as in (B) above. (E) Correlation of VEC-CMR E/A ratio with Doppler echocardiography E/A ratio (F) Bland-Altman analysis between VEC-CMR E/A ratio and Doppler echocardiography E/A ratio in the same format as in (B) above. SD, standard deviation.

6.4.10 Correlation of VEC-CMR E/Em ratio with invasive measurements of left ventricular end diastolic filling pressure in patients with impaired LV systolic function.

A weak-moderate correlation between E/Em(S+Lav) and invasively recorded LVEDP was present in the study cohort with impaired LV systolic function. The remaining VEC-CMR indices had no significant correlation with LVEDP (Figure 6.19).

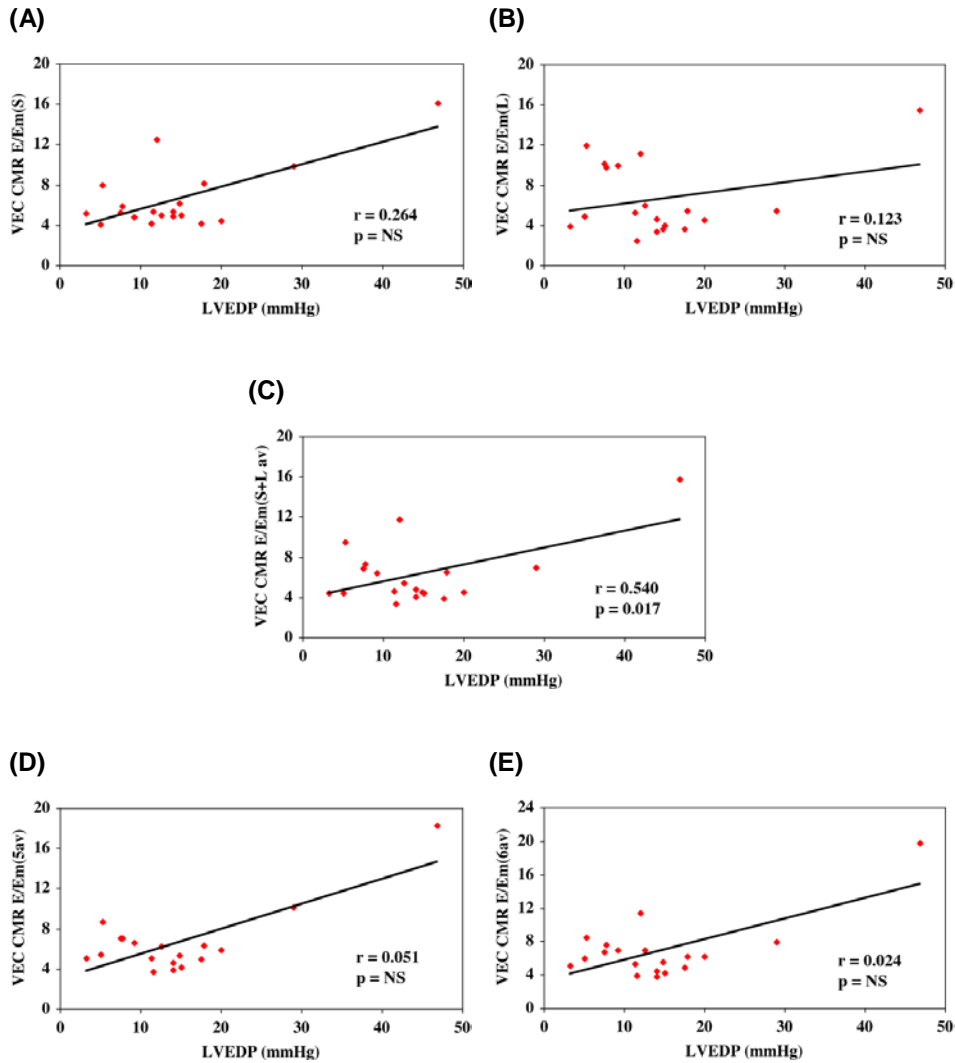


Figure 6.19. Correlation of LVEDP with (A) VEC-CMR E/Em(S), (B) VEC-CMR E/Em(L), (C) VEC-CMR E/Em(S+L+av), (D) VEC-CMR E/Em(5av) and (E) VEC-CMR E/Em(6av) in N=19 patients (LVEF<55%). E, peak mitral inflow velocity; Em, early diastolic tissue relaxation velocity; LVEDP, left ventricular end-diastolic filling pressure; VEC-CMR, velocity encoded cardiac magnetic resonance imaging

6.4.11 Correlation and intertechnique agreement of VEC-CMR E/Em ratio with PWTDE E/Em ratio in patients with impaired LV systolic function.

There was no significant correlation between VEC-CMR and echo indices of E/Em in patients with impaired LV systolic function (Figure 6.20).

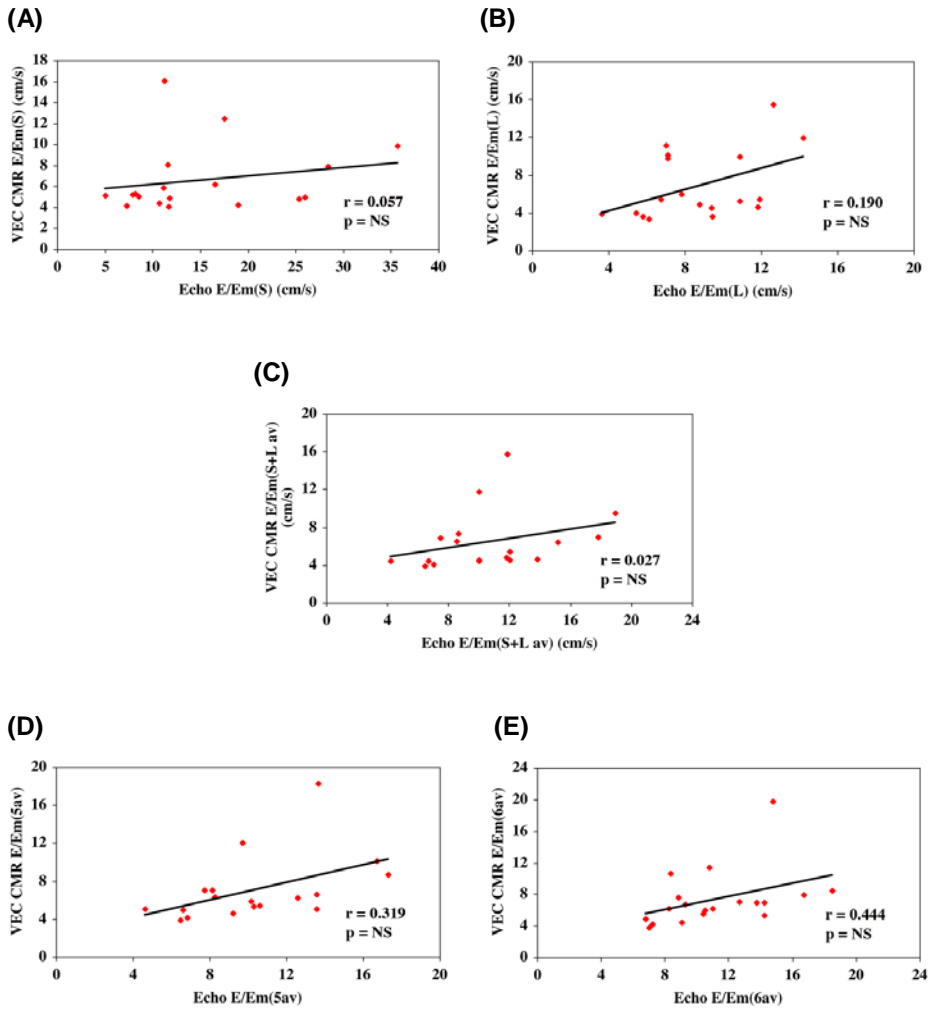


Figure 6.20. Correlation between echo and CMR-derived E/Em ratios in patients with preserved LVEF (LVEF < 55; N = 19): (A) Echo vs. VEC-CMR E/Em(S), (B) echo vs. VEC-CMR E/Em(L), (C) echo vs. VEC-CMR E/Em(S+L av), (D) echo vs. VEC-CMR E/Em(5av) and (E) echo vs. VEC-CMR E/Em(6av). E, peak mitral inflow velocity; Em, early diastolic tissue relaxation velocity; LVEDP, left ventricular end-diastolic filling pressure; VEC-CMR, velocity encoded cardiac magnetic resonance imaging.

6.4.12 Receiver-operator characteristics for VEC-CMR E/Em ratios

In the absence of mitral valve disease, LVEDP approximates mean left atrial pressure (LAP). The upper limit of normal for both LVEDP and LAP is 12mmHg, as shown in Table 1.10. Receiver-operator characteristics were studied for VEC-CMR E/Em(S), E/Em(L) and E/Em(S+Lav) ratios to establish cut-off values for normal and elevated LV filling pressures by CMR. In our study LVEDP \leq 12mmHg was defined as normal and LVEDP $>$ 12mmHg was indicative of elevated LV filling pressure. This chosen threshold value was the same as the threshold value used for invasive left heart catheter data in both the original echo Doppler-catheterisation study by Ommen et al,⁴ and subsequent echo Doppler-catheterisation study by Kasner et al.⁶

On ROC analysis, E/Em(S) \geq 9.6 predicted elevated LV filling pressures with a specificity of 90.10%, and E/Em(S) $<$ 4.4 predicted normal LV filling pressures with a specificity of 89.50%, with E/Em(S) of 4.5-9.5 representing an overlap zone.

E/Em(L) \geq 10.2 predicted elevated LV filling pressures with a specificity of 90.90%, and E/Em(L) $<$ 3.6 predicted normal LV filling pressures with a specificity of 94.70%, with E/Em(L) of 3.7-10.1 representing an overlap zone.

E/Em(S+Lav) \geq 8.7 predicted elevated LV filling pressures with a specificity of 90.90%, and E/Em(S+Lav) $<$ 3.9 predicted normal LV filling pressures with a specificity of 94.70%, with E/Em(S+Lav) 4.0-8.6 representing an overlap zone.

6.4.13 Diagnosing diastolic dysfunction by VEC-CMR in a heterogeneous patient cohort, based on a modification of the EAE/ASE 2010 guidelines

Since the recruitment of our study cohort, the EAE and ASE have published new guidelines in the form of a step-wise algorithm for diagnosing diastolic dysfunction in patients with preserved (Figure 1.31) and impaired (Figure 1.32) systolic function.¹⁴ Current EAE/ASE recommendations for diagnosing diastolic dysfunction involves the non-invasive quantification and identification of elevated LAP. The EAE/ASE guidelines for assessing

LV diastolic function have been written for patients undergoing spectral and tissue Doppler echocardiography. We have used velocity-encoded magnetic resonance to record mitral inflow velocity, E/A ratio and E/Em ratios. Our VEC-CMR protocol for assessing diastolic function is based on a similar principle (although vastly different imaging physics) to echocardiographic mitral E velocity, E/A and E/Em ratios, and this method requires the use of different normative cut-off values specific to CMR. We have therefore modified the EAE/ASE guidelines, as described below, for use by VEC-CMR by calculating new normative values specific to the CMR protocol used.

Current EAE/ASE guidelines use a mitral E velocity cut-off value of 50cm/s. The inter-technique bias between mitral E velocity calculated by echo and by CMR was 10.98cm/s. Therefore, we determined an equivalent VEC-CMR mitral E velocity cut-off value of 39cm/s.

Current EAE/ASE guidelines use E/A cut-off values of 1 and 2. The inter-technique bias between E/A ratios calculated by echo and by CMR was -0.17. Therefore we determined VEC-CMR E/A equivalent threshold values of 1.17 and 2.17.

Our VEC-CMR E/Em normative cut-off values were determined by ROC analysis as previously described in section 6.4.11.

Based on the above modifications, we re-analysed our VEC-CMR data, creating a modified version of current EAE/ASE guidelines for diagnosing diastolic dysfunction that was specific to VEC-CMR (see Figures 6.21 and 6.22 below).

Modified EAE/ASE diagnostic algorithm for the estimation of left ventricular filling pressures in patients with normal LV systolic function: Modified for analysis of VEC-CMR indices

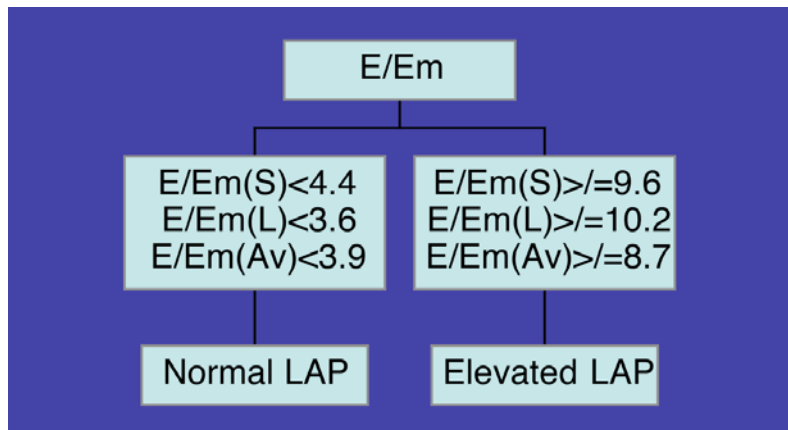


Figure 6.21. Simplified EAE/ASE diagnostic algorithm for the estimation of left ventricular filling pressures in patients with normal LVEFs: Modified for use in patients undergoing VEC-CMR.

Diastolic dysfunction was assessed in the 22 patients with normal LV systolic function (LVEF \geq 55%) using a version of the EAE/ASE diagnostic algorithm, modified by us for use in VEC-CMR scanning (Figure 6.21). Ten patients had E/Em ratio's in the indeterminate range and were excluded from the analysis. The presence or absence of elevated diastolic filling pressures could be assessed in the remaining 12 patients (55%) using the above algorithm. Five of the 6 patients with elevated LVEDP, and all of patients with normal LVEDP were accurately diagnosed using the above algorithm (Fishers exact test: $p=0.015$). The sensitivity, specificity, positive and negative predictive values were 83.30%, 100.00%, 100.00% and 85.71% respectively.

Modified EAE/ASE diagnostic algorithm for the estimation of left ventricular filling pressures in patients with impaired LV systolic function: Modified for analysis of VEC-CMR indices

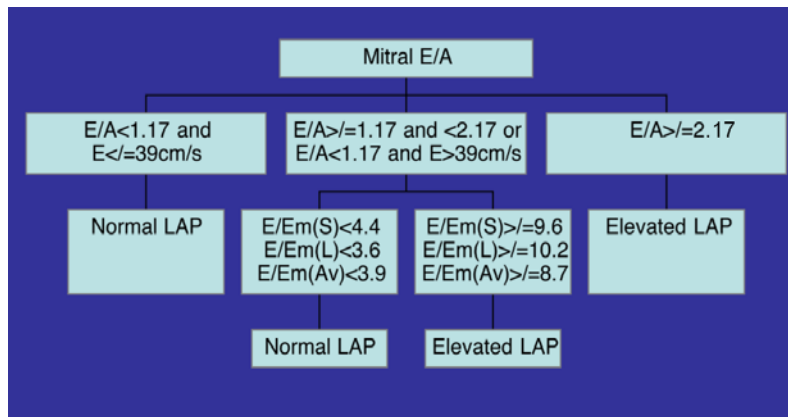


Figure 6.22. Simplified EAE/ASE diagnostic algorithm for the estimation of left ventricular filling pressures in patients with impaired LVEFs: Modified for use in patients undergoing VEC-CMR.

Diastolic dysfunction was assessed in the 19 patients with impaired LV systolic function (LVEF<55%) using a version of the EAE/ASE diagnostic algorithm, modified by us for use in VEC-CMR scanning (Figure 6.22). Fourteen patients had E/Em ratio's in the indeterminate range and were excluded from the analysis. The presence or absence of elevated diastolic filling pressures could only be assessed in 5 patients (26%) using the above algorithm. One of the 2 patients with elevated LVEDP, and one of the 3 patients with normal LVEDP were accurately diagnosed using the above algorithm (Fishers exact test: p=NS). The sensitivity, specificity, positive and negative predictive values were 50.00%, 33.33%, 33.33% and 50% respectively.

6.4.14 Reproducibility

Intra- and inter-observer variability for CMR measures of mitral E velocity, mitral A velocity, E/A ratio, Em(S), Em(L), E/Em(S), E/Em(L) and E/Em(L+Sav) are expressed as the co-efficient of variation, and as the mean bias, limits of agreement and standard deviation of the difference as shown in Tables 6.2 and 6.3. Reproducibility of transmitral Doppler echocardiography is well documented with intra- and inter-observer correlations ≥ 0.89 for transmitral flow velocities.³³² Reproducibility of mitral annular tissue velocities are excellent with an intra-class correlation co-efficient of 0.9.³³³

Index of LV diastolic function	% Co-efficient of variation	Mean bias	Limits of agreement	SDD
<u>CMR PARAMETERS</u>				
1) Mitral E velocity	2.57	-1.32	-9.67 to 7.03	4.17
2) Mitral A velocity	0.78	0.23	-1.42 to 1.92	0.83
3) E/A ratio	3.16	-0.05	-0.34 to 0.24	0.15
4) Em(S)	4.37	0.46	-1.02 to 1.93	0.74
5) Em(L)	8.84	0.86	-3.24 to 4.95	2.05
6) E/Em(S)	6.57	-0.45	-1.82 to 1.19	0.69
7) E/Em(L)	11.19	-0.32	-2.07 to 1.42	0.87
8) E/Em(S+Lav)	8.20	-0.41	-1.39 to 0.57	0.49

Table 6.2. Intra-observer variability for CMR measurements of LV diastolic function. . A, peak late transmitral inflow velocity associated with atrial contraction; E, peak early transmitral inflow velocity; Em, early peak myocardial tissue relaxation velocity; L, basal LV lateral wall; S, basal septum.

Index of LV diastolic function	% Co-efficient of variation	Mean bias	Limits of agreement	SDD
<u>CMR PARAMETERS</u>				
1) Mitral E velocity	1.26	0.27	-3.65 to 4.19	1.96
2) Mitral A velocity	3.27	1.01	-4.08 to 6.11	2.55
3) E/A ratio	3.66	-0.03	-0.25 to 0.18	0.11
4) Em(S)	9.92	0.96	-2.29 to 4.21	1.63
5) Em(L)	10.94	1.37	-3.68 to 6.42	2.52
6) E/Em(S)	9.22	-0.68	-3.06 to 1.70	1.19
7) E/Em(L)	11.74	-0.39	-2.05 to 1.26	0.83
8) E/Em(S+Lav)	8.75	-0.57	-1.81 to 0.67	0.62

Table 6.3. Inter-observer variability for CMR measurements of LV diastolic function. A, peak late transmitral inflow velocity associated with atrial contraction; E, peak early transmitral inflow velocity; Em, early peak myocardial tissue relaxation velocity; L, basal LV lateral wall; S, basal septum.

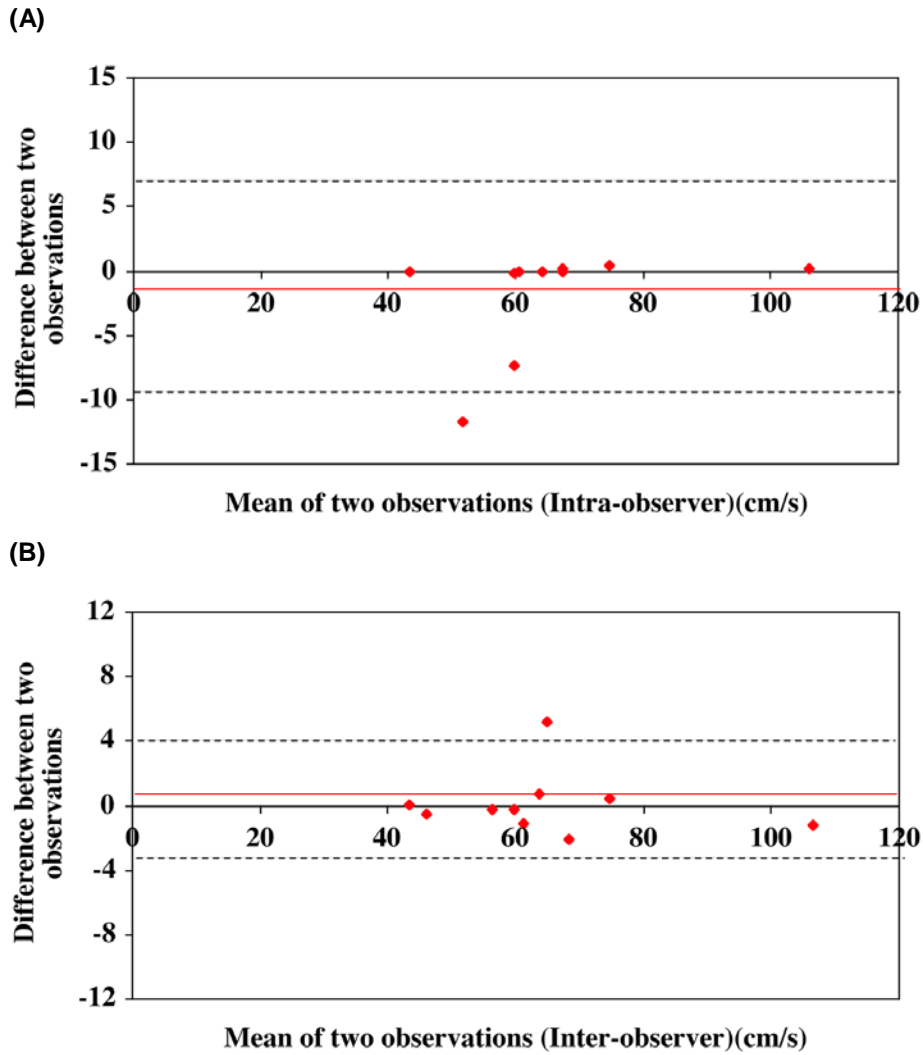


Figure 6.23. Bland-Altman Plot of (A) intra-observer variation and (B) inter-observer variation for measuring mitral E velocity using cardiac magnetic resonance imaging (cm/s).

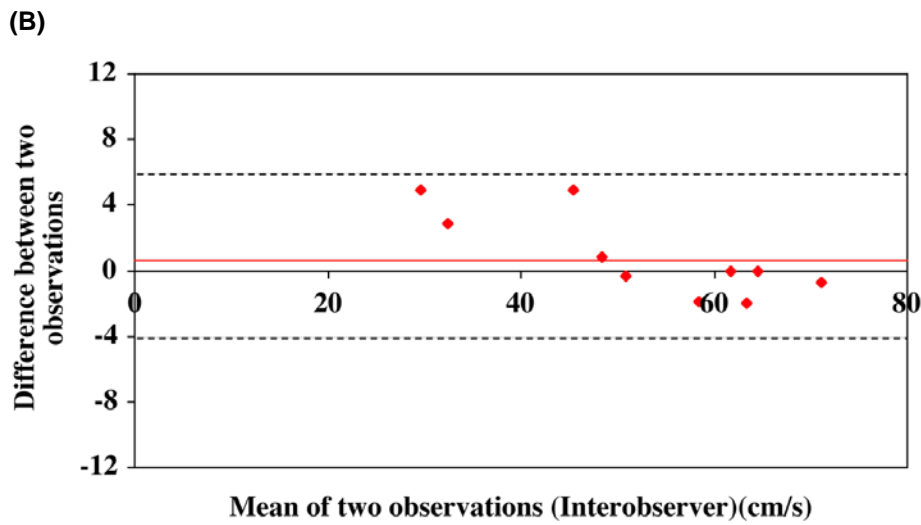
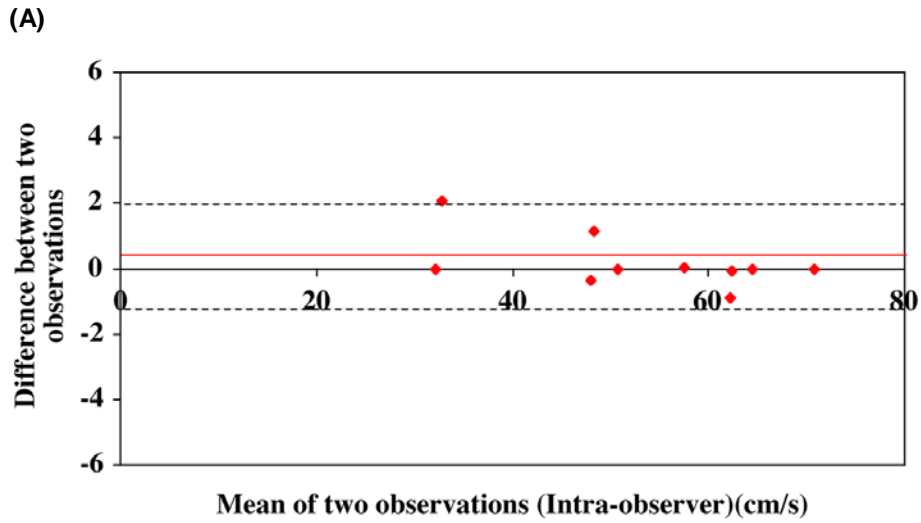
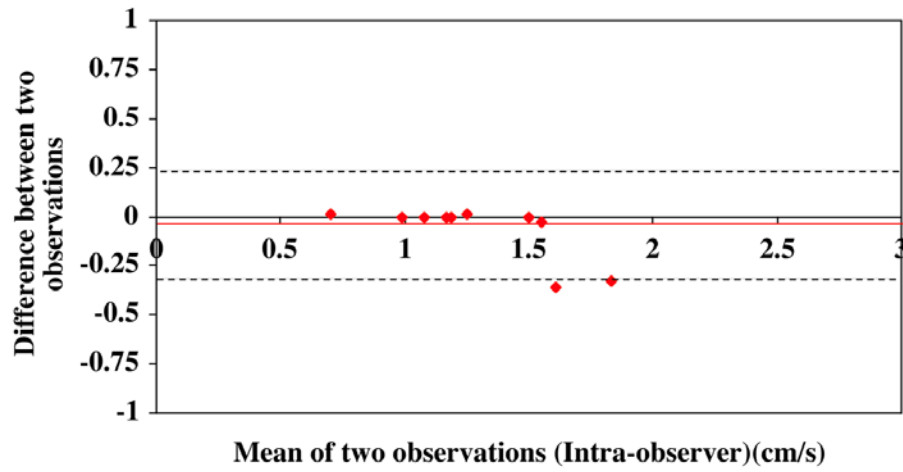


Figure 6.24. Bland-Altman Plot of (A) intra-observer variation and (B) inter-observer variation for measuring mitral A velocity using cardiac magnetic resonance imaging (cm/s).

(A)



(B)

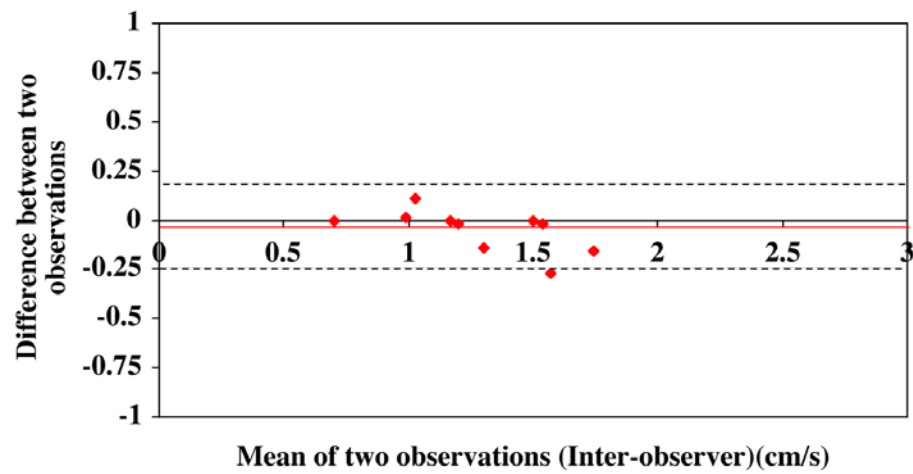


Figure 6.25. Bland-Altman Plot of (A) intra-observer variation and (B) inter-observer variation for measuring mitral E/A ratio using cardiac magnetic resonance imaging.

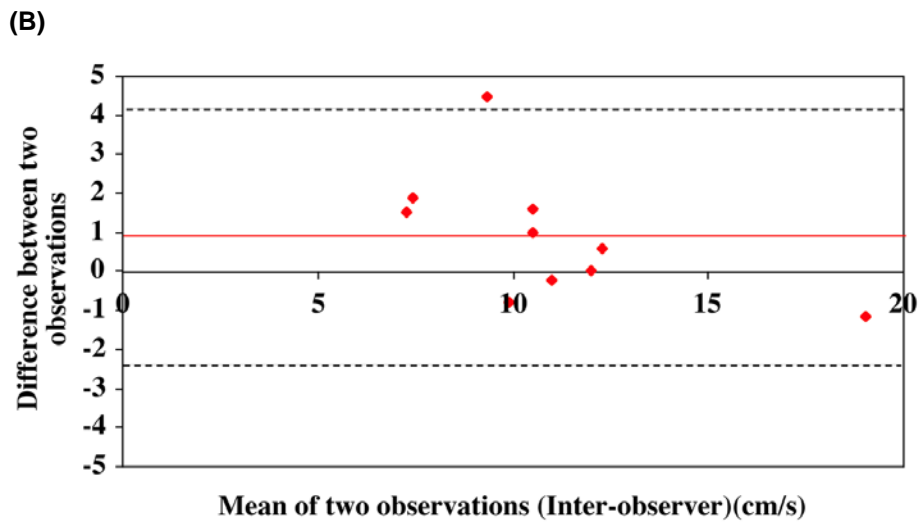
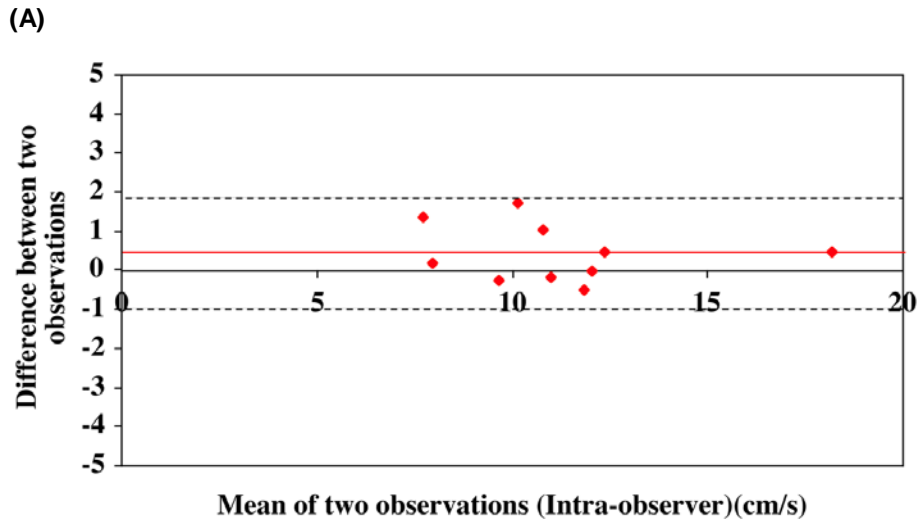


Figure 6.26. Bland-Altman Plot of (A) intra-observer variation and (B) inter-observer variation for measuring peak myocardial tissue velocity of the basal LV septum (EmS) by cardiac magnetic resonance imaging (cm/s).

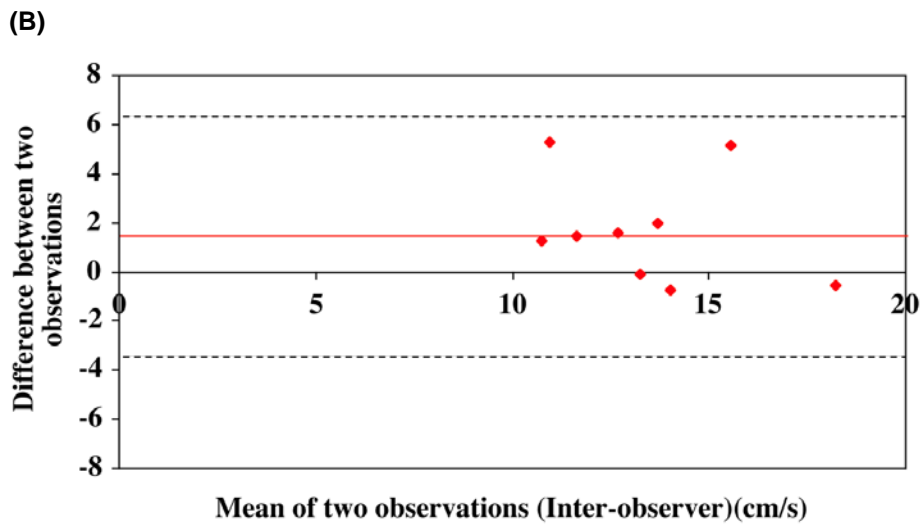
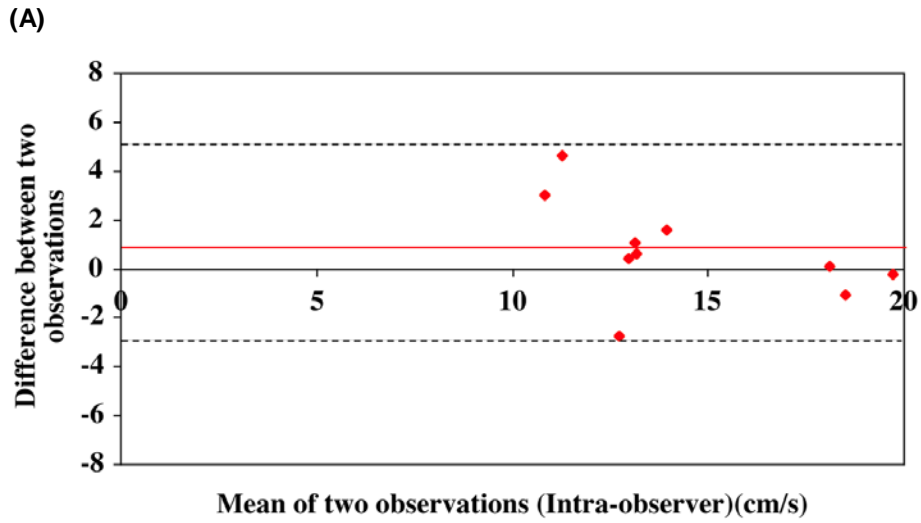
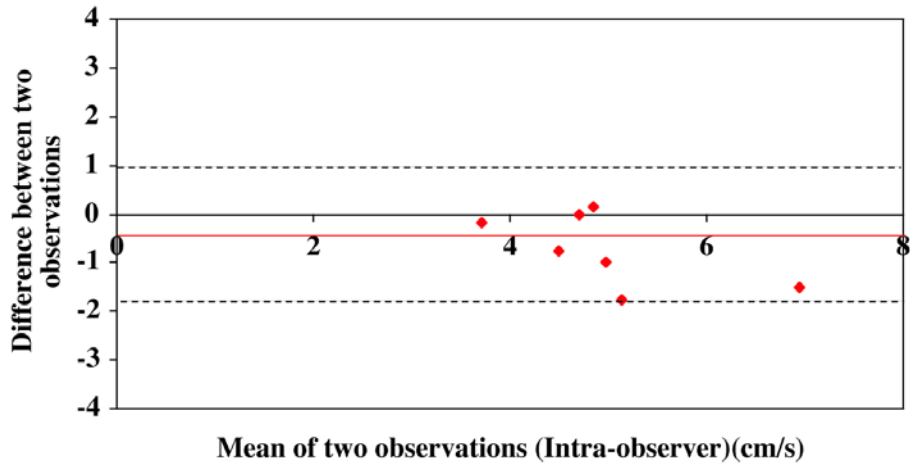


Figure 6.27. Bland-Altman Plot of (A) intra-observer variation and (B) inter-observer variation for measuring peak myocardial tissue velocity of the basal LV lateral wall (EmL) by cardiac magnetic resonance imaging (cm/s).

(A)



(B)

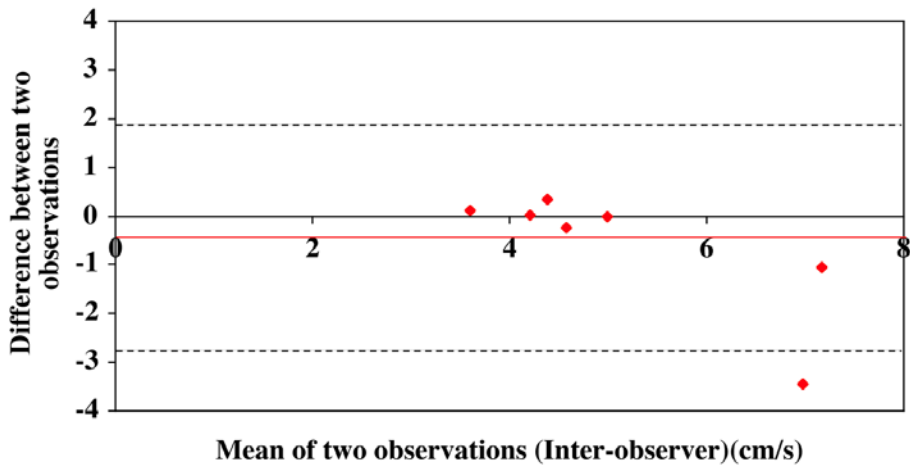


Figure 6.28. Bland-Altman Plot of (A) intra-observer variation and (B) inter-observer variation for measuring E/EmS ratio by cardiac magnetic resonance imaging.

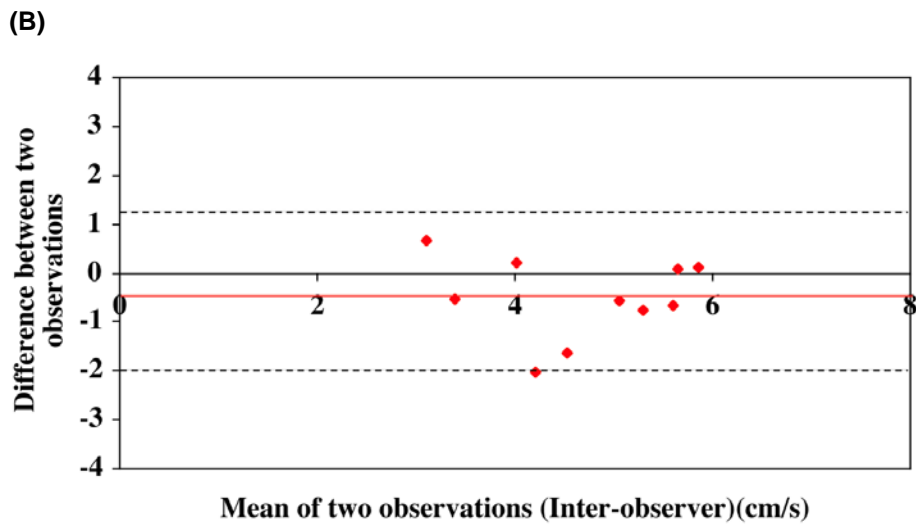
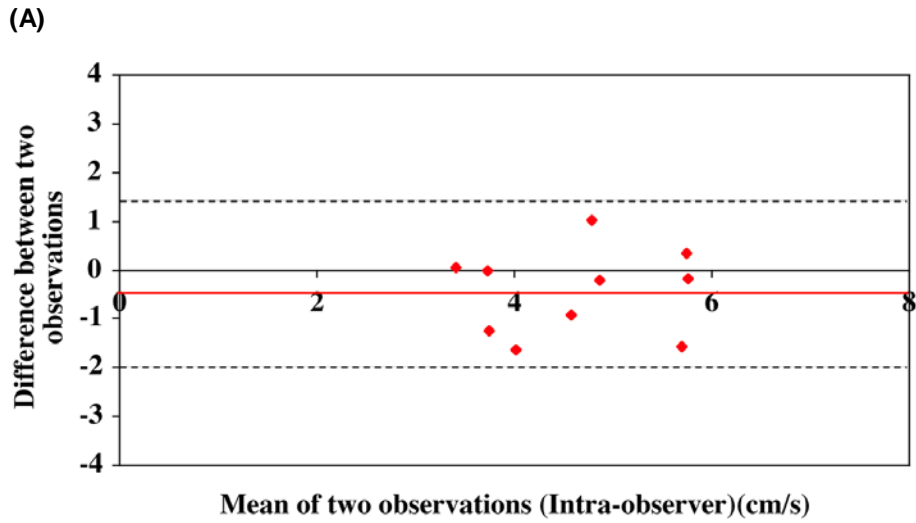


Figure 6.29. Bland-Altman Plot of (A) intra-observer variation and (B) inter-observer variation for measuring E/EmL by cardiac magnetic resonance imaging.

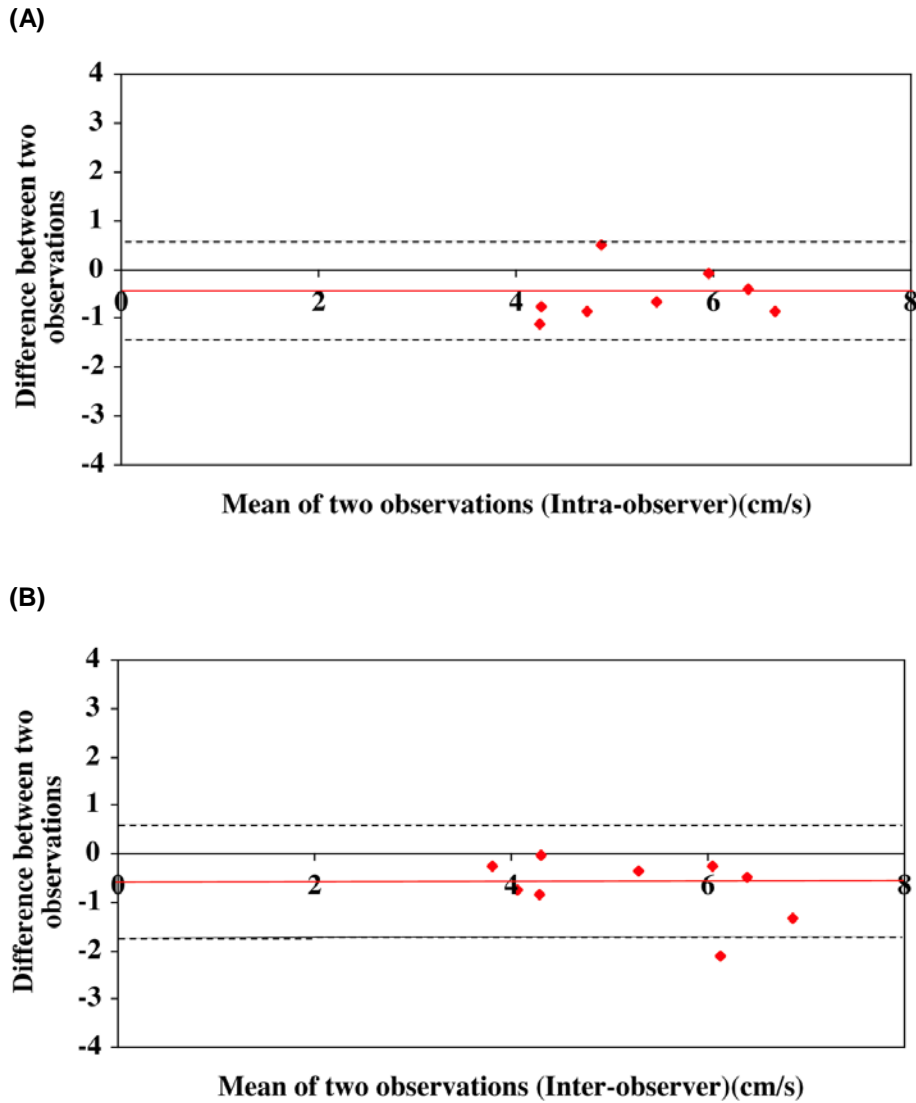


Figure 6.30. Bland-Altman Plot of (A) intra-observer variation and (B) inter-observer variation for measuring E/EmS+Lav ratio by cardiac magnetic resonance imaging.

6.5. DISCUSSION

The first objective of this study was to examine the feasibility of using a VEC-CMR imaging protocol to calculate E/Em ratio as a non-invasive estimate of left ventricular diastolic filling pressure. The second objective was to examine the accuracy of this new technique in heterogeneous population of patients exhibiting a wide range of LVEF, by directly comparing VEC-CMR E/Em ratios against LVEDP recorded invasively during left heart catheter studies. The third objective of this study was to examine the relationship of E/Em ratios recorded using VEC-CMR with E/Em recorded using pulsed-wave tissue Doppler echocardiography. Since completion of our study recruitment, there have been several single centre studies questioning the accuracy of echo-derived E/Em for estimating LV filling pressures in certain patient cohorts.¹⁵⁻¹⁹ A recent study by Mullens et al found no correlation between E/Em and PCWP measured in patients with severely impaired LVEFs.¹⁶ As a result of increasing research in this area, and since completion of our study recruitment, the American Society of Echocardiography and European Association of Echocardiography have issued new guidelines for diagnosing diastolic dysfunction.¹⁴ These guidelines include two new step-wise protocols for diagnosing elevated mean left atrial pressures (as a definitive marker of diastolic dysfunction) using E/Em and other echocardiographic parameters of diastolic function in patients with normal and impaired left ventricular systolic function respectively. The guidelines recommend E/Em as the first line index for diagnosing diastolic dysfunction in patients with preserved LVEF. For patients with impaired LV systolic function, an assessment of diastology is recommended using peak transmitral E-wave velocity, E/A ratio and mitral deceleration times as first line indices for diagnosing diastolic dysfunction as shown in Figure 1.32. In response to these new guidelines, we have re-analysed our data, using our own modification of these protocols tailored specifically for use with diastolic indices measured using the cardiac magnetic resonance protocols described above. This guideline modification for use by VEC-CMR will require validation in a separate patient cohort before its use in clinical practice should be contemplated.

6.5.1. Comparing VEC-CMR peak transmitral inflow velocities, myocardial tissue velocities and E/A ratios with spectral and tissue Doppler echo recordings and LV filling pressures

Mitral inflow velocities (E and A) measured by VEC-CMR were lower than those measured by spectral Doppler echocardiography. This may be partly due to the lower temporal resolution of VEC-CMR (30 phases/cycle) when compared to Doppler echocardiography (frame rate >90/cycle). There was a moderately good inter-modality correlation between echo and CMR mitral E velocities, and between echo and CMR mitral A velocities, and a moderate inter-modality correlation in E/A ratios. This finding is consistent with previously published data comparing CMR and echo mitral inflow patterns, and most likely reflects the similar sampling sites used by the two imaging modalities, at the level of the mitral valve leaflet tips.²²³⁻²²⁵ By comparison, early diastolic relaxation myocardial tissue velocities (VEC-CMR Em) measured using VEC-CMR were significantly higher than the early diastolic relaxation mitral annular tissue velocities measured using tissue Doppler echocardiography (PWTDE Em). There was no significant correlation between Em values recorded using VEC-CMR and those using pulsed-wave tissue Doppler echocardiography. There may be several reasons for this. Em tissue velocities were measured by echocardiography from apical long-axis views of the heart by using pulsed-wave TDE from the junction of the mitral annulus and basal LV myocardium, as is standard practice. Using this method a TVI velocity trace is recorded from a pulsed sample volume that remains in a static position throughout the cardiac cycle and the mitral annulus moves up and down through the pulse sampling volume in the long-axis. By comparison, myocardial tissue velocities were recorded by VEC-CMR using through-plane views of the heart. Using this method, the base of the heart actually move in and out of plane if the velocity-encoded slice is selected at the level of the mitral annulus, and so data throughout the whole of the cardiac cycle cannot be recorded. For this reason, our VEC-CMR slice selection was at approximately two thirds of the length of the LV long-axis, at the level of the upper basal LV myocardium, and not at the level of the mitral annulus. Furthermore using PWTDE, the sampled Em velocity is at the level of the junction of the mitral annulus with basal LV *endocardium*. Using VEC-CMR, the Em region of interest was within the middle of the basal LV *myocardium*. During image acquisition every attempt was made to ensure carefully selected on-axis apical views through the middle of

all 6 LV walls by echocardiography. During VEC-CMR analysis of the 6 LV myocardial tissue velocities recorded for each study subject, care was taken to ensure the 6 regions of interest within the basal LV myocardium selected reflected as closely as possible the 6 LV wall positions (anteroseptum, anterior, lateral, posterior, inferior and septal) recorded from the 3 apical echocardiographic views of the heart. Selecting the 6 region of interest sites within the basal myocardium from VEC-CMR through-plane views relied on a visual judgement of the position and delineation of the six LV wall mid-points and boundaries as demonstrated previously in Figure 6.3, and there may therefore have been an unavoidable degree of variability between echo and CMR region of interest positions. Furthermore, the amplitudes of the recorded PWTDE measurements are dependent on the angle of insonation of the ultrasound beam from the transducer. Any Doppler angulation beyond zero degrees would therefore result in a reduction in the maximal recorded Em tissue velocity, as per the Doppler shift equation. The measurement of peak myocardial tissue velocities using VEC-CMR is not angle dependent. Although care was taken to minimise the Doppler angulation during echo scanning to <20 degrees, any deviation from zero degrees would result in an underestimate of echo-recorded Em velocities compared to CMR-recorded Em velocities. Our finding is consistent with that of another recently published study by Jung et al, who noted an increase in peak Em velocities recorded by CMR compared to echo-measured CMR velocities from various different but comparable regions of interest within the ventricular myocardium.²⁰

In this study, we noted no relationship between invasively recorded LVEDP and peak transmitral E wave velocity, recorded by either VEC-CMR or Doppler echocardiography. There was no relationship between invasively recorded LVEDP and E/A ratio, recorded by either VEC-CMR or Doppler echocardiography. These findings are consistent with previously published data.^{13,191,192}

6.5.2. Comparing VEC-CMR E/Em with echo E/Em and LV filling pressures

Using VEC-CMR, E velocity was lower and Em velocity higher than measured using echocardiography and this combination resulted in calculated E/Em ratios being significantly lower when measured using VEC-CMR compared to Doppler echocardiography. Over a wide range of LVEF's, E/Em(S), E/Em(L) and E/Em(S+Lav)

ratios measured by VEC-CMR had no correlation with the equivalent E/Em ratios measured by echocardiography. When Em velocities were averaged from 5 or 6 LV walls, there was a weak-moderate correlation between CMR and echo techniques, and this may reflect a smoothing effect in site selection velocities. In study subjects with preserved LVEF there was a moderate correlation between VEC-CMR E/Em and echo E/Em. There was no correlation in E/Em ratios between imaging modalities in patients with impaired LV systolic function. This may reflect the fact that the majority of our patients in this study had known or suspected coronary artery disease, and hence of the 19 patients with impaired ventricular function, 12 (63%) had regional wall motion abnormalities. Em velocities may be affected by changes in regional as well as global function. As the Em velocities recorded by PWTDE for each LV wall were at a more basal and subendocardial site than the corresponding VEC-CMR Em velocities in patients with ischaemic heart disease and regional wall motion abnormalities, this could account for the poor correlation between CMR and echo-E/Em ratios in patients with impaired LV systolic function and is a recognised limitation of this study.

Our VEC-CMR Em velocities were recorded from the basal LV myocardium and not the mitral annulus. Although this may affect the absolute Em velocity recorded, it should not significantly affect the validity of the resultant E/Em ratio as a reflection of the diastolic filling pressure of the left ventricle. The early diastolic myocardial tissue relaxation velocity Em, measured by VEC-CMR, is used to correct the peak transmitral E wave velocity for the influence of the time constant of myocardial relaxation, such that VEC-CMR E/Em should closely reflect changes in the LV diastolic filling pressure. When VEC-CMR E/Em was compared directly to LVEDP in all patients (n=41) exhibiting a broad range of LVEF, only E/Em(S) had a weak correlation with LVEDP. The remaining E/Em indices exhibited no significant correlation to LVEDP measurements. Similarly, the cohort of patient with impaired LV systolic function, only E/Em(S+Lav) had any correlation with invasively measured LV filling pressures. The remaining VEC-CMR E/Em ratios showed no correlation to LVEDP measurements. In both cases, the limited correlation, may have been influenced by the presence of regional ischaemia and regional wall motion abnormalities. Although, it can be argued that this is a limitation of the study, these results are also important and valid. Ischaemic cardiomyopathy is the most common cause of LV systolic dysfunction in clinical practice. Current echocardiographic guidelines suggest

averaging Em velocities recorded from the septal and lateral sides of the mitral annulus to minimise the influence of regional changes, but do not preclude the use of E/Em ratio in patients with regional wall motion abnormalities.¹⁴ If E/Em ratio by CMR correlates poorly with LVEDP in patients with impaired ventricular function and regional wall motion abnormalities, then this technique should not be used to estimate LVEDP in this patient cohort.

By comparison, in our cohort of patients with preserved LVEF, VEC-CMR E/Em(S), E/Em(L) and E/Em(S+Lav) had a moderate correlation with LVEDP. Measuring Em averaged from 5 or 6 sites within the ventricular myocardium significantly increases analysis times when compared to measuring Em from the septal and lateral positions only, limiting the clinical application of this technique. Averaging Em from 5 or 6 sites within the LV myocardium did not improve the correlation with LVEDP when compared to E/Em(S), E/Em(L) and E/Em(S+Lav) (p=NS), and therefore we do not recommend doing so.

Recent EAE/ASE guidelines now recommend two distinct diagnostic algorithms for the non-invasive estimation of LV filling pressures in patients with normal and depressed LVEFs respectively. For this reason we re-analysed our VEC-CMR data as categorical, rather than numerical variables, using simplified versions of the two EAE/ASE diagnostic algorithms, with modified normative cut-off values specific to VEC-CMR which we determined from receiver-operator characteristics. Using our specific CMR modification of the EAE/ASE guidelines for assessing diastolic function, we have demonstrated that VEC-CMR E/Em has a high sensitivity and high specificity for correctly diagnosing both normal and elevated LV filling pressures in individuals with preserved LV systolic function, but not in those with significant LV systolic impairment.

6.5.3 Comparing VEC-CMR E/Em results in this study with current research

We found the Em velocities recorded by CMR were significantly higher than those recorded using TDE techniques. While the site selection differences of the Em region of interests within the ventricular myocardium between the two techniques may have in part accounted for this finding in our patient population, it is unlikely to be the only explanation.

Jung and colleagues have published two studies, in separate patient cohorts comparing Em velocities recorded by VEC-CMR and TDE at similar sites within the LV. In the first study, standard VEC-CMR temporal resolution scanning was used (temporal resolution: 62-ms VEC-CMR vs. 40ms- TDE) in a cohort of 29 healthy volunteers.³³⁴ In the second study, a high-temporal resolution magnetic resonance tissue phase mapping sequence (temporal resolution: 13.8ms) was used in 12 healthy volunteers and 2 individuals with left ventricular hypertrophy, and compared with similar site TDE Em measurements.²⁰ Both studies found a marked inter-technique discordance in peak Em velocity measurements, with Em velocities acquired using VEC-CMR being significantly higher than those recorded using the pulsed-wave TDE method.^{20,334}

To our knowledge, there is only one other small single centre study by Paelinck and colleagues which examines the use of VEC-CMR for diagnosing diastolic dysfunction. This small pilot study explores the relationship of VEC-CMR E/Em with LV filling pressures in a cohort of 18 patients with left ventricular hypertrophy and preserved LV systolic function.¹⁹⁴ This study differs from ours in several ways. Firstly, they only include patients with preserved systolic function, whereas we have chosen to validate the technique in patients with both preserved and impaired LVEFs. Secondly, they measured mean pulmonary capillary wedge pressure (mPCWP) during right heart catheter as an estimate of left ventricular filling pressure, using mPCWP>15mmHg as indicative of elevated diastolic filling pressure. Although, mPCWP and LVEDP have been shown to have a close relationship ($r=0.81$) they are not the same.⁷ PCWP may not accurately reflect LVEDP in patients with pulmonary artery hypertension and significant mitral valve pathology. Although, this limitation may not be relevant in Paelinck's homogeneous study population, it is in our deliberately heterogeneous patient cohort which included 4 patients with primary pulmonary hypertension, and one patient with pulmonary hypertension secondary to a secundum ASD. We felt it was preferable and more accurate to measure LVEDP directly during left heart catheterisation, using LVEDP of 12mmHg as our normative threshold value for the reasons previously described. Despite these differences in study design and methodology, the results of our subgroup analysis of study subjects with preserved LVEF broadly compliments that of the Paelinck study. Both studies show moderate correlation between invasive measures of LV diastolic filling and various VEC-CMR E/Em ratios. Both studies also show moderate correlation between echo and VEC-

CMR E/Em ratios, with the exception of VEC-CMR E/Em recorded from the lateral LV wall, which did not correlate with echo E/Em(L) in either study.

To our knowledge, our study is the first to examine the use of VEC-CMR E/Em ratios as a non-invasive estimate of LVEDP, and hence diastolic function, in individuals with systolic heart failure secondary to both ischaemic and non-ischaemic causes. We found that peak transmitral E wave velocity divided by the mean of the septal and lateral Em velocities had a moderate correlation with LVEDP in patients with impaired ventricular function, whereas E/Em(S) and E/Em(L) individually did not. As 63% of our cohort with impaired LV function had ischaemic heart disease, we also averaged Em from recordings taken from all six basal LV walls, to minimise the effect of regional dysfunction. This did not appear to make any difference, with E/Em(5av) and E/Em(6av) failing to correlate with measured LVEDP. The reason for is unclear and warrants further investigation. Unfortunately, the small numbers of patients in this study prevents further meaningful subgroup analysis of those with depressed LVEFs.

6.5.4 Study limitations

This small pilot study was designed to establish if velocity encoded CMR tissue phase mapping sequences could be used to non-invasively estimate LV diastolic filling pressures in a manner analogous to echo E/Em. To be valid for use in clinical practice, we believed the technique had to be valid in a heterogenous population exhibiting a range of LVEF, as seen in our clinical practice. The results of our study compliment [those of Paelinck](#), and suggest VEC-CMR E/Em may be clinically useful for diagnosing diastolic dysfunction in individuals with preserved LV systolic function. The accuracy of this technique in patients with impaired LVEF remains less clear. Unfortunately the small size and heterogeneous nature of our study cohort with impaired LVEF, precluded further meaningful subgroup analysis of this group, and warrants further study in the future.

New EAE/ASE guidelines recommend two differing step-wise algorithms for diagnosing diastolic dysfunction on patients with a) preserved LVEF and b) impaired LVEF. In patients with preserved LVEF, low E/Em ratios are indicative of a normal LVEDP, and high E/Em ratios indicative of a high LVEDP.¹⁴ [When we re-analysed our data using a](#)

[modification of the EAE/ASE step-wise algorithm for individuals with preserved LVEF, 45% of our study cohort had E/Em ratios in the intermediate range.](#) Where E/Em is of an intermediate value, LVEDP may be normal or elevated, and the EAE recommend that additional echo features, such as elevated LA volumes (>34ml/m²), need to be present to confirm the diagnosis of diastolic dysfunction in this intermediary cohort. Unfortunately these guidelines were published following the recruitment of our study cohort, and an LA volume stack was not part of our CMR protocol. The cohort of patients with preserved LVEF and intermediate E/Em, could not be analysed further to determine if diastolic function was present and this is a significant limitation of our study. [Although CMR E/Em ratios were highly specific for accurately predicting normal or elevated LVEDP in the 55% of individuals in whom E/Em fell within the diagnostic range, we must conclude that overall CMR is likely to be a poor predictor of LVEDP in clinical practice due to the large number of subjects \(45%\) with E/Em ratios falling into the indeterminate range.](#)

Ideally we would have liked to recruit an unselected heterogenous patient population into this study. However, due to the inherent risk of left heart catheterisation, we felt this was difficult to justify in ethical terms, and so patients undergoing invasive LVEDP recordings had to have a clinical indication for the left heart catheterisation study. For this reason, our study cohort may have a higher prevalence of coronary artery disease than that of a truly unselected population, and this may have biased our results.

Left ventricular haemodynamics are best measured invasively using micro-manometer conductance catheters. Unfortunately expense and limited availability prevented the use of a micro-manometer catheter in this study and LVEDP was measured by the interventional cardiologist at the time of left heart catheterisation using a traditional fluid-filled catheter system. Although this method may not be as accurate and detailed as measuring pressure-volume loops it is the reference standard by which LVEDP is quantified in routine clinical practice, and we would argue is superior to measuring PCWP which has been used as a surrogate marker of mLAP/LVEDP in several Doppler echo E/Em-invasive catheter comparison studies.^{5,16,335,336}

6.5.5 Conclusion and future work

VEC-CMR E/Em(S), E/Em(L) and E/Em(S+Lav) ratios have a moderate correlation with LVEDP in patients with preserved LVEF. This finding suggests that velocity encoded magnetic resonance tissue phase mapping can be used to estimate left ventricular diastolic filling pressures and diagnose left ventricular diastolic dysfunction in patients with preserved LV systolic function. Using a modification of the EAE/ASE guidelines for diagnosing diastolic dysfunction in patients with preserved LVEF, modified specifically for use by VEC-CMR derived velocity indices, VEC-CMR E/Em was both sensitive and specific for correctly diagnosing and excluding elevated diastolic filling pressures. However, a significant number of patients had VEC-CMR E/Em values which fell within the indeterminate zone, [limiting the clinical application of the technique](#), and this cohort requires further review. Further work could include secondary measures in this cohort, such as the assessment of left atrial volume by CMR. A larger prospective study of patients with 1) normal LVEF and symptoms consistent with heart failure and 2) normal LVEF and no symptoms of heart failure is now required. Invasive LV filling pressure needs to be recorded in this study and the CMR imaging protocol should include an atrial short axis stack of steady state free precession imaging in addition to the VEC-CMR protocol described above.

The accuracy of VEC-CMR E/Em in estimating LV diastolic filling pressures in patients with impaired ventricular function remains unclear. Further work is required. A future study of VEC-CMR E/Em velocity ratios indexed against LVEDP in patients with impaired LV systolic function secondary to dilated cardiomyopathy (in the absence of regional wall motion abnormalities) would provide useful insight into both the accuracy and the prognostic implications of an elevated VEC-CMR E/Em ratio in this patient cohort.

Formatted: Font: 24 pt

CHAPTER 7

Formatted: Font: 24 pt

RIGHT VENTRICULAR FUNCTION

***“TEN QUANTATATIVE METHODS FOR
ANALYSING RIGHT VENTRICULAR
SYSTOLIC FUNCTION USING TWO-
DIMENSIONAL AND TISSUE DOPPLER
ECHOCARDIOGRAPHY: A COMPARISON***

WITH CARDIAC MAGNETIC RESONANCE IMAGING”

Formatted: Normal, Indent: Left: 0 cm, First line: 0 cm, Line spacing: single

CHAPTER 7: RV SYSTOLIC FUNCTION

7.1 BACKGROUND

The right ventricle was historically viewed as a passive conduit connecting the venous circulation to the pulmonary circulation. Until relatively recently the RV was considered less important than the LV in maintaining normal cardiovascular haemodynamics, and therefore study of the RV has been largely neglected in favour of research into left ventricular physiology. It is not until recent years that the true importance of this “forgotten” ventricle in cardiovascular pathophysiology is finally being appreciated. It is now well recognised that right ventricular systolic function is of clinical and prognostic importance in a variety of cardiac diseases.^{82,337-340} Despite this knowledge, systematic quantitative assessment of right ventricular function is not uniformly performed during echocardiographic imaging studies, and a visual assessment of RV function remains the standard by which RV systolic function is assessed in many centres. This is due in part to the complex geometry of the right ventricle, rendering volumetric assessments of RV function by 2DE inaccurate, and also to the paucity of ultrasound studies providing normal values of right heart function. Furthermore, the myofibre architecture of the RV lacks the middle constrictor fibre layer seen within the LV, and therefore relies more heavily on its long axis contractility to maintain RVEF.⁶³ Due to the geometric complexity of the RV and

the predominance of RV long axis contractility, there has been recent interest in assessing RV systolic function by non-volumetric methods in particular TDE, myocardial deformation imaging and methods quantifying measures of tricuspid annular motion. In response to increasing echocardiographic study in this area, the American Society of Echocardiography published in 2010 revised guidelines, endorsed by both the European Association of Echocardiography and the Canadian Society of Echocardiography, for the echocardiographic assessment of the right heart in adults.³⁷ The guidelines review ten non-volumetric methods for quantifying RV systolic function, and for selected methods, suggest normal reference ranges based on data pooled from several studies. The guidelines conclude that visual assessment of RV systolic function should be combined with at least one quantitative index of RV function – either tricuspid annular plane systolic excursion (TAPSE), RV myocardial performance index (RV MPI), pulsed-wave tissue Doppler peak systolic velocity of the lateral tricuspid annulus (RV PWTDE S') or fractional area change (FAC). The guidelines also consider the use of RV isovolumic acceleration (RV IVA) and strain imaging, but do not at present recommend the clinical use of these techniques due to the current paucity of data and lack of reference ranges.³⁷

Standardizing assessment of RV function is important for both clinical and prognostic reasons and will improve service delivery of cardiac diagnostic imaging within and between centres. To our knowledge, there are no head-to-head studies comparing multiple different non-volumetric indices of RV function in a heterogeneous population of patients. At the time of writing it remains unclear which if any, of the available quantitative 2DE non-volumetric assessments of RV function is superior to the others when compared to CMR, is the most reproducible, has the highest potential clinical application and should therefore be the echocardiography method of choice for assessing RV function in the heterogeneous population of patients seen in clinical practice.

Although there is no “gold standard” for assessing RV systolic function, the superior spatial resolution of CMR, coupled with its ability to image the heart in any plane, makes it the widely accepted reference standard for quantifying right ventricular volumes and ejection fraction.

The aim of this study was to compare ten non-volumetric 2DE methods for quantifying RV systolic function, indexed against CMR-RVEF as the reference standard, in a heterogeneous population of patients exhibiting a wide range of RVEFs. Methods reviewed in the ASE guidelines include measurement of RV dP/dT and regional tissue Doppler strain. The use of RV dP/dT for quantifying RV function requires the presence of significant tricuspid regurgitation (TR) and therefore cannot be used in patients without TR. Furthermore dP/dT is load dependent and may be inaccurate in patients with severe TR due to the neglect of the inertial component of the Bernoulli equation and the rise in right atrial pressure. For a technique to have high clinical application, it needs to be accurate and applicable to all. For these reasons the ASE do not recommend RV dP/dT for routine use and we therefore chose to exclude this measurement from our study. From both our own experience and the experience of others, we know that measurement of regional strain using tissue Doppler techniques is susceptible to significant inaccuracy due to angle dependency, high signal-to-noise ratio and wide limits of agreement caused by high inter-observer variation in manual region of interest site selection and manual temporal tracking.^{166,341-343} For these reasons tissue Doppler strain techniques are not recommended by the ASE, and are not included in our study. The remaining eight non-volumetric indices of RV function described by the ASE/EAE/CSE guidelines are included in our study.³⁷ In addition to these indices, we have chosen to include two differing assessments of RV strain measured using the more accurate speckle tracking technique, plus one novel tissue Doppler index of tricuspid annular plane systolic excursion developed by us, which we have not found previously described in the current literature. Each RV index is described in detail below.

7.2 STUDY AIM

The aim of this study was to compare ten non-volumetric 2DE methods for quantifying RV systolic function, indexed against CMR-RVEF as the reference standard, in a heterogeneous population of patients exhibiting a wide range of RVEFs.

7.3 METHODS

7.3.1 Study Design

This study was approved by the Regional Ethics Committee and study subjects gave written informed consent. Sixty patients exhibiting a broad spectrum of RVEF's (Range 24-73%) were prospectively studied. They were recruited from outpatient clinics, elective echocardiography and cardiac catheterisation lists.

All study subjects underwent standard 2DE (GE Vivid 7) and CMR (1.5T Siemens Sonata) consecutively. RVEF was calculated by CMR as described below. Ten non-volumetric echocardiographic indices of global RV systolic function were assessed from 2DE as described below. The ten echocardiographic methods for quantifying RV function were then correlated against CMR-RVEF, and compared against each other. Where normative cut-off values for the technique have previously been published by the ASE/EAE/CSE, these cut-off values were applied to ROC curves to determine the sensitivity and specificity of the specified RV index in our patient cohort. For RV indices in which no normative threshold values have been determined, ROC analysis was performed to establish normal RV function cut-off values for each echocardiographic method. As visual assessment of the right ventricle is the standard by which RV systolic function is still quantified in many centres, patients were also visually assessed as having normal, mild, moderate or severe RV dysfunction on echocardiography by a British Society of Echocardiography accredited operator blinded to the CMR results.

7.3.2 Patient Selection

A heterogeneous population of patients in sinus rhythm, exhibiting a broad spectrum of RV systolic function, was studied. Patients were excluded if they had a contraindication to CMR, had severe calcific tricuspid valve disease, moderate-severe tricuspid annular calcification, tricuspid annular ring or prosthesis, or if it was not possible to image the right heart clearly from the apical 4-chamber view.

7.3.3 Imaging Methods.

CMR and 2DE were performed consecutively, within 30 minutes of each other, to ensure similar heart rates and cardiac loading conditions.

Cardiac Magnetic Resonance.

The CMR RV systolic function acquisition protocol was performed as previously described in section 3.4.2.

Two-dimensional Echocardiography.

2DE imaging was performed using a Vivid 7 scanner, (GE Medical Systems, Wauwatosa, WI). All patients were imaged in the left lateral decubitus position and depth and frame rate were optimised. The right ventricle was imaged from the parasternal short axis, parasternal long axis and apical-4 chamber views of the heart. Study subjects were then imaged in the supine position and the right ventricle was further assessed from the subcostal view of the heart. A visual assessment of global right ventricular function was made from review of the above 2D images. Harmonic imaging was used consistently throughout each study.

Tricuspid inflow and Pulmonary outflow spectral Doppler acquisition for assessing RV Myocardial Performance Index

A pulsed-wave Doppler signal was recorded through the pulmonary valve from the parasternal short axis view taking care to ensure a Doppler angle of <20degrees. If it was not possible to obtain a clear Doppler envelope from this view, then a spectral Doppler recording was made through the pulmonary valve in either the modified parasternal long axis RV outflow view or the subcostal short-axis view of the heart. A pulsed-wave Doppler signal was then recorded through the tricuspid valve from the apical 4-chamber view of the heart. The spectral Doppler traces were stored for subsequent post-processing.

Acquiring colour M-mode data sets for the assessment of Tricuspid Annular Plane Systolic Excursion

Right ventricular M-Mode measurements were made from the apical-4 chamber view of the heart in paused expiration. The M-Mode cursor was placed at the junction of the lateral tricuspid annulus and right ventricular free wall one centimetre from the insertion point of

the tricuspid valve leaflet as per EAE guidelines.³³² The subsequent time-motion mode recording was acquired with a sweep speed of 100mm/s to ensure consistency in temporal resolution. To further improve accuracy a colour tissue Doppler trace was superimposed on the M-Mode recording as shown in Figure 7.3, with the red-blue interface representing peak systolic tricuspid annular excursion during systole prior to the onset of diastolic relaxation of the RV. Colour Doppler M-mode recordings were stored for subsequent post-processing.

Acquiring pulsed-wave tissue Doppler traces for assessing the tricuspid annular peak systolic tissue velocity and tissue Doppler-derived RV myocardial performance index.

Tissue Doppler imaging now allows the recording of longitudinal myocardial tissue velocities and mitral and tricuspid annular velocities. The tricuspid annular peak systolic tissue velocity (PWTDE S') is a measure of the longitudinal contractile function of the right ventricle. A tissue Doppler velocity trace of the RV was measured by placing a pulsed-wave sample volume at the junction of the right ventricular free wall and lateral tricuspid annulus one centimetre from the insertion point of the tricuspid valve leaflet, in the apical 4-chamber view of the heart.³³² To improve accuracy, care was taken to ensure a Doppler angle of <20 degrees, and translational motion of the heart was reduced by acquiring the image in paused expiration. The pulsed-wave tissue Doppler trace was then stored for subsequent analysis. The tissue Doppler myocardial performance index was also calculated from this velocity trace.

Right ventricular TDI-Q acquisition for analysis of colour tissue Doppler systolic velocities, isovolumic acceleration and tissue Doppler tricuspid annular plane systolic excursion.

Colour tissue Doppler images of the right ventricle were acquired from the apical 4-chamber views with frame rates ≥ 100 frames/sec and pulse repetition frequencies between 500 Hz to 1 KHz. Three consecutive beats were stored and analysed during post processing. A continuous-wave Doppler tracing of pulmonary outflow was recorded through the pulmonary valve from the parasternal short axis view to enable calculation of event timings during post-processing.

Acquiring RV data sets for assessing RV Fractional Area Change

The RV was imaged from the apical 4-chamber view of the heart in the zoomed mode taking care to optimise RV endocardial wall definition and avoid apical foreshortening. Subsequent RV data sets were stored.

Acquiring RV data sets for assessing RV global strain and RV free wall strain using 2D speckle tracking software.

The ventricles were imaged from the apical windows as previously described. Care was taken to optimise endocardial wall definition of the RV. Images of the RV were acquired from the apical 4-chamber view taking care to avoid apical foreshortening. An apical long axis view of the RV was acquired to enable event-timing markers to be added during post-processing of the data sets.

7.3.4 Image Analysis.

Cardiac Magnetic Resonance

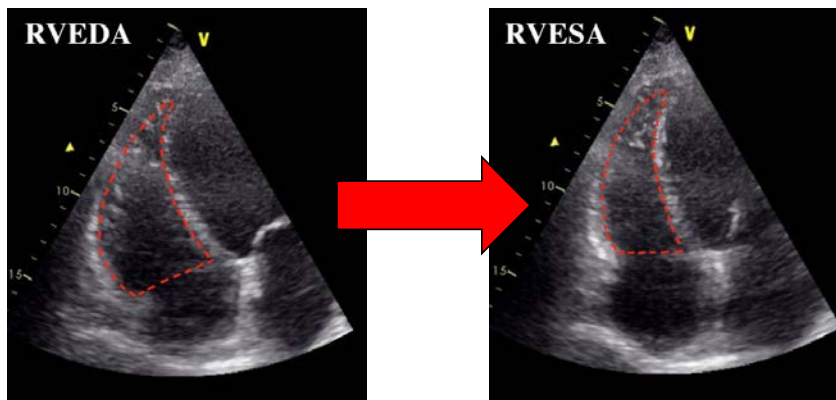
RV volumes were quantified and RVEF calculated by CMR using the method described in section 3.4.2. Normal RV systolic function was defined as a CMR-derived RVEF $\geq 47\%$ as is standard practice.

Two-dimensional Echocardiography

1) Measuring RV fractional area change (FAC)

The RV FAC was calculated from an optimised apical four-chamber view of the RV acquired as described above. End-diastole was determined as the frame after mitral valve closure and the RV end diastolic area (RVEDA) was measured by tracing the RV endocardial border from the tricuspid annulus, along the RV free wall to the apex and back down the interventricular septum.³⁷ A straight line then connects the medial and lateral

tricuspid annular points (see Figure 7.1). Trabeculations, tricuspid leaflets and chords were included in the RV chamber. End-systole was defined as the frame displaying the smallest cavity area. RV end systolic area (RVESA) was measured using the same method as described for RVEDA. The RV FAC was then calculated from the equation: $RV\ FAC = (RVEDA - RVESA) / RVEDA \times 100\%$.³⁷ According to ASE/EAE/CSA guidelines, a $FAC \geq 35\%$ is indicative of normal RV systolic function.³⁷



$$FAC(\%) = (RVEDA - RVESA) / RVEDA \times 100\%$$

Figure 7.1. Calculating the RV fractional area change. The endocardial border of the RV traced in the apical 4-chamber view, from the lateral tricuspid annulus, along the free wall to the apex, then down the interventricular septum to medial tricuspid annulus. The medial and lateral borders of the tricuspid annulus are then connected by a straight line. This is performed in end-diastole, to calculate RV end-diastolic area, and then repeated in end-systole. The percentage fractional area change is calculated using the equation shown above. Trabeculation, tricuspid leaflets and chords are included in the RV chamber. FAC, fractional area change; RVEDA, right ventricular end-diastolic area; RVESA, right ventricular end-systolic area.

2) Measuring RV myocardial performance index (MPI) by spectral Doppler

The MPI is a simple, relatively load independent measure of RV function based on the ratio of the sum of the isovolumic contraction and relaxation times of the right ventricle (IVCT+IVRT) divided by the right ventricular ejection time (RVET). The RV MPI was calculated from the acquired spectral Doppler envelopes of tricuspid inflow and pulmonary outflow using the equation: $MPI = (a-b)/b$, where: $a-b = (IVCT+IVRT)$ and $b = RVET$ as shown in Figure 7.2. Using this method, the upper normative limit of RV MPI=0.40.³⁷

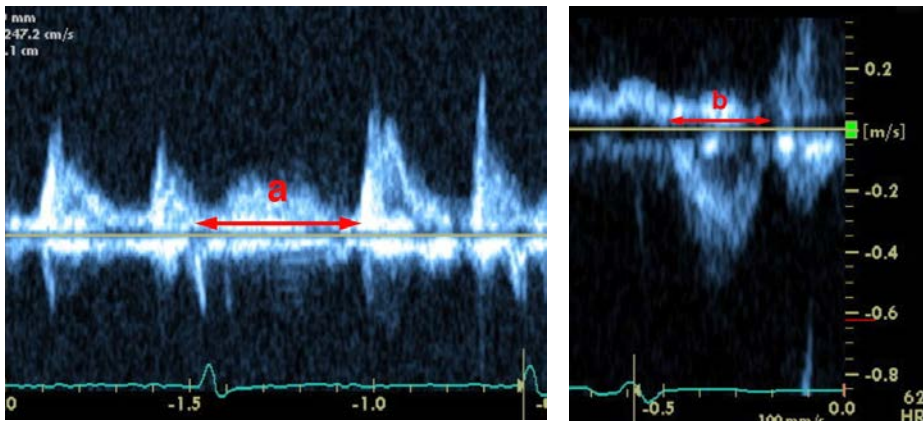


Figure 7.2. Calculating the RV Myocardial Performance Index (MPI) by spectral Doppler. MPI is the ratio of the sum of the isovolumic contraction and relaxation times (IVCT+IVRT) divided by the right ventricular ejection time (RVET (b)) and is calculated by the equation $MPI = (a-b)/b$.

3) Measuring RV myocardial performance index (MPI) by pulsed-wave tissue Doppler

The RV MPI was also calculated from a pulsed-wave tissue Doppler velocity trace of the lateral tricuspid annulus/RV free wall, as shown in Figure 7.3. Using TDE, the MPI is calculated from a single Doppler trace, thus minimising error due to variation in the R-R interval between cardiac cycles. Using this method, the upper normative limit of tissue Doppler myocardial performance index (RV TDE-MPI) is 0.55.³⁷

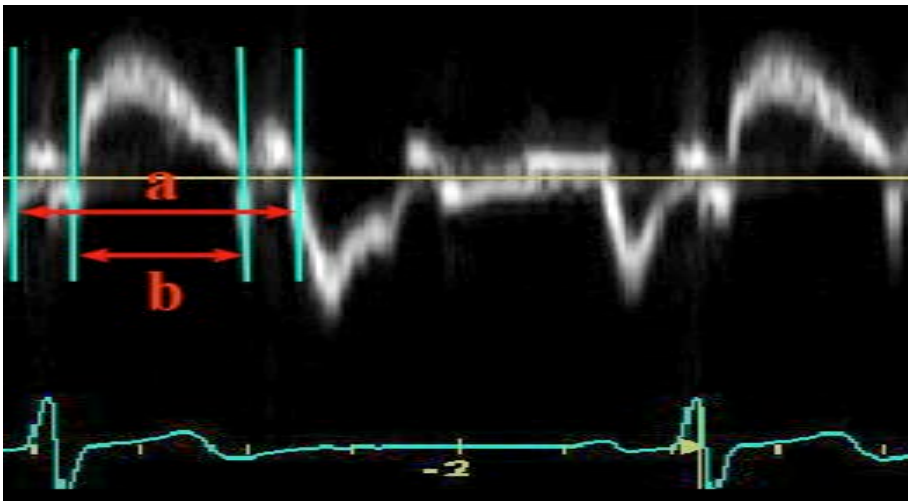


Figure 7.3. Calculating the RV Myocardial Performance Index (MPI) by tissue Doppler. MPI is the ratio of the sum of the isovolumic contraction and relaxation times (IVCT+IVRT) divided by the right ventricular ejection time (RVET (b)) and is calculated by the equation $MPI=(a-b)/b$.

4) *Measuring tricuspid annular plane systolic excursion with colour M-Mode (M-Mode TAPSE)*

The M-Mode TAPSE score was measured as the peak systolic displacement from the end-diastolic reference point, and occurred at the red-blue colour M-Mode interface as shown in Figure 7.4. ASE/EAE/CSA guidelines recommend a M-Mode TAPSE score of ≤ 16 mm as indicative of impaired RV systolic function.³⁷

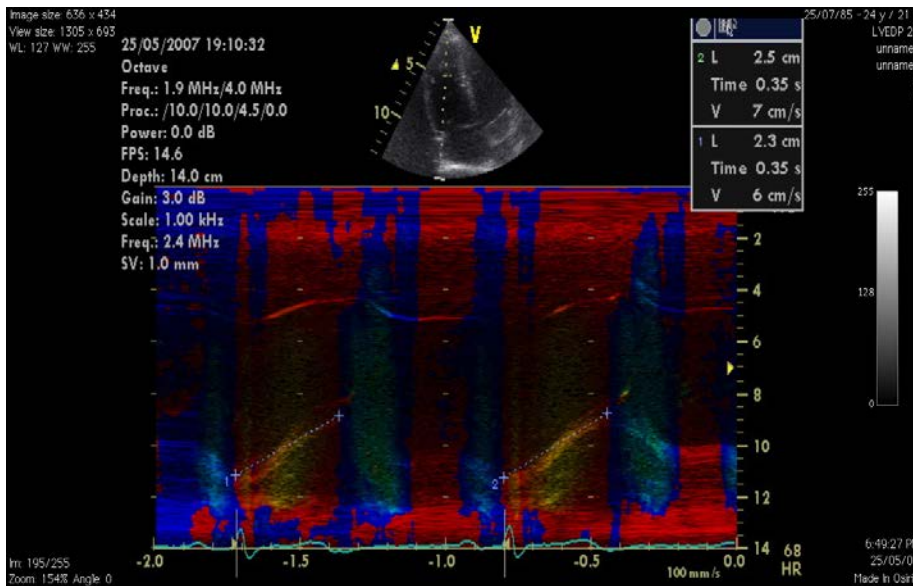


Figure 7.4. Measuring the tricuspid annular plane systolic excursion score using colour M-Mode (M-Mode TAPSE) . A slope caliper is used to measure the degree of systolic excursion in the longitudinal plane of the heart.

5) Measuring tricuspid annular peak systolic tissue velocity by pulsed-wave tissue Doppler (RV PWTDE S')

The tricuspid annular peak systolic tissue velocity (S') was measured as the peak deflection in systole above the isoelectric line, and occurs after the isovolumic contraction spike as shown in Figure 7.5. ASE/EAE/CSA guidelines recommend a lower normative limit of 10cm/s for PWTDE S' .³⁷

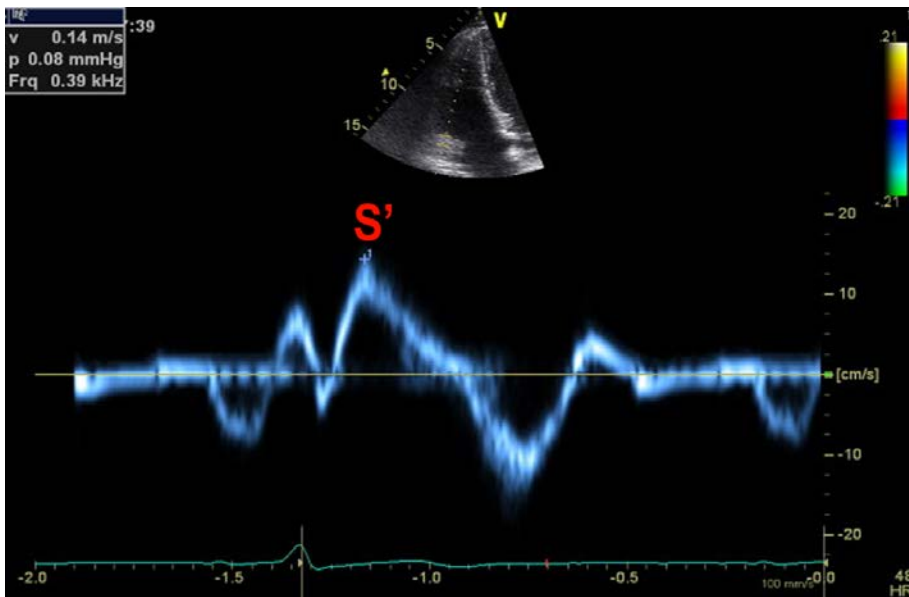


Figure 7.5. Recording the tricuspid annular peak systolic tissue velocity using pulsed-wave tissue Doppler imaging (RV PWTDE S').

A pulsed-wave sample volume is placed at the junction of RV free wall and lateral tricuspid annulus and the resultant tissue Doppler velocity pattern recorded. The peak systolic tissue velocity (S') is the peak deflection seen in systole above the isoelectric line, and occurs after the isovolumic contraction spike as shown.

6) Measuring tricuspid annular systolic tissue velocity by colour tissue Doppler (CTDE S')

Pulmonary valve opening and closure times were recorded by placing event-timing markers at the start and end of the recorded pulmonary outflow spectral envelope. The recorded pulmonary event timing markers were then superimposed on the tissue velocity/time graph

during post processing. Tissue velocity parameters were measured from the colour images during further post processing. The tissue Doppler sample volume, also known as the ROI (region of interest) marker was placed at the junction of the basal right ventricular free wall with the lateral tricuspid annulus, and the ROI was manually tracked throughout the cardiac cycle. Colour tissue Doppler velocity maps display the mean of the recorded systolic velocities within the ROI and so the peak systolic deflection measured is usually lower than the peak systolic velocity recorded by pulsed-wave tissue Doppler (Figure 7.6).

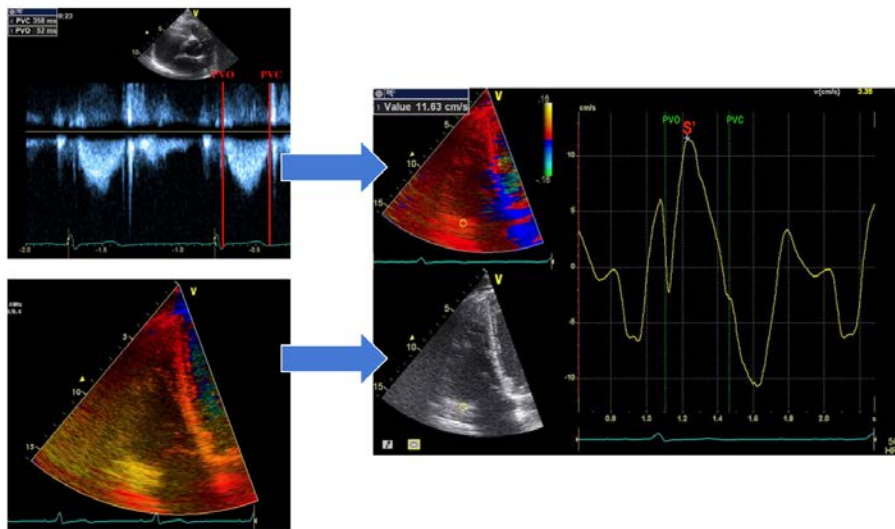


Figure 7.6. Measuring the tricuspid annular peak systolic tissue velocity using colour tissue velocity echocardiography imaging (RV CTDE S')

Pulmonary valve opening and closure event timing markers are recorded from a spectral Doppler trace of pulmonary outflow recorded in the parasternal short axis view, and superimposed on the resultant colour TDE graph. The raw colour TDE data set is recorded from the apical 4-chamber view of the heart with high temporal resolution (≥ 100 fr/sec). The region of interest (ROI) marker is positioned at the junction of the lateral tricuspid annulus and RV free wall ~ 1 cm from the tricuspid valve leaflet insertion point and motion is manually tracked throughout the cardiac cycle. The resultant colour TDE velocity trace is shown in the right side of the

image. S' is measured as the maximal systolic deflection present between pulmonary valve opening (PVO) and pulmonary valve closure (PVC).

7) *Measuring right ventricular myocardial acceleration during isovolumic contraction – “Isovolumic acceleration”(RV IVA)*

Event timing markers were superimposed on the colour TDE graph as previously described. A tissue velocity trace obtained at the junction of the lateral tricuspid annulus and basal right ventricular free wall was recorded as described above. The peak velocity of isovolumic contraction (IVV) and the isovolumic acceleration time (AT) were recorded from the isovolumic contraction deflection on the tissue velocity graph as shown in Figure 7.7. The IVA was calculated as the ratio of IVV:AT.

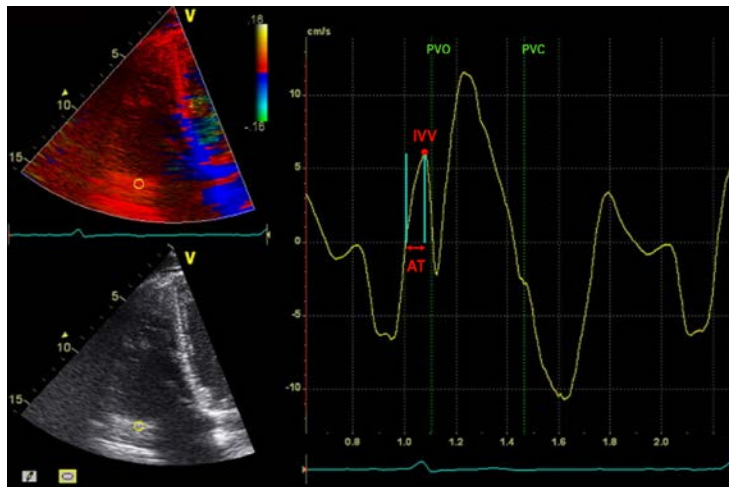


Figure 7.7. Measuring myocardial acceleration during isovolumic contraction of the right ventricle (RV IVA).

The peak velocity of isovolumic contraction (IVV) and the isovolumic acceleration time (AT) are recorded as shown. IVA is then calculated as the ratio of IVV:AT. PVO, pulmonary valve opening; PVC, pulmonary valve closure.

8) *Measuring tricuspid annular peak systolic excursion by colour tissue Doppler (TDE TAPSE)*

Event timing markers were superimposed on the colour TDE graph as previously described. A ROI sample volume was placed at the junction of the lateral tricuspid annulus and basal right ventricular free wall as previously described. Tissue Doppler myocardial displacement was selected from the TDI-Q analysis software and the ROI was manually tracked throughout the cardiac cycle to create a myocardial displacement graph as shown in Figure 7.8. The tricuspid annular peak systolic displacement was recorded as the peak systolic deflection on the graph prior to pulmonary valve closure.

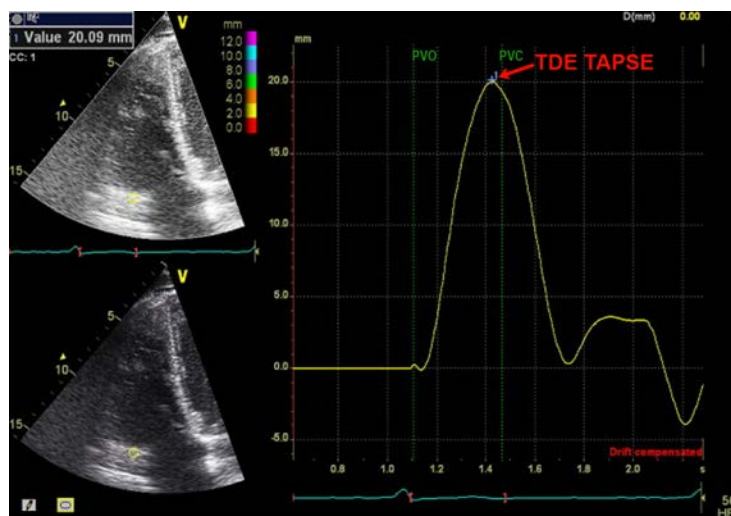


Figure 7.8. Measuring tricuspid annular peak systolic excursion using colour tissue Doppler displacement imaging (TDE TAPSE).

A ROI sample volume was placed at the junction of the lateral tricuspid annulus and basal right ventricular free wall and tracked manually throughout the cardiac cycle. The tricuspid annular peak systolic displacement was recorded as the peak systolic deflection on the graph prior to pulmonary valve closure. PVO, pulmonary valve opening; PVC, pulmonary valve closure.

9) Measuring right ventricular global strain (RVGS)

Event-timing markers were applied to the speckle tracking strain data sets as previously described to enable temporal analysis within the systolic component of the cardiac cycle. Right ventricular speckle tracking strain analysis was performed using GE Automated Functional Imaging software. The semi-automated endocardial border tracking system was applied to the right ventricle in the apical 4-chamber view of the heart by manually selecting the RV apex and the junctions between the basal RV free wall and lateral tricuspid annulus and basal interventricular septum and medial tricuspid annulus respectively. The endocardial border tracking system was re-positioned manually by selecting the appropriate coloured dots, until the operator was satisfied that each myocardial segment was being tracked correctly throughout that cardiac cycle. Once the operator was satisfied, the positions were finalised by selecting the approve button and a global 2D strain score was automatically generated from the quadrant analysis of the right ventricular free wall and septum as shown in Figure 7.9.



Figure 7.9. Right ventricular global strain (RVGS) recorded from the apical 4-chamber view.

A regional strain score is automatically applied to each myocardial segment in the RV free wall and septum. A global strain score is automatically calculated from the segmental strain score and is displayed in the top left picture of the quadrant. In this example the longitudinal global strain score for the right ventricle is -26.6%

10) Measuring right ventricular free wall strain (RVFWS).

As the interventricular septum, for imaging purposes, is traditionally considered as part of the left ventricle, it is unclear how much it contributes towards right ventricular systolic contraction. For this reason right ventricular free wall strain was analysed by excluding the longitudinal regional strain scores generated by the interventricular septum. The speckle tracking software was applied to the RV in the apical 4-chamber view as previously described. The right ventricular free wall strain (RVFWS) was calculated as the average of the basal, mid and apical regional longitudinal strain scores within the RV free wall as shown in Figure 7.10.

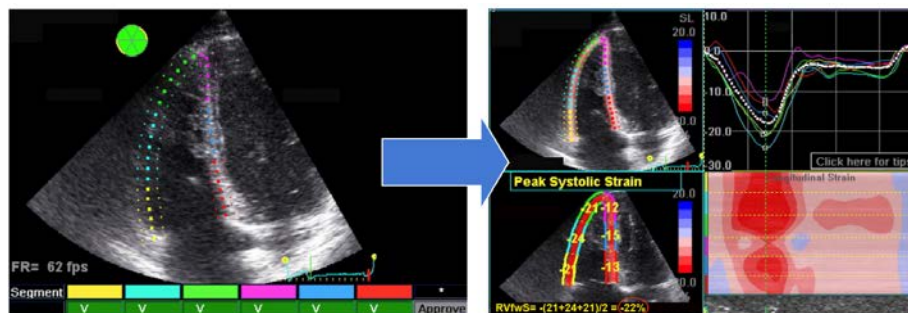


Figure 7.10. Measuring right ventricular free wall strain (RVFWS) using 2D speckle tracking software. RVFWS is measured as the mean of the 2D strain recordings from the basal, mid and apical RV free wall segments. In this example $RVFWS = -(21+24+22)/3 = -22\%$

7.3.5 Acquisition and Analysis times.

For an imaging technique to have widespread clinical application it must be quick and easy to perform. The acquisition and analysis times for each non-volumetric index of RV function were recorded.

7.3.6 Visual assessment of RV systolic function

A visual “eyeball” assessment of the right ventricle function is common practice in 2D echocardiography and remains the standard by which many centres report on RV systolic function. For this reason, the echocardiograms of the study subjects were visually assessed by a British Society of Echocardiography accredited operator blinded to the CMR results, and RV systolic function was reported semi-quantitatively as normal, mild, moderate and severely impaired. Due to the small numbers in this study, patients with moderate and severe RV dysfunction were classified as one sub-group. For each RV quantitative index measured, the mean \pm 2SD was calculated for each of the three sub-groups of patients with normal, mildly impaired and moderately-severely impaired RV systolic function. The mean value for each subgroup was compared to each adjacent subgroup, to ensure each echocardiographic technique had the ability to discriminate between differing subgroups of RV function.

7.3.7 Reproducibility

Interobserver and intraobserver variability for CMR-RVEF and for the ten echocardiographic indices of RV function were assessed in 10 patients exhibiting a range of RVEFs (RVEF range: 26-68% by CMR analysis). All measurements of RV function were assessed by two independent BSE accredited observers. These measurements were subsequently repeated by one observer at six months.

7.3.8 Statistical Analysis.

Values are expressed as mean \pm standard deviation (SD). All data sets were tested for normality. Each echocardiographic technique was correlated against CMR-RVEF using a bivariate correlation (Pearson correlation coefficient for parametric data and Spearman correlation coefficient for non-parametric data). For parametric data, linear regression analysis was used to directly compare the echocardiographic indices of RV function indexed against CMR-RVEF as the reference standard. A value of $p < 0.05$ was considered significant. Receiver operator characteristic (ROC) curves were estimated for each method and the area under the curve was calculated.

The reproducibility of CMR-RVEF and the ten non-volumetric 2DE indices of RV function were assessed by calculating the co-efficient of variation for intra- and inter-observer measurements. Bland-Altman analysis was also used to determine the mean bias and limits of agreement for intra- and inter-observer measurements. Results are expressed as mean bias ± 1.96 SD. A value of $p < 0.05$ was considered significant.

7.4 RESULTS

7.4.1 Patient characteristics

CMR and all 10 echocardiographic indices of RV function were successfully measured in 50 of the 60 patients. The remaining patients were excluded from the study. Clinical characteristics of the study population are described in Table 7.1.

Gender (M:F)	37:13
Mean age (yrs)	56±14
Clinical Diagnosis	
- Ischaemic heart disease*	17
- Valvular heart disease	5
- Dilated cardiomyopathy	1
- Pulmonary hypertension	3
- Atrial septal defect	1
- Coronary artery spasm	1
- Hypertensive heart disease	2
- Type 2 Diabetes & Metabolic syndrome	10
- No cardiac diagnosis	11

Table 7.1. Clinical characteristics of study subjects who completed both RV-CMR and 2D echocardiography protocols (n=50). F, female; M, male

* diagnosed either on coronary angiography, or clinical diagnosis of angina/previous myocardial infarction.

7.4.2 Correlation of ten echocardiographic indices of RV function against CMR RVEF

The ten echocardiographic indices of RV systolic function were correlated against CMR-RVEF in all patients (N=50; RVEF range: 26-73%). RvfwS ($p<0.001$, $r=-0.770$) and RVGS ($p<0.001$, $r=-0.750$) correlated strongly with CMR-RVEF (Figure 7.11 and Figure 7.12).

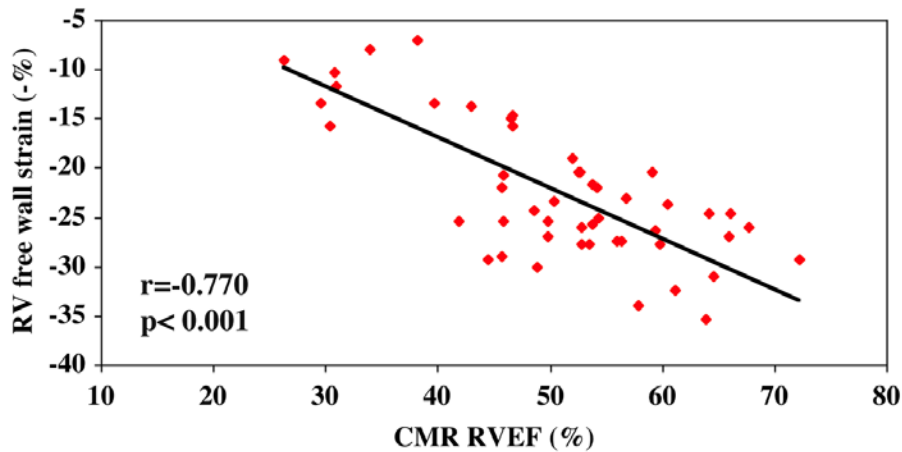


Figure 7.11. Correlation of RVFWS with CMR-RVEF in 50 subjects (RVEF range: 26-73%). CMR, cardiac magnetic resonance imaging; RVEF, right ventricular ejection fraction RVFWS, right ventricular free wall strain.

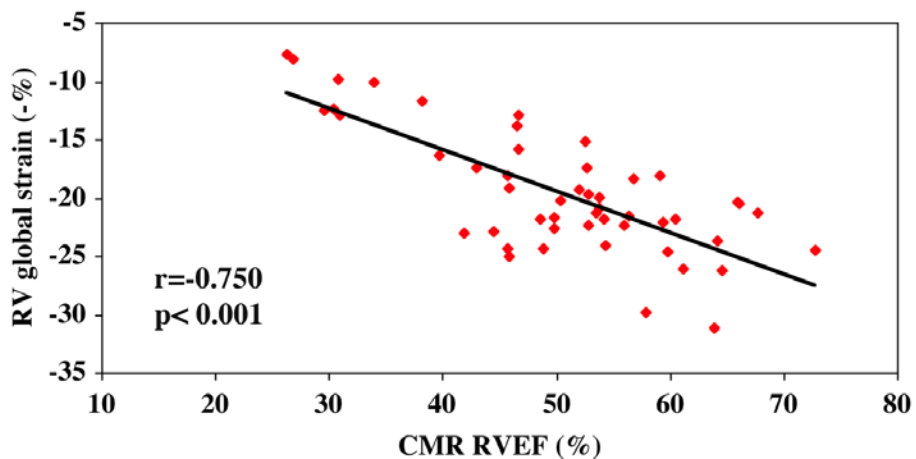


Figure 7.12. Correlation of RVGS with CMR-RVEF in 50 subjects (RVEF range: 26-73%). CMR, cardiac magnetic resonance imaging; RVEF, right ventricular ejection fraction RVGS, right ventricular global strain.

RV FAC ($p < 0.001$, $r = 0.582$), M-Mode TAPSE ($p < 0.001$, $r = 0.581$), RV CTDE S' ($p < 0.001$, $r = 0.523$), RV PWTDE S' ($p < 0.001$, $r = 0.509$) and TDE TAPSE ($p < 0.001$, $r = 0.488$) all had a modest correlation with CMR-RVEF (Figures 7.13 to 7.17).

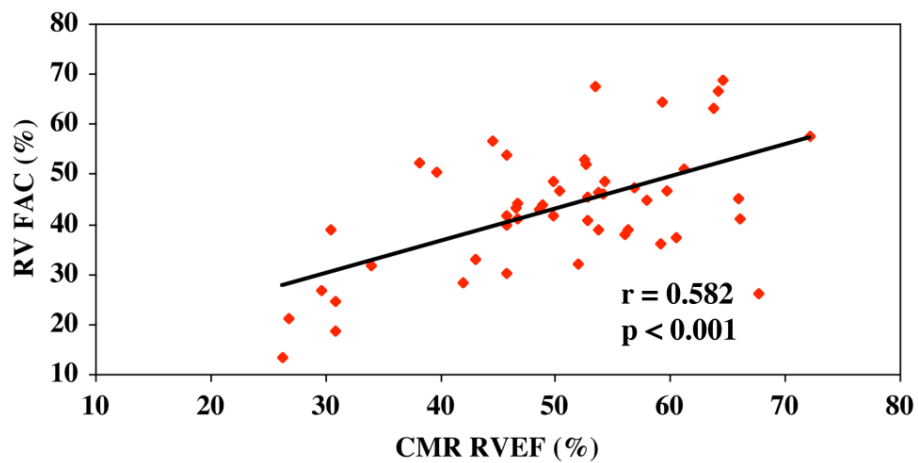


Figure 7.13. Correlation of RV FAC with CMR-RVEF in 50 subjects (RVEF range: 26-73%). CMR, cardiac magnetic resonance imaging; RVEF, right ventricular ejection fraction; RV FAC, right ventricular fractional area change.

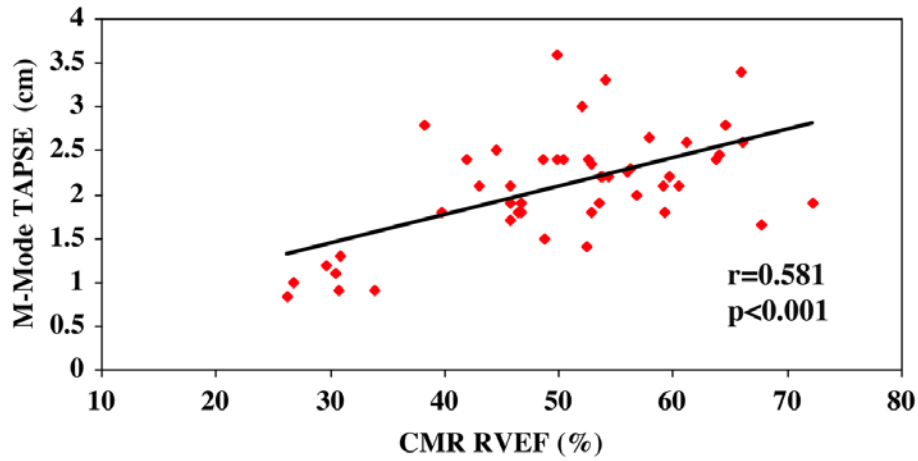


Figure 7.14. Correlation of M-Mode TAPSE Sm with CMR-RVEF in 50 subjects (RVEF range: 26-73%). CMR, cardiac magnetic resonance imaging; RVEF, right ventricular ejection fraction; TAPSE, tricuspid annular plane systolic excursion.

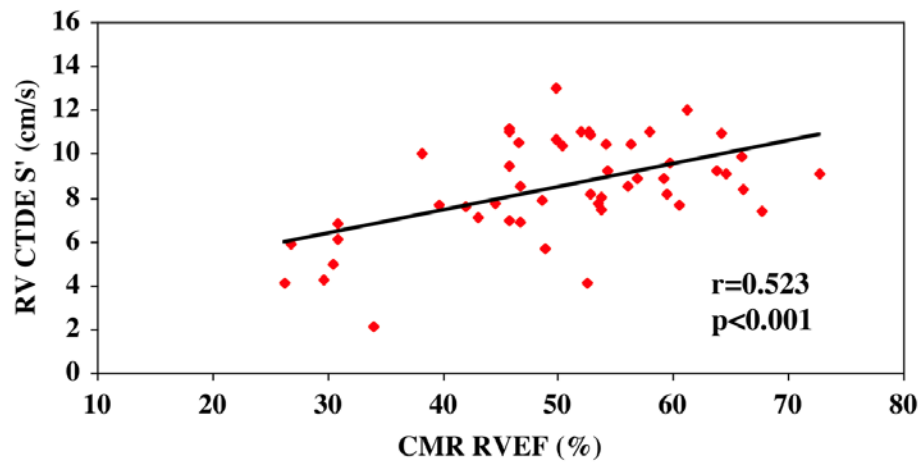


Figure 7.15. Correlation of RV CTDE S' with CMR-RVEF in 50 subjects (RVEF range: 26-73%). CMR, cardiac magnetic resonance imaging; RVEF, right ventricular ejection fraction; RV CTDE S', right ventricular colour tissue Doppler systolic velocity.

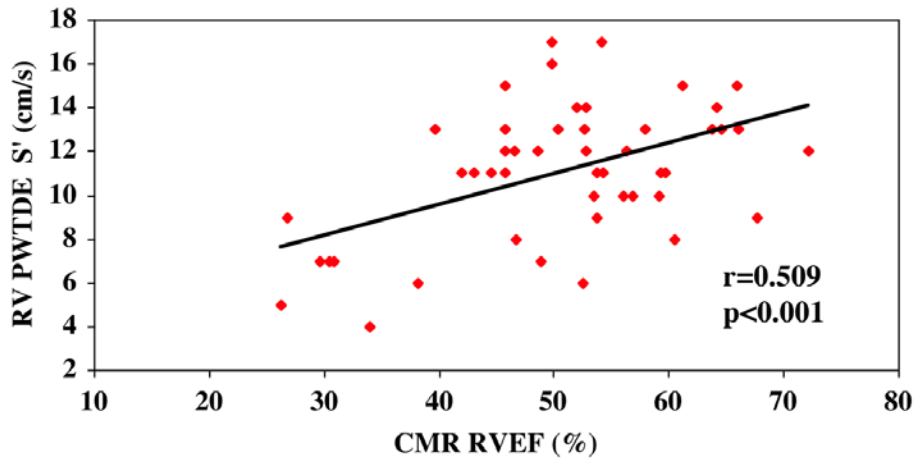


Figure 7.16. Correlation of RV PWTDE S' with CMR-RVEF in 50 subjects (RVEF range: 26-73%). CMR, cardiac magnetic resonance imaging; RVEF, right ventricular ejection fraction; RV PWTDE S', right ventricular pulsed-wave tissue Doppler systolic velocity.

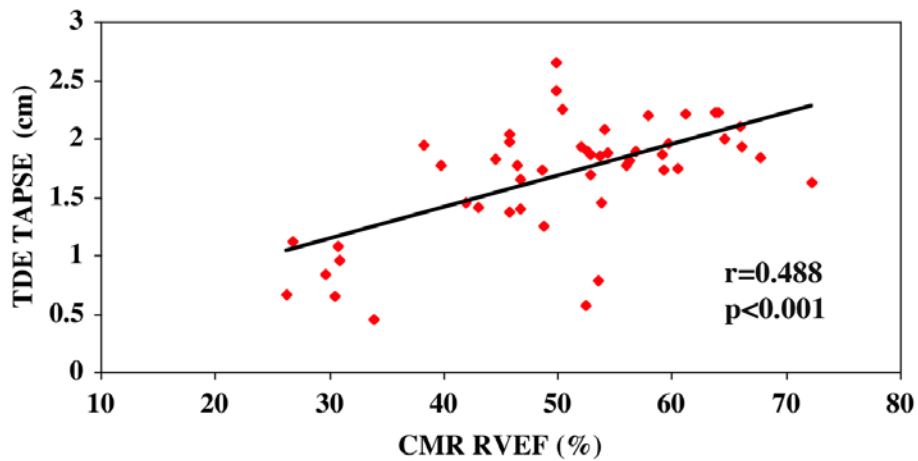


Figure 7.17. Correlation of TDE TAPSE with CMR-RVEF in 50 subjects (RVEF range: 26-73%). CMR, cardiac magnetic resonance imaging; RVEF, right ventricular ejection fraction; TDE TAPSE, tissue Doppler echocardiography-derived tricuspid annular plane systolic excursion.

RV TDE-MPI ($p=0.031$, $r=0.306$) had a weak correlation with CMR-RVEF (Figure 7.18).

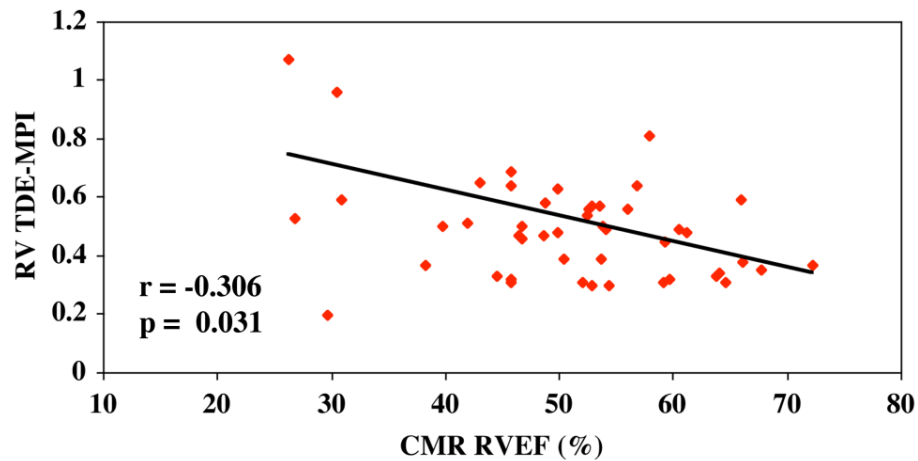


Figure 7.18. Correlation of RV TDE-MPI with CMR-RVEF in 50 subjects (RVEF range: 26-73%). CMR, cardiac magnetic resonance imaging; RVEF, right ventricular ejection fraction; RV MPI, right ventricular myocardial performance index.

RV MPI ($p=NS$, $r=-0.262$) and RV IVA ($p=NS$, $r=0.166$) had no correlation with CMR-RVEF (Figure 7.19 and 7.20) and were therefore excluded from further subgroup analysis.

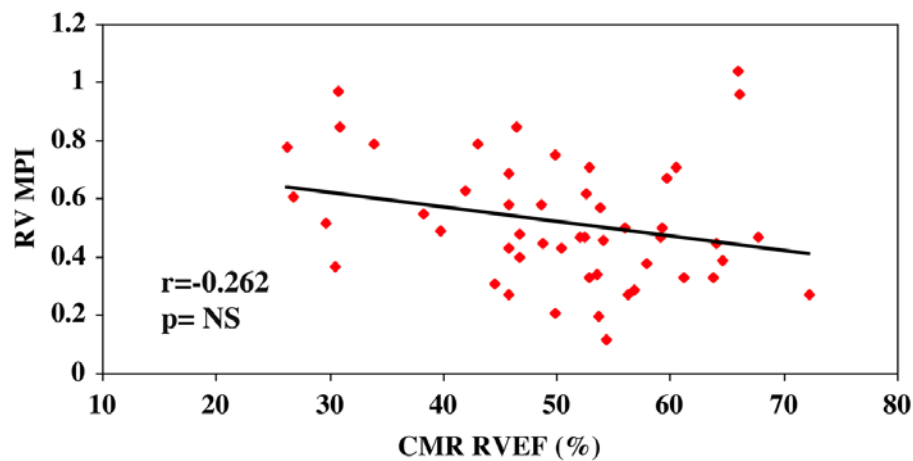


Figure 7.19. Correlation of RV MPI with CMR-RVEF in 50 subjects (RVEF range: 26-73%). CMR, cardiac magnetic resonance imaging; RVEF, right ventricular ejection fraction; RV MPI, right ventricular myocardial performance index.

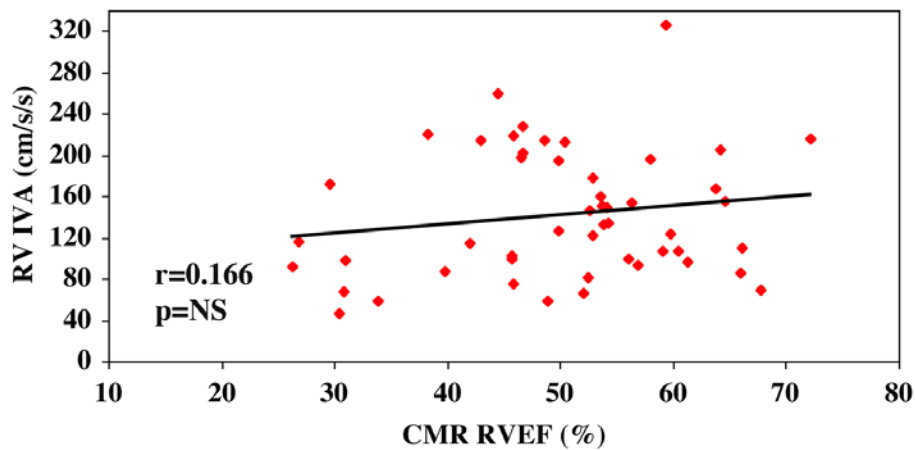


Figure 7.20. Correlation of RV IVA with CMR-RVEF in 50 subjects (RVEF range: 26-73%). CMR, cardiac magnetic resonance imaging; RVEF, right ventricular ejection fraction; RV IVA, right ventricular isovolumic acceleration.

7.4.3 Receiver operator characteristics

Eight echocardiographic indices of RV function (RVFWS, RVGS, RV FAC, M-Mode TAPSE, RV CTDE S', RV PWTDE S', TDE TAPSE and TDE-MPI) correlated with CMR-RVEF as detailed in section 7.4.2 above. ROC analysis was performed to examine the accuracy of these indices in correctly identifying patients with normal (RVEF \geq 47%) and abnormal (RVEF<47%) RV systolic function as determined by CMR.

For RV indices in which normative threshold values have already been published and endorsed in the ASE/EAE/CSE 2010 Guidelines for assessing the right heart in adults (ref), (i.e. FAC=35%, PWTDE S'=10cm/s, M-Mode TAPSE=16mm, TDE-MPI=0.55), the sensitivity and specificity of these normative threshold values were determined in our cohort of heterogenous patients. For the echo techniques used in which normative reference

values are as yet unclear (i.e. RVFWS, RVGS, CTDE S' and TDE-TAPSE), optimum normative cut-off values were determined from ROC analysis.

RV free wall strain

Of the eight RV echocardiographic indices RVFWS exhibited the largest area under the curve (AUC: 0.853). RVFWS \geq -22.50% predicted RVEF<47% with a sensitivity of 78.90% and a specificity of 80.6% (Figure 7.21).

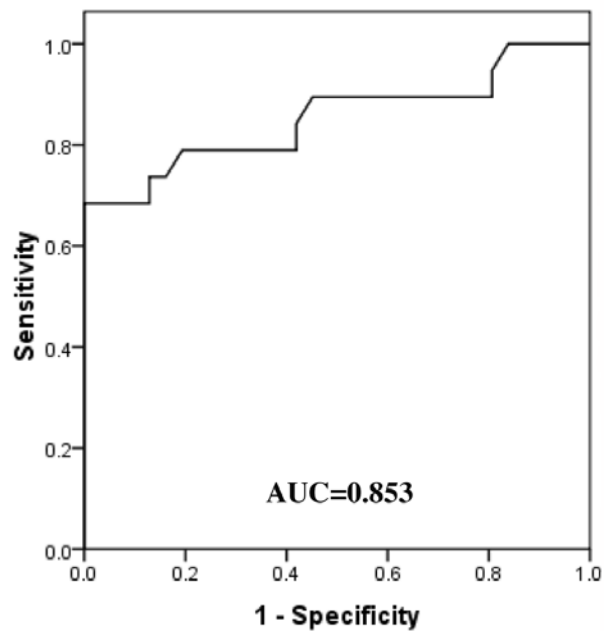


Figure 7.21. ROC curve of RVFWS indexed against CMR-RVEF.

A normal cut-off value of -22.50% identified RV systolic dysfunction with a sensitivity of 78.90% and a specificity of 80.6%. AUC, area under the curve; CMR, cardiac

magnetic resonance; RV, right ventricle; RVEF, right ventricular ejection fraction; RVfws, right ventricular free wall strain.

RV global strain

RVGS \geq -18.05% predicted RVEF < 47% with a sensitivity of 73.70% and a specificity of 93.5% (AUC: 0.822) (Figure 7.22).

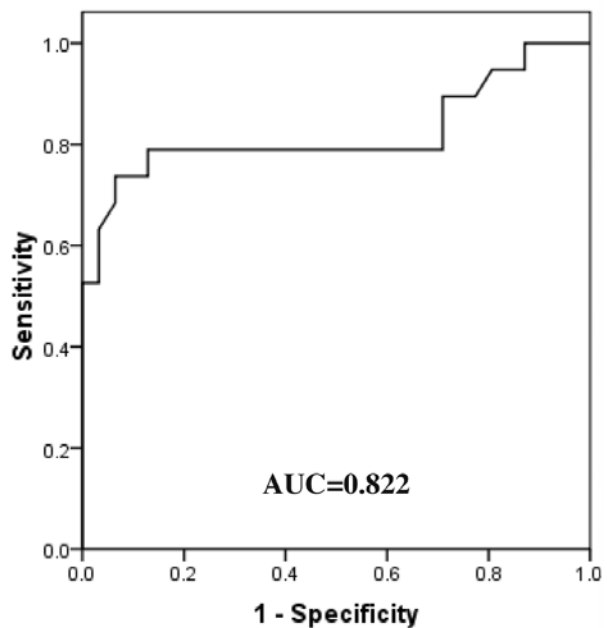


Figure 7.22. ROC curve of RVGS indexed against CMR-RVEF.

A normal cut-off value of -18.05% identified RV systolic dysfunction with a sensitivity of 73.70% and a specificity of 93.50% . AUC, area under the curve; CMR, cardiac magnetic resonance; RV, right ventricle; RVEF, right ventricular ejection fraction; RVGS, right ventricular global strain.

M-Mode TAPSE

The ASE guidelines for assessing RV function recommend the use of TAPSE (performed using the M-Mode method) and ASE, EAE and British Society of Echocardiography guidelines suggest a TAPSE score of $>16\text{mm}$ as indicative of normal RV systolic function based on radionuclide and other comparison studies.^{37,244,245,287} Using this cut-off value,

M-Mode TAPSE<1.6cm was highly specific at predicting RVEF<47% by CMR (specificity=93.50%) but with a low sensitivity of 36.80% (AUC: 0.791) (Figure 7.23).

An alternative threshold value of 18.5mm, improved sensitivity to 57.9%, but at the expense of specificity (specificity=83.9%).

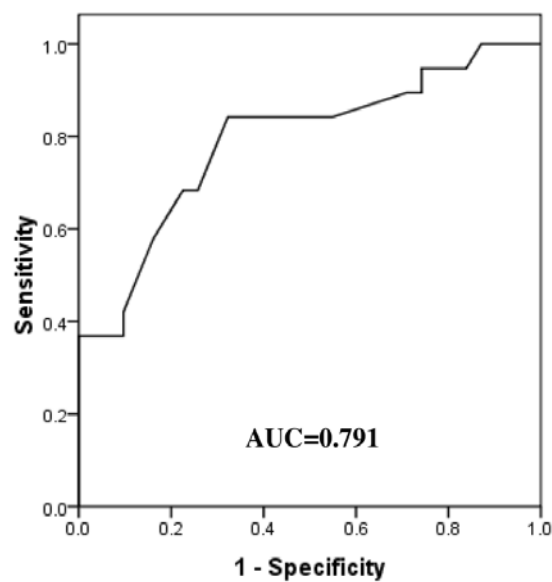


Figure 7.23. ROC curve of M-Mode TAPSE indexed against CMR-RVEF.

A normal cut-off value of 1.6cm identified RV systolic dysfunction with a sensitivity of 36.80% and a specificity of 93.50%. AUC, area under the curve; CMR, cardiac magnetic resonance; RV, right ventricle; RVEF, right ventricular ejection fraction; TAPSE, tricuspid annular plane systolic excursion.

Tissue Doppler TAPSE

TDE TAPSE<1.44cm predicted RVEF<47% with a sensitivity of 52.60% and a specificity of 90.30% (AUC: 0.730) (Figure 7.24).

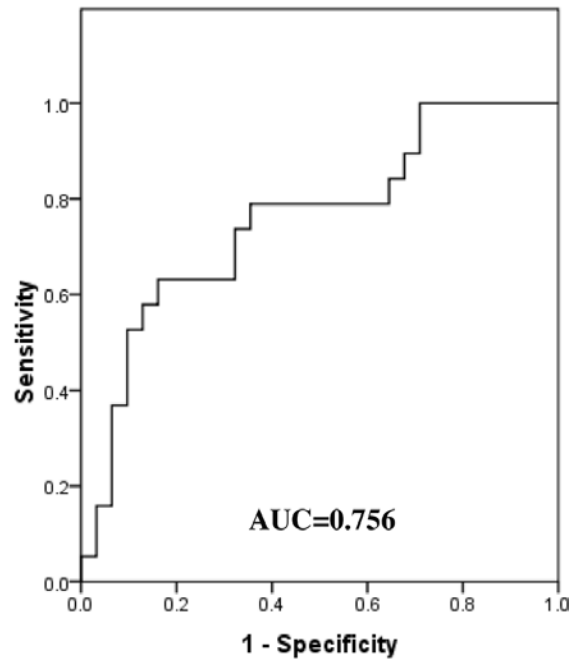


Figure 7.24. ROC curve of TDE TAPSE indexed against CMR-RVEF.

A normal cut-off value of 1.4cm identified RV systolic dysfunction with a sensitivity of 52.60% and a specificity of 90.30%. AUC, area under the curve; CMR, cardiac magnetic resonance; RV, right ventricle; RVEF, right ventricular ejection fraction; TDE TAPSE, tissue Doppler echocardiography-derived tricuspid annular plane systolic excursion.

Fractional area change

The ASE guidelines for assessing RV function recommend the use of RV FAC using a threshold value of 35% as the lower normative limit.³⁷ Using this cut-off value, RV FAC was highly specific at predicting RVEF<47% by CMR (specificity=93.50%) but with a low sensitivity of 47.4% (AUC: 0.734) (Figure 7.25).

An alternative threshold value of 44.5%, improved sensitivity to 78.9%, but at the expense of specificity (specificity=61.3%).

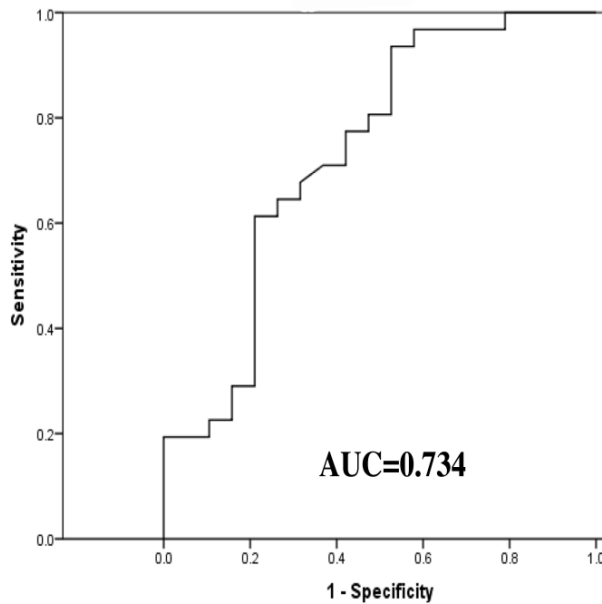


Figure 7.25. ROC curve of RV FAC indexed against CMR-RVEF.

A normal cut-off value of 35% identified RV systolic dysfunction with a sensitivity of 52.60% and a specificity of 90.30%. AUC, area under the curve; CMR, cardiac magnetic resonance; FAC, fractional area change RV, right ventricle; RVEF, right ventricular ejection fraction.

PWTDE S'

The ASE guidelines for assessing RV function in adults recommend the use of RV PWTDE S' and suggest a S' of 10cm/s as the lower reference limit of normal based on pooled data from 43 studies of over 2000 normal controls.^{37,291} Using this cut-off value, RV PWTDE

$S' < 10$ cm/s only had a moderate specificity of 77.50% and a low sensitivity of 52.60% for predicting $\text{CMR-RVEF} < 47\%$ (AUC: 0.734).

An alternative threshold value of $S' < 8.5$ cm/s improved specificity to 90.30%, but at the expense of sensitivity (sensitivity=47.40%) (Figure 7.26).

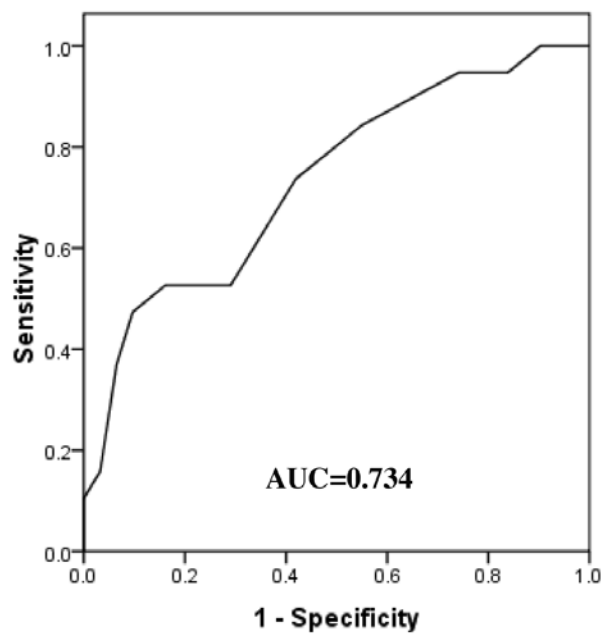


Figure 7.26. ROC curve of RV PWTDE S' indexed against CMR-RVEF.

A normal cut-off value of 8.5 cm/s identified RV systolic dysfunction with a sensitivity of 47.40% and a specificity of 90.30%. AUC, area under the curve; CMR, cardiac magnetic resonance; RV, right ventricle; RV PWTDE S' , right ventricular pulsed-wave tissue Doppler systolic velocity; RVEF, right ventricular ejection fraction.

CTDE S'

RV CTDE $S' < 7.7$ cm/s predicted $\text{RVEF} < 47\%$ with a sensitivity of 68.40% and a specificity of 83.90% (AUC: 0.730) (Figure 7.27).

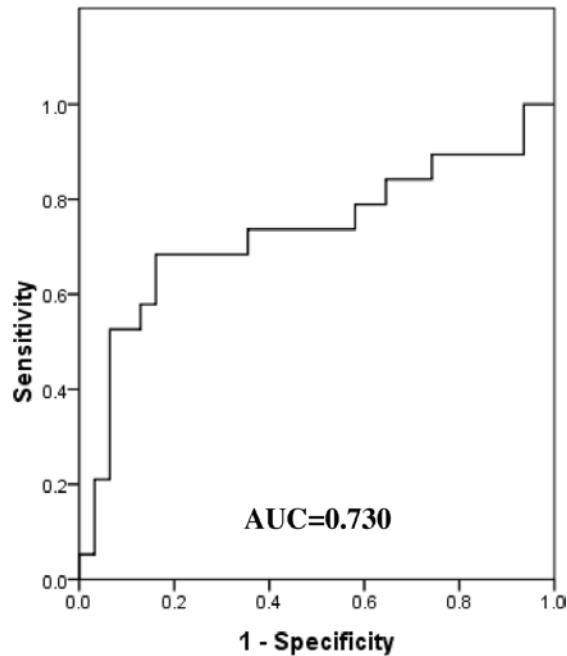


Figure 7.27. ROC curve of RV CTDE S' indexed against CMR-RVEF.

A normal cut-off value of 7.7cm/s identified RV systolic dysfunction with a sensitivity of 68.40% and a specificity of 83.90%. AUC, area under the curve; CMR, cardiac magnetic resonance; RV, right ventricle; RV CTDE S', right ventricular colour tissue Doppler systolic velocity; RVEF, right ventricular ejection fraction.

TDE MPI

The ASE guidelines for assessing RV function in adults endorse the use of RV TDE-MPI for estimating RV function in complement, but not in isolation, with other quantitative and non-quantitative indices of RV function. The ASE recommend an upper normative

reference limit of 0.55 for RV TDE-MPI.³⁷ Using this cut-off value, RV TDE-MPI >0.55 had a poor sensitivity and specificity of 57.9% and 33.3% respectively for predicting CMR-RVEF <47% (AUC: 0.621).

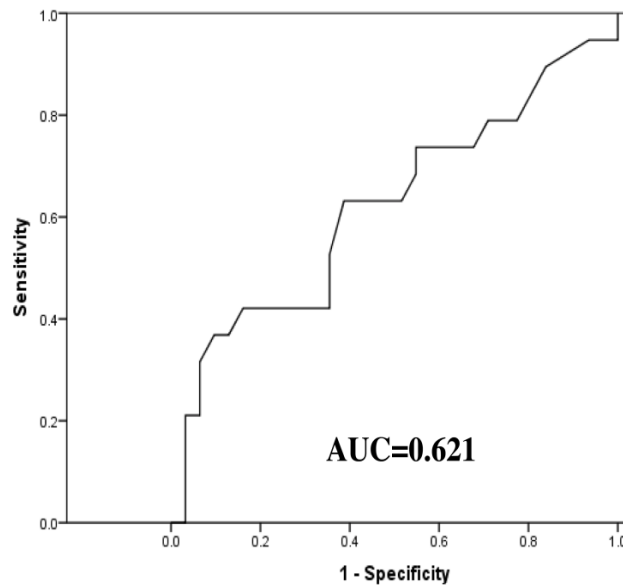


Figure 7.28. ROC curve of RV TDE-MPI indexed against CMR-RVEF.

A normal cut-off value of 0.55 identified RV systolic dysfunction with a sensitivity of 32.30% and a specificity of 57.90%. AUC, area under the curve; CMR, cardiac magnetic resonance; RV, right ventricle; RVEF, right ventricular ejection fraction; RV TDE-MPI, right ventricular tissue Doppler myocardial performance index.

7.4.4 Regression analysis of echo RV indices indexed against CMR-RVEF

On bivariate correlation, RV MPI and RV IVA failed to correlate with CMR-RVEF and were therefore excluded from regression analysis. On regression analysis, in patients exhibiting a wide range of RV function (RVEF range: 26-73%, n=50), RVFWS had a

significantly stronger correlation with CMR-RVEF than all other RV echocardiographic parameters for quantifying RV systolic function ($p=0.013$, $T=-2.61$). When RVFWS was excluded from the analysis, RVGS exhibited the strongest correlation to CMR-RVEF, when compared the remaining echocardiographic indices of RV function ($p<0.001$, $T=-3.99$). When both RVFWS and RVGS were excluded from the analysis, RV FAC exhibited the strongest correlation to CMR-RVEF when compared to the remaining echocardiographic RV parameters ($p=0.009$, $T=2.75$). Upon exclusion of RVFWS, RVGS and RV FAC, no remaining echocardiographic index of RV systolic function exhibited a superior correlation over all other remaining indices, when compared to CMR-RVEF as the reference standard.

7.4.5 Calculation of right ventricular ejection fraction

From linear regression analysis, the RVFWS can be converted into a RVEF equivalent score (RVEFES) using the regression equation below:

Equation 7.1 $RVEFES = -1.16(RVFWS) + 24.55$.

7.4.6 Comparison of the ten echocardiographic indices of RV systolic function with visual assessment of RV systolic function.

The echocardiograms of all 50 patients were visually assessed and RV systolic function was categorized as normal, mild, moderately or severely impaired. Due to the small numbers of patients in this study, patients with moderately and severely impaired RV function were combined into one category. The mean values for patients with normal, mild and moderately-severely impaired RV function were recorded for each echocardiographic index. The mean difference between each functional subgroup was compared with the adjacent subgroup to examine the power of each echocardiographic index of RV function to discriminate between different categories of RV function/dysfunction. Results are shown in Table 7.2.

Quantitative Index of	Normal	Mild	Moderate-severe
-----------------------	--------	------	-----------------

RV systolic function	RV function	RV dysfunction	RV dysfunction
CMR-RVEF (%)	55.82±7.30	45.65±2.20 ^ϵ	30.86±3.82 ^ϵ
RVFWS (-%)	-25.56±4.41	-20.04±6.20 ^ϕ	-9.67±4.11 ^ϕ
RVGS (-%)	-21.81±3.38	-18.91±4.77*	-10.58±2.63 ^ϕ
RV FAC (%)	47.87±10.14	37.79±9.28 ^ϕ	25.72±9.08*
RV CTDE S' (cm/s)	9.28±1.71	8.04±1.87 ^{NS}	5.55±2.31*
RV PWTDE S' (cm/s)	12.21±2.47	10.13±2.17*	6.50±1.51 ^ϕ
M-Mode TAPSE (cm)	2.33±0.48	1.91±0.28 ^ϕ	1.25±0.65*
TDE TAPSE (cm)	1.88±0.39	1.55±0.26 ^ϕ	0.97±0.46 ^ϕ
RV MPI	0.46±0.20	0.61±0.16 ^{NS}	0.68±0.20 ^{NS}
RV TDE-MPI	0.48±0.21	0.50±0.11 ^{NS}	0.89±0.42*
RV IVA (cm/s ²)	145.31±57.78	163.76±69.36 ^{NS}	109.15±59.74 ^{NS}

Table 7.2. Comparison of CMR-RVEF and ten echocardiographic indices of RV function with visual assessment of RV systolic function. Each category of RV dysfunction is compared to the category above (i.e. Mild RV dysfunction is compared to normal RV function; moderate-severe RV dysfunction is compared to mild RV dysfunction). **NS = not significant; * = p<0.05; ϕ = p<0.01; ϵ = p<0.001**

CMR, RVFWS, RVGS, RV PWTDE S', M-Mode TAPSE and TDE TAPSE were able to discriminate both visually mild RV dysfunction from visually normal RV function, and visually moderate-severe RV dysfunction from visually mild RV dysfunction. RV CTDE S' discriminated visually moderate-severe RV dysfunction from mild RV dysfunction, but

not mild RV impairment from visually normal RV function. The difference between means between the normal and mildly impaired RV categories and between the mildly impaired and moderately-severely impaired categories were not significant for either RV MPI or RV IVA.

7.4.7. Acquisition and analysis times

The acquisition and analysis times for each index of RV function are shown in Table 7.3.

Quantitative Index of RV systolic function	Additional Acquisition time	Analysis Time

RVFWS (-%)	15 sec min	2 min
RVGS (-%)	15 sec min	1 min 30 sec
RV FAC (%)	15 sec	1 min 30 sec
RV CTDE S' (cm/s)	35 sec	1min 25 sec
RV PWTDE S' (cm/s)	15 sec	15 sec
M-Mode TAPSE (cm)	15 sec	15 sec
TDE TAPSE (cm)	35 sec	1min 6 sec
RV MPI	30 sec	51 sec
RV TDE-MPI	15 sec	45 sec
RV IVA (cm/s ²)	35 sec	2 min

Table 7.3. The additional acquisition and analysis time for each index of RV function, performed during acquisition of a full standard transthoracic echocardiogram study. Min, minute; sec, second

7.4.8. Reproducibility

Intra- and inter-observer variability for CMR-RVEF and all ten echocardiographic indices of RV function are expressed as the co-efficient of variation, and as the mean bias, limits of

agreement and standard deviation of the difference (Table 7.4 and 7.5). The corresponding Bland-Altman plots are shown in Figures 7.29 to 7.39.

Imaging modality used to quantify RV function	% Co-efficient of variation	Mean bias	Limits of agreement	SDD
CMR PARAMETER				
RVEF (%)	5.90%	0.19	-8.70 to 9.07	4.44
ECHO PARAMETERS				
2DE :				
1) RV FAC (%)	13.13%	-3.15	-17.09 to 10.79	6.97
2) RV MPI	8.38%	-0.02	-0.15 to 0.11	0.06
3) M-Mode TAPSE (cm)	4.22%	-0.00	-0.17 to 0.17	0.09
TDE:				
4) RV PWTDE S' (cm/s)	2.23%	-0.32	-1.35 to 0.72	0.52
5) RV CTDE S' (cm/s)	2.40%	-0.08	-0.86 to 0.71	0.39
6) RV IVA (cm/s ²)	13.96%	12.50	-72.71 to 97.71	42.61
7) TDE MPI	9.63%	0.05	-0.11 to 0.21	0.08
8) TDE TAPSE (cm)	1.32%	-0.07	-0.86 to 0.72	0.39
9) RVGS (-%)	-2.31%	-0.09	-2.18 to 2.00	1.05
10) RVFWS (-%)	-3.89%	0.12	-3.77 to 4.00	1.94

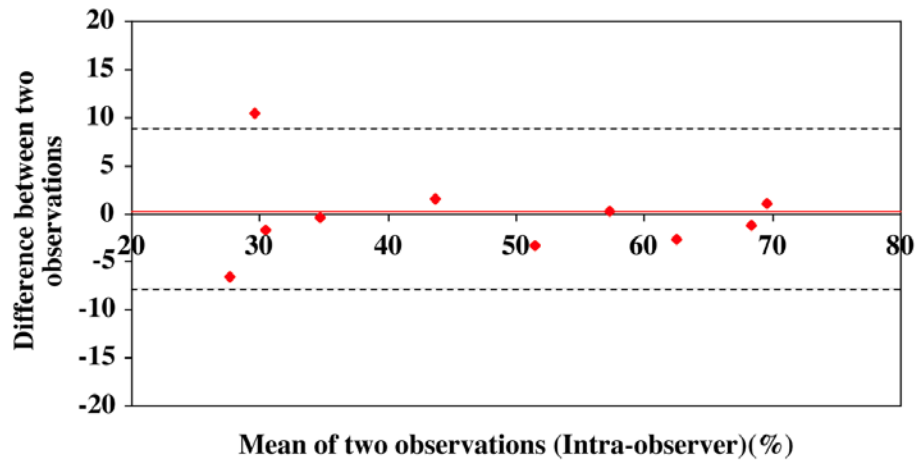
Table 7.4. Intra-observer variability for measurements of right ventricular systolic function

Imaging modality used to quantify RV function	% Co-efficient of variation	Mean bias	Limits of agreement	SDD
CMR PARAMETER				

RVEF (%)	8.44%	1.78	-11.35 to 13.71	6.27
ECHO PARAMETERS				
2DE :				
1) RV FAC (%)	17.42%	-1.33	-20.69 to 18.03	9.68
2) RV MPI	18.95%	0.11	-0.32 to 0.54	0.21
3) M-Mode TAPSE (cm)	7.91%	0.03	-0.32 to 0.38	0.18
TDE:				
4) RV PWTDE S' (cm/s)	1.29%	-0.14	-0.99 to 0.70	0.42
5) RV CTDE S' (cm/s)	2.69%	0.09	-0.69 to 0.88	0.39
6) RV IVA (cm/s ²)	18.52%	8.05	-94.37 to 110.48	51.21
7) TDE MPI	18.98%	-0.14	-0.54 to 0.26	-0.20
8) TDE TAPSE (cm)	4.12%	0.30	-1.62 to 2.23	0.96
9) RVGS (-%)	-3.12%	0.40	-1.65 to 2.46	1.03
10) RVFWS (-%)	-3.03%	0.43	-2.36 to 3.22	1.40

Table 7.5. Inter-observer variability for measurements of right ventricular systolic function.

(A)



(B)

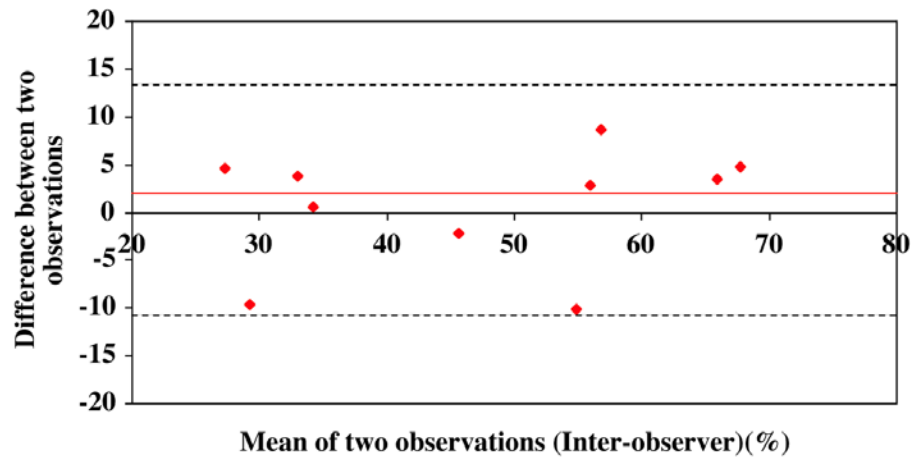
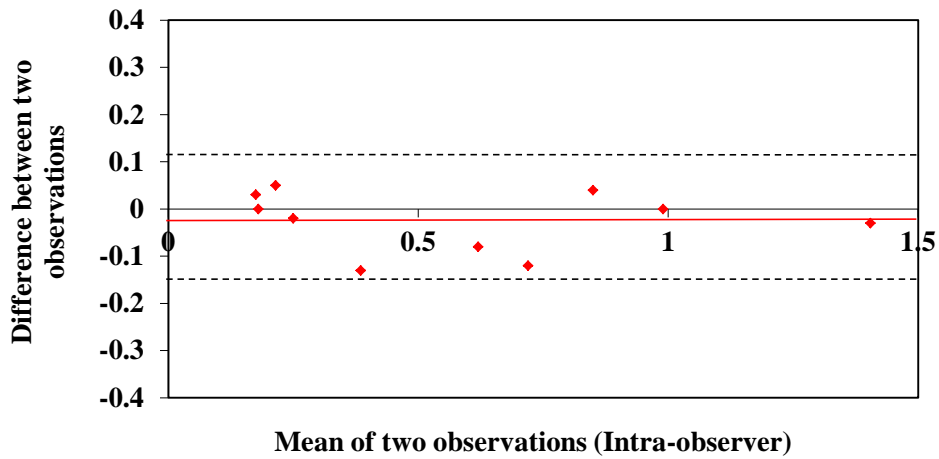


Figure 7.29. Bland-Altman Plot of (A) intra-observer variation and (B) inter-observer variation for measuring RV systolic function using cardiac magnetic resonance imaging (RVEF %)

(A)



(B)

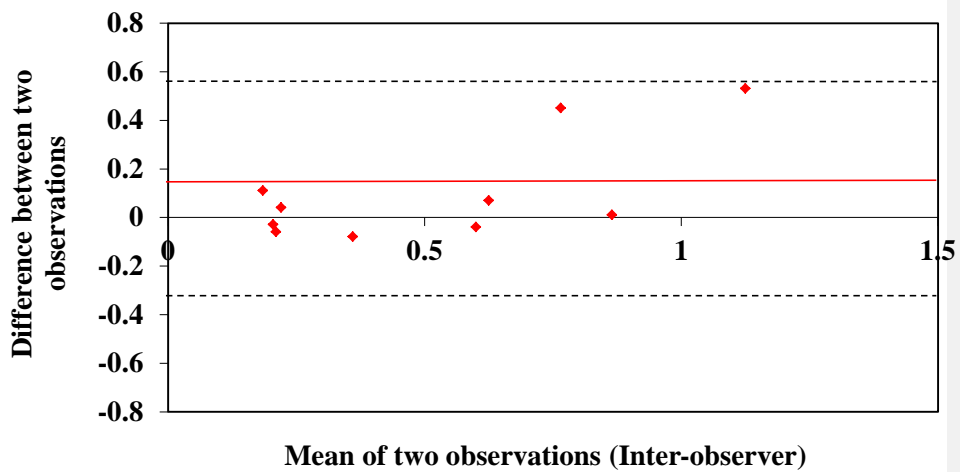
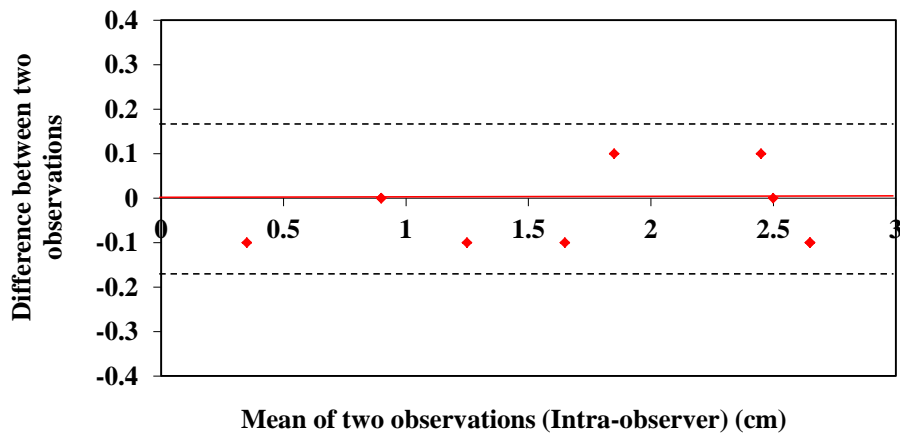


Figure 7.30. Bland-Altman Plot of (A) intra-observer variation and (B) inter-observer variation for measuring RV systolic function using RV myocardial performance index derived by spectral Doppler (MPI)

(A)



(B)

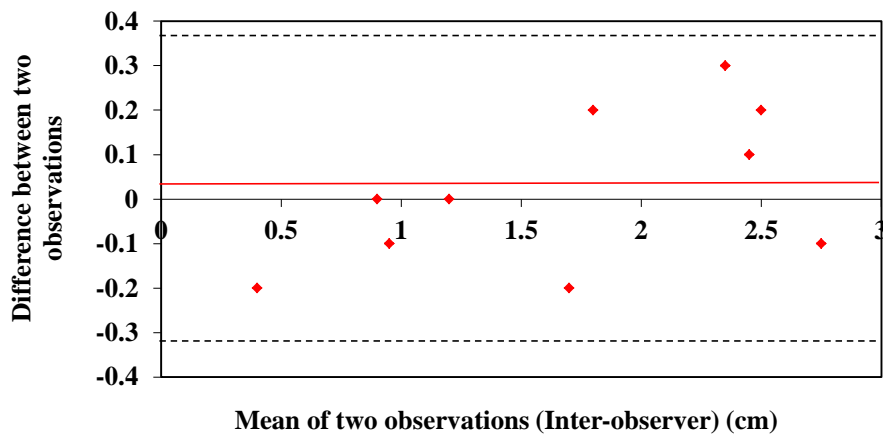
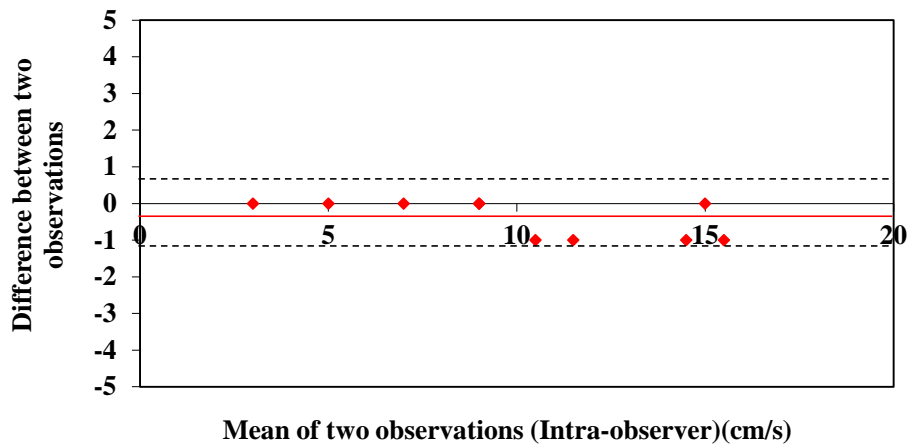


Figure 7.31. Bland-Altman Plot of (A) intra-observer variation and (B) inter-observer variation for measuring RV systolic function using colour M-Mode tricuspid annular plane systolic excursion (MM TAPSE) (cm)

(A)



(B)

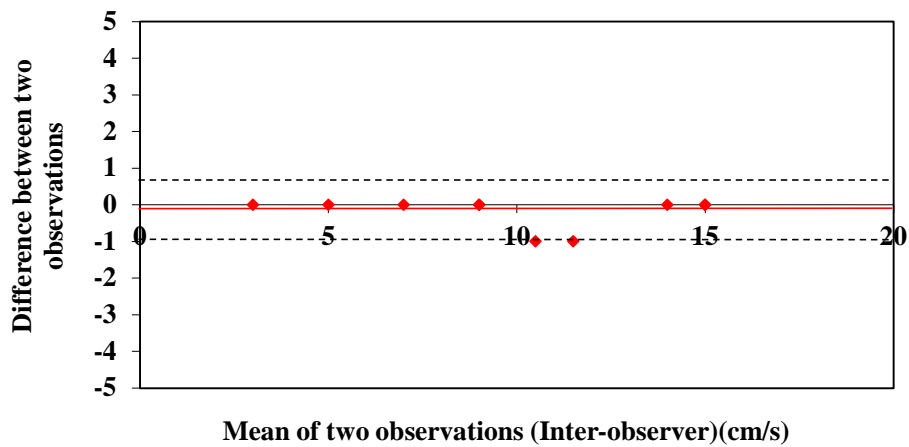
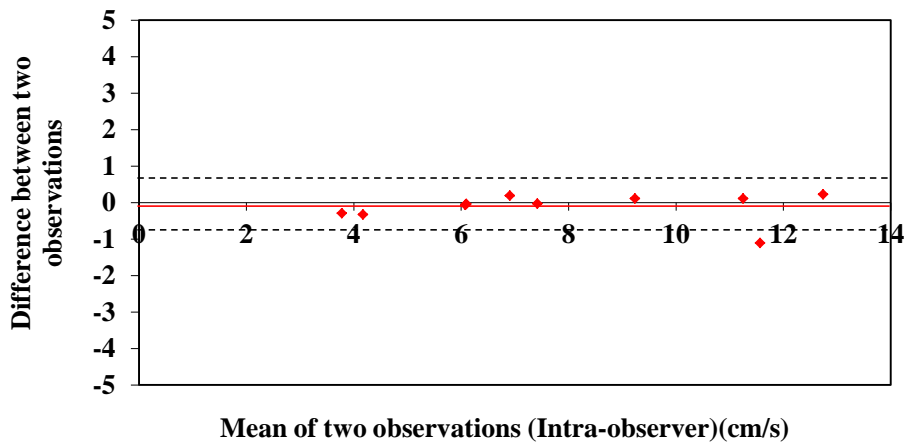


Figure 7.32. Bland-Altman Plot of (A) intra-observer variation and (B) inter-observer variation for measuring RV systolic function using tricuspid annular peak systolic velocity measured using pulsed wave tissue Doppler (PWTDE S') (cm/s)

(A)



(B)

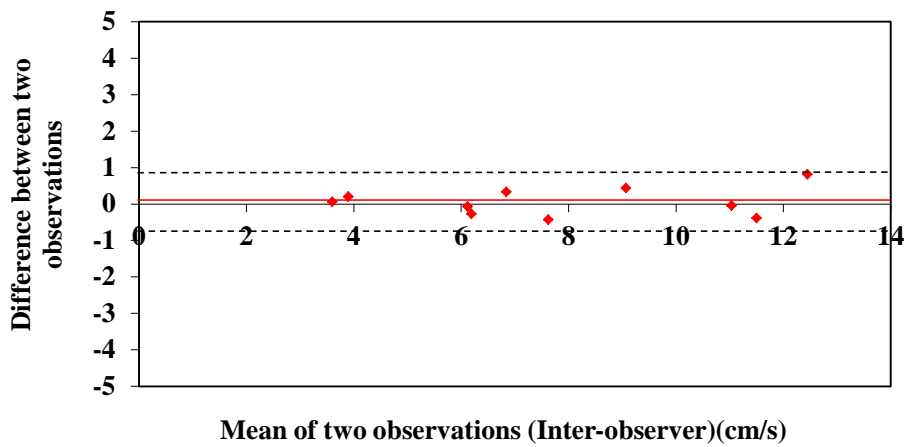
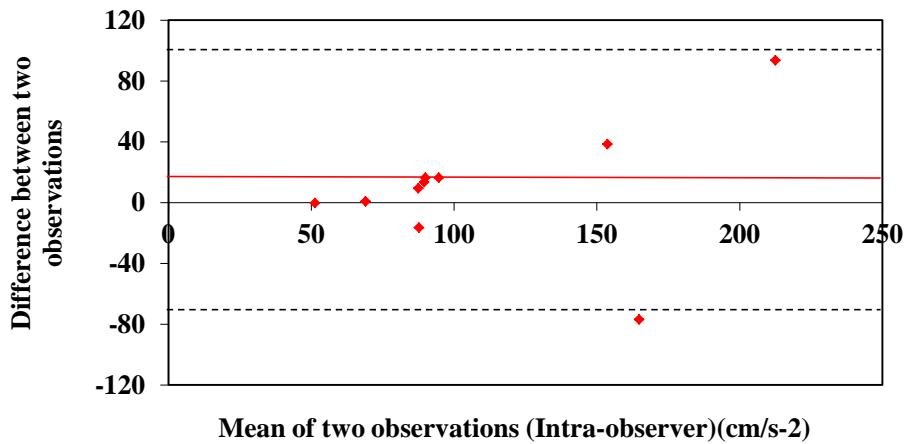


Figure 7.33. Bland-Altman Plot of (A) intra-observer variation and (B) inter-observer variation for measuring RV systolic function using tricuspid annular peak systolic velocity measured using colour tissue Doppler (CTDE S') (cm/s)

(A)



(B)

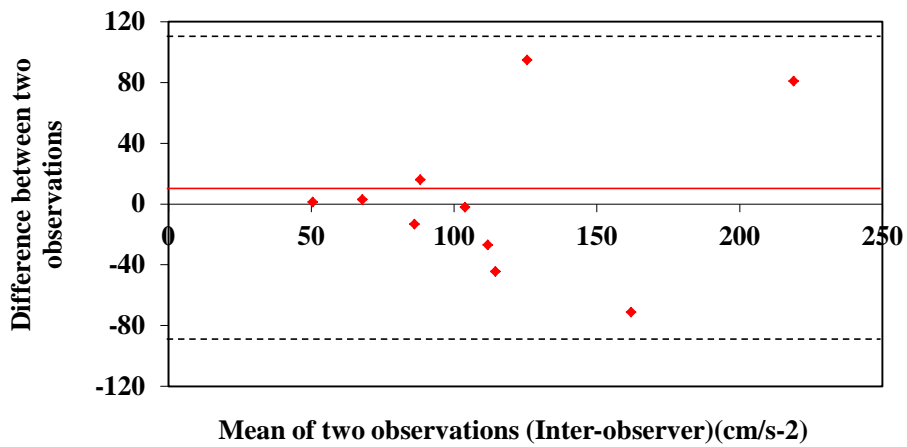
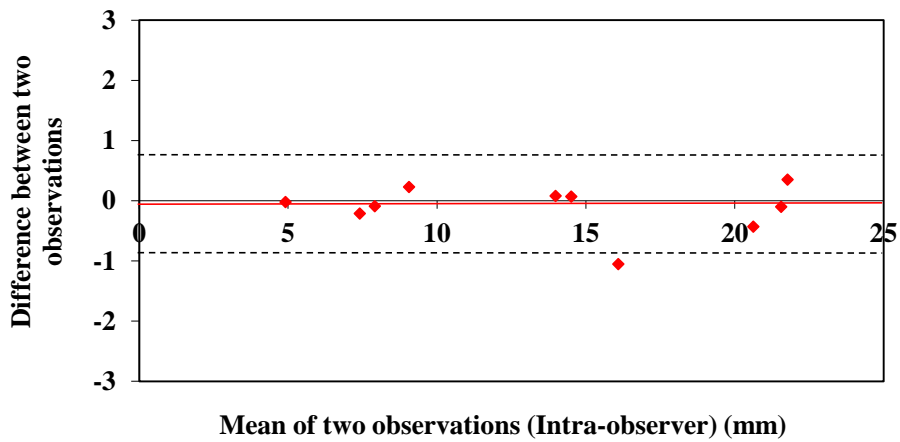


Figure 7.34. Bland-Altman Plot of (A) intra-observer variation and (B) inter-observer variation for measuring RV systolic function using isovolumic acceleration (IVA) (cm/s²)

(A)



(B)

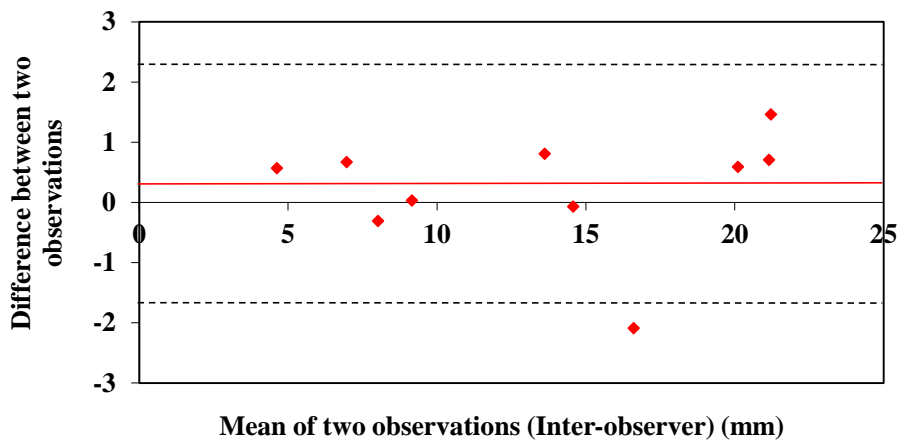
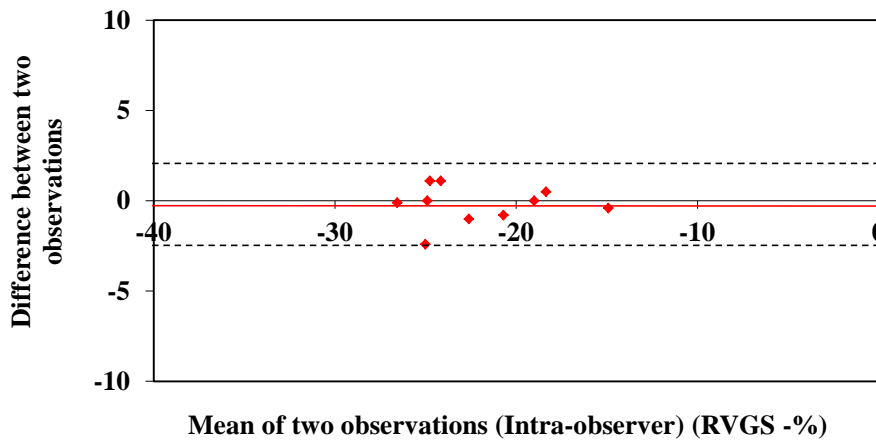


Figure 7.35. Bland-Altman Plot of (A) intra-observer variation and (B) inter-observer variation for measuring RV systolic function using tricuspid annular peak systolic displacement measured using colour tissue Doppler (TDE TAPSE) (mm)

(A)



(B)

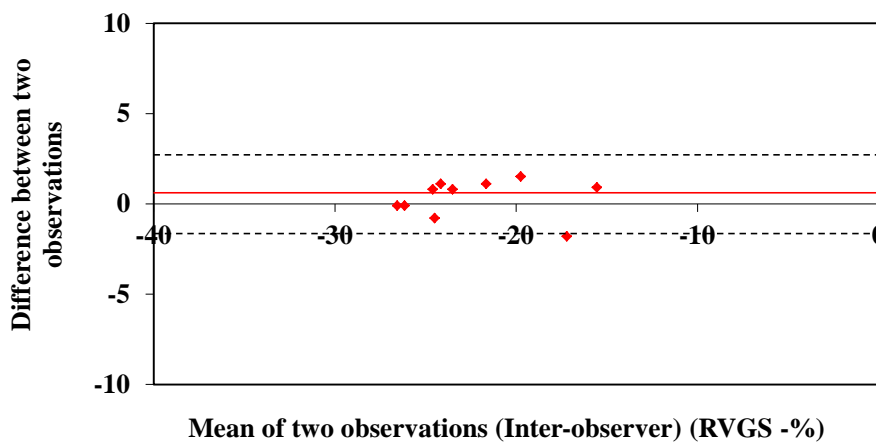
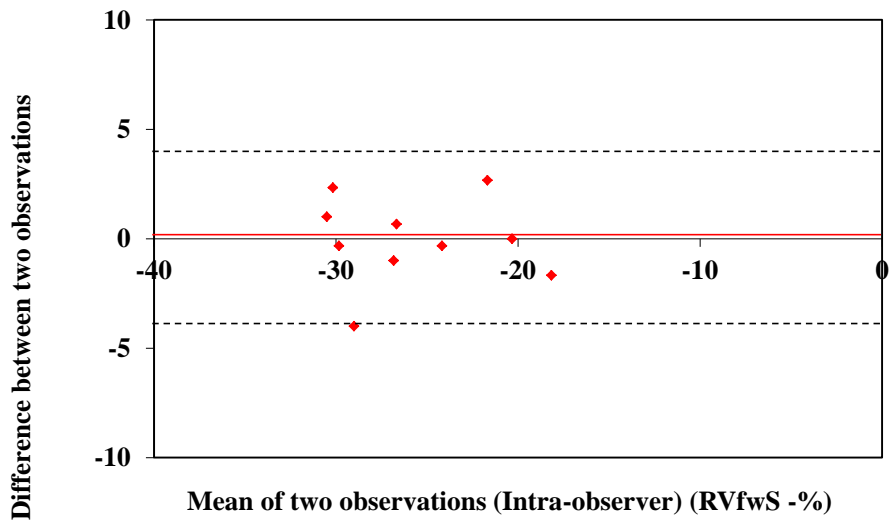


Figure 7.36. Bland-Altman Plot of (A) intra-observer variation and (B) inter-observer variation for measuring RV systolic function using RV Global strain score (RVGS) (-%)

(A)



(B)

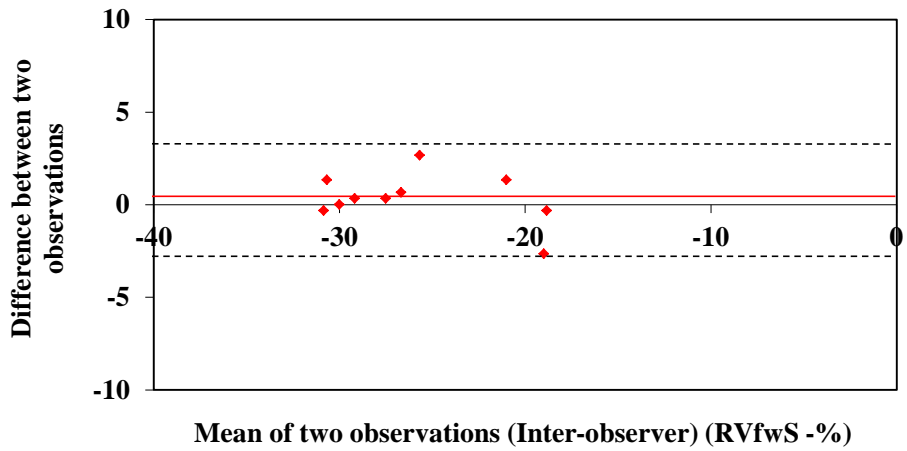
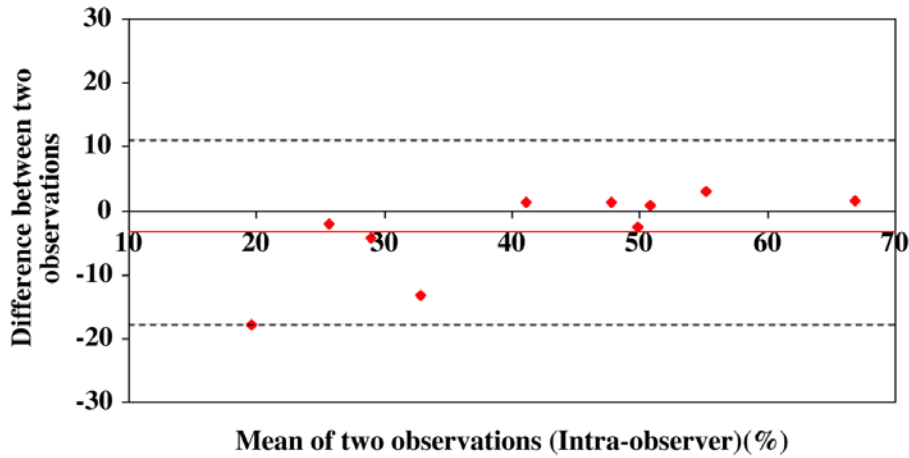


Figure 7.37. Bland-Altman Plot of (A) intra-observer variation and (B) inter-observer variation for measuring RV systolic function using RV free wall strain score (RVFWS) (-%)

(A)



(B)

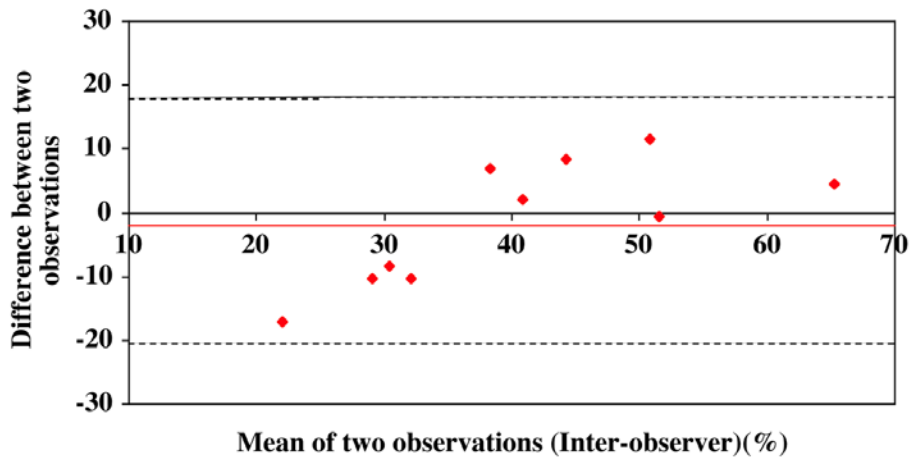
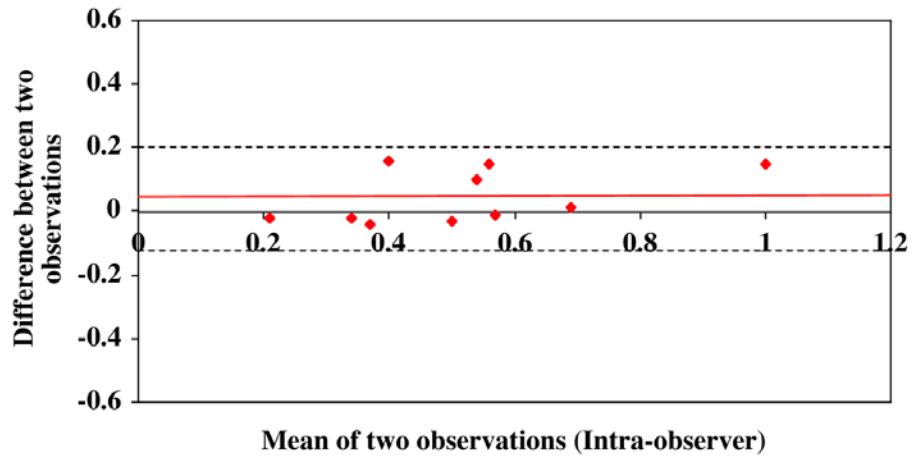


Figure 7.38. Bland-Altman Plot of (A) intra-observer variation and (B) inter-observer variation for measuring RV systolic function using RV fractional area change (RVFAC) (%)

(A)



(B)

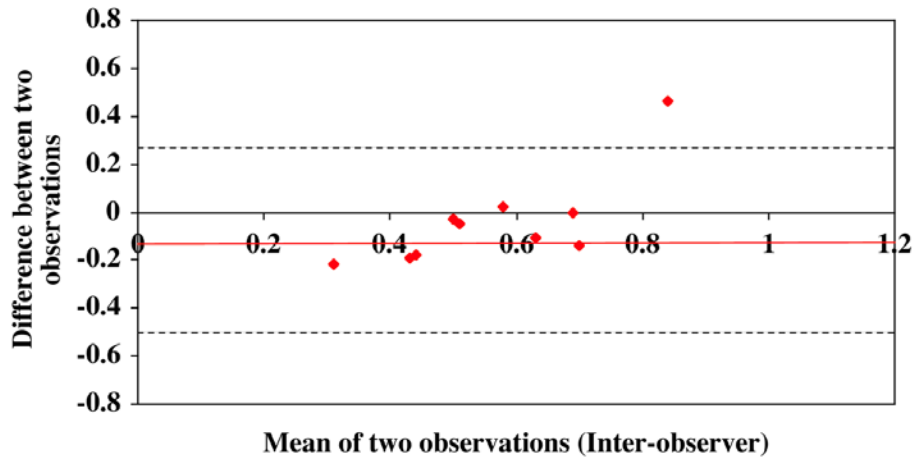


Figure 7.39. Bland-Altman Plot of (A) intra-observer variation and (B) inter-observer variation for measuring RV systolic function using RV myocardial performance index derived by tissue Doppler (TDE MPI)

7.5 DISCUSSION

This study has compared ten easily performed 2DE measures of RV function against each other in an unselected population when indexed against CMR as the reference standard. Our study demonstrates that RVFWS, assessed using 2D speckle tracking, has a stronger correlation with CMR-RVEF than all other indices of RV function and is highly reproducible. Due to the semi-automated nature of the speckle tracking software, data analysis times were short (<3minutes), ensuring this technique has a highly clinical application. On ROC analysis, RVFWS had both a high sensitivity and specificity for detecting abnormal RV systolic function, with a normative cut-off value of -22.5% . Furthermore, RVFWS can be converted into a more user-friendly RVEF equivalent score using the regression equation: $RVEFES = -1.16(RVFWS) + 24.55$.

We assessed both RVFWS and RVGS to establish the effect including the interventricular septum had on subsequent RV analysis. This study clearly demonstrated that assessing the average longitudinal strain value from the RV free wall had a stronger relationship to RVEF than a combined assessment of RV free wall and interventricular septum. Therefore when speckle tracking strain imaging is available, strain imaging of the RV free wall should be performed. RV FAC had a poorer correlation with CMR-RVEF when compared to speckle tracking strain imaging techniques, but a stronger correlation with CMR-RVEF than the remaining echocardiographic indices of RV function. The robustness of this technique however is limited by its moderate reproducibility. Using the normative cut-off value of $\leq 1.6\text{cm}$ recommended by the ASE/EAE/CSE guidelines, TAPSE had a high specificity, but moderately-low sensitivity for correctly identifying RV systolic dysfunction. M-Mode TAPSE had a moderately good correlation with CMR-RVEF and had acceptable reproducibility. RV CTDE S', RV PWTDE S' and TDE TAPSE were all highly reproducible techniques, but had only moderate correlation with CMR-RVEF. RV IVA and RV MPI did not correlate with RVEF. This result may not be as surprising as it first seems. RVEF is a volumetric assessment of RV systolic function. The RV relies heavily on longitudinal contraction during systole to maintain ejection fraction, so measures of RV longitudinal strain (RVfWS and RVGS) and measures of tricuspid annular motion (M-Mode TAPSE, TDE TAPSE, RV CTDE S', RV PWTDE S') should correlate with RVEF. IVA is a non-invasive measure of myocardial contractility, and RV MPI is an index of global RV performance, combining systolic and diastolic functional components.

Although both are still indices of RV performance, they do measure different physiological events compared to RVEF. However the high intra- and inter-observer variability of these two techniques limit their clinical application in an unselected population. Furthermore, when compared to visual assessment of RV systolic function, RV MPI and RV IVA were unable to discriminate between different categories of RV dysfunction. For these reasons, the result of this study does not support the use of RV MPI or RV IVA in routine clinical practice.

The accurate evaluation of RV function by 2D-ultrasonography is difficult given its complex geometry, interrelationship with the left ventricle, anatomical location within the thorax and sensitivity to changes in pulmonary pressures. While volumetric calculation of ejection fraction has for many years been the ubiquitous measure of left ventricular systolic performance, 2DE estimation of RVEF is unreliable due to the heterogeneity of methods, numerous geometric assumptions and technical limitations of the echocardiographic imaging windows. Due to its superior spatial resolution and unlimited ability to image the heart in any plane, CMR has become largely accepted as the reference standard for assessing the right heart. However, there remain major limitations to its widespread use due to initial cost and inability of some individuals to enter an enclosed space. RVEF quantification by 3DE has recently been made possible due to advances in 3DE software. However the limited normative data available is from small single centre studies, and suggests intermodality discordance between the techniques with 3DE underestimating RV volumes when compared to CMR. This discordance is believed due to imprecise endocardial wall definition by 3DE secondary to the poor visualisation of anterior RV wall segments by 3DE, the abundant RV trabeculae and variations in the demarcation of the basal RV and RVOT boundaries.²⁴⁰ For these reasons the joint ASE/EAE/CSE guidelines do not yet endorse the use of 3DE RVEF in routine clinical practice until more validation studies are available.

Recent international guidelines have reviewed the 2DE and TDE indices available for the quantitative assessment of RV systolic function.³⁷ While the guidelines recommend the use of several quantitative indices of RV function in addition to qualitative RV assessment, they draw no conclusions as to which method is preferred above the others. We have sought to compare all of these indices of RV function in an unselected population of patients

exhibiting a wide range of RVEFs. We are not the first study to do so. Miller and colleagues have previously compared RV MPI, RV PWTDE S' and M-Mode TAPSE and concluded that all three techniques were comparable based on a similar areas under the curve on ROC analysis. Unfortunately, these RV parameters were indexed against 2DE biplane Simpson's RVEF as the reference standard. This is a technique the American Society of Echocardiography, European Association of Echocardiography, Canadian Society of Echocardiography and British Society of Echocardiography do not recommend due to multiple geometric assumptions and inherent inaccuracy.³⁷ Furthermore, in this study a Simpson's RVEF<50% was considered abnormal, whereas the joint ASE/EAE/CSE guidelines state the lower normative reference limit for RVEF from pooled studies is actually 44% with a 95% confidence interval of 38% to 50%.³⁷ To our knowledge, our study is the first to directly compare ten different quantitative 2DE indices of RV function indexed against RVEF calculated by CMR, the internationally accepted reference standard. Current ASE/EAE/CSE guidelines review the use of 2D speckle tracking strain for quantifying RV function, but make no recommendations for routine clinical use due to the paucity of research data and lack of normative values. The results of our study suggest RVFWS is highly specific and sensitive at detecting RV dysfunction with a lower normative reference value of -22.5%. We have demonstrated that RVFWS is a technique that is accurate, reproducible and quick to perform, and therefore has the potential to be a routine clinical tool of the future for the quantifying RV systolic function.

7.5.1 Study limitations

[In this study we assessed both intra- and inter-observer variation in data analysis for each of the 10 described echo indices of RV systolic function, based on pre-acquired echocardiographic data. Due to time constraints, limitations in both imaging sessions and patient availability, we were unable to repeat scans using an independent operator. We were therefore unable to assess inter-observer variation in data acquisition \(the 'repeatability' of the methods\) and we accept this as a significant limitation of our study.](#)

In this study we assessed RVFWS and RVGS using GE Vivid 7 AFI speckle tracking strain software. We cannot comment on the accuracy of 2D strain for quantifying RV systolic function using software from other manufacturers. From the results of our study, we

derived a regression equation to enable us to convert RVFWS into a more user-friendly and recognisable RVEFES. Validation of this formula is required in an independent cohort of patients before this regression equation should be considered for clinical use.

7.5.2 Conclusion

In patients exhibiting a wide range of RVEFs, RVFWS is a highly reproducible measure of RV systolic function that had a stronger correlation to CMR-derived RVEF, when compared to nine alternative echocardiographic indices of RV function. Using a normative cut-off value of -22.5% , RVFWS detects RV systolic dysfunction with a high sensitivity and specificity.

Formatted: Font: 24 pt

CHAPTER 8

Formatted: Font: 24 pt

GENERAL DISCUSSION, CONCLUSIONS AND

FUTURE WORK

CHAPTER 8: DISCUSSION, CONCLUSIONS, FUTURE WORK

Formatted: Font: Times, 12 pt, Not Bold

Formatted: Line spacing: single

8.1 GENERAL DISCUSSION

Quantification of cardiac ventricular function is the most common request in cardiac imaging and one of the most fundamental assessments in the cardiac patient. However, the accurate assessment of cardiac ventricular function is far from simple and remains a constant challenge for the non-invasive cardiac imaging specialist. Cardiac contraction/relaxation during each cardiac cycle is a complex multi-stage multi-planar and

multi-directional pressure-dependent active process which involves myofilament coupling, long-axis shortening, radial thickening and circumferential torsion and twist during systole and myofilament uncoupling, myocardial relaxation and ventricular compliance, circumferential “untwisting”, pressure-gradient induced ventricular suction and LV filling and atrial contraction during diastole. Conventionally, the assessment of cardiac ventricular function is sub-classified into right and left, systolic and diastolic, regional and global function. Within each of these sub-classifications, the quantification of ventricular function may vary depending on both the imaging mode and imaging method used, and in some cases, may also vary depending on the experience of the operator. To minimise error, improve accuracy and reliability, the governing bodies within the specialties of echocardiography and cardiac magnetic resonance imaging have set international guidelines and standards for the quantification of left ventricular systolic,^{38,237} left ventricular diastolic¹⁴ and right ventricular function.^{37,237}

The advance in non-invasive cardiac imaging technology over the past few years has been phenomenal. In a symbiotic relationship, the advance in non-invasive cardiac imaging technology has greatly improved our understanding of ventricular function, which in turn has enabled the development and refinement of further imaging software programmes. A classic example being the development of speckle-tracking myocardial deformation imaging. As we become increasingly able to image the heart with high spatial and temporal resolution, we will likely reach a point whereby new imaging methods supersede the accuracy and reproducibility of current gold standard methods for quantifying ventricular function. Historically, this has already occurred on several occasions. The recording of haemodynamic and functional data during left heart catheterisation and left ventriculogram, was once the gold standard for assessing LV systolic function. This was superseded by the development of echocardiography, which in turn has been superseded by CMR quantification of LVEF. In clinical practice however, the cost, availability and safety profile of a “gold standard” investigation will be the determining factor in whether or not a patient receives this test, or a cheaper, more widely available and safer alternative.

The primary research aims of this thesis were therefore both clinical and pragmatic. The primary aims of this thesis were specifically directed at validating new non-invasive imaging methods for quantifying global left ventricular systolic function, left ventricular

diastolic function and right ventricular systolic function against internationally accepted reference standards in a heterogenous population of patients, as seen in clinical practice. Furthermore in all sub-classifications of ventricular function studied, in addition to being validated against the current imaging reference standard, our new imaging methods were also compared to the most widely used alternative methods for assessing LV systolic, LV diastolic and RV systolic function in clinical practice. A further aim of this thesis was to therefore establish if our new methods were superior to current methods used in clinical practice, when compared to the imaging reference standard. For example, CMR-derived LVEF is the widely accepted reference standard for quantifying left ventricular systolic function, with 3D echocardiography emerging as a close second. However, due to cost and limited availability of CMR and 3DE, 2DE Simpson's biplane method of discs remains the widespread standard by which LVEF is quantified in clinical practice. For this reason, in chapter 4 and chapter 5 we validated our new imaging methods for quantifying LV systolic function against CMR-derived LVEF, but also compared them against 2DE Simpson's biplane method of discs. Invasive measurement of intracardiac pressures during left heart catheterisation remains the reference standard for assessing LV diastolic filling pressures, however, due to both patient discomfort and the inherent risks of cardiac catheterisation, tissue Doppler echocardiography E/Em has become the non-invasive method used to estimate LV filling pressures in clinical practice. For this reason, in chapter 6 we validated our new VEC-CMR E/Em ratio against invasively recorded LVEDP and compared it to echo-derived E/Em ratios.

Due to the complex nature of cardiac contractile function, and the intimate and interdependent relationship between cardiac systole and diastole, RV and LV function and changes in cardiac preload and afterload, no single two-dimensional quantitative measure of LV systolic function, LV diastolic function or RV systolic function can accurately capture all the changes that occur during that specified phase of the cardiac cycle. However, that was not the aim of this thesis. Our aim was to establish new methods for quantifying global ventricular function that are more sensitive, accurate and reproducible than current widely employed imaging techniques, and to prove that these new methods correlate closely to current reference standards.

2D speckle tracking strain is a myocardial deformation imaging technique that is used to assess regional changes in ventricular function in clinical research. It has been found to be sensitive in detecting sub-clinical ventricular dysfunction in a variety of pathologies³⁴⁴⁻³⁵¹ and also is useful as an indicator of prognosis.³¹³ We hypothesised that detailed Lagrangian strain analysis of all 16 AHA myocardial segments of the left ventricle could be averaged to establish a global strain score of the LV that would accurately reflect changes in LV systolic function. We have demonstrated that our GSS has a significantly stronger correlation and higher reproducibility than 2DE biplane Simpson's rule for quantifying LV systolic function when compared to CMR-derived LVEF as the reference standard. During the recruitment period of our study we only had access to longitudinal strain speckle tracking software, although radial strain software is now commercially available. As our strain imaging software was able to record systolic deformation in only one contractile plane of the heart, it is perhaps unsurprising that our 3D volumetric assessment of LVEF using Philips iE33 3DE scanner, had a closer correlation with CMR LVEF than GSS. At the start of this year General Electric Incorporated completed the development of 4D-speckle tracking software programme. This software aims to quantify myocardial deformation in 3 contractile planes of the heart in addition to quantification of regional volumetric change. Future work should therefore include validation of this 4D speckle software against CMR and strain software from other manufacturers. Until then, the results of our study suggest that GSS may be a more accurate and reproducible alternative to biplane Simpson's rule for the quantification of LV systolic function by 2DE. This finding requires confirmation in a larger diverse population before the GSS should be used in routine clinical practice.

The cost of a 1.5T MRI scanner is in the region of one million pounds. A Philips iE33 3DE scanner costs £98,711.³⁵² Speckle tracking software costs £2,500.³⁵² A standard CMR scan costs £380.³⁵² By comparison the tariff for a standard 2D transthoracic echocardiogram is £57.³⁵² In addition to its accuracy and reproducibility the clinical application of a technique also depends on its simplicity and its wide-spread availability. Although speckle-tracking strain is a cheaper alternative to CMR for quantifying LV systolic function, many cardiac imaging departments world-wide may not be able to afford the cost of this specialist software. For this reason, in Chapter 5, we examined the use of a modified regional wall motion scoring index for calculating LVEF, and compared this to CMR-LVEF. Again, our findings suggest that the RWMSI-derived LVEF had a closer correlation and better inter-

technique concordance with CMR-LVEF, when compared to biplane Simpson's LVEF. The clear advance of this technique is that it is quick and easy to perform and does not require the use of specialist software. It can therefore be used on any echo machine, in any echo laboratory world-wide, giving it huge potential clinical application. The disadvantage is that the technique is clearly subjective and has poorer reproducibility than GSS (interobserver variability: 11.2% vs. 3.2%). It must also be noted in this study that validation and reproducibility of our modified RWMSI equation was performed by experienced British Society of Echocardiography accredited imaging specialists. We would not recommend use of this technique by trainees or inexperienced individuals due to its inherent subjectivity. Within these limitations, our results suggest that use of the modified RWMSI, by experienced individuals, may be a superior alternative to biplane Simpson's rule. Future work should include recruitment of larger patient numbers, to enable valid sub-group assessment of the accuracy and inter-technique concordance of the RWMSI in patients with mild, moderate and severely impaired LV systolic function compared to CMR-LVEF.

Diastolic function is a complex multi-stage process that is difficult to quantify in absolute terms. In recent years the prevalence and importance of diastolic dysfunction has become increasingly recognised. Diastolic dysfunction is now believed to account for up to 50% of clinical heart failure cases.^{168,169} The accurate diagnosis of diastolic dysfunction has been classified as being of "paramount clinical importance" by the EAE/ASE.¹⁴ The development of tissue Doppler echocardiography has resulted in a move away from load-dependent semi-quantitative assessments of mitral inflow patterns, to more simple quantitative non-invasive estimates of LV filling pressures based on echo E/Em ratio. In this area, CMR lags behind echo. At present there is no standard method for assessing diastolic function by CMR. In chapter 6 we sought to explore the clinical utility of using phase encoded velocity mapping CMR sequences to estimate LV filling pressure (and hence diastolic function), by comparing VEC-CMR E/Em with invasively recorded LVEDP, with mixed results. We found that VEC-CMR E/Em had a significant correlation with LVEDP in study subjects with preserved LVEF, but a weak correlation in those with impaired LV systolic function. The reason for this is unclear, but our results compliment recent echo findings of E/Em in patients with systolic heart failure.¹⁶ Ours was a small

pilot study, designed to explore the feasibility and potential clinical utility of the technique, and our findings require further validation in a larger prospective study.

Technically, there is no “gold standard” for quantifying RV systolic function, however, due to the high spatial resolution of CMR and the ability to image the heart in any plane, CMR is the widely accepted reference standard for quantifying RVEF. The resolution of the RV by 3DE is generally poorer than that of the LV, and at present the EAE/ASE guidelines do not recommend the use of 3DE for quantifying RVEF in routine clinical practice.³⁷ Due to the complex geometry of the RV, quantification of RVEF by 2DE is inaccurate and should not be used.³⁷ The 2010 EAE/ASE guidelines review 10 non-volumetric alternative methods for quantifying RV systolic function by 2DE, and recommend at least one of these quantitative indices be measured in addition to a qualitative assessment of RV function, in every routine TTE performed.³⁷ Due to a paucity of head-head comparison studies on the subject, the guidelines fail to make a clinical recommendation as to which 2D index of RV function is superior to the remaining methods and should therefore be the standardised method of choice in routine clinical practice. In chapter 7, we therefore attempt to answer this important clinical question by performing a direct comparison study of these 10 non-volumetric indices of RV function, indexed against CMR RVEF as the reference standard. In our study we have demonstrated that longitudinal speckle tracking strain of the RV free wall had a significantly closer correlation with RVEF than all other non-volumetric echo indices of RV systolic function. Current EAE/ASE guidelines review the methodology behind strain imaging, but do not as yet endorse its use in routine clinical practice due to a paucity of normative data and reproducibility data.³⁷ For this reason, we have determined normative threshold values for the technique by studying receiver-operator characteristics. We have also demonstrated that the technique is reproducible. Furthermore, due to the semi-automated nature of the software, the technique is easy to perform and the analysis time for calculating RV free wall strain is ~2 minutes. For these reasons, we believe this technique has a potentially far reaching clinical application. What remains unclear at present, is if the normative cut-off values for RVFWS determined using GE speckle tracking software, will correspond to the same values for RVFWS which are calculated using speckle-tracking software produced by other manufacturers. Future work now should include a comparison study of RVFWS indices measured using speckle tracking software from various manufacturers. The same rule must also apply for our LV global strain score.

8.2 CONCLUSION

Non-invasive cardiac imaging is a constantly evolving specialty, and regular review of current practice for the assessment of cardiac ventricular function is required as new multi-modal imaging techniques become available. Due to the small patient numbers within our studies, the preliminary findings of this thesis clearly require validation in a larger, more diverse patient population before any of these techniques should be used in routine clinical practice. However, the results of this thesis suggest that when compared to CMR as the reference standard, speckle tracking strain imaging, using the methods described in detail above, may be the best 2D echocardiographic imaging method available for accurately assessing both left and right ventricular systolic function in a heterogenous population of patients as seen in clinical practice. When speckle tracking strain imaging is not available, the use of the modified regional wall motion scoring index, by experienced individuals, may provide a superior alternative to 2D biplane Simpson's method of discs. We have also demonstrated that phase encoded velocity mapping CMR E/Em ratios can be used to estimate LVEDP in individuals with preserved LVEF, but not impaired LV systolic function and this may therefore may provide a potential new method for assessing diastolic function by CMR.

Comment [DZ2]: Rae
This chapter is good and I think needs trimming by a few pages, if you can. Otherwise, it is good to go

APPENDIX A

Formatted: Font: 24 pt

EXAMPLE PATIENT INFORMATION SHEET

ROYAL ADELAIDE HOSPITAL & WAKEFIELD HOSPITAL

VOLUNTEER INFORMATION SHEET

“Non-invasive indices for the assessment of load independent cardiac function: Comparison of Cardiac Magnetic Resonance Imaging (CMR) and Transthoracic Echocardiography (TTE) techniques versus invasive Left Ventricular End Diastolic Pressure (LVEDP) ”

Principal Investigator: Dr Rae Duncan

Co-investigators: Prof Stephen Worthley, Prof Gary Wittert, Dr Matthew Worthley, Prof Prashanthan Sanders, Dr Julie Bradley, Mr Angelo Carbone, Mr Greg Brown, Ms Diana Pilkington, Ms Kerry Brackenridge, Dr Darryl Leong

YOUR PARTICIPATION IS VOLUNTARY

You are invited to take part in a study looking at non-invasive ways of imaging (scanning) the heart, to measure the pressure in the main pumping chamber of the heart at the end of each heartbeat. This pressure reading gives your doctor information on how well the heart is able to relax (diastolic function) after each heart muscle contraction (systolic function). The purpose of this sheet is to provide you with information so you can make an informed decision as to whether you wish to participate part in this study. This is a research project and you do not have to be involved. If you do not wish to participate, your medical care will not be affected in any way.

BACKGROUND

During each heartbeat, the heart contracts and then relaxes. Contraction of the heart is termed “systolic function” and relaxation of the heart is termed “diastolic function”. Abnormalities in either contraction (termed systolic dysfunction) and abnormalities in relaxation (termed diastolic dysfunction) of the heart can cause the signs and symptoms of heart failure. Systolic dysfunction can usually be detected easily, and sometimes before the development of symptoms, by performing a scan of the heart - either an echo (ultrasound) scan or a cardiac MRI scan. Early detection results in early treatment and monitoring by doctors to prevent problems developing. By calculating the ejection fraction (the fraction of blood pumped out of the heart with each heartbeat), the systolic function of an individual’s heart can be monitored accurately over many years. Diastolic function is not so easy to measure. Diastolic function can be measured by measuring the pressure in the main

pumping chamber of the heart, the left ventricle, during the relaxation phase of the heart. The accepted “Gold Standard”, or best way of doing this, is by inserting a catheter (a long thin tube), via a blood vessel in the leg, into the ventricle, and to measure pressure and volume changes in the left ventricle throughout the cardiac cycle. The pressure at end of the hearts relaxation period – the left ventricular end diastolic pressure (LVEDP) – is also measured this way. These are standard clinical measurements which, can be recorded in individuals like yourself, during a cardiac catheter procedure. Because a cardiac catheter procedure involves taking X-ray pictures, doctors try to keep the number of times a catheter procedure is performed in any individual, to a minimum. For this reason it is not practical or recommended that a cardiac catheter procedure be used to monitor the diastolic function of an individual over an extended time period of several years as this would involve several repeat procedures. Instead, echocardiography has been used to assess diastolic function, as it is non-invasive, quick and does not involve X-rays. However, the standard methods for assessing diastolic function with echo are limited by the fact that they are not quantitative, and they are not as accurate or reproducible as the cardiac catheter “Gold Standard”. There have been major advances in the quality of cardiac imaging recently both in the development of tissue Doppler echo techniques and in cardiac MRI scanning. Both of these methods of heart scanning are non-invasive, safe, painless and do not involve any exposure to ionising radiation. Both of these new imaging techniques, now give the opportunity to measure diastolic function quantitatively and to calculate LVEDP non-invasively. We would like to validate these techniques by comparing the LVEDP and diastolic pressure-volume curves your doctor records during your cardiac catheter procedure with the figures we record during echo and cardiac MRI scanning.

WHAT IS THE PURPOSE OF THE TRIAL?

The overall aim of this project is to investigate the use of both echo and cardiac MRI protocols in calculating LVEDP, and to validate the results against LVEDP and/or left ventricular pressure-volume curves recorded during cardiac catheterisation. We hope that if we can validate these techniques in this study, we may be able to use tissue Doppler echo or cardiac MRI routinely in the future to monitor diastolic dysfunction in patients who suffer from heart failure.

WHAT WILL YOU HAVE TO DO?

If you agree to participate in this study, we will ask and record relevant aspects of your medical history – this is simply to ensure that you are suitable for our study and you have no problems that would prevent you from entering the MRI scanner. We will invite you to attend Adelaide Cardiac Imaging (Wakefield Clinic, Wakefield Street, Adelaide) early on the morning of your catheter procedure. We would like to perform an echo scan of your heart (which takes approximately 30-40 minutes) followed by an MRI scan (which takes approximately 60 minutes) prior to your catheter procedure (which takes approximately 20 minutes).

What is an Echo exam and what is involved?

An echo is an ultrasound scan of the heart, and works on a similar principal to the ultrasound scan used to scan pregnant women. You will be asked to lie on a couch and a microphone like device (a transducer probe) will be placed on your chest. The transducer transmits and receives sound waves that travel through the chest wall to the heart and

reflect back again. The reflected sound waves are translated into moving images of the heart. An echo is non-invasive, painless, without radiation and carries no side effects.

What is an MRI exam and what is involved?

MRI is a test which uses a powerful magnet with special radiofrequency pulses to produce radiofrequency signals (echoes) from within the body. These echoes produce a very detailed picture of the part of the body being studied (in this case the heart). The MRI scanner consists of a very short circular tunnel and a narrow table. During the scan you simply lie on your back on the table and your body goes through the tunnel of the scanner. The scan will take approximately 45-60 minutes to perform. MRI is also non-invasive, painless, without radiation and carries no significant side effects, however you will hear a loud knocking or buzzing sound at various intervals. Some patients can find an MRI scan distressing. You will be provided with earplugs and if you wish, we can offer you music to listen to during the scan.

As part of this research study, all the scans are free. We may also be able to assist in transport arrangements to Wakefield Hospital for those with difficulty.

ADVERSE EFFECTS

Both echo and MRI scans are safe. Overall, there is very little risk involved in this research study. Some individuals can find the MRI scanner a little claustrophobic or uncomfortable.

CONFIDENTIALITY

Your participation in this study is strictly confidential. All information collected for research purposes is only available to the study investigators and will not be released to other medical or research staff without your consent. If information from this study is published in any form, it will be done so in a way that does not allow you to be personally identified.

CONTACT DETAILS

Should you have any questions about this study please feel free to contact:

Dr Rae Duncan (08) 8222 2473

INDEPENDENT CONTACT

If you wish to speak to someone not directly involved in the study about your rights as a volunteer, or about the conduct of the study, you may also contact the Chairman, Research Ethics Committee, on (08) 8405 3333.

APPENDIX B

Formatted: Line spacing: 1.5 lines,
Don't adjust space between Latin and
Asian text

Formatted: Font: 24 pt

EXAMPLE PATIENT CONSENT FORM

Formatted: Line spacing: 1.5 lines

ROYAL ADELAIDE HOSPITAL & WAKEFIELD HOSPITAL

CONSENT FORM

I, THE UNDERSIGNED HEREBY CONSENT TO MY INVOLVEMENT IN THE PROJECT TITLED:

““Non-invasive indices for the assessment of load independent cardiac function: Comparison of Cardiac Magnetic Resonance Imaging (CMR) and Transthoracic Echocardiography (TTE) techniques versus invasive Left Ventricular End Diastolic Pressure (LVEDP) ”

conducted by Dr Rae Duncan, Prof Stephen Worthley, Dr Matthew Worthley, Prof Prashanthan Sanders, Dr Julie Bradley, Mr Angelo Carbone, Mr Greg Brown, Mrs Diana Pilkington, Ms Kerry Brackenridge, Dr Darryl Leong.

1. I understand the nature, purpose and contemplated effects of the research project. It has been fully explained to my satisfaction and I have been given the opportunity to ask questions about the project. I have also read the Information Sheet and I agree to take part in the study. My consent is given voluntarily.
2. I understand that I may not directly benefit from taking part in this study.
3. I understand that while information gained during the study may be published, I will not be identified and my personal results will remain confidential.
4. I understand that I can withdraw from the study at any stage.
5. I understand that I should not become pregnant during the course of this trial. In the event of a pregnancy occurring, I agree to notify the investigator as soon as is practically possible.
6. I understand that this study has been approved by the Research Ethics Committees of the Royal Adelaide and Wakefield Hospitals.
7. I have had the opportunity to discuss taking part in this investigation with a family member or friend

Name of subject (PRINT): _____

Signed: _____

Date: _____

Address: _____

Contact number: _____

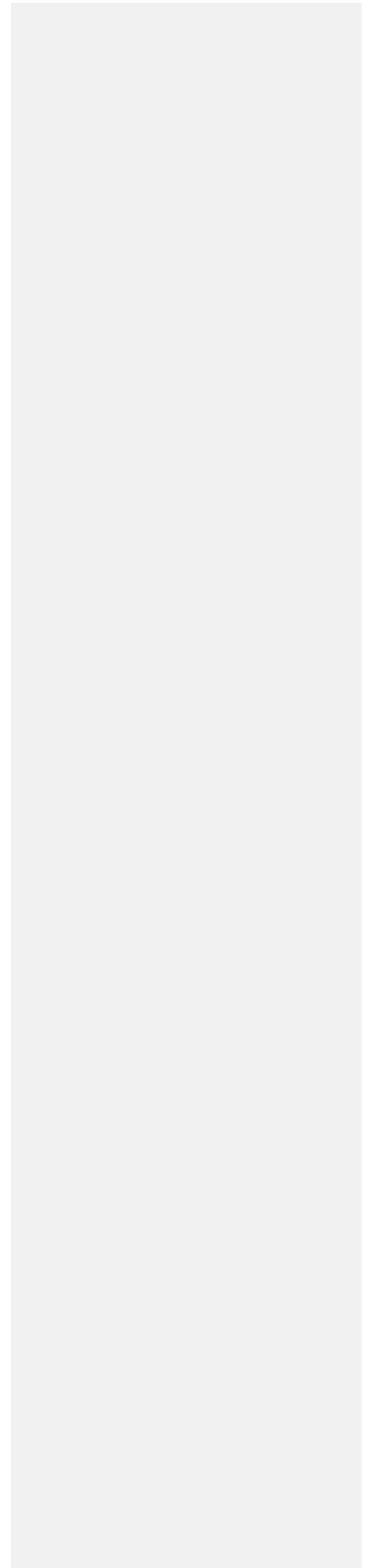
I certify that I have explained the study to the patient/volunteer and consider that he/she understands what is involved.

Signed: _____ Dated: _____
(Investigator)

APPENDIX C

Formatted: Font: 24 pt

BRITISH SOCIETY OF ECHOCARDIOGRAPHY INVESTIGATOR AWARD WINNER CERTIFICATE



The following Abstract presenter has been awarded 1st place in the
BSE 2011 Investigator of the Year Award

Formatted: Font: Times New Roman,
28 pt, Bold, Underline

Dr Rae F Duncan

Abstract Title

A study of the 16-segment regional wall motion scoring index and biplane Simpson's rule for the calculation of left ventricular ejection fraction: A comparison with cardiac magnetic resonance

Authors:

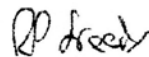
^{1,2}Rae F Duncan, MBChB, BSc, MSc, MRCP; ¹Ben K Dundon, MBBS FRACP; ¹Adam J Nelson, BSc; ²James Pemberton, MBBS MD MRCP; ¹Kerry Williams, Dip Appl Sci; ¹Matthew I. Worthley, MBBS; PhD, FRACP; ²Azfar Zaman, MBChB, BSc, MD, FRCP; ²Honey Thomas, MBBS, MD, MRCP; ²Anna Johnson, BSc; ¹Stephen G. Worthley, MBBS, PhD, FRACP.

¹Cardiovascular Research Centre, Royal Adelaide Hospital and University of Adelaide, Adelaide, South Australia 5000, Australia

²Department of Cardiology, The Freeman Hospital and Institute of Cellular Medicine, Newcastle University, Newcastle-upon-Tyne, UK

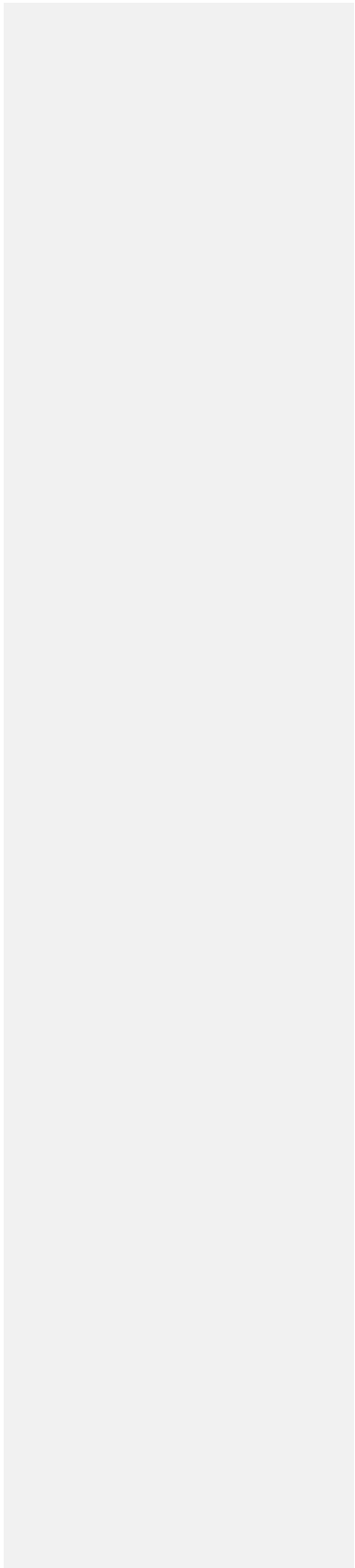


Dr Navroz Masani
President



Dr Rick Steeds
Chair, Education Committee

|



The following Abstract presenter has been awarded 1st place in the
BSE 2011 Investigator of the Year Award

Formatted: Font: Times New Roman,
28 pt, Bold, Underline

Dr Rae F Duncan

Abstract Title

A study of the 16-segment regional wall motion scoring index and biplane Simpson's rule for the calculation of left ventricular ejection fraction: A comparison with cardiac magnetic resonance

Authors:

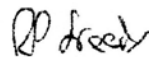
^{1,2}Rae F Duncan, MBChB, BSc, MSc, MRCP; ¹Ben K Dundon, MBBS FRACP; ¹Adam J Nelson, BSc; ²James Pemberton, MBBS MD MRCP; ¹Kerry Williams, Dip Appl Sci; ¹Matthew I. Worthley, MBBS; PhD, FRACP; ²Azfar Zaman, MBChB, BSc, MD, FRCP; ²Honey Thomas, MBBS, MD, MRCP; ²Anna Johnson, BSc; ²Stephen G. Worthley, MBBS, PhD, FRACP.

¹Cardiovascular Research Centre, Royal Adelaide Hospital and University of Adelaide, Adelaide, South Australia 5000, Australia

²Department of Cardiology, The Freeman Hospital and Institute of Cellular Medicine, Newcastle University, Newcastle-upon-Tyne, UK



Dr Navroz Masani
President



Dr Rick Steeds
Chair, Education Committee

APPENDIX D

Formatted: Font: 24 pt

**BRITISH SOCIETY OF
ECHOCARDIOGRAPHY
INVESTIGATOR AWARD
FINALIST
CERTIFICATE**

The following Abstract presenter has been shortlisted for the
BSE 2011 Investigator of the Year Award

Formatted: Font: 18 pt

Dr Rae F Duncan

Abstract Title

Right ventricular free wall strain has a closer correlation with right ventricular ejection fraction than other echocardiographic indices of right ventricular function: Validation with cardiac magnetic resonance imaging

Authors:

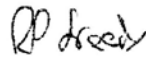
^{1,2} Duncan RF, ² Nelson AJ, ² Dundon BK, ¹ Schuster J, ² Worthley MI, ² Carbone A, ² Williams K, ¹ Taylor R, ¹ Johnson A, ¹ Zaman A, ² Worthley SG.

¹ Department of Cardiology, The Freeman Hospital and Institute of Cellular Medicine, Newcastle University, Newcastle-upon-Tyne, UK

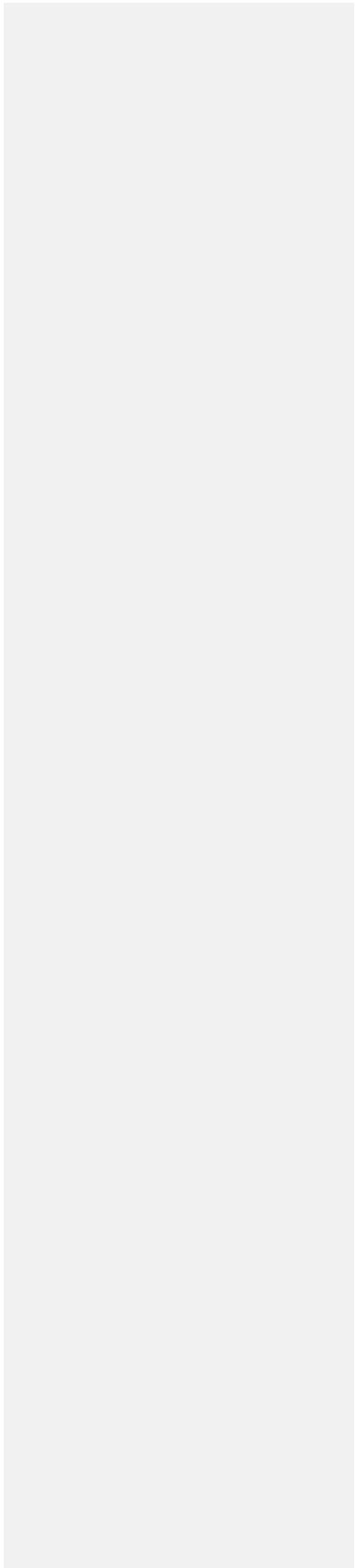
² Cardiovascular Research Centre, Royal Adelaide Hospital and University of Adelaide, Adelaide, South Australia 5000, Australia



Dr Navroz Masani
President



Dr Rick Steeds
Chair, Education Committee





REFERENCES

REFERENCES

1. Witteles RM, Knowles JW, Perez M, et al. Use and overuse of left ventriculography. *American Heart Journal* 2012;163:617-623.
2. Cournaud A. Cardiac catheterisation; development of the technique, its contributions to experimental medicine, and its initial applications in man. *Acta Medicine Scandinavia Supplement* 1975;579:3-32.
3. Wells PNT. Milestones in cardiac ultrasound: echoes from the past. History of cardiac ultrasound. *International Journal of Cardiac Imaging* 1993;9:S3-S9.
4. Ommen SR, Nishimura RA, Appleton CP, et al. Clinical utility of Doppler echocardiography and tissue Doppler imaging in the estimation of left ventricular filling pressures; A comparative simultaneous Doppler-catheterisation study. *Circulation* 2000;102:1788-1794.
5. Nagueh SF, Middleton KJ, Kopelen HA, et al. Doppler tissue imaging: A non-invasive technique for evaluation of left ventricular relaxation and estimation of filling pressures. *Journal of the American College of Cardiology* 1997;30:1527-1533.
6. Kasner M, Westermann D, Steendijk P, et al. Utility of Doppler echocardiography and tissue Doppler imaging in the estimation of diastolic function in heart failure with normal ejection fraction: A comparative Doppler-conductance catheterisation study. *Circulation* 2007;116:637-647.

7. Sharma GVRK, Woods PA, Lambrew CT, et al. Evaluation of a non-invasive system for determining left ventricular filling pressure. *Archives of Internal Medicine* 2002;162:2084-2088.
8. Arteaga RB, Hreybe H, Patel D, et al. Derivation and validation of a diagnostic model for the evaluation of left ventricular filling pressures and diastolic function using mitral annulus tissue Doppler imaging. *American Heart Journal* 2008;155:924-929.
9. De Boeck BWL, Cramer MJM, Oh JK, et al. Spectral pulsed tissue Doppler imaging in diastole: A tool to increase our insight in and assessment of diastolic relaxation of the left ventricle. *American Heart Journal* 2003;146:411-419.
10. Dokainish H, Zoghbi WA, Lakkis NM, et al. Incremental predictive power of B-type natriuretic peptide and tissue Doppler echocardiography in the prognosis of patients with congestive heart failure. *Journal of American College of Cardiology* 2005;45:1223-6.
11. Sharma R, Pellerin D, Gaze DC, et al. Mitral peak Doppler E-wave to peak mitral annulus velocity ratio is an accurate estimate of left ventricular filling pressure and predicts mortality in end-stage renal disease. *Journal of the American Society of Echocardiography* 2006;19:266-73.
12. Dokainish H, Sengupta R, Pillai M, et al. Correlation of tissue Doppler and two-dimensional speckle myocardial velocities and comparison of derived ratios with invasively measured left ventricular filling pressures. *Journal of the American Society of Echocardiography* 2009;22:284-289.
13. Nagueh SF, Lakkis NM, Middleton KJ, et al. Doppler estimation of the left ventricular filling pressures in patients with hypertrophic cardiomyopathy *Circulation* 1999;99:254-61.

14. Nagueh SF, Appleton CP, Gillebert TC, et al. EAE/ASE Recommendations: Recommendations for the evaluation of left ventricular diastolic function by echocardiography. *European Journal of Echocardiography* 2009;10:165-193.
15. D'Souza KA, Mooney DJ, Russell AE, et al. Abnormal septal motion affects early diastolic velocities at the septal and lateral mitral annulus, and impacts on estimation of the pulmonary capillary wedge pressure. *Journal of the American Society of Echocardiography* 2005;18:445-453.
16. Mullens W, Borowski AG, Curtin RJ, et al. Tissue Doppler imaging in the estimation of intracardiac filling pressure in decompensated patients with advanced systolic heart failure. *Circulation* 2009;119:62-70.
17. Tschope C, Paulus WJ. Doppler echocardiography yields dubious estimates of left ventricular diastolic pressures. *Circulation* 2009;120:810-820.
18. Geske JB, Sorajja P, Nishimura RA, et al. Evaluation of left ventricular filling pressures by Doppler echocardiography in patients with hypertrophic cardiomyopathy: Correlation with direct left atrial pressure measurement at cardiac catheterization. *Circulation* 2007;116:2702-2708.
19. Soloman SD, Stevenson LW. Recalibrating the barometer: is it time to take a critical look at non-invasive approaches to measuring filling pressures? *Circulation* 2009;119:13-15.
20. Jung B, Foll D, Bottler P, et al. Detailed analysis of myocardial motion in volunteers and patients using high temporal resolution MR tissue phase mapping. *Journal of Magnetic Resonance Imaging* 2006;24:1033-1039.
21. Heidenreich PA, Steffens J, Fujita N, et al. Evaluation of mitral stenosis with velocity-encoded cine-magnetic resonance imaging. *American Journal of Cardiology* 1995;75:365-369.

22. Teo KSL, Carbone A, Piantadosi C et al. Cardiac MRI assessment of left and right ventricular parameters in Healthy Normal Australian Volunteers. *Heart, Lung and Circulation* 2008; 17: 313-317.
23. Hori Y, Yamada N, Higashi M, et al. Rapid evaluation of right and left ventricular function and mass using real-time true FISP cine MR imaging without breath-hold: comparison with segmented true-FISP cine MR imaging with breath-hold. *Journal of Cardiovascular Magnetic Resonance* 2003;5(3):439-450.
24. Lorenz CH, Walker ES, Morgan VL, et al. Normal human right and left ventricular mass, systolic function, and gender differences by cine magnetic resonance imaging. *Journal of Cardiovascular Magnetic Resonance* 1999;1:7-21.
25. Buechel EV, Kaiser T, Jackson C, et al. Normal right and left ventricular volumes and myocardial mass in children measured by steady state free precession cardiovascular magnetic resonance. *Journal of Cardiovascular Magnetic Resonance* 2009;11:19.
26. Pattynama PM, Lamb HJ, Velde EA, et al. Reproducibility of MRI –derived measurements of right ventricular volumes and myocardial mass. *Journal of Magnetic Resonance Imaging* 1995;13:53-63.
27. Thiele H, Nagel E, Patetsh I, et al. Functional cardiac MR imaging with steady-state free precession (SSFP) significantly improves endocardial border delineation without contrast agents. *Journal of Magnetic Resonance Imaging* 2001;14:362-367.
28. Maciera AM, Prasad SK, Khan M, et al. Reference to right ventricular systolic and diastolic function normalised to age, gender and body surface area from steady-state free precession cardiovascular magnetic resonance. *European Heart Journal* 2006;27:2879-2888.

Formatted: Font: Not Bold

29. Maciera AM, Prasad SK, Khan M, et al. Normalized left ventricular systolic and diastolic function by steady state free precession cardiovascular magnetic resonance. *Journal of Cardiovascular Magnetic Resonance* 2006;8:417-426.
30. Helbing WA, Rebergen SA, Maliopaard C, et al. Quantification of right ventricular function with magnetic resonance imaging in children with normal hearts and with congenital heart disease. *American Heart Journal* 1995;130:828-837.
31. Alfakih K, Plein S, Thiele H, et al. Normal human left and right ventricular dimensions for MRI as assessed by turbo gradient echo and steady-state free precession imaging sequences. *Journal of Magnetic Resonance Imaging* 2003;17:323-329.
32. Alfakih K, Plein S, Thiele H, et al. Comparison of right ventricular volume measurement between segmented k-space gradient-echo and steady-state free precession magnetic resonance imaging. *Journal of Magnetic Resonance Imaging* 2002;16:253-258.
33. Grothues F, Moon JC, Bellenger NG, et al. Interstudy reproducibility of right ventricular volumes, function and mass with cardiovascular magnetic resonance. *American Heart Journal* 2004;147:218-223.
34. Jauhianen T, Järvinen VM, Hekali PE. Evaluation of methods for MR imaging of human right ventricular heart volumes and mass. *Acta Radiologica* 2002;43:587-592.
35. Marcu C, Beek A, Van Rossum A. Cardiovascular magnetic resonance for the assessment of right heart involvement in cardiac and pulmonary disease. *Heart and Lung Circulation* 2006;15:362-370.
36. Sievers B, Addo M, Kirchberg S, et al. Impact of the ECG gating method on ventricular volumes and ejection fractions assessed by cardiovascular magnetic

- resonance imaging. *Journal of Cardiovascular Magnetic Resonance* 2005;7:441-446.
37. Rudski LG, Wyman WL, Afilalo J, et al. Guidelines for the echocardiographic assessment of the right heart in adults: A report from the American Society of Echocardiography, endorsed by the European Society of Echocardiography, a registered branch of the European Society of Cardiology, and the Canadian Society of Echocardiography. *Journal of the American Society of Echocardiography* 2010;23:685-713.
38. Lang RM, Bierig M, Devereux RB, et al; Chamber Quantification Writing Group; American Society of Echocardiography's Guidelines and Standards Committee; European Association of Echocardiography. Recommendations for chamber quantification: A report from the American Society of Echocardiography's Guidelines and Standards Committee and the Chamber Quantification Writing Group, developed in conjunction with the European Association of Echocardiography, a branch of the European Society of Cardiology. *Journal of the American Society of Echocardiography* 2005;18:1440-1463.
39. Anderson RH, Ho SY, Redmann K, et al. The anatomical arrangement of the myocardial cells making up the ventricular mass. *European Journal of Cardiothoracic Surgery* 2005; 28: 515-525.
40. Camm AJ (2002). Ch 13: Cardiovascular Disease. *Kumar P and Clark M: Clinical Medicine Fifth Edition* (pp701-832). Edinburgh, London, New York, Philadelphia, St Louis, Sydney, Toronto: WB Saunders.
41. Ciba Medical Illustrations: The Heart. 1969;5:16.
42. Anderson B (2000). Ch 14: Doppler assessment of left ventricular systolic and diastolic function. *Echocardiography: The normal examination and echocardiographic measurements* (pp 189-227). Queensland, Australia: MGA graphics.

43. Edward Life Sciences. Normal haemodynamic parameters in the Adult. 2011. doi: ht.edwards.com/scin/edwards/sitecollectionimages/products/presep/ar05688_parameters.
44. Cohn JN, Ferrari R, Sharpe N. Cardiac remodelling- Concepts and clinical implications; a consensus paper from an international forum on cardiac remodelling. *Journal of the American College of Cardiology* 2000;35:569-582.
45. Davis BA, O'Sullivan C, Jarritt PH, et al. Value of sequential monitoring of left ventricular ejection fraction in the management of thalassemia major. *Blood* 2004;104:263-269.
46. Curtis JP, Sokol SI, Wang Y, et al. The association of left ventricular ejection fraction, mortality, and cause of death in stable outpatients with heart failure. *Journal of the American College of Cardiology* 2003;42:736-742.
47. Kelly MJ, Thompson PL, Quinlan MF. Prognostic significance of left ventricular ejection fraction after acute myocardial infarction. A bedside radionuclide study. *British Heart Journal* 1985;53:16-24.
48. Specchia G, De Servi S, Scire A, et al. Interaction between exercise training and ejection fraction in predicting prognosis after a first myocardial infarction. *Circulation* 1996;94:978-982.
49. Ekman I, Kjork E, Anderson B. Self-assessed symptoms in chronic heart failure – Important information for clinical management. *The European Journal of Heart Failure* 2006; doi: 10.1016/j.ejheart.2006.10.020.
50. Ekman I, Cleland JCF, Swedberg K et al. Symptoms in patients with heart failure are prognostic predictors. Insights from COMET. *Journal of Cardiac Failure* 2005; 11: 288-292.

51. Buckberg GD, Castella M, Gharib M, et al. Active myocyte shortening during the 'isovolumetric relaxation' phase of diastole is responsible for ventricular suction; 'systolic ventricular filling'. *European Journal of Cardiothoracic Surgery* 2006;29:98-106.
52. Yu CM, Sanderson JE, Shum IO, et al. Diastolic dysfunction and natriuretic peptides in systolic heart failure. Higher ANP and BNP levels are associated with restrictive filling pattern. *European Heart Journal* 1996;17:1694-1702.
53. Paelinck BP, Vrints CJ, Bax JJ, et al. Tissue cardiovascular magnetic resonance imaging demonstrates regional diastolic dysfunction in remote tissue early after inferior myocardial infarction. *Journal of Cardiovascular Magnetic Resonance* 2007;9:877-882.
54. Wang M, Yip G, Yu CM, et al. Independent and incremental prognostic value of early mitral annulus velocity in patients with impaired left ventricular systolic function. *Journal of the American College of Cardiology* 2005;45:272-277.
55. Samad BA, Olson JM, Alam M. Characteristics of left ventricular diastolic function in patients with systolic heart failure: A Doppler tissue imaging study. *Journal of the American Society of Echocardiography* 2005;18:896-900.
56. Moller JE, Sindergaard E, Poulsen SH, et al. Pseudonormal and restrictive filling patterns predict left ventricular dilation and cardiac death after a first myocardial infarction: a serial colour M-mode Doppler echocardiographic study. *Journal of American College of Cardiology* 2000;36:1841-1846.
57. Duncan R, Dundon B, Nelson A, et al. Does isolated diastolic dysfunction truly exist?: insights from myocardial deformation imaging. Unpublished data.
58. Yip G, Wang M, Zhang Y, et al. Left ventricular long axis function in diastolic heart failure is reduced in both diastole and systole: time for a redefinition. *Heart* 2002;87:121-125.

59. Ho KK, Anderson KM, Kannel WB, et al. Survival after the onset of congestive heart failure in Framington Heart Study subjects. *Circulation* 1993;88:107-115.
60. Vasan RS, Larson MG, Benjamin EJ, et al. Congestive heart failure in subjects with normal versus reduced left ventricular ejection fraction: prevalence and mortality in a population-based cohort. *Journal of the American College of Cardiology* 1999;33:1948-55.
61. Hogg K, Swedberg K, McMurray J. Heart failure with preserved left ventricular systolic function: Epidemiology, clinical characteristics and prognosis. *Journal of the American College of Cardiology* 2004;43:317-327.
62. Harvey W (1628). *Exercitatio Anatomica de Motu Cordis et Sanguinis*. Frankfurt, Germany: Sumptibus Gvilielmi Fitzeri.
63. Vitarelli A, Terzano C. Do we have two hearts? New insights in right ventricular function supported by myocardial imaging echocardiography. *Heart Failure Reviews* 2010;15:39-61.
64. Haddad F, Hunt SA, Rosenthal DN, et al. Right ventricular function in cardiovascular disease, Part I: Anatomy, physiology, aging and functional assessment of the right ventricle. *Circulation* 2008;117:1436-1448.
65. Buckberg GD and the RESTORE Group. The Ventricular septum: The lion of right ventricular function and its impact on right ventricular restoration. *European Journal of Cardiothoracic Surgery* 2006;295:S272-S278
66. Goldstein JA. Pathophysiology and management of Right Heart Ischaemia. *Journal of the American College of Cardiology* 2002;40:841-853
67. Goldstein JA. Right heart ischaemia: Pathophysiology, natural history and clinical management. *Progress in Cardiovascular Diseases* 1998;40:325-341.

68. Selton-Suty C, Juiliere Y. Non-invasive investigations of the right heart: How and why? *Archives of cardiovascular disease* 2009;102:219-232.
69. Boettler P, Claus P, Herbots L, et al. New aspects of the ventricular septum and its function: an echocardiographic study. *Heart* 2005;91:1343-1348
70. Sheehan F, Redington A. The right ventricle: anatomy, physiology and clinical imaging. *Heart* 2008;94:1510-1515,
71. Bleeker GB, Steendijk P, Holman ER, et al. Assessing right ventricular function: the role of echocardiography and complementary technologies. *Heart* 2006;91:i19-i26.
72. Lindqvist P, Calcuttea A, Henein M. Echocardiography in the assessment of right heart function. *European Journal of Echocardiography* 2008;9:225-234
73. Dell'Italia LJ, Walsh RA. Application of a time varying elastance model to right ventricular performance in man. *Cardiovascular Research* 1988;22:864-874.
74. Damiano RJ, La Follette P Jr, Cox JL et al. Significant left ventricular contribution to right ventricular systolic function. *American Journal of Physiology* 1991;261:H1514-1524.
75. Hoffman D, Sisto D, Frater RW, et al. Left-to-right ventricular interaction with a non-contracting right ventricle. *Journal of Thoracic Cardiovascular Surgery* 1994;107:1496-1502.
76. Goldstein JA, Tweddell JS, Barizlai B, et al. Importance of left ventricular function and systolic interaction to right ventricular performance during right heart ischaemia. *Journal of the American College of Cardiology* 1992;19:704-711.

77. Laster SB, Shelton TJ, Barzilai B, et al. Determinants of the recovery of right ventricular performance following experimental chronic right coronary artery occlusion. *Circulation* 1993;88:696-708.
78. Laster SB, Ohnishi Y, Saffitz JE, et al. Determinants of the recovery of right ventricular dysfunction: disparate mechanisms of benefit related to duration of ischaemia. *Circulation* 1994;90:1398-1409.
79. Goldstein JA, Harada A, Yagi Y, et al. Haemodynamic importance of systolic ventricular interaction, augmented right atrial contractility and atrioventricular synchrony in acute right ventricular dysfunction. *Journal of the American College of Cardiology* 1990;16:181-189.
80. Goldstein JA, Tweddell JS, Barzilai B, et al. Right atrial ischaemia exacerbates haemodynamic compromise associated with experimental right ventricular dysfunction. *Journal of the American College of Cardiology* 1991;18:1564-1572.
81. Mehta SR, Eikelboom JW, Natarajan MK et al. Impact of right ventricular involvement on mortality and morbidity in patients with inferior myocardial infarction. *Journal of the American College of Cardiology* 2001;37:37-43.
82. Zehender M, Kasper W, Kauder E et al. Right ventricular infarction as an independent predictor of prognosis after acute inferior myocardial infarction. *New England Journal of Medicine* 1993;328:981-988.
83. Marmor A, Geltman EM, Biello DR, et al. Functional response of the right ventricle to myocardial infarction: dependence of the site of left ventricular infarction. *Circulation* 1981;64:1005-1011.
84. Mueller RL, Sanborn TA. The history of interventional cardiology: cardiac catheterisation, angioplasty, and related interventions. *American Heart Journal* 1995;129:146-172.

85. Cournand A. Cardiac catheterisation; development of the technique, its contributions to experimental medicine, and its initial applications in man. *Acta Medicine Scandinavia Supplement* 1975;579:3-32.
86. Forssmann W. Sondierung des rechten Herzens. *Klin Wochenschr* 1929;8:2085.
87. Cournand A, Riley RL, Breed ES, et al. Measurement of cardiac output in man using the technique of catheterisation of the right auricle or ventricle. *Journal of Clinical Investigation* 1945;24:106-116.
88. Krishnamoorthy VK, Sengupta PP, Gentile F, et al. History of echocardiography and its future applications in medicine. *Critical Care Medicine* 2007; 35: S309-S313.
89. Edler I, Lunstorm K. History of echocardiography. *Ultrasound in Medicine and Biology* 2004;30:1565-1644.
90. Feigenbaum H, Popp RL, Chip JN, et al. Left ventricular wall thickness measured by Ultrasound. *Archives of Internal Medicine* 1968; 121: 391.
91. Feigenbaum H, Popp RL, Wolfe SB, et al. Ultrasound measurements of the left ventricle: A correlative study with angiocardiography. *Archives of Internal Medicine* 1972; 129: 461.
92. Feigenbaum H, Wolfe SB, Popp RL, et al. Correlation of ultrasound with angiocardiography in measuring left ventricular diastolic volume. *American Journal of Cardiology* 1969; 23: 11.
93. Feigenbaum H, Zaky A, Nasser WK. Use of ultrasound to measure left ventricular stroke volume. *Circulation* 1967; 35: 1092.
94. Blumgart HL, Yens OC. Studies on the velocity of blood flow: 1. The method utilised. *Journal of Clinical Investigation* 1927;4:1-13.

95. Love WD. Isotope technics in clinical cardiology. *Circulation* 1965;32:309-315.
96. Bisi G, Sciagra R, Santoro GM, et al. Myocardial scintigraphy with tc-99m-teboroxime: its feasibility and the evaluation of its diagnostic reliability. A comparison with thallium-201 and coronary angiography. *Giornale Italiano di Cardiologia* 1992;22:795-805.
97. Roguin A. Nikola Tesla; the man behind the magnetic field unit. *Journal of Magnetic Resonance Imaging* 2003;21:1019-1022.
98. Bloch F, Hanson W, Packard M. Nuclear infraction. *Physics Review* 1946;69:127.
99. Purcell E, Torrey H, Pound R. Resonance absorption by nuclear magnetic moments in a solid. *Physics Review* 1946;69:37-38.
100. Lauterbur PC. Image formation by induced local interactions: examples of employing nuclear magnetic resonance. *Nature* 1973;242:190-191.
101. Mansfield P, Grannell PK. NMR "diffraction" in solids? *Journal of Physics C: Solid State Physics* 1973;6:L422-426.
102. Geva T. Magnetic resonance imaging: Historical perspective. *Journal of cardiovascular magnetic resonance* 2006;8: 573-580.
103. Rinck PA. A short history of magnetic resonance imaging. *Spectroscopy Europe* 2008;20:7-9.
104. Goldman M, Pohost G, Ingwall S, et al. Nuclear magnetic resonance imaging: potential cardiac applications. *American Journal of Cardiology* 1980;46:1278-83.

- 105.Hawkes R, Holland G, Moore W, et al. Nuclear magnetic resonance (NMR) tomography of the normal heart. *Journal of Computer Assisted Tomography* 1981;5:605-12.
- 106.Heidelberger E, Petersen S, Lauterbur P. Aspects of cardiac diagnosis using synchronized NMR imaging. *European Journal Radiology* 1983;3:S281-S285.
- 107.Hurlock GS, Higashino H, Mochizuki T. History of cardiac computed tomography: single to 320-detector row multislice computed tomography. *International Journal of Cardiovascular Imaging* 2009;25: S31-S42.
- 108.Siemens Medical solutions. Computed Tomography: It's history and technology. Available at:www.medical.siemens.com/siemens/en_US/gg.ct.FBA./files/brochures/CT.history_and_technology.pdf
- 109.Brodoefel H, Kramer U, Reimann A, et al Dual-source CT with improved temporal resolution in assessment of left ventricular function: a pilot study. *American Journal of Roentgenology* 2007;189:1064-1070.
- 110.Health Protection Agency for the Administration of Radioactive Substances Advisory Committee, Nov 2010. A Review of the supply of Molybdenum-99, the impact of recent shortages and the implications for Nuclear Medicine Services. Report available online at: www.arsac.org.uk
- 111.Gibbons RJ, Araoz PA, Williamson EE. The Year in Cardiac Imaging. *Journal of the American College of Cardiology* 2009;53:54-70.
- 112.Metcalf MJ (2005). Ch 9: The Cardiovascular System. Sharp PF, Gemmell HG, Murray AD:*Practical Nuclear Medicine (third Edition)*. London;Springer-Verlag Limited
- 113.Quinones MA, Otto CM, Stoddard M, et al. Recommendations for quantification of Doppler echocardiography: a report on the Doppler Quantification Task Force of the

- Nomenclature and Standards Committee of the American Society of Echocardiography. *Journal of the American Society of Echocardiography* 2002;15:167-84.
114. Brophy JM, Dagenais GR, McSherry F, et al. A multivariate model for predicting mortality in patients with heart failure and systolic function. *American Journal of Medicine* 2004;116:300-304.
115. SOLVD Investigators. Effect of Enalapril on mortality and the development of heart failure in asymptomatic patients with reduced left ventricular ejection fractions. *New England Journal of Medicine* 1992;327:685-691.
116. SOLVD Investigators. Effect of Enalapril on survival patients with reduced left ventricular ejection fractions and congestive heart failure. *New England Journal of Medicine* 1991;325:293-302.
117. The CONSENSUS Trial group. Effects of enalapril on mortality in severe congestive heart failure: results of the Cooperative North Scandinavian Enalapril Survival Study (CONSENSUS). *New England Journal of Medicine* 1987;316:1429-1435.
118. The Acute Infarction Ramipril Efficiency (AIRE) Study Investigators. Effect of ramipril on mortality and morbidity of survivors of acute myocardial infarction with clinical evidence of heart failure. *Lancet* 1993;342:821-828.
119. Pfeffer MA, Braunwald E, Moye LA, et al, for the SAVE Investigators. Effect of captopril on mortality and morbidity in patients with left ventricular dysfunction after myocardial infarction: results of the survival and Ventricular Enlargement Trial (SAVE). *New England Journal of Medicine* 1992;327:669-677.
120. Chinese Cardiac Study Collaborative Group. Oral captopril versus placebo among 13634 patients with suspected acute myocardial infarction: interim report from the Chinese Cardiac Study (CCS-1). *Lancet* 1995;345:686-687.

121. CIBIS II Study Group. The Cardiac Insufficiency Bisoprolol Study II (CIBIS II): a randomised clinical trial. *Lancet* 1999;353:9-13.
122. MERIT-HF Study Group. Effect of metoprolol CR/XL in chronic heart failure: Metoprolol CR/XL Randomised Intervention Trial in Congestive Heart Failure (MERIT-HF). *Lancet* 1999;353:2001-2007.
123. Packer M, Coats A, Fowler M, et al. Effect of carvedilol on survival in severe chronic heart failure. *New England Journal of Medicine* 2001;334:1651-1658.
124. Poole-Wilson PA, Swedberg K, Cleland JGF, et al. Comparison of carvedilol and metoprolol on clinical outcomes in patients with chronic heart failure in the Carvedilol Or Metoprolol European Trial (COMET): randomised controlled trial. *Lancet* 2003;362:7-13.
125. Pitt B, Zannad F, Remme W, et al. The effect of spironolactone on morbidity and mortality in patients with severe heart failure. *New England Journal of Medicine* 1999;341:709-717.
126. Pitt B, Remme W, Zannad F, et al; Eplerenone Post-Acute Myocardial Infarction Heart Failure Efficacy and Survival (EPHESUS) Study Investigators. Eplerenone, a selective aldosterone blocker, in patients with left ventricular dysfunction after myocardial infarction. *New England Journal of Medicine* 2003;348:2271.
127. American College of Cardiology and American Heart Association Task Force on Practice Guidelines, developed in collaboration with the Society of Cardiovascular Anaesthesiologists, endorsed by the Society for Cardiovascular Angiography and Interventions and the Society of Thoracic Surgeons. ACC/AHA 2006 Guidelines for the management of patients with valvular heart disease. *Journal of the American College of Cardiology* 2006;48:e1-e148.

128. Abraham WT, Fisher WG, Smith AL, et al. Cardiac resynchronisation in chronic heart failure: The Multicentre InSync Randomised Clinical Evaluation. *New England Journal of Medicine* 2002;346:1845-1853.
129. Auricchio A, Stellbrink C, Sack F, et al. The Pacing Therapies for Congestive Heart Failure (PATH-CHF) study: rationale, design and end-points of a prospective randomized multicentre study. *American Journal of Cardiology* 1999;83:130D-135D.
130. Cazeau S, Leclercq C, Lavergne T, et al. Effects of multisite biventricular pacing in patients with heart failure and intraventricular conduction delay. The Multisite Stimulation in Cardiomyopathies (MUSTIC) Study Investigators. *New England Journal of Medicine* 2001;344:873-880.
131. Linde C, Leclercq C, Rex S, et al. Long term benefits of biventricular pacing in congestive. Results from the multisite stimulation in cardiomyopathy (MUSTIC) study. *Journal of the American College of Cardiology* 2002;40:111-118.
132. Abraham WT, Young JB, Smith AL, et al. Combined cardiac resynchronization and implantable cardioverter defibrillator in advanced chronic heart failure: The MIRACLE-ICD trial. *Circulation* 2004;110:2864-2868.
133. Higgins SL, Hummel JD, Niazi IK et al. Cardiac resynchronization therapy for the treatment of heart failure in patients with intraventricular conduction delay and malignant ventricular tachyarrhythmias. *Journal of the American College of Cardiology* 2003;42:1454-1459.
134. Bristow MR, Saxon LA, Boehmer J, et al. Cardiac-Resynchronisation Therapy with or without an Implantable Defibrillator in Advanced Chronic Heart Failure. *New England Journal of Medicine* 2004;350:2140-2150.

135. Cleland J, Daubert JC, Erdmann E, et al. The Effect of Cardiac Resynchronisation on Morbidity and Mortality in Heart Failure. *New England Journal of Medicine* 2005;352:1539-1549.
136. National Institute for Health and Clinical Excellence (NICE) technology appraisal guidance 120. Cardiac resynchronisation therapy for the treatment of heart failure. May 2007. Available at <http://guidance.nice.org.uk/TA120/niceguidance/pdf/English>.
137. The Antiarrhythmics versus Implantable Defibrillators (AVID) Investigators. A comparison of anti-arrhythmic-drug therapy with implantable defibrillators in patients resuscitated from near fatal ventricular arrhythmias. *New England Journal of Medicine* 1997;337:1576-1583.
138. Goldenberg I, Moss AJ, Zareba W, et al; MADIT-II Investigators. Time dependence of defibrillator benefit after coronary revascularization in the Multicentre Automatic Defibrillator Implantation Trial (MADIT)-II. *Journal of the American College of Cardiology* 2006;47:1811-1817
139. National Institute for Health and Clinical Excellence (NICE) technology appraisal guidance 95. Implantable cardioverter defibrillators for the treatment of arrhythmias. January 2006. Available at <http://guidance.nice.org.uk/TA95/niceguidance/pdf/English>.
140. Jones AL, Barlow M, Barrett-Lee PJ, et al. Management of cardiac health in trastuzumab-treated patients with breast cancer; updated United Kingdom National Cancer Research Institute recommendations for monitoring. *British Journal of Cancer* 2009;100:684-692.
141. Anderson B (2000). Ch 9: Two-dimensional echocardiographic measurements and calculations. *Echocardiography: The normal examination and echocardiographic measurements* (pp 87-104). Queensland, Australia: MGA graphics.

- 142.Thomson HL, Basmadjian AJ, Rainbird AJ, et al. Contrast echocardiography improves the accuracy and reproducibility of left ventricular remodelling measurements: A prospective, randomly assigned, blinded study. *Journal of the American College of Cardiology* 2001;38:867-875.
- 143.Jacobs LD, Salgo IS, Goonewardena S, et al. Rapid online quantification of left ventricular volume from real-time three-dimensional echocardiographic data. *European Heart Journal* 2006;27:460-468.
- 144.Kuhl HP, Schreckenber M, Rulands D, et al. High resolution transthoracic real-time three dimensional echocardiography – Quantification of cardiac volumes and function using semi-automated border detection and comparison with cardiac magnetic resonance imaging. *Journal of the American College of Cardiology* 2004; 43:2083-2090.
- 145.Kim WY, Sogaard P, Kristensen BO, et al. Measurement of left ventricular volumes by 3-dimensional echocardiography with tissue harmonic imaging: a comparison with magnetic resonance imaging. *Journal of the American Society of Echocardiography* 2001;14:169-179.
- 146.Bu L, Munns S, Zang H et al. Rapid full volume data acquisition by real-time 3-dimensional echocardiography for assessment of left ventricular indexes in children: a validation study compared with magnetic resonance imaging. *Journal of the American Society of Echocardiography* 2005;18:299-305.
- 147.Jenkins C, Bricknell K, Hanekom L et al. Reproducibility and accuracy of echocardiographic measurements of left ventricular parameters using real-time three dimensional echocardiography. *Journal of the American College of Cardiology* 2004;44:878-886.
- 148.Miller C, Pearce K, Jordan P, et al. Comparison of real time 3D echocardiography and CMR for left ventricular volume assessment in unselected patients. *European Journal of Cardiovascular Imaging* 2012;13:187-195.

149. Bellenger NG, Burgess MI, Ray SG, et al. Comparison of left ventricular ejection fraction and volumes in heart failure by echocardiography, radionuclide ventriculography and cardiovascular magnetic resonance: Are they interchangeable? *European Heart Journal* 2000;21:1387-1396.
150. Gardner BI, Bingham SE, Allen MR, et al. Cardiac magnetic resonance versus transthoracic echocardiography for the assessment of cardiac volumes and regional function after myocardial infarction: an intrasubject comparison using simultaneous intrasubject recordings. *Cardiovascular Ultrasound* 2009; 7: 38 doi: 10.1186/1476-7120-7-38.
151. Chuang ML, Hiberd MG, Salton CJ, et al. Importance of imaging method over imaging modality in non-invasive determination of left ventricular volumes and ejection fraction: Assessment by two- and three-dimensional echocardiography and magnetic resonance imaging. *Journal of the American College of Cardiology* 2000; 35: 477-484.
152. Sakuma H, Globits S, Bourne MW, et al. Improved reproducibility in measuring LV volumes and mass using multicoil breath-hold cine MR imaging. *Journal of Magnetic Resonance Imaging* 2005;6:124-127.
153. De Ferrari GM, Petracci B, Frattini, et al. Long term effects of aggressive rhythm control strategy in patients with permanent atrial fibrillation and advanced heart failure. *Heart Rhythm* 2005;2:S116.
154. Hebbar AK, Hueston WJ. Management of common arrhythmias: Part II. Ventricular arrhythmias and arrhythmias in special populations. *American Family Physician* 2002;65:2491-2497.
155. Anter E, Jessup M, Callans DJ. Atrial fibrillation and heart failure: treatment considerations for a dual epidemic. *Circulation* 2009;119:2516-2525.

156. Cunningham D, Charles R, Cunningham M, et al. Heart Rhythm Devices: UK National Survey 2009. Available online at: <http://www.agwscs.nhs.uk/files/heart20rhythm20device20national20report>.
157. Doppler CJ (1988). Über das farbige Licht der Doppelsterne und einige andere Gestirne des Himmels. Reprinted in: *Christian Doppler, Leben und Werk. Der Dopplereffekt*. Amt der Salzburger Landesregierung,
158. Price DJA, Wallbridge DR, Stewart MJ. Tissue Doppler imaging: current and potential clinical applications. *Heart* 2000;84:ii11-ii18.
159. Sengupta PP, Jagdish CM, Pandion NG. Tissue Doppler echocardiography: Principles and applications. *Indian Heart Journal* 2002; 54: 368-378.
160. Galiuto L, Ignone G, DeMaria AN. Contraction and relaxation velocities of the normal left ventricle using pulsed-wave tissue Doppler echocardiography. *American Journal of Cardiology* 1998;81:609-614.
161. D'Hooge J, Heimdal A, Jamal F, et al. Regional strain and strain rate measurements by cardiac ultrasound: Principles, implementation and limitations. *European Journal of Echocardiography* 2000;1:154-170.
162. Dandel M, Lehmkuhl H, Knosalla C, et al. Strain and strain rate imaging by echocardiography – basic concepts and clinical applicability. *Current Cardiology Reviews* 2009;5:133-148.
163. Rabben SI, Irgens F, Haukanes A, et al. An analysis of the angle dependence in strain (rate) imaging of the left ventricle. *Ultrasonics* 2003;1:13-16.
164. Schuster P, Faerestrød S. Techniques for identification of left ventricular asynchrony for cardiac resynchronization therapy in heart failure. *Indian Pacing and Electrophysiology* 2005;5:175-185.

- 165.Boettler P, Claus P, Herbots L, et al. An echocardiographic study: New aspects of the ventricular septum and its function. *Heart* 2005;91:1343-1348.
- 166.Edvardsen T, Gerber BL, Garot J, et al. Quantitative assessment of intrinsic regional myocardial deformation by Doppler strain rate echocardiography in humans: Validation against three-dimensional tagged magnetic resonance imaging. *Circulation* 2002;106:50-56.
- 167.Zaglavara T, Pillay T, Karvounis H, et al. Detection of myocardial viability by dobutamine stress echocardiography: incremental value of diastolic wall thickness measurement. *Heart* 2005;91:613-617.
- 168.Abhayaratna WP, Marwick TH, Smith WT, et al. Characteristics of left ventricular diastolic dysfunction in the community: An echocardiographic survey. *Heart* 2006;92:1259-1264.
- 169.Owan TE, Hodge DO, Herges RM, et al. Trends in prevalence and outcome of heart failure with preserved ejection fraction. *New England Journal of Medicine* 2006;355:251-259.
- 170.Paulus WJ, Tschope C, Sanderson JE, et al. How to diagnose diastolic heart failure: a consensus statement on the diagnosis of heart failure with normal left ventricular ejection fraction by the Heart Failure and Echocardiographic Associations of the European Society of Cardiology. *European Heart Journal* 2007;28:2539-2550.
- 171.Owan TE, Redfield MM. Epidemiology of diastolic heart failure. *Prognosis of Cardiovascular Disease* 2005;47:320-332.
- 172.Bhatia RS, Tu JV, Lee DS, et al. Outcome of heart failure with preserved ejection fraction in a population based study. *New England Journal of Medicine* 2006;355:260-269.

173. Aurigemma P. Diastolic heart failure – a common and lethal condition by any name. *New England Journal of Medicine* 2006;355:308-310.
174. Grossman W. Diastolic function and congestive heart failure. *Circulation* 1990;81:Suppl III:III-1-7.
175. Hadano Y, Murata K, Yamamoto T, et al. Usefulness of mitral annular velocity in predicting exercise tolerance in patients with impaired left ventricular systolic function. *American Journal of Cardiology* 2006;97:1025-1028.
176. Skaluba SJ, Litwin SE. Mechanisms of exercise intolerance. Insights from tissue Doppler imaging. *Circulation* 2004;109:972-977.
177. Somaratne JB, Whalley GB, Gamble GD, et al. Restrictive filling pattern is a powerful predictor of heart failure events post acute myocardial infarction and in established heart failure: a literature based meta-analysis. *Journal of Cardiac Failure* 2007;13:346-52.
178. Rossi A, Ciccoira M, Folia G, et al. Amino-terminal propeptide of type III procollagen is associated with restrictive mitral filling pattern in patients with dilated cardiomyopathy: a possible link between diastolic dysfunction and prognosis. *Heart* 2004;90:650-4.
179. Hansen A, Haass M, Zugck C, et al. Prognostic value of Doppler echocardiographic mitral inflow patterns: Implications for risk stratification in patients with congestive heart failure. *Journal of the American College of Cardiology* 2001;37:1049-1055.
180. Whalley GA, Doughty RN, Gamble GD, et al. Pseudonormal mitral filling pattern predicts hospital re-admission in patients with congestive heart failure. *Journal of the American College of Cardiology* 2002;39:1787-95.

- 181.Zile MR, Brutsaert DL. New concepts in diastolic dysfunction and diastolic heart failure: Part 1: diagnosis, prognosis and measurements of diastolic function. *Circulation* 2002;105:1387-1393.
- 182.Zile MR, Brutsaert DL. New concepts in diastolic dysfunction and diastolic heart failure: Part 2: causal mechanisms and treatment. *Circulation* 2002;105:1503-1508.
- 183.Keogh AM, Baron DW, Hieke JB. Prognostic guides in patients with idiopathic or ischemic dilated cardiomyopathy for cardiac transplantation. *American Journal of Cardiology* 1990;65:903-908.
- 184.Stevenson WG, Stevenson LW, Middlekauff HR, et al, for the ESCAPE Investigators and ESCAPE Study Coordinators. Evaluation study of congestive heart failure and pulmonary artery catheterization effectiveness:the ESCAPE trial. *Journal of the American Medical Association* 2005;294:1625-1633.
- 185.Haskell RJ, French WI. Accuracy of left atrial and pulmonary artery wedge pressure in pure mitral regurgitation in predicting ventricular end-diastolic pressure. *American Journal of Cardiology* 1988;136-141.
- 186.Weiner RS, Welch HG. Trends in the use of the pulmonary artery catheter in the United States 1993-2004. *Journal of the American Medical Association* 2007;298:423-429.
- 187.Zile MR, Baicu CF, Gaasch WH. Diastolic heart failure – abnormalities in active relaxation and passive stiffness of the left ventricle *New England Journal of Medicine* 2004;350:1953-1959.
- 188.Rimmington H, Chambers J (1998). Ch 1: The left ventricle. *Echocardiography: A practical guide for reporting* (pp 1-14). London, New York: The Parthenon publishing group limited.

189. Nishimura RA, Tajik AJ. Evaluation of diastolic filling of the left ventricle in health and disease. *Journal of the American College of Cardiology* 1997;30:8-18.
190. Yamamoto K, Nishimura RA, Redfield MM. Assessment of mean left atrial pressure from the left ventricular pressure tracing in patients with cardiomyopathies. *American Journal of Cardiology* 1996;78:107-10.
191. Yamamoto K, Nishimura RA, Chaliki HP, et al. Determination of left ventricular filling pressure by Doppler echocardiography in patients with coronary artery disease: critical role of left ventricular systolic function. *Journal of the American College of Cardiology* 1997;30:1819-26.
192. Nishimura RA, Appleton CP, Redfield MM, et al. Noninvasive Doppler echocardiographic evaluation of left ventricular filling pressures in patients with cardiomyopathies: a simultaneous Doppler echocardiographic and cardiac catheterization study. *Journal of the American College of Cardiology* 1996;28:1226-33.
193. Alam M, Wardell J, Andersson E, et al. Effects of first myocardial infarction on left ventricular systolic and diastolic function with the use of mitral annular velocity determined by pulsed wave Doppler tissue imaging. *Journal of the American Society of Echocardiography* 2000;13:343-52.
194. Paelinck BP, de Roos A, Bax JJ, et al. Feasibility of tissue magnetic resonance imaging: a pilot study in comparison with tissue Doppler imaging and invasive measurement. *Journal of the American College of Cardiology* 2005;45:1109-1116.
195. Abali G, Tokgozoglu L, Ozcebe OI, et al. Which Doppler parameters are load independent? A study in normal volunteers after blood donation. *Journal of the American Society of Echocardiography* 2005;18:1260-1266.

- 196.Olsen NT, Jons C, Fritz-Hansen T, et al. Pulsed-wave tissue Doppler and colour tissue Doppler echocardiography: calibration with M-Mode agreement and reproducibility in a clinical setting. *Echocardiography* 2009;26:638-644.
- 197.Sohn DW, Chai IH, Lee DJ et al. Assessment of mitral annulus velocity by Doppler tissue imaging in the evaluation of left ventricular diastolic function. *Journal of the American College of Cardiology* 1997;30:474-480.
- 198.Agricola E, Galderisi M, Oppizzi M, et al. Doppler tissue imaging: A reliable method for estimation of left ventricular filling pressure in patients with mitral regurgitation. *American Heart Journal* 2005;150:610-615.
- 199.Bruch C, Stypmann J, Gradaus R, et al. Usefulness of tissue Doppler imaging for estimation of filling pressures in patients with primary or secondary mitral regurgitation. *American Journal of Cardiology* 2004;93:324-328.
- 200.Rivas-Gotz C, Manolios M, Thohan V, et al. Impact of left ventricular ejection fraction on estimation of left ventricular filling pressures using tissue Doppler and flow propagation velocity. *The American Journal of Cardiology* 2003;91:780-784.
- 201.Little WC, Oh JK. Echocardiographic evaluation of diastolic function can be used to guide clinical care. *Circulation* 2009;120:802-809.
- 202.Cheng CP, Freeman GL, Santamore WP, Constantinescu MS, Little WC. Effect of loading conditions, contractile state and heart rate on early diastolic left ventricular filling in conscious dogs. *Circulation Research* 1990;66:814-823.
- 203.Rovner A, Greenberg N, Thomas JD, et al. Relationship of diastolic intraventricular pressure gradients and aerobic capacity in patients with heart failure. *American Journal of Physiology. Heart and Circulatory Physiology* 2005;289:H2081-H2088.

- 204.Hasegawa H, Little WC, Ohno M, et al. Diastolic mitral annular velocity during the development of heart failure. *Journal of the American College of Cardiology* 2003;41:1590-1597.
- 205.Oh JK, Tajik J. The return of cardiac time intervals: the Phoenix is rising. *Journal of the American College of Cardiology* 2003;42:1471-1474.
- 206.Lester SJ, Tajik AJ, Nishimura RA, et al. Unlocking the mysteries of diastolic function: Deciphering the Rosetta Stone 10 years later. *Journal of the American College of Cardiology* 2008;51:679-689.
- 207.Rivas-Gotz C, Khoury DS, Manolios M, et al. Time interval between onset of mitral inflow and onset of early diastolic velocity by tissue Doppler: a novel index of left ventricular relaxation: experimental studies and clinical application. *Journal of the American College of Cardiology* 2003;42:1463-1470.
- 208.Bruch C, Klem I, Breithardt G, et al. Diagnostic usefulness and prognostic implications of the mitral E/E' ratio in patients with heart failure and severe secondary mitral regurgitation. *American Journal of Cardiology* 2007;100:860-865.
- 209.Okhura H, Takada Y, Kubo T, et al. Tissue Doppler-derived index of left ventricular filling pressure, E/E', predicts survival of patients with non-valvular atrial fibrillation. *Heart* 2006;92:1248-52.
- 210.Wang M, Yip GW, Wang AY, et al. Peak early diastolic mitral annulus velocity by tissue Doppler imaging adds independent and incremental prognostic value. *Journal of American College of Cardiology* 2003;41:820-826.
- 211.Wang M, Yip GW, Wang AY, et al. Tissue Doppler imaging provides incremental prognostic value in patients with systemic hypertension and left ventricular hypertrophy. *Journal of Hypertension* 2005;23:183-91.

212. Yu CM, Sanderson JE, Marwick TH, et al. Tissue Doppler Imaging: A new prognosticator for cardiovascular diseases. *Journal of the American College of Cardiology* 2007;49:1903-1914.
213. Yamamoto T, Oki T, Yamada H, et al. Prognostic value of the atrial systolic mitral annular motion velocity in patients with left ventricular systolic dysfunction. *Journal of the American Society of Echocardiography* 2003;16:333-339.
214. Hillis GS, Moller Je, Pellikka PA, et al. Noninvasive estimation of left ventricular filling pressure by E/E' is a powerful predictor of survival after acute myocardial infarction. *Journal of the American College of Cardiology* 2004;43:360-367.
215. Buchalter MB, Weiss JL, Rogers WJ, et al. Noninvasive quantification of left ventricular rotational deformation in normal humans using magnetic resonance imaging myocardial tagging. *Circulation* 1990;81:1236-1244.
216. Osman NF, Kerwin WS, McWeigh ER, et al. Cardiac motion tracking using CINE harmonic phase (HARP) magnetic resonance imaging. *Magnetic Resonance in Medicine* 1999;42:1048-1060.
217. Aletra AH, Ding S, Balaban RS, et al. DENSE: displacement encoding with stimulated echoes in cardiac functional MRI. *Journal of Magnetic Resonance Imaging* 1999;137:247-252.
218. Korosoglou G, Youssef AA, Bilchick KC, et al. Real-time fast strain-encoded magnetic resonance imaging to evaluate regional myocardial function at 3.0 Tesla: comparison to conventional tagging. *Journal of Magnetic Resonance Imaging* 2008;27:1012-1018.
219. Garot J. The study of diastole by tagged MRI: are we nearly there yet? *European Heart Journal* 2004;25:1376-1377.

220. Dong SJ, Hees PS, Siu CO, et al. MRI assessment of LV relaxation by untwisting rate: a new isovolumic phase measure of tau. *American Journal of Physiology Heart and Circulatory Physiology* 2001;281:H2002-2009.
221. Westenberg JJM. CMR for assessment of diastolic function. *Current Cardiovascular Imaging Reports* 2011;4:149-158.
222. Azevedo CF, Amado LC, Kraitchman DL, et al. Persistent diastolic dysfunction despite complete systolic functional recovery after reperfused acute myocardial infarction demonstrated by tagged magnetic resonance imaging. *European Heart Journal* 2004;25:1419-27.
223. Paelink BP, Lamb HJ, Bax J, et al. Assessment of diastolic function by cardiovascular magnetic resonance. *American Heart Journal* 2002;144:198-205.
224. Rathi VK, Doyle M, Yamrozik J, et al. Routine evaluation of left ventricular diastolic function by cardiovascular magnetic resonance: A practical approach. *Journal of Cardiovascular Magnetic Resonance* 2008;10:36 doi:10.1186/1532-429x-10-36.
225. Rubinstein R, Glockner JF, Feng D, et al. Comparison of magnetic resonance imaging versus Doppler echocardiography for the evaluation of left ventricular diastolic function in patients with cardiac amyloidosis. *American Journal of Cardiology* 2009;103:718-723.
226. Braunwald E (1997). Ch 6: Cardiac Catheterisation. *Heart disease: A textbook of Cardiovascular Medicine* (pg 177-203). Philadelphia, Pennsylvania, USA: W. B. Saunders Company.
227. Nagueh SF, Rao L, Soto J, et al. Haemodynamic insights into the effects of ischaemia and cycle length on tissue Doppler-derived mitral annulus diastolic velocities. *Clinical Science* 2004;106:147-54.

228. Ha JW, Oh JK, Ling LH, et al. Annulus paradoxus: transmitral flow velocity to mitral annual velocity ratio is inversely proportional to pulmonary capillary wedge pressure in patients with constrictive pericarditis. *Circulation* 2001;104:976-978.
229. Masutani S, Little WC, Hasegawa H, et al. Restrictive left ventricular filling pattern does not result from increased left atrial pressure alone. *Circulation* 2008;117:1550-1554.
230. Lindqvist P, Calcuttea A, Henein M. Echocardiography in the assessment of right heart function. *European Journal of Echocardiography* 2008;9:225-234.
231. Baker BJ, Wilen MM, Boyd CM, et al. Relation of right ventricular ejection fraction to exercise capacity in chronic heart failure. *American Journal of Cardiology* 1984;54:596-599.
232. Burgess MI, Mogulkoc N, Bright-Thomas RJ, et al. Comparison of echocardiographic markers of right ventricular function in determining prognosis in chronic pulmonary disease. *Journal of the American Society of Echocardiography* 2002;15:633-639.
233. Burgess MI, Bright-Thomas RJ, Ray SG. Echocardiographic evaluation of right ventricular function. *European Journal of Echocardiography* 2002;3:252-262.
234. Mendes LA, Dec GW, Picard MH, et al. Right ventricular dysfunction: an independent predictor of adverse outcome in patients with myocarditis. *American Heart Journal* 1994;128:301-307.
235. Ghio S, Gavazzi A, Campana C, et al. Independent and additive prognostic value of right ventricular systolic function and pulmonary artery pressure in patients with chronic heart failure. *Journal of the American College of Cardiology* 2001;37:183-188.

236. Nath J, Vacek JL, Heidenreich PA. A dilated inferior vena cava is a marker of poor survival. *American Heart Journal* 2006;151:730-735.
237. Kramer CM, Barkhausen J, Flamm SD, et al. Standardised cardiovascular magnetic resonance (CMR) protocols, Society for Cardiovascular Magnetic Resonance; Board of Trustees task force on standardised protocols. *Journal of Cardiovascular Magnetic Resonance* 2008;10:35 doi:10.1186/1532-429X-10-35.
238. Strugnell WE, Slaughter RE, Riley RA, et al. Modified RV short axis series – a new method for cardiac MRI measurement of right ventricular volumes. *Journal of Cardiovascular Magnetic Resonance* 2005;7:769-774.
239. Tamborini G, Marsan NA, Gripari P, et al. Reference values for right ventricular volumes and ejection fraction with real-time three-dimensional echocardiography: evaluation in a large series of normal subjects. *Journal of the American Society of Echocardiography* 2010;23:109-115.
240. Van der Zwaan HB, Meijboom FJ, McGhie JS, et al. Sources of difference in volumetric RV estimation using a 9 segment model: Real time three-dimensional echocardiography versus cardiac magnetic resonance. *European Journal of Echocardiography* 2010;11(S2):ii155-ii157.
241. Shimada YJ, Shiota M, Siegel RJ, et al. Accuracy of right ventricular volumes and function determined by three-dimensional echocardiography in comparison with magnetic resonance imaging: a meta-analysis study. *Journal of the American Society of Echocardiography* 2010;23:943-953.
242. Leibundgut G, Rohner A, Grize L, et al. Dynamic assessment of right ventricular volumes and function by real-time three-dimensional echocardiography: A comparison study with magnetic resonance imaging in 100 adult patients. *Journal of the American Society of Echocardiography* 2010;23:116-126.

- 243.Kjaergaard J, Petersen CL, Kjaer A et al. Evaluation of right ventricular volume and function by 2D and 3D echocardiography compared to MRI. *European Journal of Echocardiography* 2006;7:430-438.
- 244.Miller D, Farah MG, Liner A, et al. The Relation between qualitative right ventricular ejection fraction and indices of tricuspid annular motion and myocardial performance. *Journal of American Society of Echocardiography* 2004;17:443-447.
- 245.Kaul S, Tei C, Hopkins JM, et al. Assessment of right ventricular function using two-dimensional echocardiography. *American Heart Journal* 1984;107:526-531.
- 246.Vogel M, Schmidt MR, Kristiansen SB, et al. Validation of myocardial acceleration during isovolumic contraction as a novel non-invasive index of right ventricular contractility: Comparison with ventricular pressure-volume relations in an animal model. *Circulation* 2002;105:1693-1699.
- 247.Anavekar NS, Gerson D, Skali H, et al. Two-dimensional assessment of right ventricular function: An echocardiographic-MRI correlative study. *Echocardiography* 2007;24:452-456.
- 248.Morcos P, Wesley Vick G III, Sahn DJ, et al. Correlation of right ventricular ejection fraction and tricuspid annular plane systolic excursion in tetralogy of Fallot by magnetic resonance imaging. *International Journal of Cardiovascular Imaging* 2009;25:263-270.
- 249.Helbing WA, Bosch HG, Maliepaard C, et al. Comparison of echocardiographic methods with magnetic resonance imaging for assessment of right ventricular function in children. *American Journal of Cardiology* 1995;76:589-594.
- 250.Schwerzmann M, Samman AM, Salehian O, et al. Comparison of echocardiographic and cardiac magnetic resonance imaging for assessing right ventricular function in adults with repaired tetralogy of Fallot. *American Journal of Cardiology* 2007;99:1593-1597.

251. Vogel M, Derrick G, White PA, et al. Systemic ventricular function in patients with transposition of the great arteries after atrial repair; a tissue Doppler and conductance catheter study. *Journal of the American College of Cardiology* 2004;43:100-106.
252. Grover SK, Leong DP, Molaee P, et al. Validation of echocardiographic indices of right ventricular systolic function with cardiac magnetic resonance: a comparative study. *Journal of Cardiovascular Magnetic Resonance* 2011 doi:10.1186/1532-429X-13-S1-075.
253. Tei C, Dujardin KS, Hodge DO, et al. Doppler echocardiographic index for assessment of global right ventricular function. *Journal of the American Society of Echocardiography* 1996;9:838-847.
254. Meluzin J, Spinarova L, Dusek L et al. Prognostic importance of the right ventricular function assessed by Doppler tissue imaging. *European Journal of Echocardiography* 2003;4:262-271.
255. Meluzin J, Spinarova L, Hude P et al. Prognostic importance of various echocardiographic right ventricular functional parameters in patients with symptomatic heart failure. *Journal of the American Society of Echocardiography* 2005;18:435-444.
256. Lai WW, Gauvreau K, Rivera ES, et al. Accuracy of guideline recommendations for two-dimensional quantification of the right ventricle by echocardiography. *International Journal of Cardiovascular Imaging* 2008;24:691-698.
257. Spencer KT, Kirkpatrick JN, Mor-Avi V, et al. Age dependency of the Tei index of myocardial performance. *Journal of the American Society of Echocardiography* 2004;17:350-352.

- 258.Lax JA, Bermann AM, Cianciulli TF, et al. Estimation of the ejection fraction in patients with myocardial infarction obtained from the combined index of systolic and diastolic left ventricular function: A new method. *Journal of the American Society of Echocardiography* 2000;13:116-123.
- 259.Moller JE, Sondergaard E, Poulson SH, et al. Serial Doppler echocardiographic assessment of left and right ventricular performance after a first myocardial infarction. *Journal of the American Society of Echocardiography* 2001;14:249-255.
- 260.Parthenakis FI, Kanakaraki MK, Kanoupakis EM, et al. Value of Doppler index combining systolic and diastolic myocardial performance in predicting cardiopulmonary exercise capacity in patients with congestive heart failure: effects of dobutamine. *Chest* 2002;121:1935-1941.
- 261.Tei C, Dujardin KS, Hodge DO, et al. Doppler index combining systolic and diastolic myocardial performance: Clinical value in cardiac amyloidosis. *Journal of the American Society of Echocardiography* 1996;28:658-664.
- 262.Tei C, Nishimura RA, Seward JB, et al. Non-invasive Doppler-derived myocardial performance index: Correlation with simultaneous measurements of cardiac catheterisation measurements. *Journal of the American Society of Echocardiography* 1997;10:169-178.
- 263.LaCorte JC, Cabreriza SE, Rabkin DG, et al. Correlation of the Tei index with invasive measurements of ventricular function in a porcine model. *Journal of the American Society of Echocardiography* 2003;16:442-447.
- 264.Bruch C, Schmermund A, Marin D, et al. Tei index in patients with mild-moderate congestive heart failure. *European Heart Journal* 2000;21:1888-1895.
- 265.Caldas MC, Meira ZA, Barbosa MM. Evaluation of 107 patients with sickle cell anaemia through tissue Doppler and myocardial performance index. *Journal of the American Society of Echocardiography* 2008;2008:1163-1167.

- 266.Lavine SJ. Effect of heart rate and preload on index of myocardial performance in the normal and abnormal left ventricle. *Journal of the American Society of Echocardiography* 2005;18:133-141.
- 267.Ascione L, De Michele M, Accadia M, et al. Myocardial global performance index as a predictor of in-hospital cardiac events in patients with first myocardial infarction. *Journal of the American Society of Echocardiography* 2003;16:1019-1023.
- 268.Dujardin KS, Tei C, Yeo TC, Hodge Do, Rossi A, Seward JB. Prognostic value of a Doppler index combining systolic and diastolic performance in idiopathic dilated cardiomyopathy. *American Journal of Cardiology* 1998;82:1071-1076.
- 269.Lavine SJ. Index of myocardial performance is afterload dependent in the normal and abnormal left ventricle. *Journal of the American Society of Echocardiography* 2005;18:342-350
- 270.Yeo TC, Dujardin KS, Tei C, et al. Value of Doppler derived index combining systolic and diastolic time intervals in predicting outcome in primary pulmonary hypertension. *American Journal of Cardiology* 1998;81:1157-1161.
- 271.Chockalingam A, Gnanavelu G, Alagesan R, et al. Myocardial performance index in evaluation of acute right ventricular myocardial infarction. *Echocardiography* 2004;21:487-494.
- 272.Morner S, Lindqvist P, Waldenstrom A, et al. Right ventricular dysfunction in hypertrophic cardiomyopathy as evidenced by the myocardial performance index. *International Journal of Cardiology* 2008;124:57-63.
- 273.Eidem BW, O'Leary PW, Tei C, et al. Usefulness of the myocardial performance index for assessing right ventricular function in congenital heart disease. *American Journal of Cardiology* 2000;86:654-658.

274. Eidem BW, Tei C, O'Leary PW, et al. Non-geometric quantitative assessment of right and left ventricular function: Myocardial performance index in normal children and patients with Ebstein anomaly. *Journal of the American Society of Echocardiography* 1998;11:849-856.
275. Yoshifuku S, Otsuji Y, Takasaki K, et al. Pseudonormalised Doppler total ejection isovolume (Tei) index in patients with right ventricular acute myocardial infarction. *American Journal of Cardiology* 2003;91:527-531.
276. Petitjean C, Rougon N, Cluzel P. Assessment of myocardial function; a review of quantification methods and results using tagged MRI. *Journal of Cardiovascular Magnetic Resonance* 2005;7:501-516.
277. Weidemann F, Eyskens B, Jamal F et al. Quantification of regional and global radial and longitudinal function in healthy children using ultrasound-based strain rate and strain imaging. *Journal of the American Society of Echocardiography* 2002;15:20-28.
278. Jurcut R, Giusca S, La Gerche A, et al. The echocardiographic assessment of the right ventricle: what to do in 2010? *European Journal of Echocardiography* 2010;11:81-96.
279. Dambrauskaite V, Herbots L, Claus P et al. Differential changes in regional right ventricular function before and after a bilateral lung transplantation: an ultrasonic strain and strain rate study. *Journal of the American Society of Echocardiography* 2003;16:432-436.
280. Sevimli S, Gundogdu F, Aksakal E et al. Right ventricular strain and strain rate properties in patients with right ventricular myocardial infarction. *Echocardiography* 2007;24:656-663.

- 281.Sugiura E, Dohi K, Onishi K, et al. Reversible right ventricular regional non-uniformity quantified by speckle-tracking strain imaging in patients with acute pulmonary thromboembolism. *Journal of the American Society of Echocardiography* 2009;22:1353-1359.
- 282.Rushmer RF, Krystal DK. Changes in configuration of the ventricular chambers during the cardiac cycle. *Circulation* 1951;4:211-218.
- 283.Kukulski T, Hubbert L, Arnold M, et al. Normal regional right ventricular function and its change with age: A Doppler myocardial imaging study. *Journal of the American Society of Echocardiography* 2000;13:194-204.
- 284.Urheim S, Caudro S, Frantz S et al. Relationship of tissue displacement and strain to invasively determined right ventricular stroke volume. *American Journal of Cardiology* 2005;96:1173-1178.
- 285.Ueti OM, Camargo EE, Ueti AA, et al. Assessment of right ventricular function with Doppler echocardiographic indices derived from tricuspid annular motion: Comparison with radionuclide angiography. *Heart* 2002;88:244-248.
- 286.Kjaergaard J, Petersen CL, Kjaer A, et al. Evaluation of right ventricular volume and function by 2D and 3D echocardiography compared to MRI. *European Journal of Echocardiography* 2006;7:430-438.
- 287.Tamborini G, Pepi M, Galli CA, et al. Feasibility and accuracy of a routine echocardiographic assessment of right ventricular function. *International Journal of Cardiology* 2007;115:86-89.
- 288.Ghio S, Recusani F, Klersy C, et al. Prognostic usefulness of the tricuspid annular plane systolic excursion in patients with congestive heart failure secondary to idiopathic or ischaemic dilated cardiomyopathy. *American Journal of Cardiology* 2000;85:837-842.

289. Wang J, Prakasa K, Bomma C, et al. Comparison of novel echocardiographic parameters of right ventricular function with ejection fraction by cardiac magnetic resonance. *Journal of the American Society of Echocardiography* 2007;20:1058-1064.
290. Meluzin J, Spinarova L, Bakala J, et al. Pulsed Doppler tissue imaging of the velocity of tricuspid annular systolic motion; a new, rapid and non-invasive method of evaluating right ventricular systolic function. *European Heart Journal* 2001;22:340-348.
291. Lindqvist P, Waldenstrom A, Henein M, et al. Regional and global right ventricular function in healthy individuals aged 20-90 years: a pulsed Doppler tissue imaging study: Umea General Population Heart Study. *Echocardiography* 2005;22:305-314.
292. Nikitin NP, Witte KK, Thackray SD, et al. Longitudinal ventricular function: Normal values of atrioventricular, annular and myocardial velocities measured with quantitative two-dimensional colour Doppler tissue imaging. *Journal of the American Society of Echocardiography* 2003;16:906-921.
293. Pauliks LB, Chan KC, Chang D, et al. Regional myocardial velocities and isovolumic contraction acceleration before and after device closure of atrial septal defects: A colour tissue Doppler study. *American Heart Journal* 2005;150:294-301.
294. Kass Da, Yamazaki T, Burkoff D et al. Determination of left ventricular end-systolic pressure-volume relationship by the conductance (volume) catheter technique. *Circulation* 1986;73:586-595.
295. Rickards AF, Bombardini T, Corbucci G, et al. An implantable intracardiac accelerometer for monitoring myocardial contractility. The multicentre PEA Study Group. *Pacing and Clinical Electrophysiology* 1996;19:2066-2071.

296. Lytrivi ID, Lai WW, Ko HH, et al. Colour Doppler tissue imaging for evaluation of right ventricular systolic function in patients with congenital heart disease. *Journal of the American Society of Echocardiography* 2005;18:1099-1104.
297. Toyono M, Harada K, Tamura M, et al. Myocardial acceleration during isovolumic contraction as a new index of right ventricular contractile function and its relation to pulmonary regurgitation in patients after repair of tetralogy of Fallot. *Journal of the American Society of Echocardiography* 2004;17:332-337.
298. Pauliks LB, Pietra BA, DeGroff CG, et al. Non-invasive detection of acute allograft rejection in children by tissue Doppler imaging: myocardial velocities and myocardial acceleration during isovolumic contraction. *Journal of Heart and Lung Transplant* 2005;24:S239-S248.
299. Popma JJ, Bittl J (2001). Ch 12: Coronary angiography and intravascular ultrasonography. *Braunwald E, Zipes DP, Libby P; Heart Disease: A Textbook of Cardiovascular Medicine Sixth Edition* (pp387-421). Philadelphia, Pennsylvania, USA: W. B. Saunders Company.
300. Wyman RM, Safian RD, Portway V et al. Current complications of diagnostic and therapeutic cardiac catheterisation. *Journal of the American College of Cardiology* 1988;12:1400-1406.
301. Ritchie RH, Wuttke RD, Hi JTY et al. The force-interval relationship of the left ventricle: A quantitative description in patients with ischaemic heart disease. *Journal of Cardiac Failure* 1995;1:273-284.
302. Alam M, Wardell J, Andersson E, et al. Characteristics of mitral and tricuspid annular velocities determined by pulsed wave Doppler tissue imaging in healthy subjects. *Journal of the American Society of Echocardiography* 1999;12:618-628.

303. Nagueh SF, Mikati I, Kopelen HA, et al. Doppler estimation of left ventricular filling pressure in sinus tachycardia: A new application of tissue Doppler imaging. *Circulation* 1998;98:1644-1650.
304. Cheitlin MD, Armstrong WF, Aurigemma GP, et al. ACC/AHA/ASE 2003 guideline update for the clinical application of echocardiography – summary article: a report of the American College of Cardiology/American Heart Association Task Force on Practice Guidelines (ACC/AHA/ASE Committee to update the 1997 Guidelines for the Clinical Application of Echocardiography). *Journal of the American College of Cardiology* 2003;42:954-970.
305. Becker M, Hoffman R, Kuhl HP, et al. Analysis of myocardial deformation based on ultrasonic pixel tracking to determine transmural myocardial infarction. *European Heart Journal* 2006;27:2560-2566.
306. Leitman M, Lysyansky P, Sidenko S, et al. Two-dimensional strain – a novel software for real-time quantitative echocardiographic assessment of myocardial function. *Journal of the American Society of Echocardiography* 2004;17:1021-1029.
307. Nakai H, Takeuchi M, Nishikage T, et al. Effect of aging on twist-displacement loop by 2-dimensional speckle tracking imaging. *Journal of the American Society of Echocardiography* 2006;19:880-885.
308. Reisner S, Lysyansky P, Agmon Y, et al. Global longitudinal strain: a novel index of left ventricular systolic function. *Journal of the American Society of Echocardiography* 2004;17:630-633.
309. Takeuchi M, Nakai H, Kokumai M, et al. Age-related changes in left ventricular twist assessed by two-dimensional speckle-tracking imaging. *Journal of the American Society of Echocardiography* 2006;19:1077-1084.

310. Takeuchi M, Nishikage T, Nakai H, et al. The assessment of left ventricular twist in anterior wall myocardial infarction using two-dimensional speckle tracking imaging. *Journal of the American Society of Echocardiography* 2007;20:36-44.
311. Marwick TH. Should we be evaluating the ventricle or the myocardium? Advances in tissue characterization. *Journal of the American Society of Echocardiography* 2004;17:168-172.
312. D'Hooge J, Konofagou E, Jamal F, et al. Two-dimensional ultrasonic strain rate measurement of the human heart in vivo. *IEEE Transactions on Ultrasonics, Ferroelectrics and Frequency Control* 2002;49:281-286.
313. Stanton T, Leano R, Marwick TH. Prediction of all-cause mortality from Global Longitudinal Speckle Strain: Comparison with Ejection Fraction and Wall Motion Scoring. *Circulation: Cardiovascular Imaging* 2009; DOI: 10.1161/CIRCIMAGING.109.862334
314. Brown J, Jenkins C, Marwick T. Use of myocardial strain to assess global left ventricular function: a comparison with cardiac magnetic resonance and 3-dimensional echocardiography. *American Heart Journal* 2009;157:157-162.e1-5.
315. McGowan JH, Martin W, Burgess MI, et al. Validation of an echocardiographic wall motion index in heart failure due to ischaemic heart disease. *European Journal of Heart Failure* 2001;3:731-737.
316. Gregoratos G, Abrams J, Epstein AE, et al. ACC/AHA/NASPE 2002 guideline update for implantation of cardiac pacemakers and antiarrhythmia devices. Summary article: a report of the American College of Cardiology/ American Heart Association task force on practice guidelines (ACC/AHA/NASPE Committee to update the 1998 Pacemaker Guidelines). *Journal of the American College of Cardiology* 2002;40:1703-1740.

317. Vanoverschelde JL, Raphael DA, Robert AR, et al. Left ventricular filling in dilated cardiomyopathy: relation to functional class and haemodynamics. *Journal of the American College of Cardiology* 1990;15:1288-1295.
318. Pinamonti B, Di Lenarda A, Sinagra G, et al; Heart Muscle Disease Study Group. Restrictive left ventricular filling pattern in dilated cardiomyopathy assessed by Doppler echocardiography: clinical, echocardiographic and haemodynamic correlations and prognostic implications. *Journal of the American College of Cardiology* 1993;22:808-815.
319. Giannuzzi P, Imparato A, Temporelli PL, et al. Doppler-derived mitral deceleration time of early filling as a strong predictor of pulmonary wedge pressure in post infarction patients with left ventricular dysfunction. *Journal of the American College of Cardiology* 1994;23:1630-1637.
320. Pozzoli M, Capomolla S, Pinna G, et al. Doppler echocardiography reliably predicts pulmonary artery wedge pressure in patients with chronic heart failure with and without mitral regurgitation. *Journal of the American College of Cardiology* 1996;27:883-893.
321. Traversi E, Pozzoli M, Cioffi G, et al. Mitral flow velocity changes after 6 months of optimised therapy provide important haemodynamic and prognostic information in patients with chronic heart failure. *American Heart Journal* 1996;132:809-819.
322. Xie GY, Berk MR, Smith MD, et al. Prognostic value of Doppler transmitral flow patterns in patients with congestive heart failure. *Journal of the American College of Cardiology* 1994;24:132-139.
323. Hurrell DG, Oh JK, Mahoney DW, et al. Short deceleration time of mitral inflow E velocity: prognostic implication with atrial fibrillation versus sinus rhythm. *Journal of the American Society of Echocardiography* 1998;11:450-457.

324. Rihal CS, Nishimura RA, Hatle LK, et al. Systolic and diastolic dysfunction in patients with clinical diagnosis of dilated cardiomyopathy. Relation to symptoms and prognosis. *Circulation* 1994;90:2772-2779.
325. Faris R, Coats A, Heinein M. Echocardiography-derived variables predict outcome in patients with non-ischaemic dilated cardiomyopathy with or without a restrictive filling pattern. *American Heart Journal* 2002;144:343-350.
326. Bella JN, Palmier V, Roman MJ, et al. Mitral ratio of peak early to late diastolic filling velocity as a predictor of mortality in middle-aged and elderly adults: the Stron Heart Study. *Circulation* 2002;105:1928-1933
327. Pinamonti B, Zecchin M, Di Lenarda A, et al. Persistence of restrictive left ventricular filling pattern in dilated cardiomyopathy: an ominous prognostic sign. *Journal of the American College of Cardiology* 1997;29:604-612.
328. Temporelli PL, Corra U, Imparato A, et al. Reversible restrictive left ventricular diastolic filling with optimized oral therapy predicts a more favourable prognosis in patients with chronic heart failure. *Journal of the American College of Cardiology* 1998;31:1591-1597.
329. Pozzoli M, Capomolla S, Sanarico M, et al. Doppler evaluations of left ventricular diastolic filling and pulmonary wedge pressure provide similar prognostic information in patients with systolic dysfunction after myocardial infarction. *American Heart Journal* 1995;129:716-725.
330. Nijland F, Kamp O, Karreman AJ, et al. Prognostic implications of restrictive left ventricular filling in acute myocardial infarction: a serial Doppler echocardiographic study. *Journal of the American College of Cardiology* 1997;30:1618-1624.
331. Sakata K, Kashiro S, Hirata S, et al. Prognostic value of Doppler transmitral flow velocity patterns in acute myocardial infarction. *American Journal of Cardiology* 1997;79:1165-1169.

332. Galdrisi M, Heinein MY, D'Hooge J, et al on behalf of the European Association of Echocardiography. Recommendations of the European Association of Echocardiography. How to use echo-Doppler in clinical trials: different modalities for different purposes. *European Journal of Echocardiography* 2011;12:339-353.
333. Gottdeiner JS, Bednarz J, Devereux R, et al. American Society of Echocardiography recommendations for the use of echocardiography in clinical trials: A report from the American Society of Echocardiography's Guidelines and Standards Committee and the Task Force on echocardiography in clinical trials. *Journal of the American Society of Echocardiography* 2004;17:1086-1119.
334. Jung B, Sneider B, Markl M, et al. Measurement of left ventricular velocities: Phase contrast MRI velocity mapping versus tissue Doppler ultrasound in healthy volunteers. *Journal of Cardiovascular Magnetic Resonance* 2004;6:777-783.
335. Nagueh SF, Mikati I, Kopelen HA, et al. Doppler estimation of left ventricular filling pressure in sinus tachycardia. A new application of tissue Doppler. *Circulation* 1998;98:1644-50.
336. Srinivasan J, Jain H, Misri J, et al. Non-invasive estimation of pulmonary capillary wedge pressure is better with lateral than with septal mitral annular tissue Doppler velocities. *Circulation* 2008;118:S725.
337. Matthews JC, Dardas TF, Dorsch MP, et al. Right sided heart Failure: diagnosis and treatment strategies. *Current Treatment Options in Cardiovascular Medicine* 2008;10:329-341.
338. De Grote P, Millaire A, Foucher-Hossein C, et al. Right ventricular ejection fraction is an independent predictor of survival in patients with moderate heart failure. *Journal of the American College of Cardiology* 1998;32:948-954.

339. Voekel NF, Quaipe RA, Leinwand LA, et al. Right ventricular function and failure: report of a National Heart Lung and Blood Institute and working group on cellular and molecular mechanisms of right heart failure. *Circulation* 2006;114:1883-1891.
340. Gorcsan J III, Murali S, Counihan PJ, et al. Right ventricular performance and contractile reserve in patients with severe heart failure. Assessment by pressure-area relations and association with outcome. *Circulation* 1996;94:3190-3197.
341. Gaballa M, Lind B, Storaas C et al. Intra- and inter-observer reproducibility in off-line extracted cardiac tissue Doppler velocity measurements and derived variables. *Proc IEEE. Engineering in Medicine and Biology* 2001;1:4-6.
342. Rabben SI, Irgens F, Haukanes A, et al. An analysis of the angle dependence in strain (rate) imaging of the left ventricle. *Ultrasonics* 2003;1:13-16.
343. Yu CM, Fung JWH, Zhang Q, et al. Tissue Doppler imaging is superior to strain rate imaging and post-systolic shortening on the prediction of reverse remodelling in both ischaemic and non-ischaemic heart failure and after cardiac resynchronisation therapy. *Circulation* 2004;110:66-73.
344. Wong CY, O'Moore-Sullivan T, Leano R, et al. Association of subclinical right ventricular dysfunction with obesity. *Journal of the American College of Cardiology* 2009;47:611-616.
345. Suigiura E, Dohi K, Onishi K, et al. Reversible right ventricular non-uniformity quantified by speckle-tracking strain imaging in patients with acute pulmonary embolism. *Journal of the American Society of Echocardiography* 2009;22:1353-1359.
346. Serri K, Reant R, Lafitte M, et al. Global and regional myocardial function quantification by two-dimensional strain: Application in hypertrophic cardiomyopathy. *Journal of the American College of Cardiology* 2006;47:1175-1181.

347. Lafitte S, Perlant M, Reant P, et al. Impact of impaired myocardial deformations on exercise tolerance and prognosis in patients with asymptomatic aortic stenosis. *European Journal of Echocardiography* 2009;10:414-419.
348. Koyama J, Ray-Sequin PA, Falk RH. Longitudinal myocardial function assessed by tissue velocity, strain, and strain rate tissue Doppler echocardiography in patients with AL (primary) cardiac amyloidosis. *Circulation* 2003;107:2446-2452.
349. Weidemann F, Breunig F, Beer M, et al. Improvement of cardiac function during enzyme replacement therapy in patients with Fabry disease: a prospective strain rate imaging study. *Circulation* 2003;108:1299-1301.
350. Dutka DP, Donnelly JE, Palka P, et al. Echocardiographic characterization of cardiomyopathy in Friedreich's ataxia with tissue Doppler echocardiographically derived myocardial velocity gradients. *Circulation* 2000;102:1276-1282.
351. Lane A, Fleming AD, Donnelly JE, et al. Differences in myocardial velocity gradient measured throughout the cardiac cycle in patients with hypertrophic cardiomyopathy, athletes and patients with left ventricular hypertrophy due to hypertension. *Journal of the American College of Cardiology* 1997;30:760-768.
352. Cardiothoracic Directorate, Freeman Hospital. Costings and Tariffs 2012.